Predictive Pre-Cooling Control for Low Lift Radiant Cooling using Building Thermal Mass

by

Nicholas Thomas Gayeski

Bachelor of Arts in Physics, Cornell University (2002)
Master of Science in Building Technology, Massachusetts Institute of Technology (2007)

Submitted to the Department of Architecture
in partial fulfillment of the requirements for the Degree of

Doctor of Philosophy in Architecture: Building Technology
at the
Massachusetts Institute of Technology

September 2010

Signature of author ……
August 6, 2010
Nicholas T. Gayeski
Department of Architecture

Certified by……
Leslie K. Norford
Professor of Building Technology, Department of Architecture
Thesis Supervisor

Accepted by……
Takehiko Nagakura
Chair of the Department Committee on Graduate Students

Thesis Committee

Leslie K. Norford
Thesis Supervisor
Professor of Building Technology
Department of Architecture
Massachusetts Institute of Technology

Peter R. Armstrong
Associate Professor of Mechanical Engineering
Mechanical Engineering Program
Masdar Institute of Science and Technology

Leon R. Glicksman
Professor of Building Technology and Mechanical Engineering
Departments of Architecture and Mechanical Engineering
Massachusetts Institute of Technology

Predictive Pre-Cooling Control for Low Lift Radiant Cooling using Building Thermal Mass

By

Nicholas Thomas Gayeski

Submitted to the Department of Architecture
on August 6, 2010 in partial fulfillment of the requirements for the
Degree of Doctor of Philosophy in Architecture: Building Technology

Abstract

Low lift cooling systems (LLCS) hold the potential for significant energy savings relative to conventional cooling systems. An LLCS is a cooling system which leverages existing HVAC technologies to provide low energy cooling by operating a chiller at low pressure ratios more of the time. An LLCS combines variable capacity chillers, hydronic distribution, radiant cooling, thermal energy storage and predictive control to achieve lower condensing temperatures, higher evaporating temperatures, and reductions in instantaneous cooling loads by spreading the daily cooling load over time.

The LLCS studied in this research is composed of a variable speed chiller and a concrete-core radiant floor, which acts as thermal energy storage. The operation of the chiller is optimized to minimize daily energy consumption while meeting thermal comfort requirements. This is achieved through predictive pre-cooling of the thermally massive concrete floor. The predictive pre-cooling control optimization uses measured data from a test chamber, forecasts of controlled climate conditions and internal loads, empirical models of chiller performance, and data-driven models of the temperature response of the zone being controlled. These data and models are used to determine a near-optimal operational strategy for the chiller over a 24-hour horizon. At each hour, this optimization is updated with measured data from the previous hour and new forecasts for the next 24 hours.

The novel contributions of this research include the following: experimental validation of the sensible cooling energy savings of the LLCS relative to a high efficiency split system air conditioner - savings measured in a full size test chamber were 25 percent for a typical summer week in Atlanta subject to standard efficiency internal loads; development of a methodology for incorporating real building thermal mass, chiller performance models, and room temperature response models into a predictive pre-cooling control optimization for LLCS; and detailed experimental data on the performance of a rolling-piston compressor chiller to support this and future research.

Thesis Supervisor: Leslie K. Norford
Title: Professor of Building Technology

This page intentionally blank

Acknowledgements

This work has been supported by the Masdar Institute of Science and Technology and the Abu Dhabi Future Energy Company. Additional funding has been drawn from the generous donations of the Mitsubishi Electric Research Laboratory to the Building Technology program. Thank you to the Massachusetts Institute of Technology for supporting me through the Presidential Graduate Fellowship program and numerous teaching assistantships, and the Martin Family for their support of sustainability research, including my own.

I am grateful and honored to have had the patient guidance of Dr. Leslie Norford, whose calm, astute and flexible mentoring helped me find research that inspired, and whose knowledge and advice helped it to fruition.

I am thankful for the omnipresent guidance and intellectual influence of Dr. Peter Armstrong. His depth of knowledge and practical teaching on measurement, instrumentation, thermal modeling, refrigeration, controls, cooling and any and all things related to buildings and energy have been a tremendous force in my intellectual and experimental development.

Thanks to Dr. Leon Glicksman for his needed reserve and critical perspective from outside the trenches of low-lift cooling. Your presence on the committee kept me wary of my own assumptions and conclusions and prompted me to think clearly and think twice.

The warmest thanks to Dr. Marilyne Andersen, whose guidance through my Masters degree and understanding and flexibility thereafter enabled me to mature and evolve as an independent building scientist, researcher and engineer.

To Sian Kleindienst and Stephen Samouhos, thanks for being conspirators, instigators, compatriots, and friends and to a bright future whatever may come, and whatever we create.

I extend my gratitude to all the friends, colleagues, and mentors who have helped and humored me along the way, especially Yanni Loukissas, Saeed Arida, Josh Lobel, Zach Lamb, Brandon Roy, Rob Darnell, Tom Pittsley, Evan Samouhos and EVCO Mechanical, Srinivas Katipamula and PNNL, the good researchers at MERL, my friends from the Boston Architectural College and other Solar Decathletes, my lab-mates from Building Technology, and the faculty, students and staff of the Departments of Architecture and Mechanical Engineering. To the faculty and students at the Masdar Institute of Science and Technology, thanks for an educational and hot summer. To Kathleen Ross, Ali Mulcahy, and Renee Caso, thanks for all your help.

Thanks to Mom and Dad, who set the foundation and let me build. Thanks to all my family, whose fun and emotional support bring me balance.

My love and gratitude to Celina and our dogs, for keeping me sane and driving me crazy and for being there every step of the way.

Contents

List of Figures

List of Tables

Nomenclature

AAT	Adjacent zone air temperature
AHU	Air handling unit
ANN	Artificial neural network
ARMAX	Auto-regressive, moving average with exogenous variables model
ASHRAE	American Society of Heating, Refrigerating and Air Conditioning Engineers
BAS	Building automation system
BPHX	Brazed plate heat exchanger
BTU	British thermal units
C	Celsius
CFD	Computational fluid dynamics
CFM	Cubic feet per minute
COP	Coefficient of performance
CRTF	Comprehensive room transfer function
CTF	Conduction transfer function
DOAS	Dedicated outdoor air system
DOE	United States Department of Energy
EER	Energy efficiency ratio
EIR	Electric input ratio, the reciprocal of COP
EMCS	Energy management and control system
EPW	EnergyPlus weather file
EVT	Evaporating temperature
f	Condenser fan speed
$GtCO_2$-eq/yr	Gigatons of carbon dioxide equivalent per year
GPM	Gallons per minute
H	Enthalpy
HPB	High performance building
HVAC	Heating, ventilating and air conditioning
Hz	Hertz
IPLV	Integrated part load value
K	Kelvin
kPa	Kilopascals
kW	Kilowatts
kWh	Kilowatt-hours
LLCS	Low lift cooling system
LLCS-SSAC	Low lift cooling system applying predictive control to a SSAC
LLCS-TABS	Low lift cooling system with a thermo-active building system
LLCS-RCP	Low lift cooling system using radiant ceiling panels and passive TES
$\dot{m}$	Mass flow rate
MIST	Masdar Institute of Science and Technology
MIT	Massachusetts Institute of Technology
MRT	Mean radiant temperature

NARX	Nonlinear autoregressive with exogenous variables model
OAT	Outdoor air temperature
OPT	Operative temperature
P	Power (or Pressure)
P_t	System power consumption at time t
PID	Proportional-Integral-Derivative control law
PCM	Phase change material
$PENEVT_t$	Evaporating temperature penalty function at time t
$PENOPT_t$	Operative temperature penalty functionat time t
PEX	Polyethylene pipe
PLR	Part load ratio
PNNL	Pacific Northwest National Laboratory
QC	Cooling rate
QI	Internal load heat rate
RC	Resistance and capacitance (in a thermal RC network)
R410A	Refrigerant R410A, consisting of 50 percent R-32 and 50 percent R125
RCP	Radiant ceiling panel
RMSE	Root mean square error
RPM	Revolutions per minute
RTU	Rooftop unit HVAC system
RWT	Chilled water return temperature
SEER	Seasonal energy efficiency ratio
Sqft	Square feet
SSAC	Split system air conditioner
T	Temperature
TABS	Thermo-active building systems (concrete-core heating and cooling)
TCs	Thermocouples
TES	Thermal energy storage
TMY	Typical meteorological year
TOU	Time-of-use electricity rate
UA	Total thermal conductance in W/K
UAE	United Arab Emirates
UST	Under-slab temperature (at the bottom of the concrete slab)
VAV	Variable air volume heating, cooling and ventilation system
VSD	Variable speed drive
W	Watts (or power)
Wh	Watt-hours
$\forall$	Volumetric flowrate
ZAT	Zone air temperature
ΔT	Temperature difference
ω	Compressor speed
φ	Operative temperature penalty weight in W/K^2

Chapter 1 Introduction

Consumption of energy through buildings and its impact on climate and environment have motivated a broad effort to seek practical and innovative energy efficiency and conservation measures for buildings. Globally, between 30 and 40 percent of primary energy consumption is through buildings [UNEP 2007]. In the U.S., around 39 percent of national primary energy consumption is through buildings and its share is projected to increase in the next twenty years [USDOE 2006]. Improved building design, retrofits of existing buildings, better lighting, efficient heating, ventilation and air conditioning (HVAC), improved control, more efficient appliances, better operations and maintenance, and numerous other approaches hold immediate potential for energy savings [McKinsey 2007]. The barriers to progress on these measures are largely systemic issues in the industry, primarily rooted in lack of education, lack of incentive, or lack of requirement through codes [Granade et al 2009].

In the long-term, there is a deeper need for new ideas and new strategies to further and prolong energy efficiency and conservation gains in buildings. In a recent report, "Unlocking Energy Efficiency in the U.S. Economy", McKinsey and Company stated as one of its five overarching strategies the need to "Foster innovation in the development and deployment of next-generation energy efficiency technologies to ensure ongoing productivity gains" [Granade et al 2009]. In other words, to sustain and further efficiency gains achievable with current technology and practices, new technologies and strategies will be required for sustainable global development. In buildings, this could mean anything from new tools for improved designs, new methods to achieve more economical retrofits, new technologies to improve performance, or new processes to improve operations and maintenance.

This research looks ahead from existing practices and trends in HVAC design, operation, monitoring and control towards an integrated approach to designing and operating a coupled passive and active cooling strategy with more intelligent control using measured building data. This strategy is called low lift cooling. Low lift cooling refers broadly to cooling strategies that leverage existing HVAC technologies to operate chillers at low pressure ratios more of the time, thereby enabling significant cooling energy savings. Typically, low lift cooling systems (LLCS) combine variable capacity chillers, hydronic distribution, radiant cooling, thermal energy storage (TES) and predictive pre-cooling control to achieve lower condensing temperatures and higher evaporating temperatures, resulting in higher average chiller efficiency and energy savings. [Armstrong et al 2009a, Armstrong et al 2009b, Jiang et al 2007, Katipamula et al 2010].

In this research, an experimental LLCS was developed, built and tested consisting of a variable capacity chiller serving a concrete radiant floor, similar to a thermo-active building system (TABS) in which chilled water pipes are embedded in the concrete slab of a building. Predictive control of the chiller was implemented to pre-cool the radiant concrete floor in anticipation of future cooling loads based on forecast climate and internal loads. Models of chiller performance and zone temperature response were identified from measured data and used to inform the predictive control algorithm. Finally, the energy and thermal comfort performance of the LLCS was compared to the performance of a high efficiency split system air conditioner (SSAC) subject to the same climate conditions and internal loads.

1.1 Energy, climate and buildings

Society's approach to and perspective on energy, climate and buildings are interdependent. Regardless of one's views on climate change, energy has become a premier challenge for the 21st century and beyond. The potential for political instabilities, local environmental impacts, increasing costs, and rising demand for energy-intensive services make energy a primary national and international priority. For those who find the uncertainties in climate change science - role of oceans, aerosols, clouds, etc - to be outweighed by the evidence for anthropogenic causes of climate change and potential adverse impacts, tackling the energy problem is even more crucial to the future of our societies.

Among these two mammoth issues, energy and climate, lies the challenge of buildings. All too often a discussion about energy and climate conjures up images of billowing smokestacks from massive power plants or industrial facilities, backed up traffic on urban highways, or oil spills from offshore drilling rigs or international tankers. All too infrequently does the discussion turn to the pervasive presence of lighting, building heating and cooling, ventilation, appliances and other auxiliary building loads that dominate energy and electrical power consumption in modern life. These building-related loads constitute the majority of energy and electric consumption throughout modern, industrialized nations. There has been a giant white elephant in the room of national energy policy for decades that energy efficiency, and especially energy efficiency in buildings, is critical towards creating a better energy policy and infrastructure.

Numerous scientists, policy-makers, and engineers have pointed towards energy efficiency and 'soft' energy technologies as a solution to energy and climate problems. Amory Lovins, in his well-known 1976 Foreign Affairs article pointed to a soft path for energy policy. The soft path employs energy efficient technologies for appliances, HVAC and lighting, renewable energy sources, and transitional technologies for fossil fuel generation to move away from dependence on oil, gas, coal, and nuclear sources of energy [Lovins 1976]. Lovins' observations are still relevant today. David Goldstein, Art Rosenfeld, and other efficiency advocates spent decades working for appliance efficiency standards. Their efforts have not been in vain. Estimates suggests that decades of improvements in refrigerator appliance standards have saved over 17 billion dollars [Goldstein 2007] as average refrigerator energy consumption dropped from 1800 kWh/year to 450 kWh/year between 1977 and 2002.

This deliberate, long-term and persistent approach to achieving energy savings through energy efficiency standards reaps real rewards. In the buildings sector in the United States, building energy codes have been the primary regulatory tool for driving efficiency. However, turnover in the building stock is very slow, and codes lag far behind state of the art technology. Driving significant building energy savings in the United States will require both aggressive retrofitting of the existing building stock and the construction of low-energy or even zero net-energy buildings. Creating new, low energy best available technologies to motivate more aggressive energy efficiency standards is an important path to improving building energy efficiency. LLCS constitute one of these potential low energy technologies.

Reducing greenhouse gas emissions in the United States will also require a sharp focus on building-related carbon dioxide emissions. McKinsey estimates that many of the least cost carbon dioxide abatement measures relate to creating better buildings. LED lighting, façade renovations, building controls, co-generation, HVAC equipment improvements and other building and appliance efficiencies make up over 50 percent of the carbon dioxide abatement potential [McKinsey 2007].

Internationally, the intergovernmental panel on climate change (IPCC) estimates that the buildings sector holds the potential for reduction of 5.3 to 6.7 Gigatons of CO_2 equivalent per year ($GtCO_2$-eq/yr) at less than $\$100/tCO_2$-eq [Levine et al 2007]. That is the largest potential among all sectors. The technical solutions referenced by the IPCC are many, including passive façades, integrated design, more efficient mechanical systems, leveraging thermal mass, better commissioning and fault detection, and building energy management systems. The barriers are also many, including poor short term cost/benefit analyses, split incentives, hidden costs, perceived risk, and organizational ignorance or inertia [Levermore 2008, Levine et al 2007]. One of the greatest challenges is that most of the energy reductions will be required in existing buildings.

For new construction, particularly in developing countries where construction and development continues at a rapid pace, applying the best design and technologies to minimize energy demand in new buildings is a major priority. The Energy Information Administration (EIA) estimates a 34 percent increase in building energy consumption in 20 years [Perez-Lombard 2007]. At the same time, the IPCC working group on residential and commercial buildings estimates that new buildings could potentially consume one quarter of the energy of a typical existing building [Levine et al 2007]. Integrated design, passive reduction of building loads, highly efficient cooling and ventilation, and building energy management systems all make the short list of technical solutions to reduce the growth of energy consumption in new buildings.

New building construction generally involves more cooling than in the past and higher demand for thermal comfort. As such, efficient cooling is rapidly becoming a critical issue for energy efficient buildings. In the United States, space cooling accounts for around 12.6 percent of the total primary energy consumption in commercial buildings [USDOE 2006], and demand for cooling continues to grow in the U.S. and abroad. In Europe, it has been estimated that the air conditioned floor area will increase from 2,100 to 3,300 billion square meters by 2020 [Brunner

et al 2006], increasing electric demand from 102 to 159 TWh per year for cooling. Furthermore, in other areas of the world cooling is or will be an even more significant fraction of energy consumption. Much of the developing world, where urbanization and building construction are fastest, is located in lower latitudes where the need for cooling is greater.

Sivak [2009] analyzed the potential growth in cooling energy demand in the 50 largest metropolitan areas in the world. This analysis showed that 38 of the largest 50 metropolitan areas are in developing countries, where building construction and demand for thermal comfort and HVAC are on the rise. Of these 38, 24 have greater cooling demands than heating demands. Sivak estimated that if cooling was provided at the same level as that in the United States, the cooling demand in Mumbai, India with a population of just 13.8 million would be equivalent to 24 percent of the cooling demand for the entire United States. Complicating matters further, Degelman [2002] projected that cooling energy loads would significantly increase in low and middle latitude cities as a result of climate change.

The need for reliable and secure energy, the impacts on climate and environment, development in cooling dominated climates, and the rising demand for cooling and comfort motivate a need for highly efficient mechanical cooling systems coupled with reduced building thermal loads through better design. The next chapter will discuss technical strategies to meet this need through highly efficient, high performance buildings and advanced cooling strategies.

1.2 High performance buildings and advanced cooling systems

There are many technologies, design options and operational strategies available to reduce the energy consumption of buildings. A high performance building (HPB) is a term broadly used to define buildings that perform better than conventional buildings. The American Society of Heating, Refrigerating and Air Conditioning Engineers' (ASHRAE) Standard 189.1, the Standard for the Design of High Performance Green Buildings, defines an HPB as:

> "a building designed, constructed and capable of being operated in a manner that increases environmental performance and economic value over time, seeks to establish an indoor environment that supports the health of occupants, and enhances the satisfaction and productivity of occupants through integration of environmentally preferable building materials and water-efficient and energy-efficient systems". [ASHRAE 2009]

In simple terms, high performance buildings are buildings that provide a better environment for occupants, better economic value, lower energy consumption, lower water consumption, and lower life-cycle costs.

There are numerous resources available describing how to create high performance buildings. ASHRAE standard 189.1 provides minimum requirements for the "siting, design, construction, and plan for operation of high performance green buildings" [ASHRAE 2009]. However, ASHRAE 189.1 requirements largely reflect just a step above the standard state of the art, as

outlined in ASHRAE 90.1, the Standard for the Energy Performance of Buildings [ASHRAE 2007c].

Going beyond standard systems with high efficiency equipment enables even greater energy savings, but often requires a more integrated and innovative approach to both building and mechanical design, construction, control and operation. Integrated design processes seek to include architects, engineers, building owners, commissioning agents, and construction managers early in the process of creating a building to facilitate better design and coordinated strategies [Lewis 2004]. In terms of energy efficiency, the intent of this integrated design approach is to coordinate building siting, form, and envelope with passive lighting, thermal, ventilation, and mechanical system strategies to create a highly energy efficient and economical building.

Reducing energy consumption and providing a comfortable environment to occupants are the two important aspects of HPB with relation to this research. Managing the impact of environmental conditions on thermal loads and lighting through passive design are the first steps towards these goals. Strategies such as effective siting and orientation of a building can reduce solar loads, provide better access to light, and enhance natural ventilation. Façade design and building envelope optimization can further provide shading, reduce heat transfer across the envelope, and provide for the implementation of passive cross-ventilation or buoyancy-driven natural ventilation strategies.

Reducing internal loads due to office equipment, lighting, and auxiliary equipment are doubly important. This strategy reduces electrical loads directly, but also reduces the thermal load and subsequent demands on HVAC equipment. Combined with proper passive thermal management, reducing equipment internal loads can lead to operational cost and capital cost savings through reductions in the size of mechanical equipment [Todesco 2004].

Integrating passive ventilation strategies with efficient mechanical ventilation and conditioning can further reduce energy consumption. Providing mixed mode ventilation systems that allow for natural ventilation or night ventilation under favorable conditions can offset the need to use mechanical equipment. The greatest reduction in HVAC energy and costs is often achieved by avoiding the need for mechanical HVAC systems altogether, sometimes or all of the time.

There are a plethora of efficient active mechanical system components currently in use in HPB. Condensing boilers, variable speed chillers, variable speed pumps and fans, energy and enthalpy recovery systems, TES, radiant systems, and dedicated outdoor air systems are some of the many technologies being deployed to achieve energy efficiency. An efficient overall system however, arises from the design, proper construction, commissioning, effective control, and appropriate operation and maintenance of a combination of these components in an integrated manner. As will be discussed in chapter 2, this research draws from this principle that existing high efficiency mechanical components can be integrated into a highly efficient system, an LLCS, so that drastic energy savings are achieved.

There are numerous examples of HPB with highly efficient systems leveraging passive design, natural ventilation and high efficiency mechanical equipment to provide cooling. Actuated façade systems providing natural ventilation have been employed in buildings such as the San Francisco Federal Building. Buoyancy-driven natural ventilation has been employed in such buildings as Lanchester Library or the Queen's Building at De Montfort University in England. Another approach is to mix active and passive strategies. Mixed-mode systems use natural ventilation for part of the building and/or part of the time but mechanical systems under conditions unfavorable for natural ventilation or during peak loads. Buildings such as the Kirsch Center for Environmental Studies or the California Academy of Sciences are naturally ventilated but with radiant concrete slabs which provide cooling under peak load conditions [McConahey 2008].

In many climates, passive strategies and natural ventilation alone cannot provide thermal comfort. If mean temperatures, and especially night-time mean temperatures, are outside of the desired range for thermal comfort it will not be possible to naturally ventilate during the day or at night. In addition, practical issues such as outdoor air quality or street noise may be prohibitive to naturally ventilating a building. In these cases, efficient mechanical systems are necessary to provide cooling for adequate thermal comfort.

Many technologies are available for *active* low-energy cooling strategies. Thermally driven heat pumps, such as absorption, adsorption or chemisorption heat pumps [Oxizidis and Papadopolous 2008], can be incorporated into systems where waste heat or solar thermal energy is available. Variable speed chillers combined with variable speed distribution systems provide low energy chilled water generation and distribution. Coupling these with chilled beams, chilled ceiling panels, or radiant concrete-cores can eliminate fan energy and raise the chilled water temperature setpoint, improving chiller efficiency. TES can be employed to shift loads from peak demand periods to the nighttime. This has the additional benefit of chiller operation at lower condensing temperatures. Recent attention has been given to a TES strategy called thermo-active building systems (TABS) in which chilled water pipes are embedding in the concrete slab of every floor of a building [Lehman et al 2007]. With TABS the building concrete structure can be pre-cooled, providing cooling to building spaces later in the day due to the thermal time lag of the concrete.

The details of these specific advanced cooling technologies, radiant cooling, TES with precooling, variable capacity chillers and hydronic distribution are discussed in chapter 2.

1.3 Energy monitoring, management and control

The final broad trend in the building industry influencing this research is the increasing availability and utility of building data. The revolution in information technology in the past thirty years is still only beginning to impact the building sector. To date, major changes include the emergence of direct digital control systems, networked building systems and components, centralized control through building automation systems (BAS), and opportunities for energy efficiency and optimization through energy management and control systems (EMCS).

Networked building systems with centralized controls are slowly becoming the norm for large new construction projects and renovations. Today, monitored data from buildings can be used to perform data-driven modeling, analysis, simulation, benchmarking, fault detection, optimization and supervisory control to improve the performance and operation of buildings [Motegi et al 2003, Brambley et al 2005, Roth et al 2005].

Opportunities still just emerging for building energy management and control include optimal whole building control systems, simulation based control and optimization, and model-based predictive control. Optimal model-based predictive control is premised on the notion that data-driven or physically based models of buildings can be created using monitored building data, and that these models can be used to determine the most energy efficient or cost effective control strategies [Quartararo 2006, Hatley et al 2005]. Some optimal control algorithms use parametric models of building systems created from known engineering quantities using simulation tools [Kolokotsa et al 2005, Clarke et al 2002, Mahdavi 2001, Henze and Krarti 2005]. Another approach is to use monitored building data to train data-driven models from measured building performance. This approach has been explored by [Braun and Chaturvedi 2002, Armstrong et al 2006a, Armstrong et al 2006b]. This thesis will follow a similar approach in implementing a model-based predictive control strategy, as described in chapters 4 and 5.

1.4 Thesis objectives and structure

The confluence of issues around energy, climate and buildings, new technologies for low-energy cooling, and the emerging role of building data in achieving efficiency provide a broad context for this work. This research seeks to advance the art of a low-energy cooling strategy, LLCS, which leverages building monitoring and control systems to greatly improve energy efficiency. The ultimate goals are to drastically reduce the energy consumption required for cooling buildings, scale down building energy demands to make building integrated power feasible, and reduce the environmental and climate impacts of buildings.

Advancing low-lift cooling requires both theoretical development and experimental testing with variable speed chillers, radiant concrete-core cooling, radiant panel cooling, dedicated outdoor air systems (DOAS), TES, thermal model identification, pre-cooling control optimization, and model-based control. This dissertation offers original contributions on the following key issues:

- A performance comparison of an LLCS cooling system with predictive pre-cooling control to a high efficiency SSAC.
- Development of a pre-cooling optimization control algorithm for LLCS that incorporates the transient response of real building thermal mass. This algorithm determines a near-optimal chiller control schedule using outside temperature and internal gain forecast, chiller performance models, and building temperature response models.
- Measurement and empirical modeling of the performance of a rolling piston compressor heat pump/chiller over a wide range of pressure ratios including low pressure ratios.

- Application of building thermal model identification methods to the problem of passive pre-cooling control optimization for concrete core radiant cooling.

The dissertation will conform to the following structure:

Chapter 2 will be a literature review of the most important research underpinning LLCS. Research on radiant cooling and pre-cooling of TES will be reviewed in detail. Prior research on low-lift cooling, its constituent systems and supporting strategies will be explained.

Chapter 3 will explain experimental research to characterize the performance of a variable speed heat pump/chiller at low pressure ratios. This will include a review of prior research on chiller performance at low-pressure ratio, an explanation of the experimental apparatus and procedure for measuring heat pump/chiller performance under low-pressure ratio conditions, and presentation of empirical curve-fit models to represent chiller performance as a function of chilled water return temperature, outdoor air temperature, compressor speed and condenser fan speed.

Chapter 4 will focus on thermal model identification methods and results for predicting zone temperature response. It will review prior research on thermal model identification. Thermal model identification methods will be applied to predicting the thermal response of a thermally massive test chamber.

Chapter 5 will discuss the development of a pre-cooling control optimization algorithm for predictive control of the variable speed chiller. The empirical performance maps and data-driven zone temperature response models developed in chapters 3 and 4 are integrated into the optimization objective function. Compressor and condenser fan speeds can be set hourly to determine the optimal chiller dispatch schedule that will minimize power consumption and maintain thermal comfort.

Chapter 6 will detail the results of designing, building and implementing control over an experimental LLCS consisting of a variable capacity chiller serving a concrete-core radiant cooling system with predictive control. The energy and thermal comfort performance of the system will be compared to a high efficiency, variable capacity SSAC with a seasonal energy efficiency ratio (SEER) of 16 BTU/Wh. Simulations will be performed to compare LLCS performance to SSAC with conventional thermostatic control and with predictive control.

Chapter 7 will conclude with a summary of the original contributions of this research and its results. A summary of alternative LLCS strategies will be reviewed along with barriers and benefits to applying LLCS on a broad scale. Finally, future LLCS research needs will be presented.

Chapter 2 Low Lift Cooling Systems

Low-lift cooling systems (LLCS) hold promise for dramatically more efficient cooling of buildings. As previously explained, an LLCS is a cooling system that leverages existing HVAC technologies to operate vapor compression chillers at low pressure ratios more of the time while still meeting human thermal comfort standards. LLCS are typically made up of a few key HVAC components and strategies that enable low pressure ratio operation. These include variable speed compressors, hydronic distribution with variable speed pumps, radiant cooling, TES, predictive pre-cooling control, and dedicated outdoor air systems.

A temperature-entropy (T-S) diagram of a vapor compression cycle and the effect of each HVAC technology in an LLCS are shown in
Figure 1. The larger polygon on the T-S diagram represents typical air-cooled chiller operation with low chilled water temperature and high, daytime condenser air temperatures. The smaller polygon on the T-S diagram represent low lift chiller operation with radiant cooling, variable speed hydronic distribution, TES, predictive pre-cooling control, and a variable capacity chiller. The use of radiant cooling and variable speed pumping allow for high chilled water temperatures and higher evaporating temperatures. Pre-cooling of TES overnight or in the early morning allows the chiller to operate when outdoor temperatures are lower, leading to lower condensing temperatures. Variable capacity chillers with variable speed compressors allow the chiller to modulate capacity in response to cooling load.

The cooling provided by both of these cycles is represented by the area under the bottom line of the vapor compression cycle. The work required to operate the vapor compression cycle is represented by the area inside the polygons. This diagram shows why chillers can operate more efficiently at low lift conditions. The LLCS can produce a similar (or greater) cooling effect as the conventional system while requiring less work. As a result, a chiller operated at low lift has a higher coefficient of performance (COP) than under typical conditions, with subsequent energy savings.

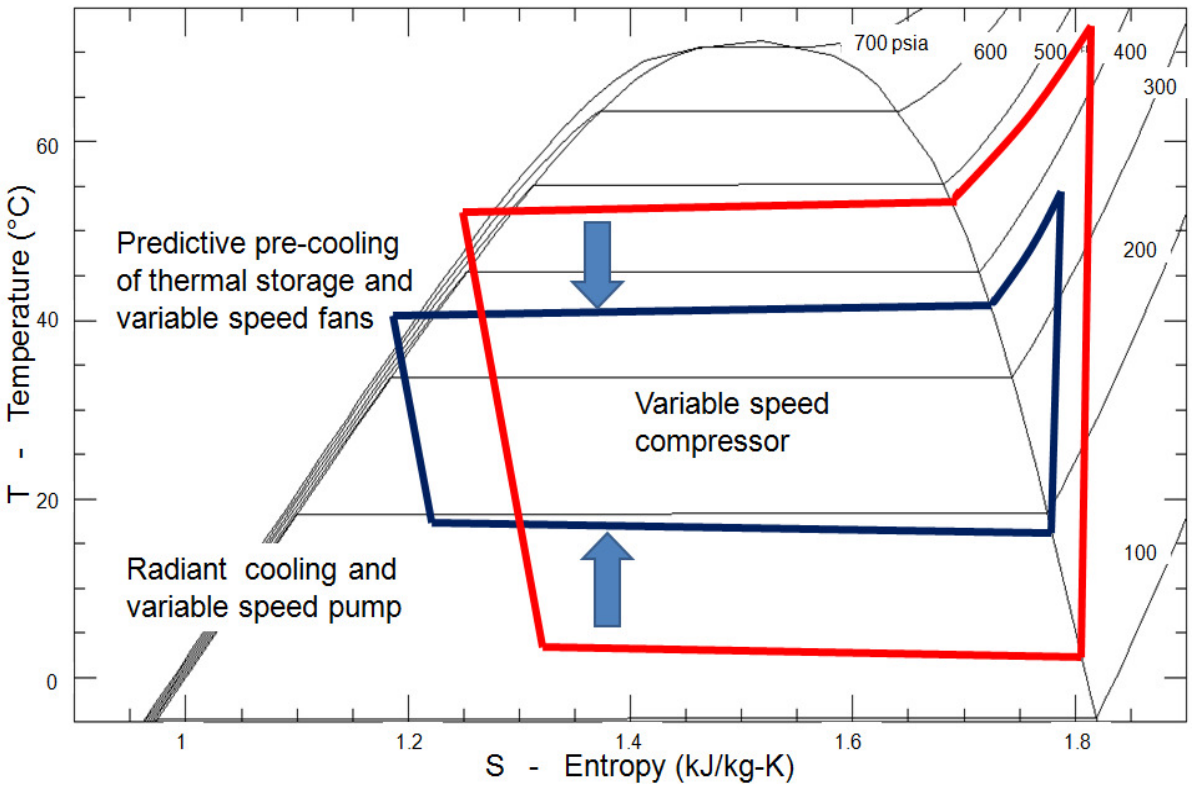

Figure 1 Effect of low lift cooling technologies in achieving low pressure ratio vapor compression

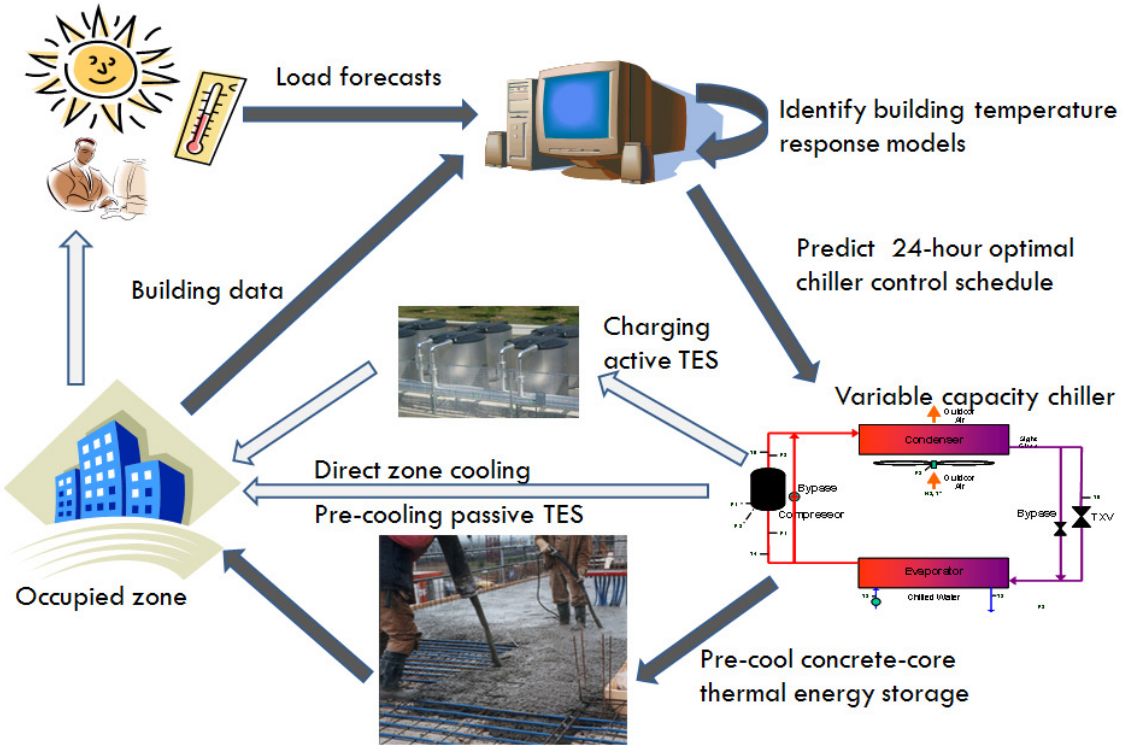

Figure 2 Low lift cooling system operational process flow

Figure 2 shows a conceptual diagram of how LLCS work. Starting at the top of the diagram, forecasts of internal loads, temperature, and solar conditions along with measured building data are gathered and delivered to a building control system (the computer in the diagram). Thermal model identification is performed on the building data to train a model of zone temperature response as a function of building loads and cooling rate input. Using this model, and a model of cooling system energy consumption, a near-optimal control schedule is determined for the chiller which may include pre-cooling of active TES, pre-cooling of thermo-active building systems (TABS), or direct cooling of a space.

Estimated energy savings of LLCS over typical variable air volume (VAV) systems common in the United States with conventional two-speed chillers are large. For typical buildings, cooling energy savings range from 37 to 84 percent depending on the climate [Katipamula et al 2010]. In high performance buildings, savings range from -9 to 70 percent of cooling energy consumption. The low end demonstrates that LLCS may not be attractive for high performance buildings in mild climates where free cooling through economizers is available. Although low-lift cooling is a relatively new concept from a systems integration viewpoint, the component cooling strategies, constituent systems and pre-cooling control strategies have a long history of research, development and implementation.

This chapter will provide a literature review of research relevant to LLCS. These include radiant cooling, pre-cooling TES, mechanical system components such as variable speed chillers, pumps and fans and dedicated outdoor air systems. Existing LLCS research will also be reviewed.

2.1 Radiant cooling

Radiant cooling is strategy by which cold surfaces absorb heat from objects (such as people), surfaces and air in a room through radiative, and to a lesser extent convective, heat transfer. Typically radiant systems consist of low thermal mass radiant panels, or thermally-massive radiant concrete-cores which have chilled water pipes embedded in concrete, or TABS. Radiant cooling enables energy savings primarily through three mechanisms. First, air temperatures in a zone can be warmer as the operative temperature is lowered by cool radiant temperatures. Second, transport energy for pumping chilled water is lower than fan energy for all-air systems. Third, chilled water temperatures, and thus evaporating temperatures, are higher which reduces the burden on the chiller. Although radiant cooling systems have been installed in many buildings, it is still an emerging technology. There is ongoing research on how best to integrate and control radiant systems of different types, in different climates, with different companion systems, and with TES [Braun et al 2001, Vangtook and Chirarattananon 2006, Armstrong et al 2009b, Roth et al 2009]. This section will review the current state of research on radiant cooling, a major sub-component of a LLCS.

The potential benefits of radiant cooling systems are many, including reduced energy consumption, improved air quality and humidity control, reduced space requirements, and potentially even lower first costs [Feustel and Stetiu 1995]. Radiant cooling operates through large, cooled surfaces which absorb radiant energy from a space, with some convective cooling

as well. Because radiant systems include a large, cool surface inside a zone humidity control must be provided separately to prevent condensation. Radiant systems also do not provide ventilation air. Typically, radiant cooling systems are combined with small ventilation systems that provide latent cooling and ventilation air. Higher potential costs, condensation, remodeling constraints, and architectural design freedom all pose real or perceived threats to the applicability of radiant cooling [Engineered Systems 2002].

Olesen [1997] explained design considerations for radiant floor cooling systems, including radiant concrete-core cooling or TABS, a conceptual diagram of which is shown in Figure 3. Typical radiant floor cooling systems require tube spacing between 75 and 300 mm to achieve adequate cooling capacity, although floor covering, slab thickness and slab thermal properties are also important considerations in design. Olesen et al [2003] describe European standards for designing radiant concrete-core cooling systems including calculation of heat transfer between chilled water and the zone based on pipe type and spacing, concrete characteristics and flow rate. Olesen et al [2000a] describes the calculation of the heat exchange coefficient between the floor surface and a space, paying special attention to reference temperatures and a more accurate method of calculating radiative and convective heat transfer separately. Typically radiant floors have a capacity of no more than 50 W/m^2, requiring designers to carefully reduce thermal loads through proper insulation, shading, and reduction in internal gains prior to specifying and designing radiant floor cooling. However, it has been shown that with direct absorption of solar radiation on the floor surface capacities can exceed 85 to 100 W/m^2 [Simmonds et al 2006, Olesen 2008].

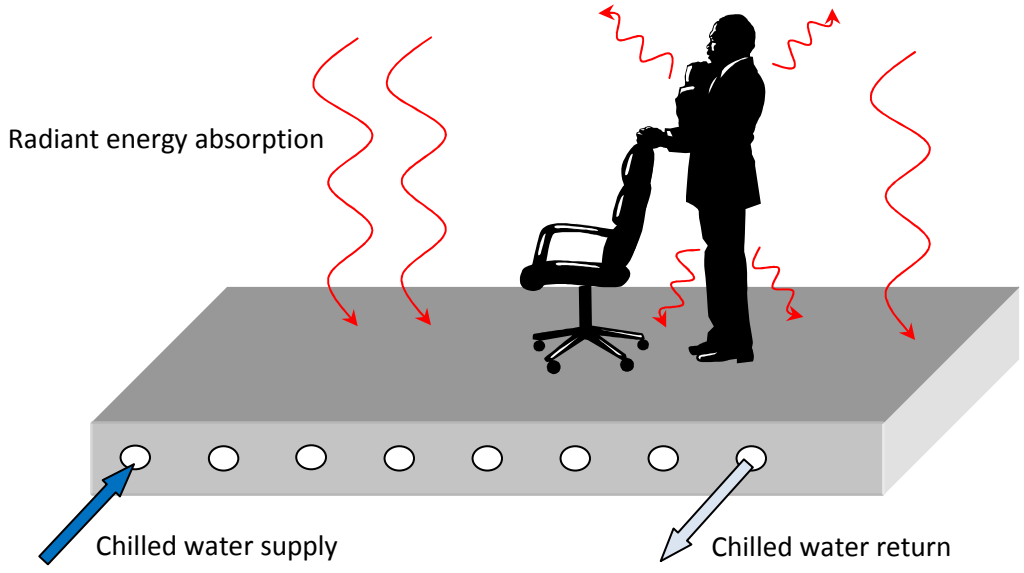

Figure 3 Conceptual diagram of a radiant concrete-core cooling system or TABS (not to scale)

A number of constraints apply to the design and control of radiant floor cooling systems. Floor surface temperatures above 18 to 19 Celsius are necessary to maintain comfort for occupants. Maintaining surface temperatures more than around two Kelvin above dewpoint temperature prevents condensation. Avoiding temperature asymmetries and vertical air temperature differences more than three Kelvin are important for thermal comfort [Olesen 1997]. Lim et al [2006] and Ryu et al [2004] investigated the use of Ondol, a traditional Korean radiant floor heating system, for radiant cooling and found that controlling supply water temperature was a more effective means of controlling floor surface temperature than on/off or variable water flow control. [Koschenz and Dorer 1999] showed the importance of minimizing convective heat loads in a space to prevent large increases in air temperature from internal loads relative to concrete surface temperatures.

[Scheatzle 2006] explained many of the real-life problems encountered in implementing concrete-core and capillary tube radiant systems in real buildings. Concrete-core radiant floor cooling can lead to large stratification without sufficient air movement, such as through ceiling fans. Embedding pipe in concrete slabs can be problematic when systems fail, and access points are important especially at valves and joints where failures may occur. Careful design and sizing of dehumidification systems are important to avoid condensation and associated mold and water damage.

Radiant cooling from the ceiling, be it through concrete core, radiant panels, or chilled beams, is also relevant to LLCS although not tested experimentally in this thesis. Radiant cooling through ceiling panels has been tried for more than 60 years [Adlam 1948] but has faced resistance due primarily to problems with condensation and mold [Dieckmann et al 2004]. Today, in Europe and increasingly in the United States radiant ceiling panel (RCP) cooling is finding new markets in tighter buildings, with controlled ventilation and dehumidification to prevent condensation problems.

[Mumma 2001] estimated that a typical RCP cooling system would cost 2$/sqft less than a conventional variable air volume (VAV) system in a commercial office building, while offering 29 percent operational cost savings. [Katipamula et al 2010] estimated an 8% additional first cost for RCP with DOAS in large office applications but expects costs to decrease as RCP market share increases. [Sodec 1999] estimated that RCP cooling first costs may be 20 percent lower than VAV systems, while occupying 40 to 55 percent less floor area. [Dieckmann et al 2004] speculated that the additional useable square footage allowed by the reduced size of mechanical equipment in radiant systems will create significant value to offset increased capital costs. Furthermore, radiant systems typically require more interaction between architects and engineers earlier in the design phase to properly design, size, and locate systems, which may add to first costs.

Energy savings estimates from radiant cooling vary widely and depend on climate, building characteristics, baseline system type, and radiant cooling type. [Leigh et al 2005] estimated that a radiant floor cooling system with supplemental ventilation and dehumidification would consume about one third of the energy of a room air conditioner in a typical house in Seoul,

South Korea. Over a set of representative climates in the United States, Stetiu [1999] concluded that radiant cooling may save on average 30 percent of the total energy consumption and 27 percent of peak power demand relative to a VAV system in a modern office building. On the other hand, Niu et al [1999] concluded through simulations that a cooled ceiling system had comparable energy consumption to a VAV system in the Dutch climate, and may perform even worse than VAV systems in colder climates such as Finland. Tian and Love [2009] found that a building in Calgary had poor control, integration and coordination between a parallel VAV system and radiant slab cooling resulting in simultaneous heating and cooling when free cooling was possible, resulting in 180 percent *more* energy consumption than a VAV system alone.

Experimental and simulation studies have shown that it is possible to control radiant slab and RCP cooling systems to effectively control thermal comfort and avoid condensation. Imanari et al [1999], Kitagawa et al [2009], Vangtook and Chirarattananon [2006], and Kim et al [2005] showed that comfortable operative temperatures, acceptable vertical air temperature gradients and reduced drafts are achievable with radiant cooling systems. However, some induced air movement and avoidance of humid conditions may be important for proper comfort, in addition to preventing condensation.

In summary, the body of research on radiant cooling systems suggests that the strategy has great potential for reduced energy consumption, reduced operational costs, less space requirements, and possibly reduced first costs. However, careful attention must be given to design integration and controls to ensure radiant cooling capacity, zone temperature response, humidity control, and ventilation achieve potential energy savings and thermal comfort. Without proper attention to these issues, the same problems of lower than expected energy performance with the additional problems of condensation, poor comfort control, and higher costs will hinder further adoption of radiant cooling systems.

2.2 Thermal energy storage and pre-cooling control

The second major strategy in LLCS is the use of thermal energy storage (TES) to shift loads and store cooling energy for later use. Employing TES in buildings is a strategy whereby energy for heating or cooling can be stored in the mass of a building, or in active thermal storage elements like ice tanks, stratified chilled water tanks, or phase change materials (PCM) to moderate temperatures or anticipate loads at another time. There is a large body of research on TES, including different types of active and passive TES, integrating TES into the building envelope through TABS, and pre-cooling control for TES. This section will review the current research on TES systems and their integration and control.

The benefits of using TES are many, but the benefit most frequently cited is the ability to shift peak thermal and electrical loads from the afternoon to the nighttime. This creates value for building owners and for the grid. First, electricity is typically cheaper at night under time-of-use or real time electricity pricing, reducing costs to the owner. For the grid, TES can allow better utilization of more efficient base-load generating plants, reduce line losses, and reduce

required spinning reserves [MacCracken 2004]. Additional benefits may include reducing the capacity, and thus costs, of mechanical equipment by reducing peak thermal loads. This research utilizes a further benefit of shifting load to nighttime, which is that variable capacity chillers can run more efficiently overnight because it is cooler outside [Roth et al 2006b]. Over the course of a cooling season, this improved nighttime efficiency can add up to significant energy savings when coupled with additional energy efficient cooling strategies.

Passive TES refers to the use of building elements, such as concrete walls or drywall with embedded capsules of PCM, to store thermal energy within the materials of a building. Passive TES may be used to dampen the diurnal temperature swing of a space, shift peak loads to later in the day, or absorb solar energy to store heat for later use.

A number of research studies have estimated the value of load shifting and pre-cooling control with passive TES. Xu and Haves [2005] found that pre-cooling with a forced air system by using low temperature setpoints during the morning occupied hours and a steadily increasing temperature setpoint schedule during peak demand hours can save 80 to 100 percent of chiller energy during peak periods. In field tests, surveys showed occupants were comfortable as long as zone temperatures remained between 70 and 76 Fahrenheit. Kintner-Meyer and Emery [1995] evaluated the potential benefits of pre-cooling with forced air systems and found significant energy savings through free-cooling in the early morning. For four cooling-dominated U.S. cities they estimated peak power reductions between 10 and 45 percent and peak period energy reductions around 40 to 50 percent.

Lee and Braun [2006, 2008] showed that demand limiting can be accomplished through optimization of zone temperature setpoints using a state space thermal RC network building model [Braun and Chaturvedi 2002]. This approach was tested at the Energy Resource Station at the Iowa Energy Center and a 30 percent reduction in peak load was achieved for a demand limiting period from 1 pm to 6 pm. Braun et al [2001] used these state space inverse models to develop a tool for evaluating thermal mass pre-cooling control strategies for forced air systems and applied it to a large commercial building in Chicago. They found that 40 percent cooling cost savings were possible by adjusting zone temperature setpoints during on and off peak periods. Conversely, when a similar approach was applied to typical buildings in California under critical peak pricing rates the financial savings were less than $50 per 1,000 square feet [Braun and Lee 2006]. This suggests that the benefits to utility companies and the grid may be greater than the benefits to building owners for certain kinds of demand shifting.

Rabl and Norford [1991] presented the use of transfer function building thermal models for predictive peak load shifting and estimate that load shifting of 10 to 20 percent is possible in typical commercial buildings. A similar approach is presented in [Armstrong et al 2006a,b] where a comprehensive room transfer function (CRTF) model is developed to forecast cooling loads and temperature trajectories for model-based predictive control. This model was presented for use in four applications: curtailment or peak load shifting, thermal mass pre-cooling, optimal chiller start, and model-based control under large disturbances or both energy savings and demand limiting.

For cooling applications, a thermo-active building system (TABS) is a HVAC strategy that integrates heat exchangers into building constructions by embedding pipes or air ducts through which chilled water or air may flow to cool the thermal mass [Lehmann et al 2007, Henze et al 2008]. This may include capillary systems with pipe embedded close to the ceiling or floor surface, concrete-core systems for which pipes are embedded within concrete slabs, or a combination of both [Pfafferott and Katz 2007].

Concrete-core TABS provide TES via the thermal mass of the slab. The slab can be charged overnight, or pre-cooled, lowering its temperature. The slab absorbs heat from the room as internal, solar and other loads warm up the space. The building mass must be pre-cooled just enough to meet the thermal loads on the building later in the day. Too much pre-cooling and the space may be too cold, too little and the space may overheat. This necessitates the use of predictive control by which day-ahead loads are forecast and TABS are pre-cooled to meet those loads. TABS may work better when coupled with faster responding systems that can adapt to prediction errors and unanticipated loads, such as Dedicated Outdoor Air Systems with additional cooling capacity or direct sensible cooling systems such as radiant ceiling panels, chilled beams, or efficient fan coil units.

There are also many active TES technologies which may be considered for LLCS pre-cooling, including aquifer TES, borehole TES, stratified chilled water tanks, or PCM storage tanks (for which PCM is not embedded in building materials) [Paksoy 2002, Dincer 2002]. Use of active TES can similarly shift loads, reduce peak demand, and allow downsizing of HVAC equipment. Market barriers to the use of active TES technologies are many. Many active TES systems cost more and require additional space when compared to the typical alternative, to simply add chiller capacity. Finally, experience with TES among engineers and facility operators are limited [Roth 2006b].

Use of TES is a well-known strategy for shifting thermal loads, reducing peak energy demand, and reducing cooling loads [Rabl and Norford 1991, Braun et al 2001, Roth et al 2006b]. In the context of low-lift, using TES for night (or early morning) pre-cooling allows chiller operation at lower condensing temperatures. Combined with higher evaporating temperatures through radiant cooling, this provides the important “low-lift” conditions for LLCS efficiency.

2.3 Component mechanical systems

There are three primary mechanical systems that are important to low-lift cooling. These are dedicated outdoor air systems (DOAS), variable speed pumps and fans, and variable capacity chillers. This section will review these three primary low-lift system components.

DOAS are air handling units that provide minimum ventilation air and latent cooling (or dehumidification). Instead of recirculating air from zones mixed with outdoor air, only outdoor air is conditioned and delivered to spaces at the minimum amount required for proper ventilation stipulated by ASHRAE 62 Standard for Acceptable Indoor Air Quality [ASHRAE 2007b]. In most buildings, moisture in outside air is the primary source of humidity. DOAS

provide dehumidification of outside air separately from sensible cooling systems, which can be provided at the zone level. As a result, DOAS provide better humidity control and indoor air quality [Dieckmann et al 2003].

DOAS can provide significant energy savings. First, when compared to typical VAV forced air systems, DOAS have much lower airflow rates which require less fan energy. DOAS can also provide energy savings through more efficient dehumidification. Including enthalpy or heat recovery across the incoming and outgoing air streams can reduce the latent load. Using the condenser heat from a direct expansion dehumidification process to reheat dehumidified air can save reheating energy. DOAS also enable additional energy savings by allowing more efficient sensible cooling systems at the zone level, such as radiant cooling systems. [Jeong et al 2003] compared DOAS coupled with RCP to a conventional VAV system and found 25 percent chiller energy savings, 71 percent fan energy savings, 100 percent *more* pumping energy, and 42 percent total annual energy consumption savings.

Many claim that DOAS offer additional advantages in terms of reduced capital costs. Dieckmann et al [2003] suggest that the use of DOAS allows reduced chiller size, reduced condenser water pump capacity, less ductwork, ultimately less floor-to-floor height requirements, and more rentable space. Despite these benefits, a market perception still exists that DOAS have high first costs, perhaps because of the perception that two systems, a DOAS and a separate sensible cooling system, will inherently cost more than one system serving ventilation and cooling needs [Dieckmann et al 2003]. Larranga et al [2008] showed that a high school retrofit with DOAS and separate sensible cooling cost $2.1 million, or $17.50/CFM, and reduced operational costs from $117.25/operating hour to $53.49/operating hour, with a payback of 3.75 years.

A second key enabling component technology for low-lift cooling is variable speed drives (VSD) for fan and pump motors. VSD fans and pumps are being widely adopted across the HVAC industry. By varying pump and fan speeds, airflow rates and water flow rates can be modulated to optimize the operation of equipment to meet a load. Lower fan and pump speeds require less energy consumption by the fan or pump's motors. Of particular interest to LLCS is the optimization of chilled water pump speed and condenser fan speed to maximize the efficiency of a chiller and minimize total HVAC energy consumption and operating costs. In an air-cooled chiller the fan speed and chilled water pump speeds can be adjusted to achieve the maximum COP for the whole system. [Bahnfleth and Peyer 2004] reviewed the state of the art in variable primary flow chilled water for chillers and concluded that variable flow, primary only chilled water systems can save 3 to 8 percent of annual plant energy, primarily through chilled water pump energy savings, and 4 to 8 percent of first costs.

Variable capacity chillers and compressors are commercially available today and have a long history of development [Hiller 1976, Takebayashi et al 1994, Mackensen et al 2002]. Varying the speed of a chiller to adapt to cooling loads allows for adjustment of a compressor's pressure ratio, the ratio between the discharge and suction pressures. Smaller pressure ratios and smaller temperature differences, or "low-lift" between condensing and evaporating

pressures and temperatures, demand less work from the compressor. Since the compressor is responsible for most of the energy consumed during a vapor compression cycle, low-lift chiller operation using variable speed, variable capacity control can provide significant energy savings [Armstrong et al 2009a, Armstrong et al 2009b].

Chiller efficiency is rated using the full-load COP or an integrated part load value (IPLV). The IPLV metric was created to better represent the seasonal performance of chillers over a wider range of conditions by looking at part-load performance at various entering condenser temperatures [Dieckmann et al 2010]. While IPLV does a better job at reflecting the average performance of a chiller, and will show the benefits of VSDs applied to chiller compressors with better part load performance, IPLV still does not reflect the wide range of entering condenser temperatures and part load fractions at which chillers will operate under real conditions. There is a significant lack of data about the performance of chillers over a wide range of conditions and pressure ratios, especially low-lift conditions and pressure ratios below 1.6 [Armstrong et al 2009a]. Chapter 3 will present data on the performance of a rotary piston compressor, air-cooled condenser heat pump over a wide range of load and conditions including low pressure ratios for use in a predictively controlled LLCS.

2.4 Low lift cooling systems

The term low-lift cooling system (LLCS) is used here to describe an integrated system combining radiant cooling, TES, a variable capacity chiller and predictive pre-cooling control to achieve energy efficient cooling. An LLCS achieves energy savings through optimal operation of the chiller throughout a 24 hour period to meet a daily cooling load. The chiller compressor speed, condenser fan speed, and chilled water distribution pump speed can be adjusted and scheduled for each hour of the day to meet the daily cooling load using minimal energy. The use of TES allows the chiller to run at times when it may be more optimal, such as overnight, then store the cooling for use later in the day when it is needed. This research focuses specifically on the use of concrete-core radiant cooling systems, or TABS, or TES.

Armstrong et al [2009a, 2009b] present a detailed description of the component systems, system models, and expected performance of an LLCS that consists of radiant cooling, a variable capacity chiller with variable speed distribution, ideal TES which can be discharged or charged arbitrarily without losses, and optimal predictive control. Computational models are developed in [Armstrong et al 2009a] for a compressor, condenser, liquid evaporator, air-side evaporator, DOAS, radiant cooling sub-system and variable speed transport that are valid under low pressure ratios and low capacity fractions of interest to LLCS. These models are used to compare different combinations of LLCS components to a baseline system comprising VAV distribution with a two speed chiller plant in [Armstrong et al 2009b].

[Armstrong et al 2009b] tested seven combinations of LLCS component systems, including different combinations of systems using variable speed chillers, radiant ceiling panels (RCP) with DOAS, and idealized TES and compared them to a baseline system consisting of a VAV air

handling unit (AHU) with an air-side economizer served by a two speed chiller without TES. The following eight cases were compared:

- VAV system with a two speed chiller (base case system to which others are compared)
- VAV system with a variable speed chiller
- VAV system with a two speed chiller and TES
- VAV system with a two speed chiller and TES
- RCP/DOAS system with a two speed chiller
- RCP/DOAS system with a variable speed chiller
- RCP/DOAS system with a two speed chiller and TES
- RCP/DOAS system with a variable speed chiller and TES

These eight mechanical system cases were simulated in a 20,000 square foot (sqft) medium office building as defined by the Advanced Energy Design Guide (AEDG) [Janargin et al 2006]. A standard performance envelope, glazing, shading, lighting and plug loads were defined based on ASHRAE 90.1 Standard for the Energy Performance of Building excluding Low-Rise Residential [ASHRAE 2004]. Two additional performance levels, a medium performance and a high performance building with increasingly better performance than ASHRAE 90.1 2004 were also simulated. The performance ratings for the different components of the buildings simulated are reproduced from [Armstrong et al 2009b] and shown in Table 1.

Table 1 Building component performance levels used in [Armstrong et al 2009b]

	Component Performance Levels to be Analyzed		
Component	**Standard**	**Mid Performance**	**High Performance**
Wall-roof U-factor	90.1-2004[(a)]	2/3 of 90.1-2004	4/9 of 90.1-2004
Window U-factor and SHGC	90.1-2004[(a)]	2/3 of 90.1-2004	4/9 of 90.1-2004
Window-to-wall ratio	40%	20%	20%+Shading[(b)]
Light and plug loads[(c)] (W/sf)	1.3 + 0.63	0.87 + 0.42	0.58 + 0.21
Fan power (W/scfm)[(d)]	0.8	0.533	0.356

(a) Values change with climate zones.
(b) Completely shade all windows from solar direct beam.
(c) Power density during hours of the highest loads defined in the DOE-2.2 weekly load schedules.
(d) Total HVAC fan power divided by total HVAC fan flow rate.

These eight mechanical systems in a medium office building with three levels of performance were simulated in five climate zones: Houston, Memphis, Los Angeles, Baltimore and Chicago. The resulting analysis showed the relative performance of the different combinations of LLCS components by building performance level in a variety of climates. The results, taken from [Armstrong et al 2009b], are shown in Figures 4, 5 and 6.

These results show that LLCS can have major energy savings in a variety of climates and buildings. Large reductions in energy savings occur with the progressive application of LLCS

component systems. In particular the jump between VAV systems and RCP/DOAS systems is pronounced. This is a result of both higher evaporating temperatures and more efficient chiller operation through the RCP as well as more efficient humidity control and reduced fan energy by the DOAS. The addition of TES separately also creates significant energy savings in each system configuration, due to efficient chiller operation at lower condensing temperatures through nighttime operation.

The combination of all of these systems - RCP/DOAS, variable capacity chillers, and TES - leads to the most significant energy savings. For the climates and building types tested in [Armstrong et al 2009b], energy savings for the full LLCS relative to a VAV system with a two speed chiller range from 70 to 74 percent for standard buildings, 46 to 73 percent for medium performance buildings, and 34 to 71 percent for high performance buildings. Most climates had savings in the 60 to 70 percent range. The lower energy savings correspond to the Los Angeles climate, where mild overnight and swing season conditions can lead to extended economizer operation and significant energy savings with a properly operated VAV system.

The Pacific Northwest National Lab (PNNL) conducted a follow up study to the analysis presented in [Armstrong et al 2009b] in which they analyzed the same eight LLCS configurations explained above using 12 modified DOE Benchmark Prototype EnergyPlus input files with two performance levels in 16 different climates. These DOE Benchmarks are representative of a range of commercial building types in the United States from small to large offices, hotels, hospitals, schools, warehouses and others. The 16 locations used in the study were selected to span the climate zones represented in ASHRAE 90.1 [Katipamula et al 2010].

The results from this recent research are similarly promising, if not more promising, than those in [Armstrong et al 2009b]. PNNL estimated that with 100 percent market penetration across 58 percent of newly constructed commercial floor area (where LLCS is applicable) the full LLCS system would save about 72 percent of cooling energy consumption relative to the DOE Benchmark systems. For standard medium office buildings, the average energy savings for the LLCS system relative to the DOE benchmark were 63 percent, while for high performance the average savings were 57 percent. Similar results with significant savings are presented for small offices, large offices, retail, healthcare facilities and other prototypical buildings. An overview of these results from [Katipamula et al 2010], which show the range in percent energy savings of the LLCS system relative to the DOE Benchmark system for a subset of the prototypical building types across all climates are shown in Table 2. The average savings across climates for standard performance buildings of different types are typically 60 to 70 percent, while the average savings for high performance buildings are typically 40 to 60 percent.

2. Low lift cooling systems

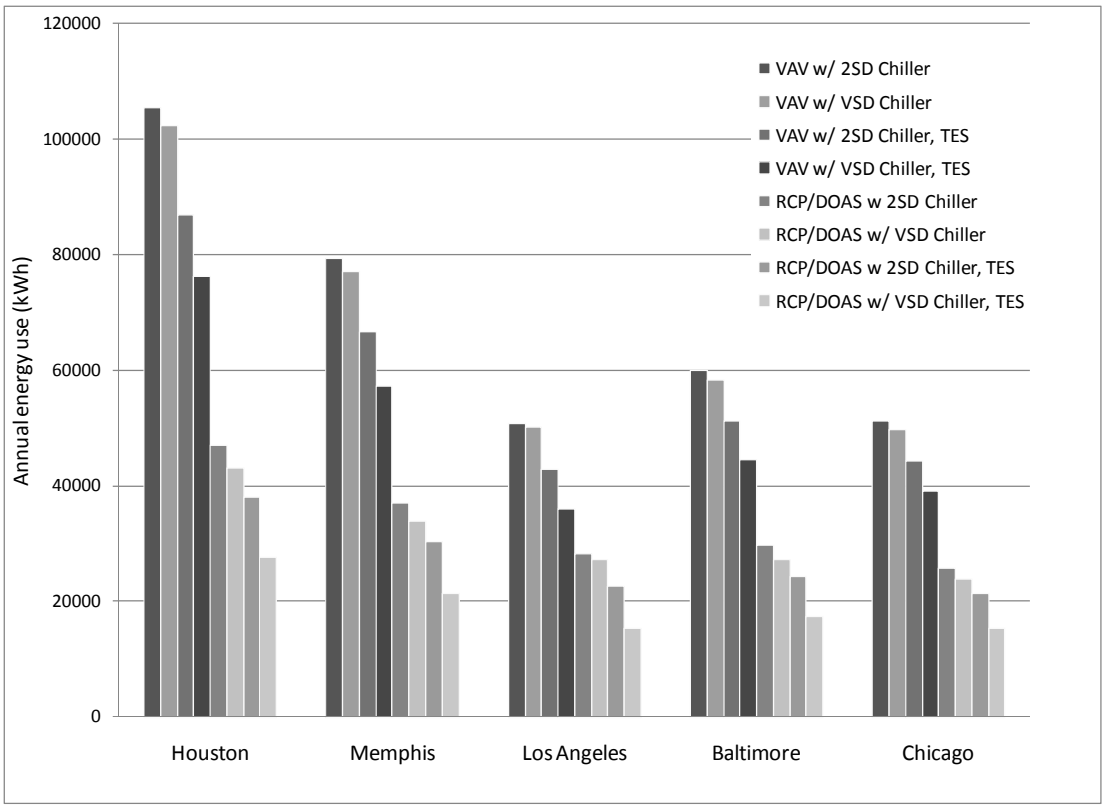

Figure 4 LLCS configuration energy consumption for a 'standard' performance building in five climates

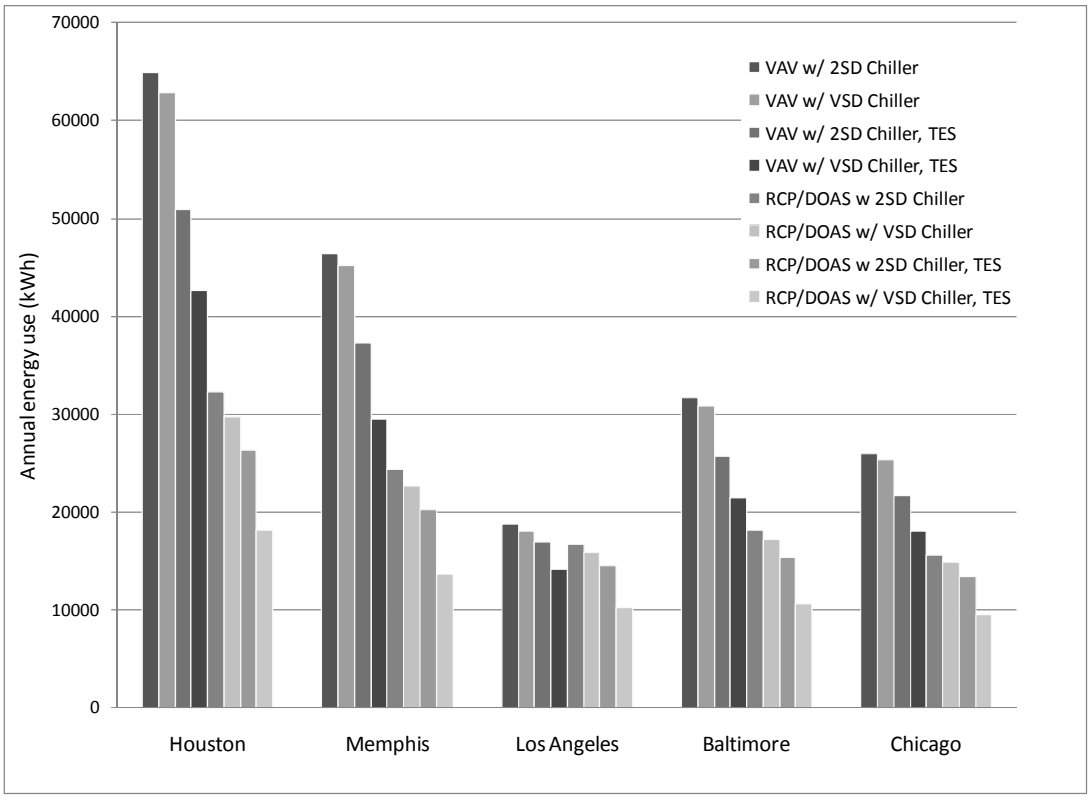

Figure 5 LLCS configuration energy consumption for a 'medium' performance building in five climates

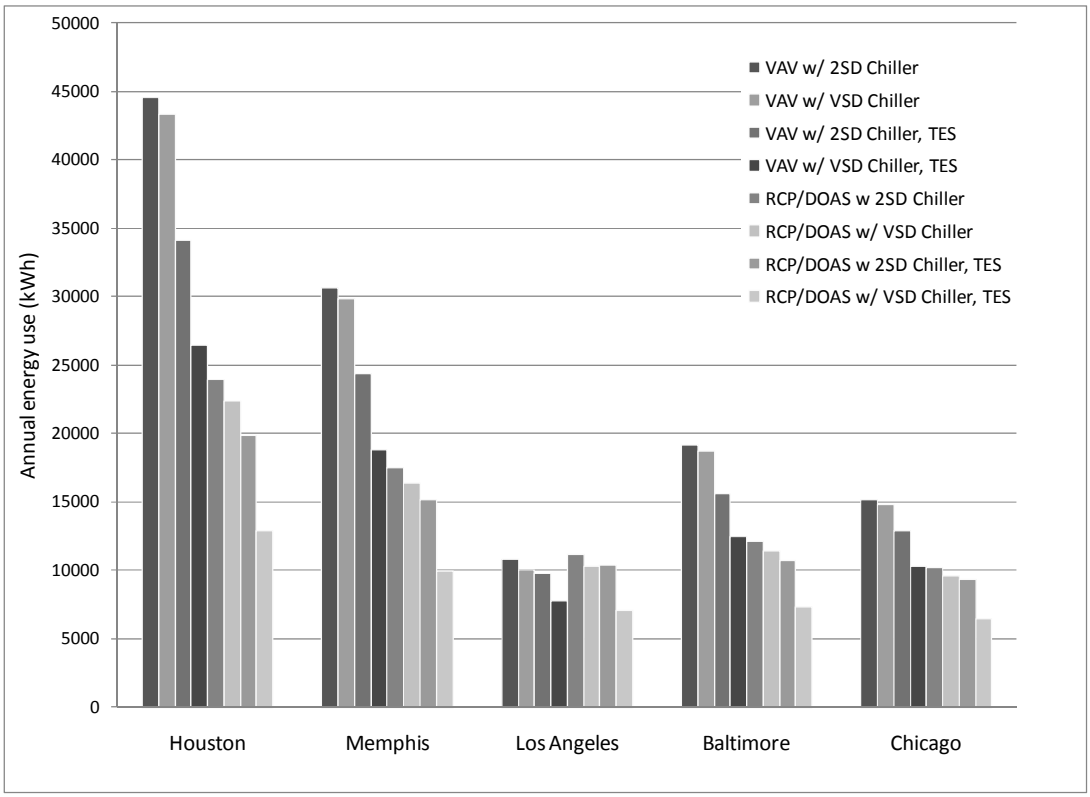

Figure 6 LLCS configuration energy consumption for a 'high' performance building in five climates

Table 2 LLCS energy savings relative to DOE benchmark by building type across 16 climates

	Standard performance building			High performance building		
Building Type	**Minimum**	**Maximum**	**Average**	**Minimum**	**Maximum**	**Average**
Office Small	68%	78%	76%	-9%	56%	40%
Office Medium	56%	67%	63%	43%	65%	57%
Office Large	37%	62%	51%	30%	54%	44%
Retail Standalone	67%	76%	72%	43%	67%	55%
Retail Strip Mall	56%	70%	65%	7%	60%	37%
Primary School	53%	69%	64%	35%	70%	56%
Secondary School	53%	69%	60%	44%	66%	53%
Supermarket	64%	79%	72%	42%	66%	58%
Warehouse	53%	81%	73%	-3%	69%	45%
Outpatient	78%	84%	81%	44%	68%	62%
Hospital	60%	78%	72%	47%	68%	61%

An important comparison to note is the energy savings of the LLCS relative to a VAV system with a variable speed chiller in a medium office building. The VAV system with a variable speed chiller is the most similar system analyzed in [Armstrong et al 2009b, Katipamula et al 2010] to the high efficiency split-system air conditioner (SSAC) used as a baseline system in this research. The simulated energy savings of LLCS relative to a VAV with a variable speed chiller in medium office buildings ranges from 1.4 to 49.7 percent in standard performance buildings, with an average savings of 32 percent. In high performance buildings, energy savings range from -2.4 to 46.8 percent with an average savings of 18.8 percent. In Atlanta, the simulated annual energy savings for a standard performance building were 28.8 percent. These savings will be important to note because the experimental LLCS described in Chapter 6 was tested in Atlanta, with standard efficiency loads.

The potential for cooling energy savings from LLCS is great. However, first cost and practical construction considerations make wide-scale implementation of LLCS in every market a challenge. In addition to energy savings potential, [Katipamula et al 2010] presented economic benefits and barriers to the application of LLCS. Potential benefits include reduced size of HVAC equipment and subsequent reduced first costs, load shifting for reduced demand charges, and better humidity control and comfort performance – benefits previously described. However, a number of barriers limit the applicability of LLCS. The need for collaboration and integrated design between architects and engineers may be problematic. LLCS retrofit applications are limited due to the need to renovate ductwork and add TES. Advanced controls add complexity that not all controls contractors or building operators can support.

[Katipamula et al 2010] investigated the incremental costs and aggregate payback for LLCS systems in the 16 climates studied. For medium office buildings the incremental costs were negative and showed a payback of zero years in all climates. In cooling dominated climates paybacks for schools and large office buildings were in the range of 5 to 10 years, while in mild and heating dominated climates payback periods were greater than 10 years. In part, the cost of LLCS reflects a premium because radiant cooling is an emerging technology and DOAS and RCP systems are not yet produced at scale. However, in the immediate future new medium office buildings, particularly in cooling dominated climates, appear to provide the most cost effective application for LLCS.

The present experimental investgation of LLCS cooling energy savings is largely motivated by the substantial energy savings estimated by the PNNL simulation studies. This research seeks to build on the work of Armstrong et al [2009a, 2009b] and Katipamula et al [2010] to map a low-lift chiller system's performance, test thermal model identification methods in the context of low-lift cooling, incorporate the behavior of a real TABS (not idealized TES) into a pre-cooling control algorithm, and experimentally test predictive, pre-cooling control of a low-lift radiant cooling system using TABS relative to a conventional variable speed split-system air conditioning system (SSAC). Chapters 3, 4, 5 and 6 will go on to explain the prior research on each of these issues separately, the development of new methods and application of existing methods to LLCS, and an experimental assessment of LLCS sensible cooling savings potential.

Chapter 3 Low lift chiller mapping and modeling

An important premise of low lift cooling is that compressors operate at higher efficiencies, or COPs, when the pressure difference, or lift, across the compressor is small. This is the major source of energy savings. Radiant cooling allows higher evaporating temperatures, and thus higher evaporating pressures, because higher chilled water temperatures are suitable for cooling a radiant concrete floor or radiant panels. TES allows for lower condensing temperatures, and thus lower condensing pressures, through nighttime operation of the chiller to pre-cool the TES or charge TABS. As a result, the difference between condensing and evaporating pressures and temperatures is reduced.

Historically, compressor and chiller efficiency ratings focus on the efficiency of the chiller at a single design load or a small set of part-loads. Because the thermal load on the chiller varies constantly over a year and cooling season, this approach ignores significant savings that could be achieved by operating the chiller at lower speeds and smaller pressure differences. Today, with the decreasing costs of and increasing efficiency and reliability of electrical inverters, or more accurately converters, variable cooling capacity chillers are available in which compressor speeds can modulate to meet loads more efficiently.

This chapter will review the state of knowledge about chiller performance at low lift conditions, present an experimental test stand for evaluating the performance of an air source heat pump with a rotary piston compressor under low lift conditions, and present empirical curve-fit models of the performance of the heat pump.

3.1 Low-lift compressor performance

Chiller performance ratings typically present the efficiency of a chiller at a very limited set of conditions. The COP of a chiller can vary with many parameters such as compressor speed, condenser fan speed, primary chilled water flowrate, outdoor temperature, chilled water temperature, or the amount of superheat and subcooling. Despite its highly variable nature, chiller performance is generally presented as a single value to enable engineers to compare and specify chillers using a common metric.

COP at design conditions presents only one value of performance, the chiller efficiency at one design load. Another metric, integrated part load value (IPLV), combines chiller performance values at four different operating conditions, with the chiller running at 25, 50, 75 and 100 percent of part load at specified condensing temperatures. The result is a weighted average

efficiency at four part load conditions. The IPLV rating assumes a chiller will typically run at given part loads a specific amount of time, while in reality a chiller may run at very different part loads and run-times depending on climate, internal loads, mechanical system design, and the attenuation of load peaks by building thermal mass. COP and IPLV, while invaluable to engineers for design and comparison, do not reflect the full range of operating conditions and efficiencies possible with a given chiller.

Dunn et al [2005] found, anecdotally, through monitoring actual system performance in four buildings that the chillers ran on average between 8 and 44 percent of their capacity most of the time. They suggest that this is in part due to over-sizing of equipment and in part due to unoccupied, night-time operation at low loads. On the other hand, Geister and Thompson [2009] found through simulation that many chiller plants, particularly those with multiple chillers, will run at *higher* part loads and lifts more often than the assumptions used for IPLV, and that actual part-load runtimes will vary significantly by climate. Their conclusion is that an hour by hour simulation with a chiller performance model is the only accurate way to estimate chiller performance and energy savings. The results of these studies and others suggest that design condition COP and IPLV are not enough to predict actual performance of equipment installed in the field.

In an LLCS cooling strategy, variable capacity chillers are employed where part load operation to achieve high efficiency is desirable and nighttime operation is enabled by TES. Understanding the performance of the chiller at a wide range of conditions beyond existing metrics is important for maximizing efficiency and energy savings in LLCS. A performance map or look-up table which specifies system power consumption, COP or electric input ratio (EIR, which is the reciprocal of COP) as a function of condensing temperature, evaporating temperature and cooling capacity can be used to model chiller performance within a predictive TES pre-cooling control algorithm. Surrogate variables might include outdoor temperature and condenser fan speed instead of condensing temperature, chilled water return temperature and chilled water pump speed instead of evaporating temperature, and compressor speed and superheat instead of cooling capacity.

Armstrong et al [2009a] developed a set of physically based models of an LLCS. These were made up of component models of a variable capacity chiller with a variable speed condenser fan and chilled water flow, a radiant cooling distribution system, an idealized TES system, and a DOAS for ventilation and dehumidification. A chiller-radiant subsystem performance map spanning low-lift conditions was created based on computational models of a reciprocating compressor, condenser, liquid evaporator, variable speed pump, variable speed fan and radiant panels. The chiller-radiant subsystem performance map is presented in Figure 7.

The performance map illustrates the efficiency, EIR, of the LLCS chiller-radiant subsystem at a wide range of conditions down to low pressure ratios as a function of outdoor temperature, zone temperature, and cooling capacity. It shows the specific power 1/COP, or EIR, in kilowatts (kW) of electricity per kW of thermal cooling delivered as a function of capacity fraction, which is equivalent to cooling delivered divided by cooling capacity at full-speed, at fixed outdoor

temperatures Tx(C) and an indoor temperature of 22.2 C (or 72 F). A refrigerant economizer is included in the chiller model. It is evident from Figure 7 that in theory much higher COPs, as high as five to 20 kW_e/kW_{th}, are possible at low capacity fraction and low outside temperatures relative to a typical chiller or heat pump COP of three or four. Enabling chillers too run at these high efficiencies more of the time is the goal of LLCS.

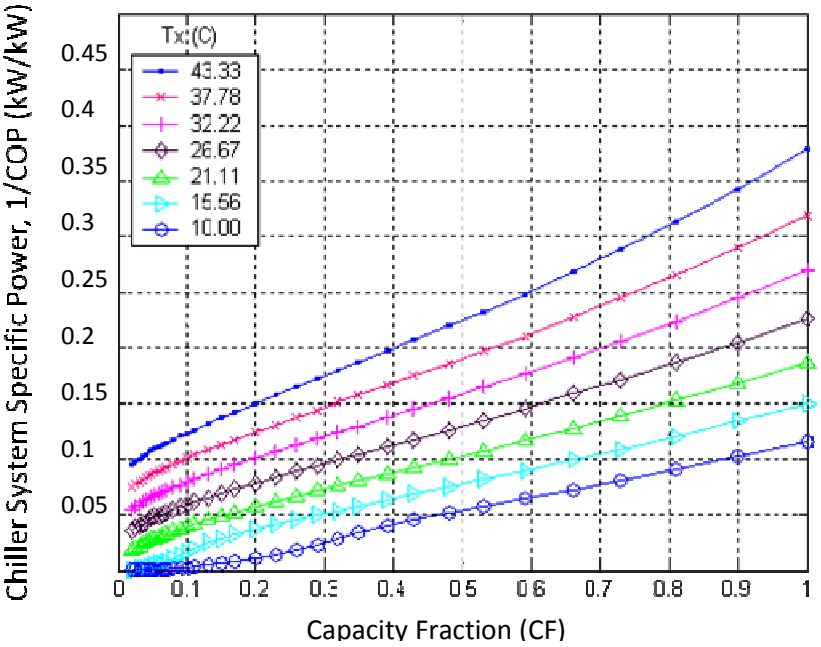

Figure 7 Chiller-radiant subsystem performance map based on first-principles modeling in [Armstrong et al 2009a]

One problem with the model in [Armstrong et al 2009a] for concrete-core radiant cooling applications is that the zone air temperature alone, which is used in the chiller model, is not a sufficient surrogate for the evaporating temperature of the chiller serving the concrete-core. In the case of concrete-core radiant floors, the return water temperature from the pipe embedded in the concrete is the variable of interest for determining chiller efficiency and performance. The return water temperature is related to the slab temperature and cooling rate, and the slab temperature is determined by past cooling rates, slab temperatures, and zone air temperatures. As a consequence, a different performance map is required for chiller-radiant concrete-core systems where current return water temperature is a variable instead of current zone air temperature.

In sections 3.2 and 3.3, a performance map of a heat pump will be measured and mapped in which zone air temperature directly influences the system efficiency. In chapter 6, which describes implementation of an LLCS with a concrete-core radiant floor cooling system, these maps will be modified to represent the performance of an air-cooled chiller in which return water temperature will replace zone air temperature as the evaporator fluid entering temperature of interest.

3.2 Experimental assessment of low-lift heat pump performance

This section will describe the development, instrumentation, and resulting measurements from a heat pump test stand designed to measure the performance of a compressor and heat pump system over a wide range of pressure ratios, condensing temperatures, evaporating temperatures, and loads. The goal of this work was twofold: to create data from which to develop improved models of variable capacity compressors, heat exchangers including pressure drops, and variable speed condenser and evaporator fan interactions; and to create a performance map of the heat pump useful for predicting optimal pre-cooling of concrete-core radiant floor as a function of outdoor temperature, evaporating temperature, compressor speed, and condenser fan speed in the LLCS experimental test chamber described in chapter 6.

The test stand was created using a Mitsubishi MUZ-A09NA-1 outdoor unit heat pump and a MSZ-A09NA indoor unit evaporator. These systems have a rotary piston compressor with an accumulator, a finned-tube single-row condenser heat exchanger with a variable speed condenser fan, a finned-tube double-row evaporator heat exchanger with a variable speed evaporator fan, and an electronic expansion valve. The working refrigerant is R410A. A schematic of the system is shown Figure 8. Only operation as an air conditioner, i.e. no including heating mode, was tested. Images of the system are shown in Figures 9, 10, 11, and 12.

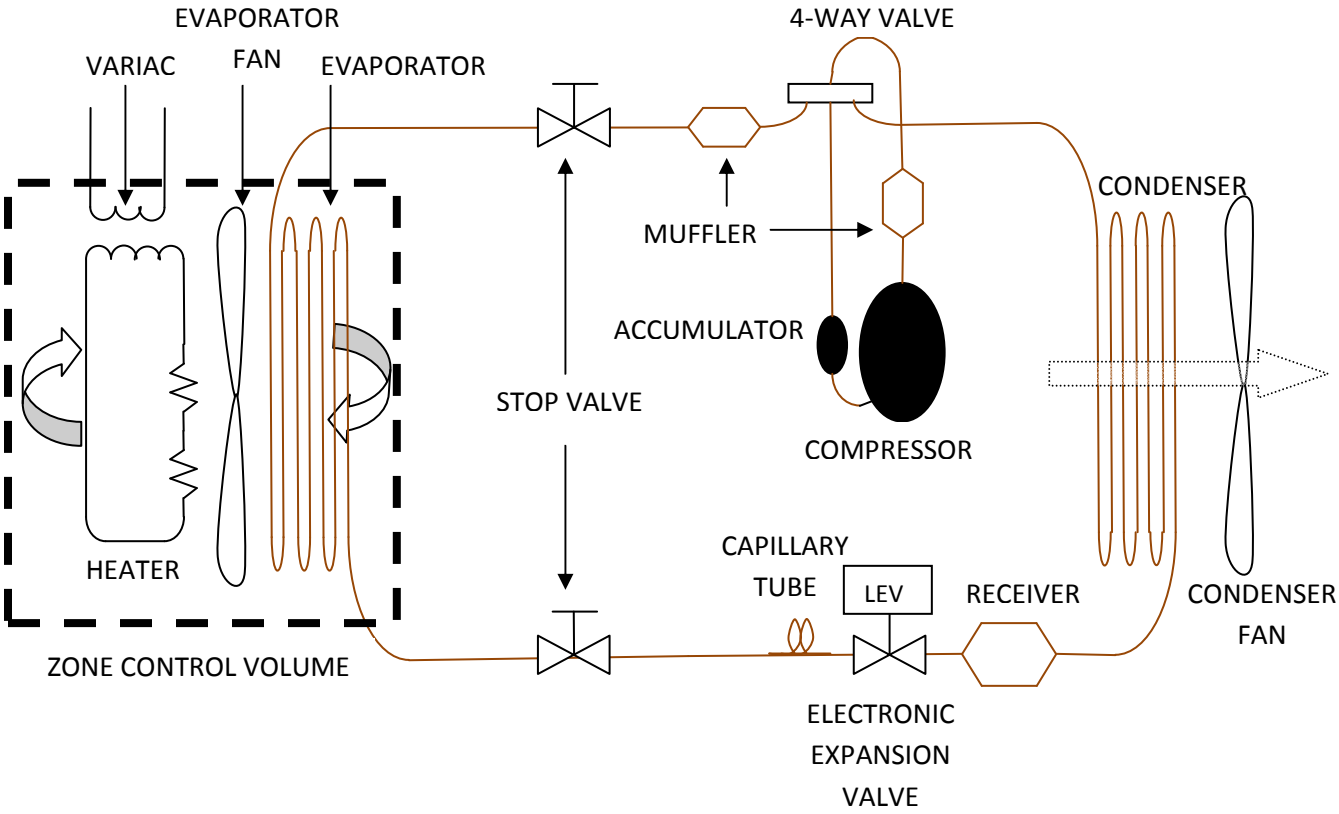

Figure 8 Heat pump experimental test stand equipment component schematic

Figure 9 Anemometer traverse for flow measurement

Figure 10 Zone control volume

Figure 11 Heat pump experimental test stand

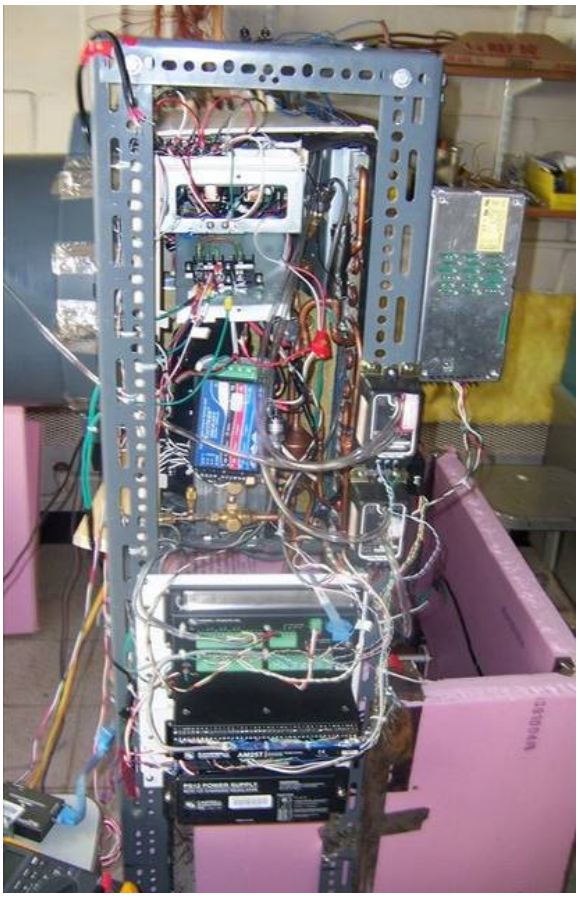

Figure 12 Data acquisition system and sensors

The evaporator was contained in a sealed control volume made of extruded polystyrene foam insulation, as shown in Figure 10. This will be called the zone control volume, because it represents are thermal zone being conditioned by the indoor unit. Air inside this zone control volume was recirculated through the evaporator by the evaporator fan, through a pair of electrical heaters serving as a thermal load, then back to the evaporator inlet. The test stand can be thought of as a secondary fluid calorimeter [ASHRAE 2005] with air as the secondary fluid.

Sensors were installed on the system to measure refrigerant temperatures and pressures, air temperatures, air temperature differences across the heat exchangers, electrical heater power providing load on the evaporator, fan power to the evaporator fan, total power to the Mitsubishi outdoor unit, DC power to the condenser fan and compressor inverters, and three phase power delivered to the condenser fan and compressor. The locations of these sensors in the system are shown in Figure 14. The details of the sensor make and models, accuracies, measurement methods and installation practices are explained in Appendix A.1.

The total thermal conductance across the zone control volume was measured to account for heat gains into the insulated enclosure which add to the cooling load on the evaporator. To do this, the temperature difference between ambient conditions (which are also condenser air conditions) and the inside of the box was measured by thermocouples installed inside and outside of the insulated zone control volume. The total power to the box heaters and fans inside of the zone control volume was also measured. A constant power was delivered to the heaters and fans inside the control volume and after a day of heating a steady state temperature difference was observed, from which the total thermal conductance could be calculated calculated in Watts per Kelvin. The conductance of the box was approximately 1.9 Watts per Kelvin.

The volumetric airflow rate through the condenser was measured using a thermal anemometer by traversing the condenser outlet air stream. Samples of air velocity were taken at 10 points along six radii as shown in Appendix A.1, following the methods for flow measurement outlined in ASHRAE Handbook Fundamentals, Chapter 14 [ASHRAE 2005]. Correlations between fan speed, airflow rate and fan power consumption were developed to avoid prohibitively time-intensive airflow rate measurements at every steady state condition. These correlations are shown in Figures 15 and 16. The ambient air pressure during each test was recorded from weather station KMACAMBR9.

Steady state performance data were collected at 131 chiller operating states spanning pressure ratios from 1.2 to 4.8, including combinations of the following conditions: condenser air inlet temperatures of 15, 22.5, 30, 37.5, and 45 Celsius; evaporator air inlet temperatures of 14, 24, and 34 Celsius, compressor speeds of 19, 30, 60, and 95 Hz, and fan speeds of 300, 450, 600, 750, 900, 1050, and 1200 RPM. The evaporator fan speed was fixed at the maximum speed because the goal of the testing was to characterize the performance of the outdoor unit for conversion to a chiller, for which only the evaporating temperature is important. Furthermore,

adding a new dimension to the test space would have greatly increased the time required for testing. At some combinations of desired test conditions, the closest achievable steady state conditions were tested. For example, if running the compressor at 95 Hz at a condenser air inlet temperature of 45 Celsius caused an overheated discharge temperature, the fastest possible compressor speed was tested instead at that condenser air temperature. A complete table of the data collected at all steady state operating conditions is available in Appendix A.2.

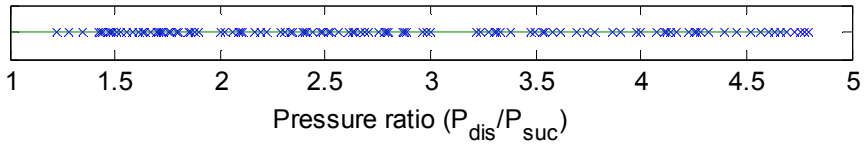

Figure 13 Range of pressure ratios spanned by 131 test conditions

The data from the experimental test stand demonstrate the potential for low-lift cooling strategies to dramatically improve the average annual electric input ratio (EIR) and COP of the air conditioner and compressor by operating at low pressure ratios. Figure 17 shows the EIR in terms of kW of electricity consumed per kW of cooling provided at the evaporator on the left, and its reciprocal, the COP, on the right. It shows both the compressor COP and the "outdoor unit" COP. The compressor COP includes three phase power consumption of the compressor alone, while the outdoor unit COP includes the power consumption due to electronics, the condenser fan inverter and condenser fan, and the compressor inverter and compressor which are all part of the outdoor unit. Evaluation of these quantities from the measured data listed in

Table 3 proceeds as follows:

Compressor kWe/kWth = Three phase power consumption / Evaporator cooling rate

(1) $$EIR_{3\phi,CMP} = 1/COP_{3\phi,CMP} = (kW_e / kW_{th}) = W_{3\phi,CMP} / \left(W_{box} + UA_{box}(T_{ambient} - T_{zone})\right)$$

Outdoor unit EIR kWe/kWth = Total outdoor unit power consumpion / Evaporator cooling rate

(2) $$EIR_{unit} = 1/COP_{unit} = W_{unit} / \left(W_{box} + UA_{box}(T_{ambient} - T_{zone})\right)$$

This view of the data shows how efficient the air conditioner and compressor can be at low pressure ratios. While data at typical pressure ratios lie within a typical COP range of three to four, at low pressure ratios, or low-lift, the outdoor unit COP increases significantly to four to ten and above while still providing significant cooling, between one and two kW. The compressor COP increases dramatically to as much as 10 to 20 kW of cooling delivered per kW of compressor power.

3. Low lift chiller mapping and modeling

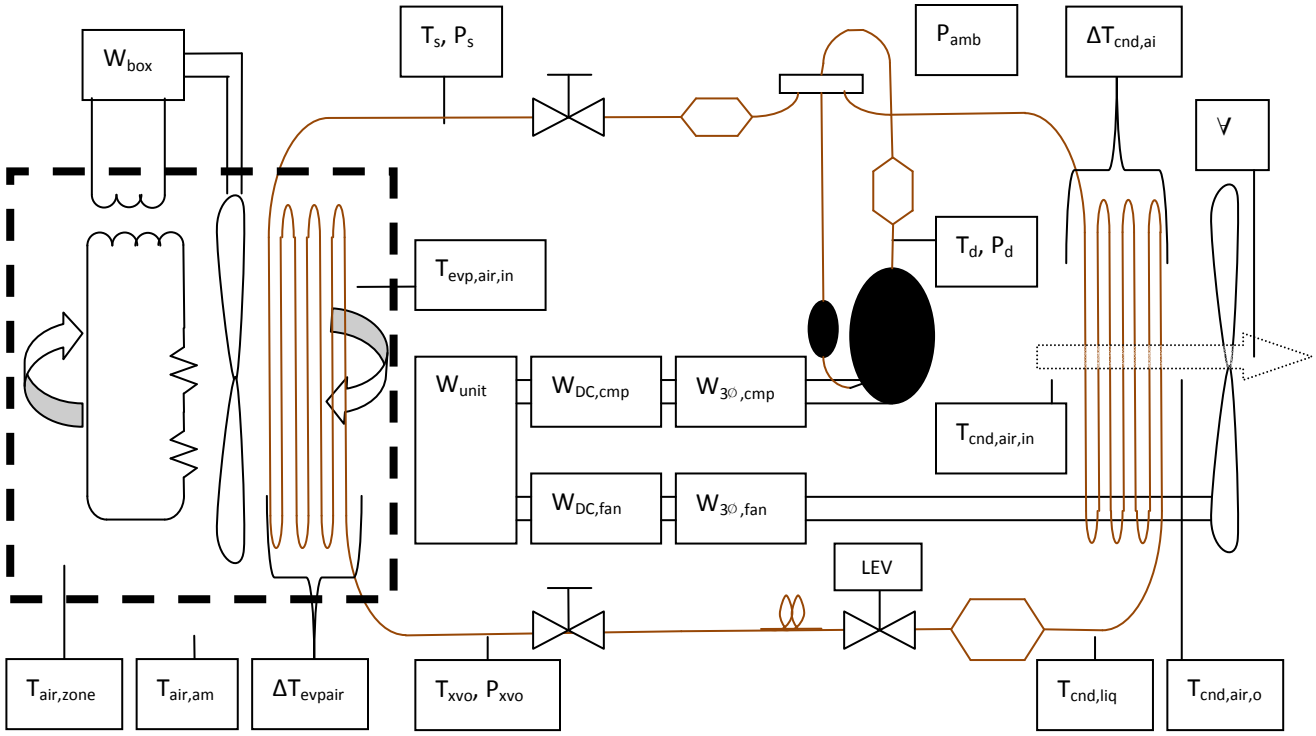

Figure 14 Heat pump experimental test stand sensor schematic

Table 3 Heat pump experimental test stand sensor descriptions

Label	Sensor description
T_s	Suction refrigerant temperature
T_d	Discharge refrigerant temperature
$T_{cnd,liq}$	Condenser outlet liquid refrigerant temperature
T_{xvo}	Expansion valve outlet refrigerant temperature
$T_{air,zone}$	Evaporator zone air temperature
$T_{evp,air,in}$	Evaporator inlet air temperature
$T_{air,am}$	Ambient air temperature
$\Delta T_{evp,air}$	Evaporator air temperature difference
$T_{cnd,air,in}$	Condenser inlet air temperature
$T_{cnd,air,out}$	Condenser outlet air temperature
$\Delta T_{cnd,air}$	Condenser air temperature difference
P_s	Suction refrigerant pressure
P_d	Discharge refrigerant pressure
P_{xvo}	Expansion valve outlet
P_{amb}	Ambient air pressure measured at local weather station
∀	Volumetric condenser air flowrate
W_{box}	Total power to the zone control volume, including fan and heaters
W_{unit}	Total power to the outdoor unit, including inverters, fan and compressor
$W_{DC,fan}$	DC power to the condenser fan inverter
$W_{DC,cmp}$	DC power to the compressor inverter
$W_{3\emptyset,fan}$	Three phase power from the inverter to the condenser fan
$W_{3\emptyset,cmp}$	Three power from the inverter to the compressor

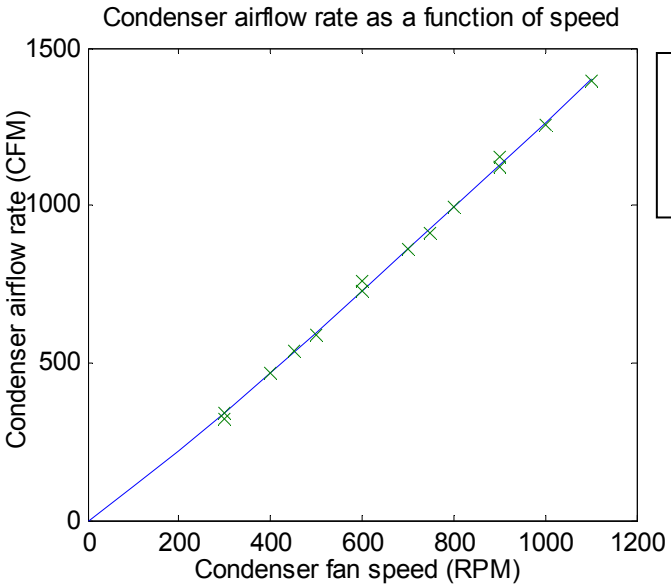

$CFM = a*RPM^b$

a = 1.328	t_a-statistic = 2.1
b = 15.5	t_b-statistic = 15.5
R-square = 0.998	

Figure 15 Condenser air flowrate as a function of fan speed

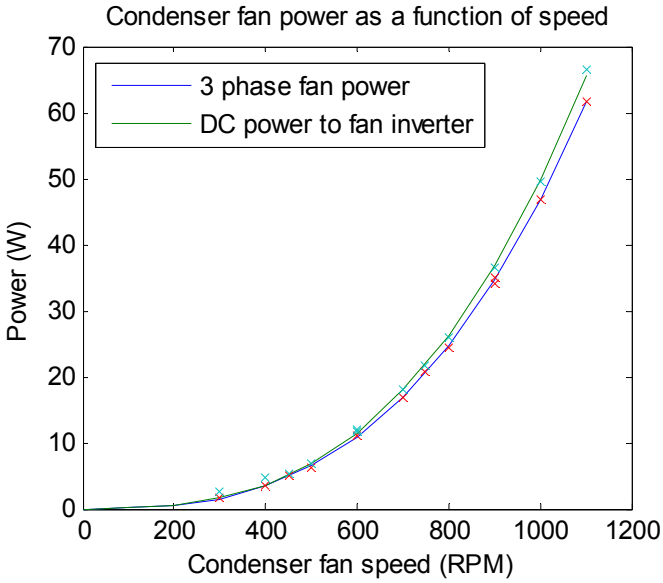

$Power\ (3\text{-}phase) = a*RPM^b$

$a = 1.153*10^{-7}$	t_a-statistic = 2
b = 2.87	t_b-statistic = 41
R-squared = 0.999	

$Power\ (DC) = a*RPM^b$

$a = 1.195*10^{-7}$	t_a-statistic = 0.9
b = 2.874	t_b-statistic = 17.9
R-squared = 0.999	

Figure 16 Condenser fan power consumption as a function of fan speed

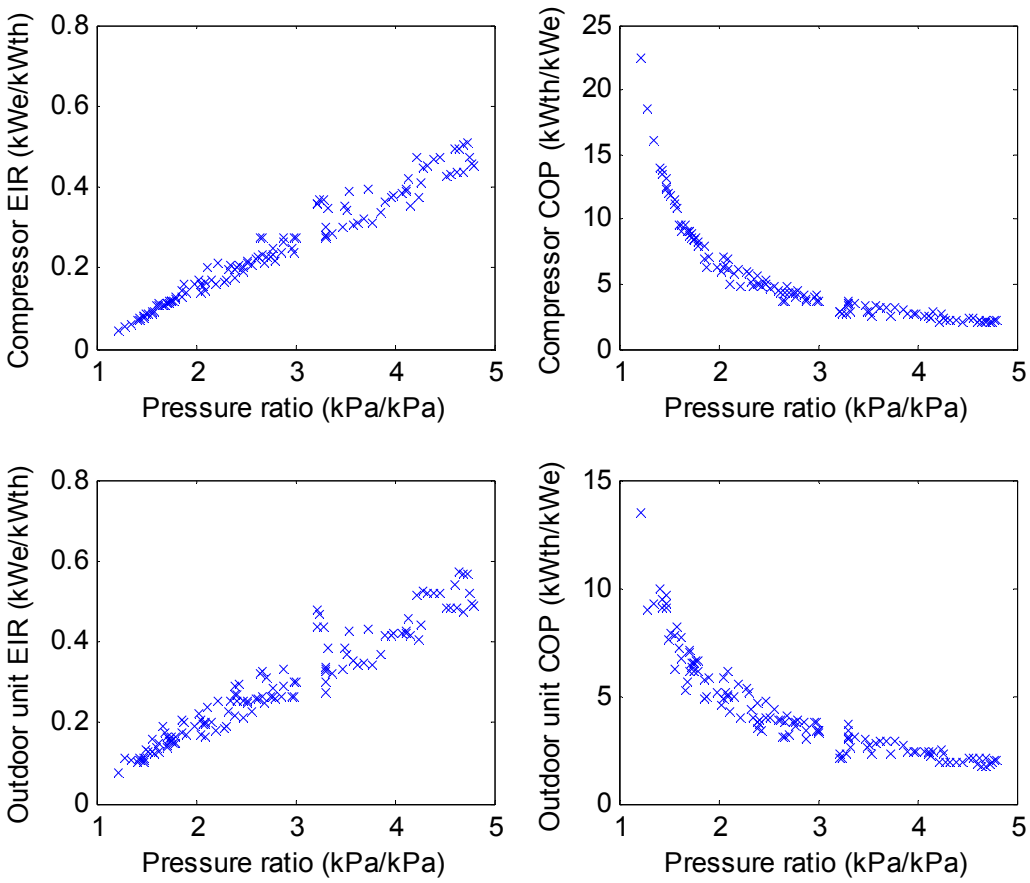

Figure 17 Compressor and outdoor unit (including condenser fan and electronics) electric input ratio, kW electricity consumed per kW cooling delivered, and coefficient of performance COP, kW cooling delivered per kW of electricity consumed as a function of pressure ratio

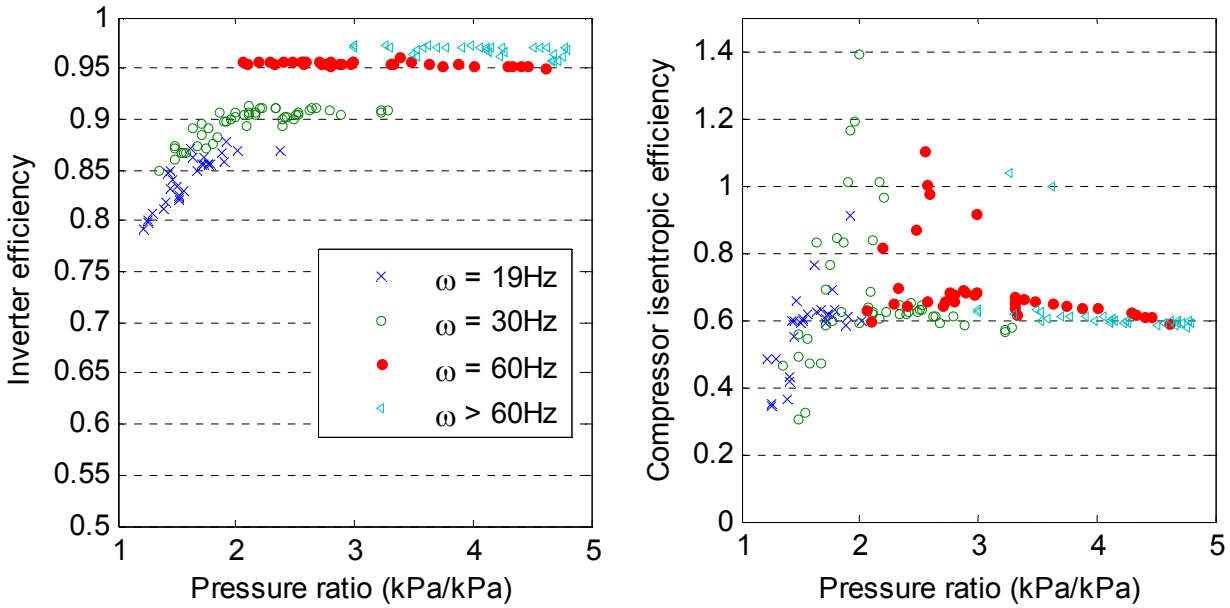

Figure 18 Efficiency of the inverter supplying the compressor and the compressor isentropic efficiency

These gains are somewhat offset in the outdoor unit COP by increased inverter losses at low speeds and increased fan power consumption. The inverter typically has efficiencies in the 90 to 95 percent region, but drops off to 80 to 90 percent at low speeds and low pressure ratio, as shown in Figure 18. The inverter efficiency has a strong dependence on compressor speed, as shown by the groups of markers in Figure 18. The isentropic efficiency of the compressor is relatively constant at 0.6, but may increase slightly at lower pressure ratios. Errors in temperature and pressure measurement cause errors in the calculation of suction entropy at low pressure ratios, resulting in poor estimates of isentropic efficiency from measurements.

Energy and mass balances were performed in order to verify the accuracy of the measurements performed at each steady state condition. The calculations include all of the measurements shown in Figure 14 except for W_{unit}, $W_{DC,fan}$ and $W_{DC,cmp}$. In a simple heat pump with zero piping and compressor jacket losses, the heat rejected at the condenser will equal the total heat absorbed at the evaporator plus the total work performed by the compressor on the refrigerant, or electrical power delivered to the compressor. The test stand includes measurements of condenser air volumetric flow, condenser air temperature difference, and condenser air pressure, from which to evaluate its specific heat and density. It also includes measurements of the three phase power delivered to the compressor and the cooling load on the evaporator. The cooling load on the evaporator includes both the electrical heater and evaporator fan power and the heat transfer into the zone control volume from the surrounding ambient conditions. With the foregoing measurements a conservation of energy check can be applied to the three important heat and work transfers:

(3) Condenser heat load $$Q_{condenser} = \rho(P_{amb}, T_{cnd,air}) c_p(P_{amb}, T_{cnd,air}) \dot{\forall} \Delta T_{cnd,air}$$

(4) Evaporator heat load $$Q_{evaporator} = W_{box} + UA_{box}(T_{amb} - T_{zone})$$

(5) Compressor power $$W_{3\phi,cmp}$$

In the equations above, $\rho(P_{amb}, T_{cnd,air})$ and $c_p(P_{amb}, T_{cnd,air})$ are the pressure and temperature dependent ambient air density and specific heat.

The energy balance shown in Figure 19 shows good agreement between the condenser heat load and the evaporator heat load plus compressor power. The relative root mean square error (RMSE) across all measurements was 4.6 percent; the relatively higher errors are present particularly at low loads. The three phase power delivered to the compressor was used rather than total unit power or DC compressor power because the heat dissipated by the electronics, the inverters and the condenser fan does not interact with the vapor compression cycle. The compressor and piping, apart from heat exchanger surfaces, were well insulated to minimize unmeasured heat transfers to or from the system.

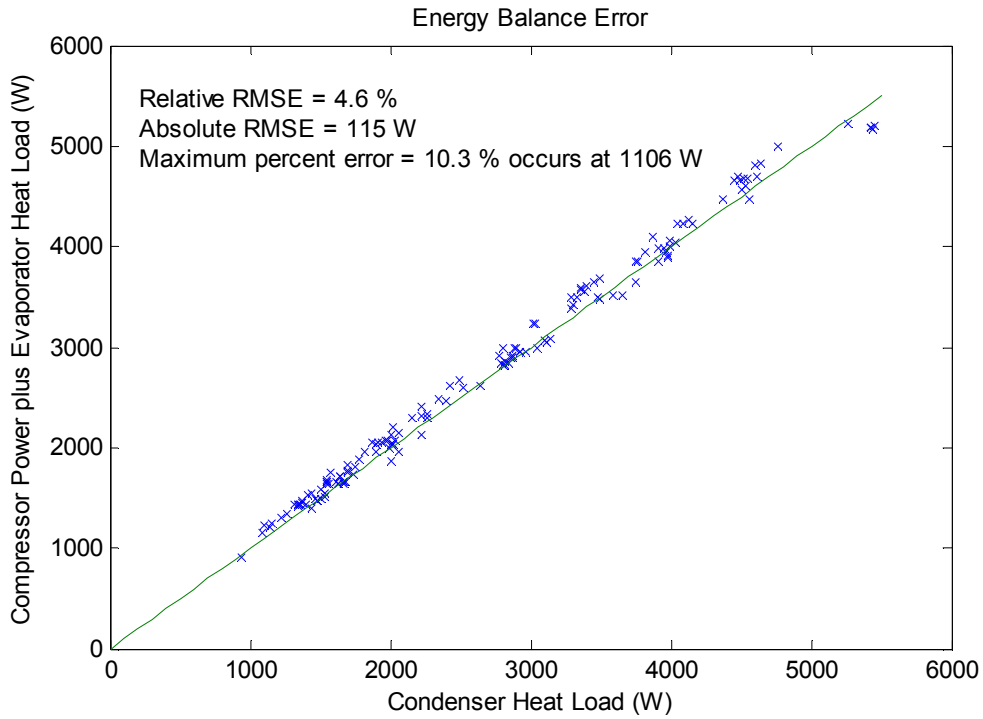

Figure 19 Steady-state energy balance validation

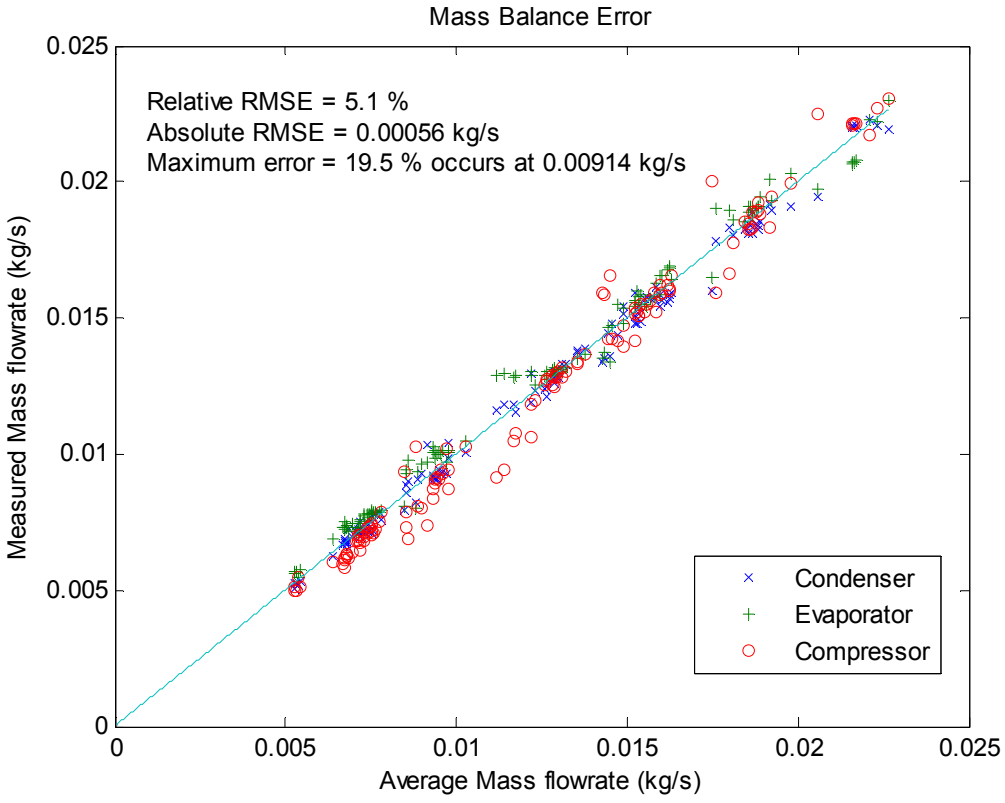

Figure 20 Steady-state mass flow rate discrepancies expressed as deviations of each of the three inferred mass flow rates from their average at each test condition

A mass balance was performed to validate the pressure and temperature measurements within the vapor compression cycle. The system is a single closed loop system and hence refrigerant mass flow rates must be the same through each component. Refrigerant mass flowrates through the compressor, condenser, and evaporator were calculated from measurements using the following equations:

(6) Compressor mass flowrate $\dot{m}_{cmp} = W_{3\phi,cmp} / \left(h(P_d, T_d) - h(P_s, T_s)\right)$

(7) Condenser mass flowrate $\dot{m}_{cond} = Q_{cond} / \left(h(P_d, T_d) - h(P_d, T_{cnd,liq})\right)$

(8) Evaporator mass flowrate $\dot{m}_{evap} = Q_{evap} / \left(h(P_s, T_s) - h(P_d, T_{cnd,liq})\right)$

In the equations above, h is the pressure and temperature dependent refrigerant enthalpy for a given condition, subscript d refers to discharge conditions, subscript s refers to suction conditions, and subscript "cnd,liq" refer to conditions of the liquid refrigerant exiting the condenser, evaluated by REFPROP [NIST 2009] for R410a.

Two assumptions are implicit in the mass flow rate calculations. First, it is assumed that the discharge pressure is sufficient to calculate the enthalpy of the condensed liquid refrigerant exiting the condenser as an incompressible fluid. This is reasonable because in liquid state the refrigerant enthalpy is nearly independent of pressure. Second, it is assumed the process of expansion through the electronic expansion valve is isenthalpic (adiabatic), and thus the enthalpy of the liquid refrigerant exiting the condenser is the same as the enthalpy of the two phase refrigerant entering the evaporator.

A comparison of these three calculated mass flow rates to the mean flowrate is shown in Figure 20. The relative RMSE for the mass flow rates was 5.1 percent with large errors at some low mass flowrate conditions. The compressor mass flowrate estimate was in error by as much as 19.5 percent at certain conditions. This may be a result of heat losses or mechanical inefficiencies in the compressor which would distort the measurements of discharge enthalpy, which is used to calculate mass flow rate. Another complication is the oil mass fraction and circulation rate. The oil mass fraction is difficult to measure and was not measured on the test stand. As a result, the enthalpies calculated from pressure and temperature measurements, which assume the fluid is refrigerant R410A, may be in error due to the presence of oil mixed with the refrigerant [Willingham 2009]. Equations (6-8) assume that the oil mass fraction is small enough that the change in refrigerant enthalpy completely dominates.

Overall, the test stand data show reasonable agreement in energy balance and mass flowrates. These data have been used by [Zakula 2010] to develop improved physics-based heat pump component models for simulating low-lift compressor and chiller performance. The data will also be used in future work at the Masdar Institute of Science and Technology (MIST) and at MIT. It has been shared with researchers at the Mitsubishi Electric Research Laboratory and the Pacific Northwest National Laboratory. The data are available in Appendix A.2 along with the mass and energy balance accuracies for each test condition.

3.3 Empirical modeling of low lift heat pump performance

The experimental data described in section 3.2 can be used to develop models of heat pump performance for integration into a predictive TES pre-cooling control algorithm. A multi-variable function or a look up table is needed which provides system cooling capacity, power consumption and/or EIR as a function of outdoor temperature, indoor temperature (or, in the case of a chiller, return or supply water temperature), compressor speed and condenser fan speed. Such models can be used to select compressor and condenser fan speeds over a 24 hour period that will meet the zone cooling load and maintain thermal comfort while minimizing energy consumption or, equivalently, maximizing average daily efficiency. This section explains the development of an empirical curve-fit model for an air conditioner with a variable speed compressor and variable speed condenser fan based on the data presented in 3.2. In chapter 6, the curve-fit model will be adapted to represent an air-cooled chiller used in an experimental LLCS installation.

There is a vast array of research on modeling of air conditioners, chillers, heat pumps and their components. [Jin 2002] provides an extensive review of the literature on heat pump and chiller modeling. [Armstrong et al 2009a] provides a model for chiller components suitable for simulating LLCS. The goal of this section is not to provide an extensive review of chiller, heat pump, compressor, condenser, or evaporator modeling methods but rather to present multi-variable curve-fit models suitable for integration in a predictive pre-cooling control algorithm. These curve-fits may ultimately be created from experimental data or from physics-based models of equipment. Physics-based models have the advantage that extrapolations of performance into untested regions of operation may be more accurate than models based on experimental data. However, for purposes of this research a curve-fit model based on extensive experimental data was deemed acceptable for optimizing compressor speed and condenser fan speed.

A number of research precedents are available for curve-fit models of heat pumps and chillers. Among energy simulation tools, it is common to represent heat pump or chiller performance as a multi-variable polynomial with the following variables: entering condenser fluid temperature; entering or exiting evaporator fluid temperature; and part load ratio (PLR), which is cooling rate over maximum steady state capacity. EnergyPlus contains a number of chiller models with forms similar to the following:

(9) $$EIR = EIR_{ref} \times f(T_{chw}, T_{cnd}) \times f(PLR) \times f(cycling)$$

In equation (9), EIR_{ref} is a reference EIR, $f(T_{chw}, T_{cndw})$ is a bi-quadratic polynomial with chilled water supply or return temperature and condenser fluid entering temperature as variables, f(PLR) is a quadratic in part load ratio, and f(cycling) is an additional term to account for performance penalties associated with on-off cycling of equipment [EnergyPlus 2009].

With the increasing prevalence of chillers and heat pumps using variable speed compressors, variable speed condenser fans and/or pumps, and variable speed evaporator fans or pumps

researchers have begun to adapt multi-variable curve-fit models to equipment with variable speed components. [Shao et al 2004] presented a curve-fit model of a variable speed compressor which used a typical bi-quadratic in evaporator and condensing temperature, such as those used in EnergyPlus, but multiplied by a single-variable quadratic in compressor speed with a correction for actual suction temperature. Application of this model to three compressors showed the ability to predict compressor power, mass flowrate, and COP to within 4 percent or less average relative error for all three compressors.

Chiller performance maps are generally smooth surfaces in multi-dimensional space for which multi-variable polynomial models may be appropriate. A generic four-variable cubic polynomial was elected for modeling the EIR, power consumption, and cooling capacity of the heat pump outdoor unit. One must be careful extrapolating polynomial models derived from experimental data outside the range of measured data. The data presented in section 3.2 spans a wide range of condenser air inlet temperatures, evaporator air inlet temperatures, and compressor speeds but a more limited set of fan speeds. This is the result of a deliberate choice to limit the number of test points due to time constraints. Combinations of 3 zone air temperature, 5 condenser air temperatures, 4 compressor speeds, and 7 condenser fan speeds would require 420 tests, each of which took at least an hour and at most 4 hours to achieve steady state. Instead, a limited set of operating points was selected to span the condenser fan speed variable at a subset of compressor speeds, outdoor air temperatures and zone air temperatures and at high, medium and low pressure ratios.

An assumption about the polynomial form had to be made to account for the limited number of condenser fan speed measurements. Even though test data were taken at condenser fan speeds that spanned the full range of fan speed, and at the extremes and mid-points for pressure ratios and compressor speeds of interest, the data was insufficient to identify the dependence of power, cooling capacity, and EIR at all the pressure ratios, compressor speeds, outdoor air temperatures, and indoor air temperatures of interest. This, in part, is because the power, cooling capacity, and EIR depends weakly on condenser fan speed relative to its dependence on compressor speed, outdoor air temperature and indoor air temperature.

A reasonable assumption was made that power, cooling capacity and EIR had a quadratic dependence on condenser fan speed. This behavior was observed for the pressure ratios and compressor speeds at which the condenser fan speed was varied, and a similar behavior was assumed at other pressure ratios and compressor speeds. This quadratic dependence was enforced by eliminating high order cross terms in the fan variable, such as cubic terms in the condenser fan speed variable. The minima of these quadratics can vary with compressor speed, outdoor air temperature and indoor air temperature. The resulting curve-fit models have the following form:

$$DV = \begin{pmatrix} C_1 + C_2 T_z + C_3 T_x + C_4 \omega_{cmp} + \\ C_5 T_z^2 + C_6 T_x^2 + C_7 \omega_{cmp}^2 + C_8 T_z T_x + C_9 T_z \omega_{cmp} + C_{10} T_x \omega_{cmp} + \\ C_{11} T_z^3 + C_{12} T_x^3 + C_{13} \omega_{cmp}^3 + \\ C_{14} T_z^2 T_x + C_{15} T_z^2 \omega_{cmp} + C_{16} T_x^2 T_z + C_{17} T_x^2 \omega_{cmp} + \\ C_{18} \omega_{cmp}^2 T_z + C_{19} \omega_{cmp}^2 T_x + C_{20} T_z T_x \omega_{cmp} + \\ C_{21} f + C_{22} f^2 + C_{23} f T_z + C_{24} f T_x + C_{25} f \omega_{cmp} \end{pmatrix} \tag{10}$$

In equation (10), DV, the dependent variable, can be either the cooling capacity Q, the whole unit power consumption P, or the EIR = 1/COP at a given outdoor air temperature T_x, indoor air temperature T_z, compressor speed ω_{cmp}, and condenser fan speed f. The minima of the EIR across the condenser fan speed variable can be found by taking a partial derivative with respect to the fan speed. The optimal fan speed as a function of outdoor air temperature, indoor air temperature, and compressor speed is given by the solution to the following equation, using the coefficients for the 1/COP curve.

$$C_{21} + 2C_{22} f + C_{23} T_z + C_{24} T_x + C_{25} \omega_{cmp} = 0 \tag{11}$$

The coefficients for each curve are provided in Appendix A.4. The resulting accuracies of this model choice are shown in Figures 21, 22 and 23 over the full range of data tested, which spans a wide range of pressure ratios, outdoor and indoor temperatures as described above.

These graphs show that a multi-variable curve fit model can approximate the measured data well, with relative RMSE of 1.7, 5.5, and 4.7 percent for cooling capacity, power consumption, and EIR respectively. The most inaccurate model is the power consumption model, which has an absolute RMSE of 27 Watts. At low compressor speeds, low pressure ratios, and low power consumption this can lead to inaccuracies as high as 10-15 percent when the unit is consuming close to 200 Watts. Despite this inaccuracy at low power consumption, these curve fit models have been used to develop a predictive pre-cooling control algorithm in chapter 5. It may be possible to derive more accurate curve fit models or look up tables for cooling capacity, power consumption and EIR (or COP) as a function of the independent and controlled variables from physics-based modeling, e.g. [Zakula 2010].

The EIRs predicted from the curve fit models are shown in Figures 24 and 25. Figure 24 shows the EIR of the air conditioner outdoor unit as a function of compressor speed. The three panels correspond to EIR curves at fixed condenser fan speeds of 300, 700 and 1100 RPM. Within each graph are multiple curves representing the EIR at a given combination of indoor and outdoor temperatures, T_z and T_x. For a given condenser fan and compressor speed, and with fixed evaporator fan speed, these are surrogate parameters to the evaporating and condensing temperatures in the vapor compression cycle.

Figure 25 shows the EIR of the outdoor unit as a function of condenser fan speed, rather than compressor speed. The three panels correspond to EIR curves at fixed compressor speeds of 20, 50 and 80 Hz. The same combinations of T_z and T_x are used as in Figure 24.

In chapters 5 and 6 it will be shown how these performance curves can be incorporated into a predictive TES pre-cooling control algorithm to optimize the performance of an air-cooled chiller over a 24 hour cycle. The curves will be adapted to represent the performance of an air-cooled chiller, rather than the split-system air-to-air heat pump presented here, using the refrigerant evaporating temperature to convert between systems.

3. Low lift chiller mapping and modeling

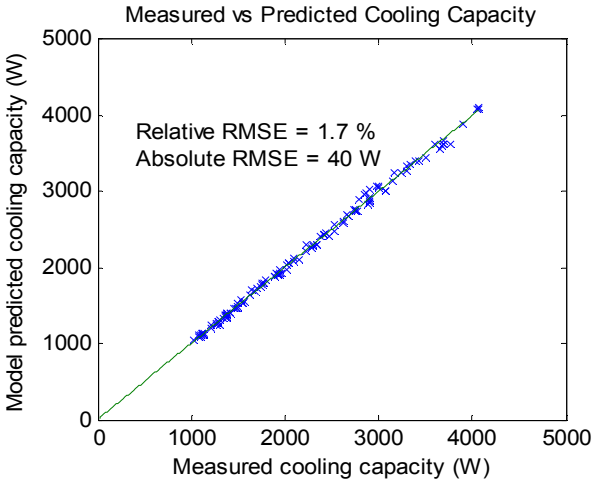

Figure 21 Validation of Curve Fit Cooling Capacity Model

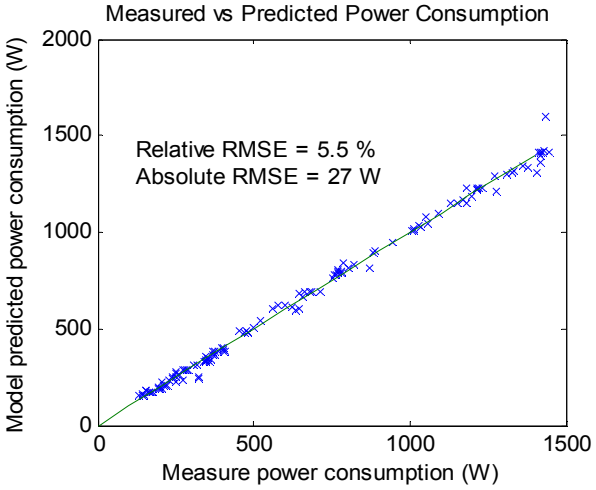

Figure 22 Validation of Curve Fit Power Model

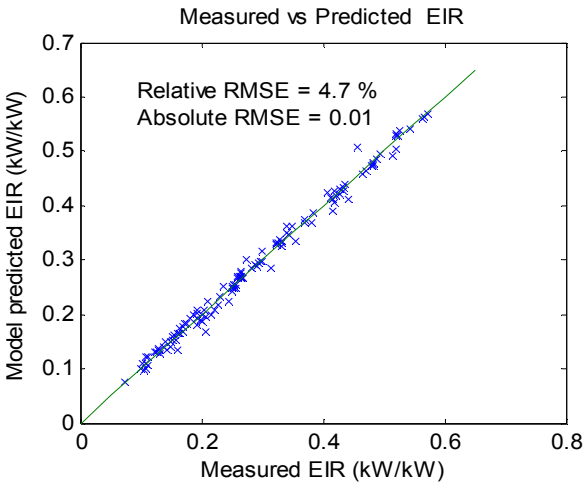

Figure 23 Validation of Curve Fit EIR Model

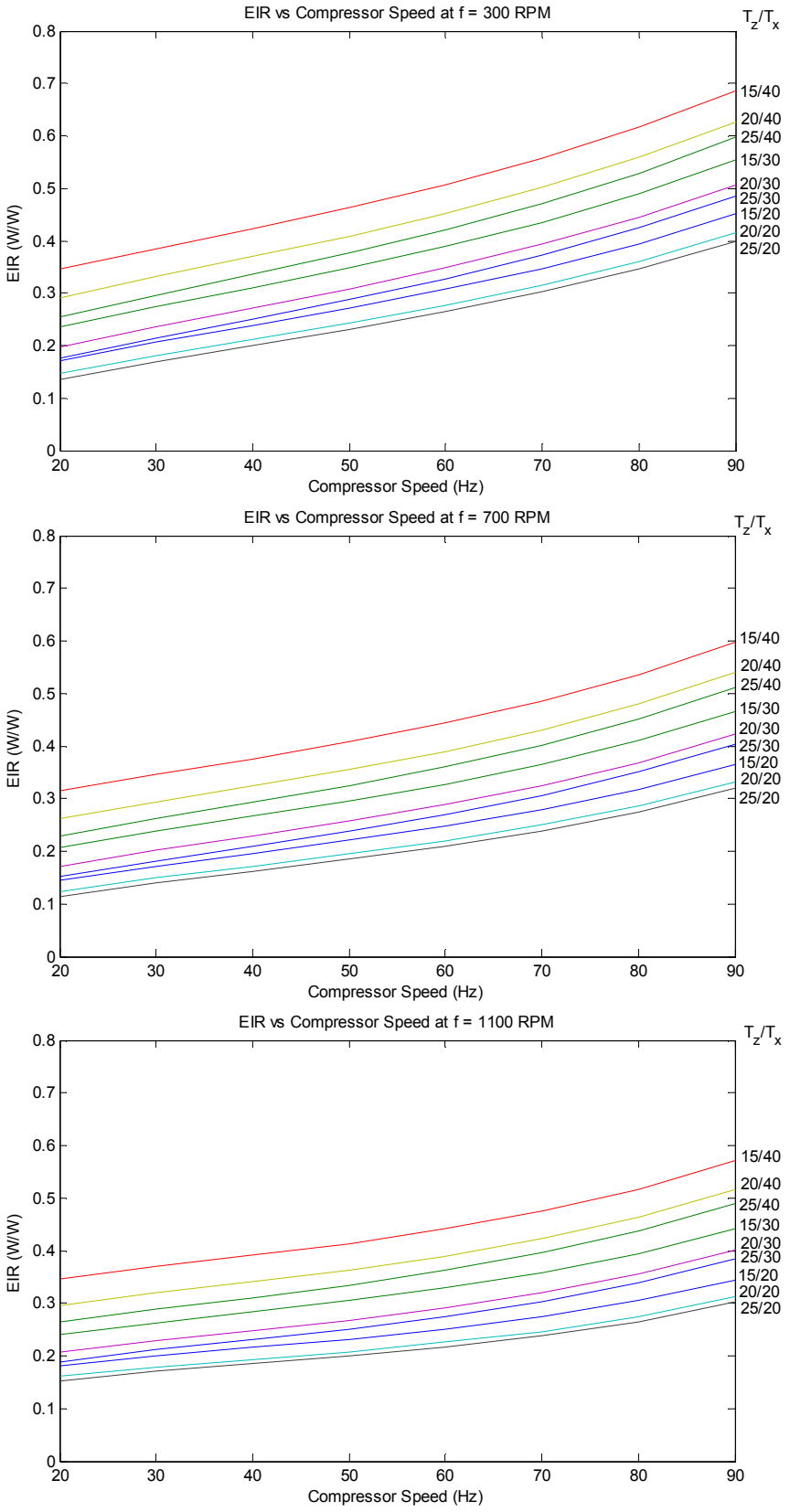

Figure 24 EIR as a function of compressor speed for combinations of Tz = 15, 20 and 25 C and Tx = 20, 30 and 40 C at condenser fan speeds of 300, 700, and 1100 RPM

3. Low lift chiller mapping and modeling

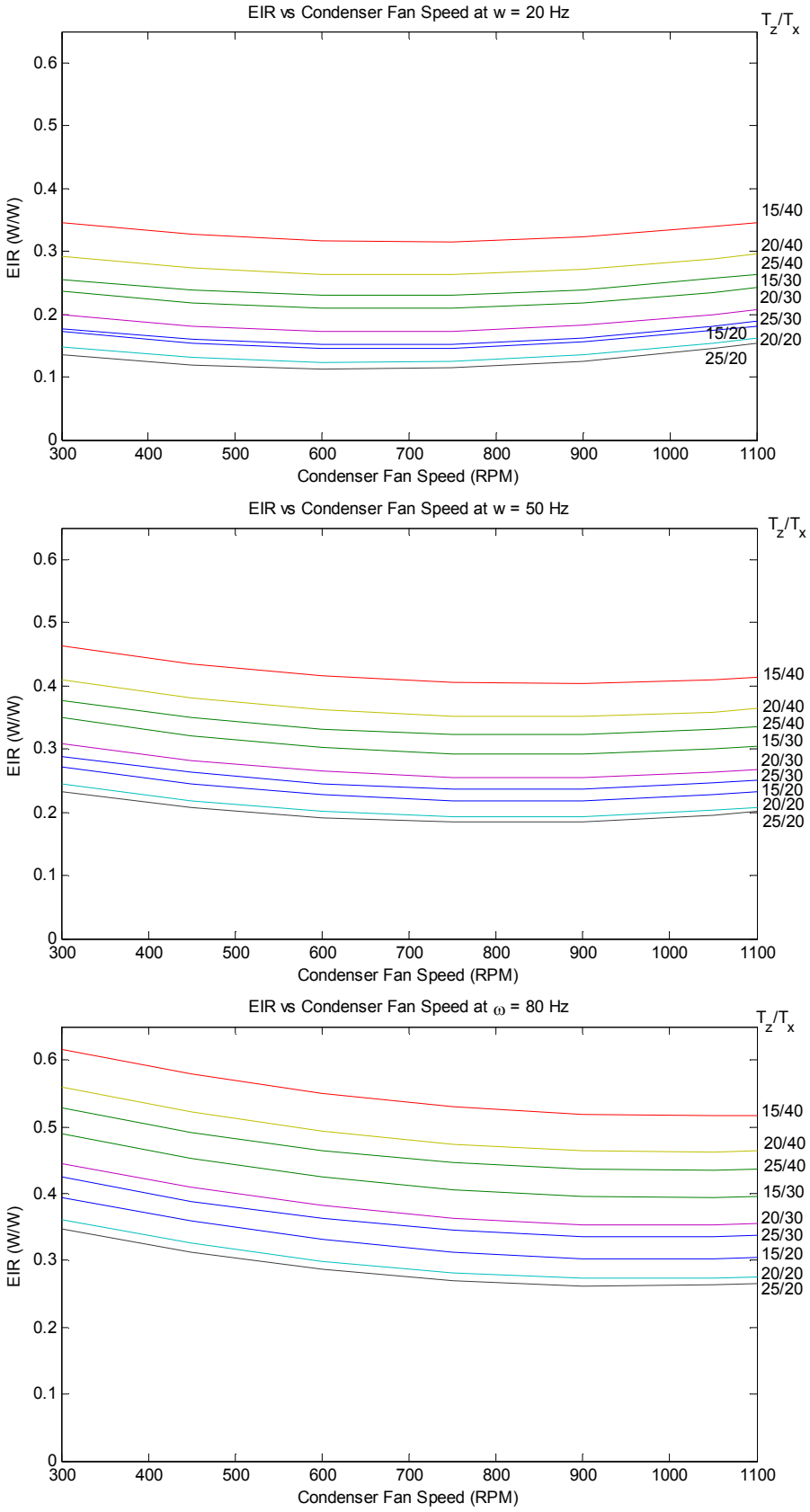

Figure 25 EIR as a function of condenser fan speed for combinations of Tz = 15, 20 and 25 C and Tx = 20, 30 and 40 C at compressor speeds of 20, 50 and 80 Hz

Chapter 4 Thermal model identification

Another important concept enabling predictive pre-cooling control for LLCS is the use of a building thermal response model to predict cooling load. In order to determine the minimal energy consumption required to meet the daily cooling load by pre-cooling TES overnight, advanced knowledge of the next day's cooling load is needed. Thermal response models can predict the thermal loads on a building or zone and predict the temperature response of the zone to those thermal loads and cooling delivered to a space.

Modeling heat transfer, energy use and thermal response in buildings has a solid and diverse foundation, drawing from the fields of physics, heat transfer, mechanical and electrical engineering to model building components and systems. Building energy and thermal modeling takes two forms, "forward" and "inverse" modeling [ASHRAE 2005]. Forward modeling is an approach in which building equipment, building materials, and heat transfer between various parts of a building are modeled using a priori information about the building. The thermal properties of materials, the types and configuration of materials in walls, windows, roofs, floors, and other components, the heat transfer and energy consumption characteristics of mechanical systems, and many other parameters must be known (or assumed) in order to 'forward' model a building. Energy simulation tools such as EnergyPlus, TRNSYS, or eQUEST which employ physics-based forward models of buildings and systems are increasingly being used to estimate energy consumption, thermal comfort performance, lighting performance and operating costs during design and renovation [Crawley et al 2005].

Inverse modeling takes a different approach. Real data from a building can be used to train models, which in turn can make predictions about building performance. For example, monitored building data has been used to train inverse models to predict building energy consumption, temperature response, and thermal loads [Armstrong et al 2006a]. The structure of models can be drawn from standard heat transfer and mechanical engineering formulations to create grey-box models with unknown parameters that have physical significance. Another approach is to create black-box models in which parameters of the model do not have physical significance. In that case, only the accuracy of prediction between a set of input variables and the outputs are important, not the physical properties of the model parameters. System identification and parameter estimation methods are used to identify black and grey box model parameters [Ljung 1999].

For this research, an inverse modeling approach will be employed. Forward modeling a building is a time-consuming process that requires detailed information about building

materials and construction. This information is not always available about the as-built construction of a building. On the other hand, inverse modeling requires only that the important temperatures and loads on a building be measured, or estimated from measurable quantities. For example, internal loads can be estimated from measured building or zone power consumption. Occupancy loads can be estimated from occupancy sensor data or can be correlated to power consumption. Solar loads can be estimated from solar irradiance measurements. These and other temperature and load measurements could be integrated into a BAS, and inverse models could be trained to predict temperature response and cooling loads. The underlying assumption in the choice of inverse models is that they will be easier to create and more accurate than forward models as BAS improve.

A number of authors have proposed inverse building thermal models suitable for identification from building data. This chapter will review building thermal inverse model types and identification methods, describe a thermal test chamber instrumented to test model identification methods, and finally apply a transfer-function-based inverse modeling approach to test chamber data. This inverse model testing was necessary to identify model structures and orders useful for predicting zone temperature response in the LLCS predictive control algorithm described in chapter 5.

4.1 Data-driven building thermal modeling

Buildings are three dimensional, non-homogeneous collections of solids, liquids and gases interacting with numerous electro-mechanical, hydrodynamic, climatic and even biological systems. Modeling the thermal behavior and energy consumption of a building and its interaction with systems in a completely rigorous way requires solution of many coupled differential and non-linear algebraic equations. Such modeling can be prohibitively time-intensive and complicated, and is not amenable to inverse modeling using measured building data, especially in the presence of significant measurement noise.

On the other hand, capturing the important dynamics of buildings relative to thermal comfort and energy performance is possible through simplified models with tractable solutions. Increasing levels of complexity can be added to models to capture certain dynamics, depending on what aspects of building performance the model is intended to predict. Numerous model formulations are possible, such as thermal resistance-capacitance (RC) networks, conduction and comprehensive room transfer functions, radiant time series models, finite difference equations, and admittance factor or frequency domain formulations [Rabl 1988]. These models may predict, for example, zone air temperatures, mean radiant temperatures, or cooling loads. Coupled with a model of an HVAC system's ability to meet a thermal load, HVAC energy consumption can be predicted.

Data-driven models are formulated with unknown parameters that can be "learned" from building data. Parameters of an inverse model are identified from training data using parameter estimation methods [Ljung 1999]. The amount of training data required for parameter estimation in order to make good predictions may depend on the model type and

the variable being predicted. Building temperature response models derived from thermal RC networks may require only a week or two of training data to create a reasonable model [Braun and Chaturvedi 2002]. On the other hand, artificial neural network models of building energy consumption may require months of training data to generate accurate models [Haberl and Thamilseran 1996].

The following sections review prior research on grey-box and black-box models that have been trained to model real buildings. The focus of this review will be transfer function models and state-space thermal RC network models, which were considered for integration into the LLCS control. Black-box methods are also briefly reviewed.

4.1.1 Transfer function models

Building temperature response is governed by the fundamental heat transfer relations for conduction, convection and radiation and the heat diffusion equation. By neglecting second order non-linearities in these relations, transfer function models can be used to represent the heat transfer equations in discrete-time, where the model is made up of coefficient-weighted time-series of physical variables. These discrete-time models can be related to physics-based state-space, thermal RC network, or lumped parameter models by use of a state transition matrix to convert from continuous time to discrete time [Jimenez and Madsen 2008]. A purely statistical view of transfer function models equates them to auto-regressive, moving average with exogenous variables (ARMAX) models, Box-Jenkins models or similar statistical models [Ljung 1999]. However, applying physical constraints to the coefficients of transfer function models can ensure that they are both stable and causal [Armstrong et al 2006a], whereas ARMAX models without constraints, in general, are not.

Transfer function models of building thermal dynamics have a long history of development. Mitalas and Stephenson [1967] and Stephenson and Mitalas [1967] created a framework for calculating room cooling loads and temperature response from heat balance equations using thermal response factors for multi-layered walls. Response factors weight time series data of exogenous outdoor and indoor temperatures and thermal loads to predict cooling loads or indoor temperature. Response factors are discrete-time impulse response functions that represent the transient thermal response of walls and other building components relating temperature and thermal load inputs on either side to indoor air temperature or cooling load outputs. Stephenson and Mitalas [1971] also showed how to use Laplace and z-transform theory to derive multi-layered wall conduction transfer functions (CTF) from a one-dimensional diffusion equation. The CTF of a wall is much more compact and computationally efficient than its response factor representation.

Seem [1987] shows how CTFs for different components of a building, i.e. for each surface, can be combined into one comprehensive room transfer function (CRTF) to represent the overall zone cooling load with one transfer function equation. The CRTF model includes modeling of long-wave radiation exchange between internal surfaces through a star network of linearized radiative heat transfer resistances. CRTFs can be used to predict cooling load for a given zone

air temperature setpoint schedule. Armstrong et al [2009a] describe CRTF models in which cooling load inputs can be used to predict zone air temperature response instead of cooling loads. These inverse CRTFs will be called temperature-CRTFs, because it is zone temperature being predicted. Although temperature-CRTFs and CRTFs are identical in form, the training and testing of these models can be very sensitive to measurement error in the independent variables.

A number of researchers have applied transfer function models to real buildings, identifying transfer function coefficients from monitored building data. Seem and Hancock [1985], Barakat [1987], and Rabl [1988] summarize earlier efforts with transfer function models such as [Forrester and Wepfer 1984, Norford et al 1985, Crawford and Woods 1985, Subbarao 1985]. Recent research has applied transfer function models to advanced control problems, such as mixed-mode ventilation, load shifting and pre-cooling control. Spindler and Norford [2009] apply transfer function modeling to predict control schedules for a mixed mode cooling system with night ventilation. Armstrong et al [2006a] applied temperature-CRTF modeling to a laboratory test zone and Russian apartment buildings, achieving models with a five percent RMSE in temperature response with 10 percent RMSE in cooling rate. Armstrong et al [2006b] describes applications of temperature-CRTF models for load shifting, pre-cooling, optimal start, and model-based control. Temperature-CRTF models of a Los Angeles office building were generated and used to estimate potential energy savings from the control strategies listed above.

4.1.2 Grey box state-space models

State-space models of building temperature response can be created from lumped parameter heat transfer models of building zones and components. Materials and composite constructions such as multi-layer walls can be represented as thermal capacitances and resistances in a thermal RC network. State-space models require specification of a structure for the thermal RC network of a building or zone. High thermal mass walls are better modeled with multiple capacitances in series to account for their distributed heat storage capacity and long time lags in heat transfer across the wall. Lightweight envelope components, such as windows, might be adequately modeled as a thermal resistance only. Thus the configuration of high thermal mass components must be known in advance to create a state-space model with an appropriate model order.

Despite the uncertainty in model order selection, state-space models are perhaps the simplest and arguably the most physically intuitive representation of building temperature response and have been widely applied for inverse modeling building performance. Many previous researchers have applied low-order thermal RC network models to real buildings to predict air temperature response and cooling loads [Sonderegger 1977, Sonderegger 1978, Pryor and Winn 1982, Balcomb 1983a, Norford et al 1985, Wilson et al 1985, Penman 1990, Coley and Penman 1992, Richalet and Neirac 1991, Athienitis 1993, Dewsen et al 1993, Madsen and Holst 1995]. These studies investigate a range of issues including the accuracy of inverse state-space

model predictions, thermal network reduction for modeling complex buildings, and applications of state-space modeling for online identification and control.

Recent research has leveraged better available computing power to test higher order models for predicting building performance and estimating the thermal characteristics of building components. Braun and Chaturvedi [2002] use a state-space model in which they apply three resistance, two capacitance (3R2C) models for *each* surface and for building internal mass to model office building cooling loads. The state space model determines an implicit structure for a transfer function model which is ultimately used for simulation and prediction. The model requires initial guesses of building parameters from known properties, unlike a direct transfer function inverse modeling approach. [Zhou et al 2008] integrates a similar state space model with detailed solar, outdoor temperature and relative humidity models for online prediction.

Jimenez and Madsen [2008] outline modeling methods useful for identifying thermal characteristics of building components through state-space inverse modeling. They include a derivation of transfer function models from discrete time state-space models, and discrete time state space models from continuous time state space models. These derivations demonstrate the relationship between thermal RC network models and transfer function models as different representations of one model. Jimenez and Madsen [2008] also include stochastic terms to accommodate measurement noise. Furthermore, they compare linear and nonlinear models. Jimenez and Madsen [2008] advocate the use of discrete-time state space models for inverse modeling because of the direct physical relationship to building component characteristics. However, they have tested their modeling methods on an experimental test building with little thermal mass. In higher thermal mass structures the assumption of a low-order state space system may cause prediction errors or other problems. In addition, their objective was to identify thermal characteristics of building components, not the temperature response or cooling load of a zone. Jimenez et al [2008] go on to explore the use of Matlab tools, including its system identification toolbox, for the identification of thermal properties associated with building components.

4.1.3 Black-box models

Other approaches to inverse building modeling have employed artificial neural networks (ANNs), black box ARMAX and Box-Jenkins models, Bayesian non-linear regressions, fuzzy-logic methods, and genetic algorithms [Krarti 2003, Haberl and Thamilseran 1998]. Haberl and Thamilseran [1996] deduce that neural networks provide the most accurate approach to predicting energy savings from retrofits. However, multiple months of training data were used to identify neural network models, which is not appropriate for real-time identification and control. A number of papers have been published describing different types of neural networks and their performance for predicting building energy consumption and savings [Kreider et al 1995, Gonzales and Zamerenno 2005, Karatsou et al 2006].

Lundin et al [2004, 2005] describe the use of ANNs for estimating the thermal characteristics of buildings, such as the total heat loss coefficient and heat capacity. Mustafaraj et al [2009] investigate the use of Box-Jenkins, Output Error, and neural network autoregressive (NARX) models to predict the temperature response of an office up to 4 hours ahead using only a few days of training data. They conclude that nonlinear NARX models are more accurate for predicting short-term temperature response than purely linear black-box models. They do not, however, compare their results to grey-box modeling methods.

Ferkl and Siroky [2010] apply black-box ARMAX and subspace state-space identification (4SID) methods to a building with radiant ceiling panels. They identified a model which predicts ceiling surface temperature and ambient air temperature with a 0.2 to 0.3 Celsius standard deviation. They observe that 4SID models were faster and easier to implement and more accurate where there was little noise, however, that ARMAX models are more accurate where measurement noise is significant.

4.1.4 Electing a temperature-CRTF inverse modeling approach

Temperature-CRTF inverse modeling was chosen from the inverse modeling methods reviewed as the most appropriate for integration into LLCS control algorithms. Temperature-CRTFs have the following generic form:

$$T_i(t) = \sum_{n=1}^{N} a_n T_i(t-n) + \sum_{w=1}^{W}\sum_{n=0}^{N} b_{w,n} T_{w,x}(t-n) + \sum_{n=0}^{N} e_n Q(t-n) \quad (12)$$

In equation (12), T_i is the interior zone temperature, $T_{w,x}$ is the temperature on the exterior of surface w, an Q is a thermal load on the zone. The coefficients a_n, $b_{w,n}$, and c_n weight the time series for each term. N refers to the model order, or the number of past terms to include in the time series for each variable.

Temperature-CRTFs have many advantages over other inverse modeling methods. First, inverse model identification is inherently a discrete time problem, because measurements from buildings are sampled at finite intervals, and temperature-CRTFs are easily applied to discrete time series data. Furthermore, temperature-CRTF models do not require assumptions about the configurations of walls and thermal resistances or capacitances within a thermal network. State-space models based on thermal RC networks require assumptions about a model structure that best fit a given building or zone and initial guess about the properties of that structure. For a concrete-core radiant floor, the appropriate number of lumped parameter capacitances to represent the concrete floor is not obvious and depends on its as-built properties. Adjusting the order of a temperature-CRTF model to account for as-built properties is simple, because the number of past terms for each variable in equation (12) can be adjusted to capture an appropriate model order.

Transfer function models are more appropriate than black box ARMAX, Box-Jenkins and related models (although they are similar) because steady state heat transfer constraints ensure that physics is obeyed. Black-box models can be non-causal and unstable, particularly when faced with data outside the range of model training data. ANN and other alternative methods have been rejected because they typically require more training data and are less suitable for predicting short term temperature response than simple temperature-CRTF models.

4.2 Experimental chamber for thermal model testing

An experimental test chamber was instrumented with numerous temperature sensors and measurements of thermal loads in order to test temperature-CRTF model identification methods. The identified temperature-CRTF models will be used for predicting zone temperature response in the predictive pre-cooling control algorithm for an experimental LLCS installation, described in chapter 6. This section will describe the experimental chamber, the instrumentation and measurements in the chamber, and the experiments performed to generate training and validation data for thermal model identification.

The chamber was originally constructed in 1996 for purposes of studying ventilation systems and validating computational fluid dynamics (CFD) models. Yang [1999] and Kobayashi [2001] describe the chamber and its properties. A diagram of the chamber geometry is shown in Figure 26 and the construction layer details are listed in Table 4.

The chamber is made up of two zones, the test chamber and the climate chamber. The test chamber represents an interior office or a generic zone inside a building. The climate chamber is an adjacent enclosed space with climate controlled by a stand-alone constant volume HVAC system. It represents an exterior or outdoor climate zone. The climate chamber conditions may be programmed to represent outdoor weather e.g., to simulate outdoor temperature conditions for a wide range of climates with temperatures as high as 50 Celsius. Climate chamber relative humidity is not currently controlled. A wall containing three double pane windows separates the test chamber from the climate chamber, to act as the “exterior wall” of the test chamber. The remaining five sides of the chamber are heavily insulated (R-30) and border an interior lab maintained typically around 20 to 25 Celsius, i.e. temperatures similar to typical test chamber temperatures to inhibit heat transfer between the test chamber and the lab. The majority of the envelope load therefore is between the test chamber and climate chamber.

The floor of the chamber has been layered with concrete pavers, or blocks, to simulate a concrete slab as shown in Figure 27. Model identification testing was performed with one layer, two layers, and three layers of concrete pavers to exercise the ability of models to simulate different amounts of thermal mass. The pavers are eight by sixteen by one and three quarter inch blocks of concrete weighing typically fifteen to fifteen and a half pounds. A schematic of the concrete paver arrangement and floor layers are shown in Appendix B.1.

Testing and application of temperature-CRTF model identification was performed in two phases. First, model identification methods were tested by exciting the chamber with different types of heat input separately. For these tests, four different thermal inputs were applied:

1) Heat input through electric radiant heating panels on the ceiling
2) Heat input through electric radiant heating underneath the concrete paver layers
3) Heat input through convective electrical heaters inside the test chamber
4) Climate chamber temperature variation with no internal heat input

These four inputs exercised the full range of thermal inputs on the chamber, including internal radiative heating, internal convective heating, thermal input through the concrete floor, and conduction and infiltration from the adjacent climate chamber. The power and total energy consumption of the electric ceiling panel heaters and the convective electrical heaters were measured using F.W. Bell or Wattnode power meters, as described in Appendix B.2. The power to the floor heating grid was direct current measured by a voltage divider and a precision current shunt.

In the second phase, thermal model identification methods were applied to the test chamber after installation of a low-lift radiant concrete floor cooling system. For these tests, a Warmboard® plywood subfloor topped by a 0.03 inch aluminum finish, to distribute heat, was installed underneath the concrete pavers. The Warmboard has half inch grooves in which PEX pipe was installed as shown in Figure 28. Chilled water was circulated through the PEX pipe to cool the concrete layers, providing a radiant cooling effect. The chilled water flow rate and supply and return water temperature differences were measured to calculate total cooling rate into the chamber, using the sensors described Appendix B.2.

The other modes of heat input, such as internal loads and climate temperature variations, were excited simultaneously with the concrete floor cooling. The climate chamber was controlled to simulate typical summer week conditions in Atlanta from typical meteorological year (TMY) weather files. Electric lights in different configurations were used to simulate internal loads. Exposed light bulbs simulated normal lighting loads. Light bulbs encased in completely encased in opaque plastic, so that the enclosure heated up and radiated infrared energy, were used to simulate thermal loads from occupants. Equipment loads were simulated using light bulbs encased in opaque plastic but with an opening to allow additional convection, providing a greater mix of convective loads relative to radiative loads. These internal loads are described in Appendix B.1.

For both model testing and application to a concrete-core cooled chamber, multiple temperature measurements were made inside and outside the chamber to characterize its temperature response. The locations of the T-type thermocouples (TCs) used for these measurements are shown in Figure 29. An explanation of the TC labels is included in Table 5. The following types of temperature were measured: air temperatures outside each surface of the test chamber; surface temperatures of each wall's inside surface; air temperatures inside each surface of the test chamber; air temperature measurements along two vertical poles at

the center of the test chamber; and a column of temperatures through the concrete slab. As mentioned previously, electrical energy consumption by the internal loads and electrical heaters and chilled water cooling rates was also measured. The details for the sensors and installation relating to all of these measurements are described in Appendix B.2.

Samples of the data gathered from model identification testing and application to the chamber with concrete floor cooling are shown in Figures 30 and 31. Figure 30 shows typical results from testing model identification methods with separate modes of thermal excitation. The following temperature measurements are shown from Figure 29: uF5 underneath the concrete pavers; xS2, an 'outdoor' air temperature in the climate chamber; sS2, an interior surface temperature; and S2, an interior air temperature. The graphs on the right hand side show the heat input to the chamber for each test, including radiant heating underneath the concrete layers, radiant panel heating from the ceiling, and convective heating inside the chamber. From top to bottom, the graphs show the results for testing the following modes of excitation: climate chamber temperature variation; convective heat input inside the chamber; radiant ceiling heat input inside the chamber; and radiant heating underneath the concrete pavers. In all cases the results shown are for three layers of pavers on the floor of the chamber.

Figure 31 shows typical data gathered from the application of thermal model identification to the chamber with a concrete floor cooling system. The chamber was excited simultaneously with thermal inputs from a radiant concrete floor chilled water loop (underneath the pavers), the internal loads, and climate temperature variations. The top graph shows temperature data, including the operative temperature calculated from room temperature measurements, the climate chamber temperature, the temperature underneath the concrete layers, and the chilled water return temperature. The bottom graph shows the power, and thus heat input, to the internal loads, previously described, and the cooling load delivered by the chilled water loop under the concrete pavers. The cooling rate from the chilled water loop was calculated from measurements of the supply and return water temperature and the water flow rate.

4. Thermal model identification

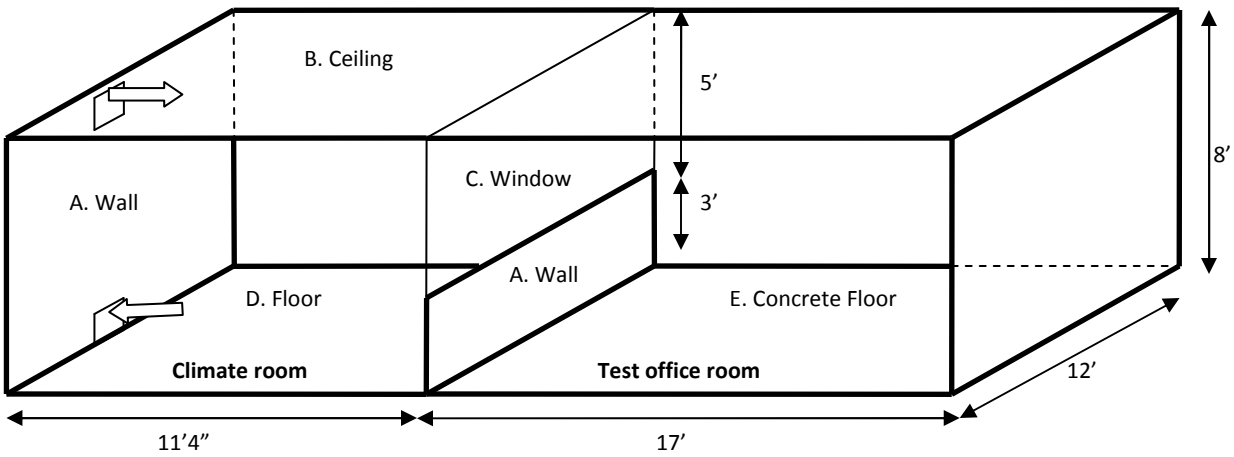

Figure 26 Experimental chamber constructions and dimensions

Table 4 Experimental test chamber construction layers

Surface	Construction layers (inside to outside)
A. Wall	5/8”gypsum board 3-1/2” air gap/2”x4” stud wall 4-1/2” “AC Foam” polyisocyanurate-foam, R-30 5/8” gypsum board
B. Ceiling	5/8”gypsum board 5-1/2” air gap/2”x6” floor joists 4-1/2” “AC Foam” polyisocyanurate-foam insulation, R-30 1/2" plywood
C. Window	1/8”clear glazing 1/2" air gap 1/8” clear glazing Actual construction is 3x 44-1/4” x 46-1/4” double pane windows separated by 3.5” frames.
D. Floor	Vinyl tile floor 1” plywood 3.5” floor joists with 3” “AC Foam” polyisocyanurary foam insulation R-20 Existing concrete floor
E. Concrete floor	1-3/4” concrete pavers (three layer tests only) 1-3/4” concrete pavers (two and three layer tests) 1-3/4” concrete pavers (one, two and three layer tests) 0.03” aluminum (cooling tests only) 1-5/8” plywood subfloor with 1/2" pex 12” on-center (cooling tests only) Vinyl tile floor 1” plywood 3.5” floor joists with 3” “AC Foam” polyisocyanurate foam insulation R-20 Existing concrete floor

Figure 27 Experimental test chamber with convective heater (white box), radiant ceiling panels (wire mesh above), and radiant floor heating (below concrete)

Figure 28 Experimental test chamber with radiant concrete floor loop, before installation of the concrete layers

4. Thermal model identification

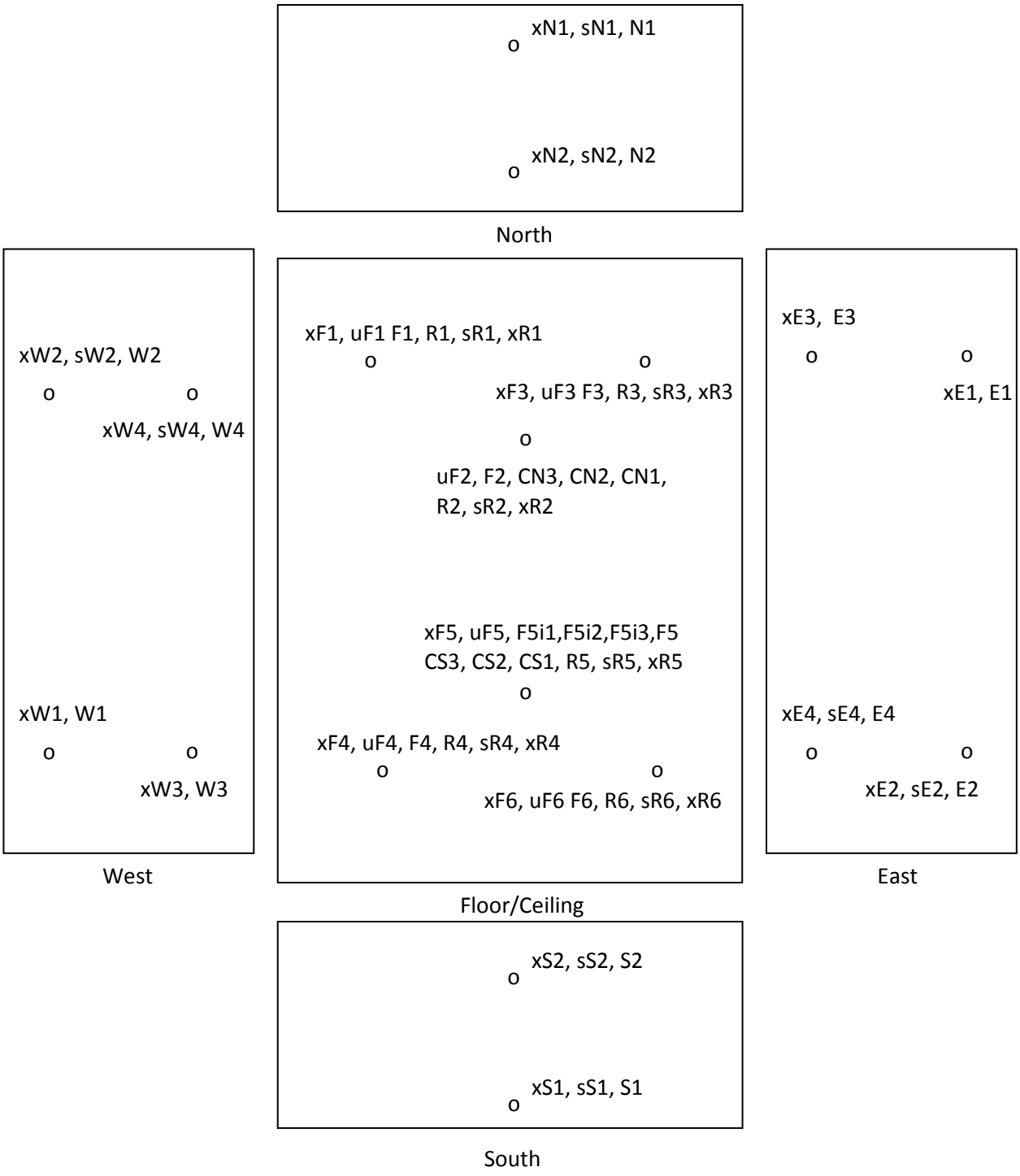

Figure 29 Experimental chamber thermocouple locations (dimensions listed in Appendix B.2)

Table 5 Thermocouple label terminology

TC Label	Description
Wall labels	N-North, S-South, E-East, W-West, R-Ceiling/roof, F-Floor, CS-Center South, CN – Center North
Modifier	x-exterior, s-surface, u-under slab

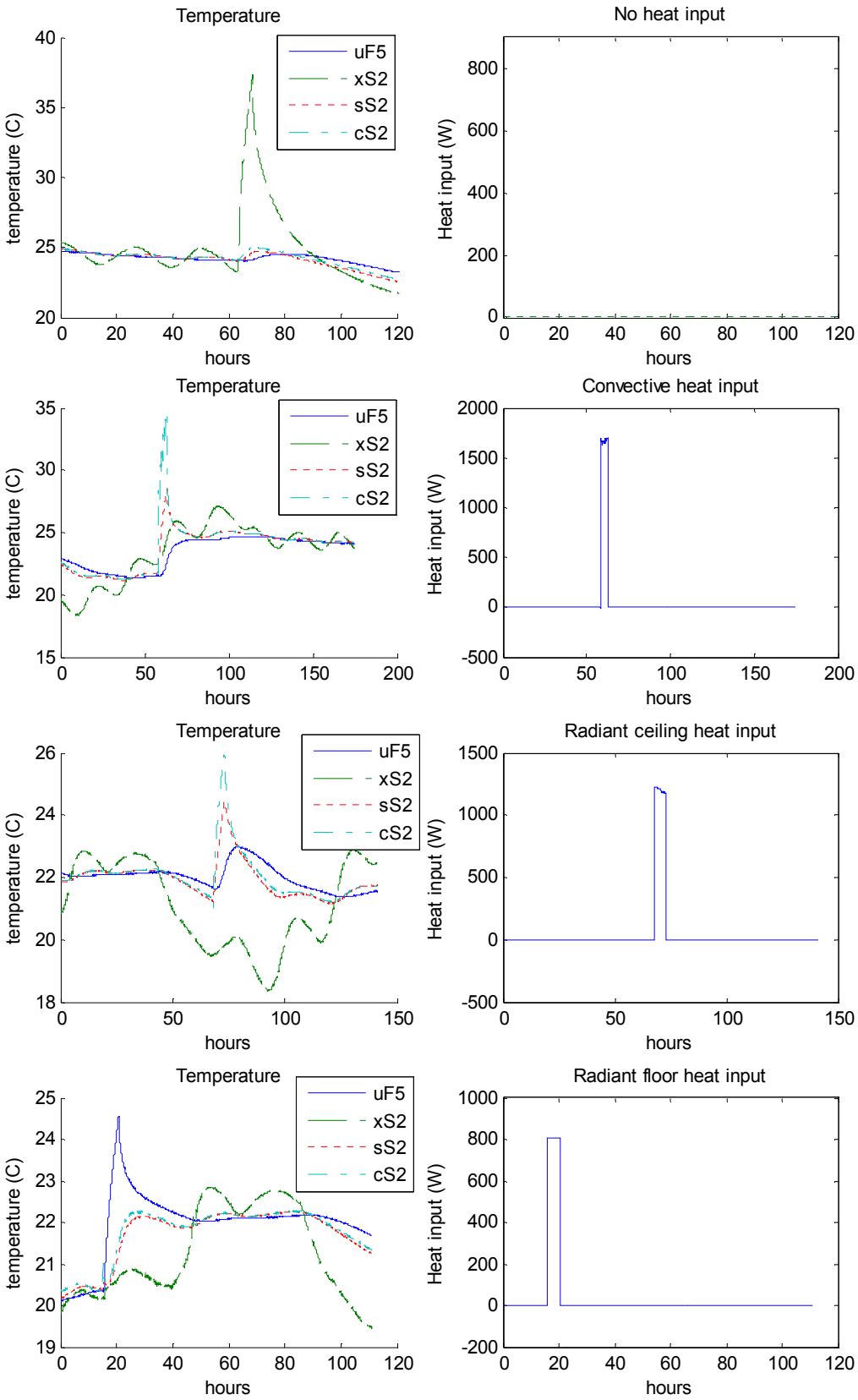

Figure 30 Measured temperature response and heat rates for model identification testing with three layers of pavers, including climate chamber temperature excitation, internal convective heat input, internal radiant heat input, and radiant concrete floor heating

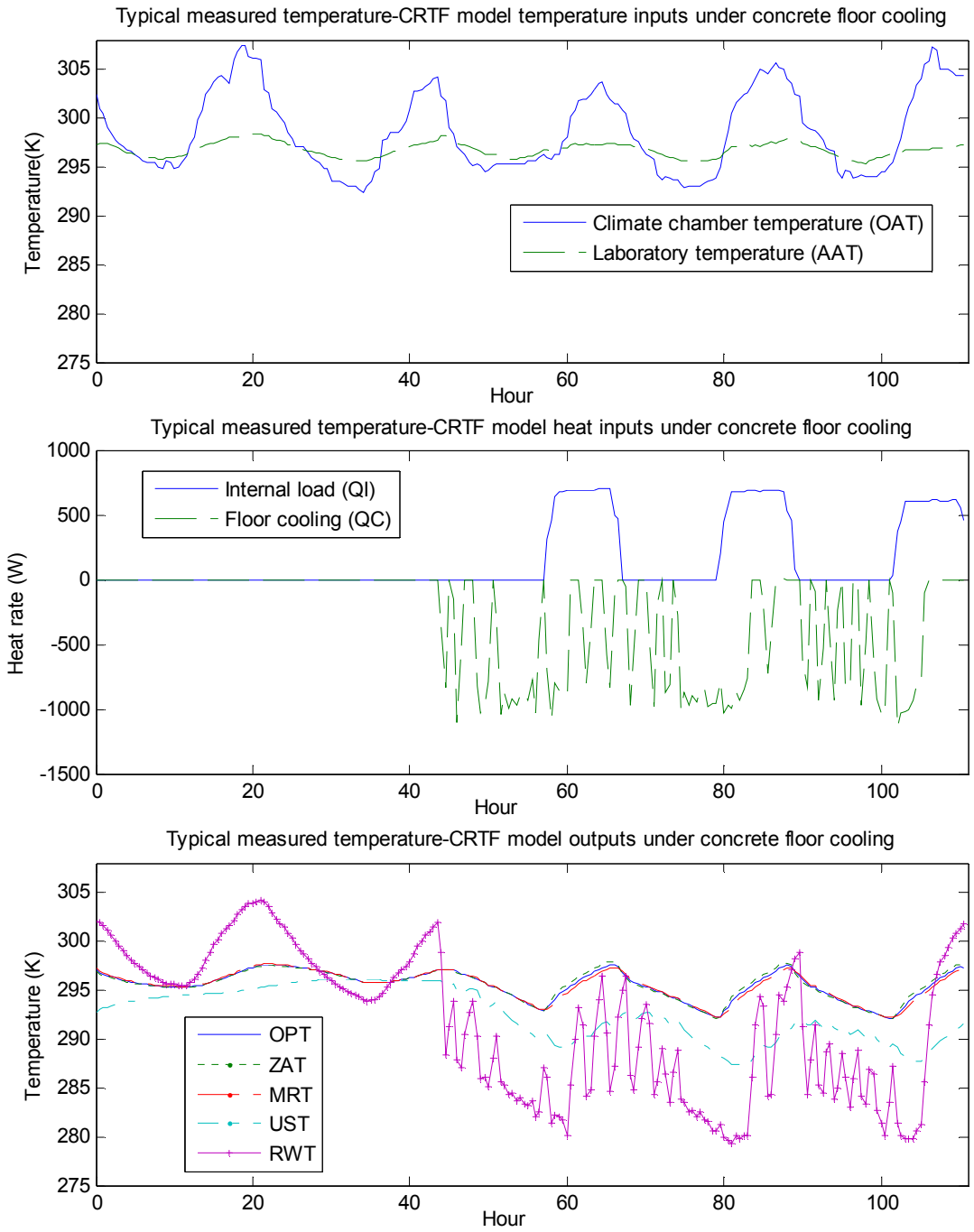

Figure 31 Measured temperature response and heat or cooling rates for application of model identification to a concrete floor cooling system with three layers of pavers. Cooling is delivered through a chilled water loop underneath the concrete layers

4.3 Test chamber thermal model identification

Gray-box temperature-CRTF models, as described in [Armstrong et al 2006a] and mentioned above, have been identified from the data described in the previous section. It will be shown that transfer function models can reliably predict zone temperature responses including mean air temperature, mean radiant temperature, and operative temperature. It will also be shown that transfer function modeling can be applied to predict a concrete floor temperature and the return water temperature when a chilled water loop is used to cool a radiant concrete floor.

The transfer function models applied here are temperature-CRTF models in which one adjacent zone temperature, an "exterior" climate chamber temperature, an internal load, and a cooling rate are related to the interior test chamber zone temperature through a transfer function model. The adjacent zone refers to the laboratory in which both the test chamber and climate chamber were housed, which is separated from both chambers by walls with continuous R-30 insulation. The model structure is as follows:

$$(13) \qquad iT(t) = \sum_{n=1}^{N} a_n iT(t-n) + \sum_{n=0}^{N} b_n OAT(t-n) + \sum_{n=0}^{N} c_n AAT(t-n) + \sum_{n=0}^{N} d_n QI(t-n) + \sum_{n=0}^{N} e_n QC(t-n)$$

In equation (13):

- iT is an interior zone temperature (either zone air temperature (ZAT), mean radiant temperature (MRT), or operative temperature (OPT)),
- OAT is an outdoor air temperature (in the climate chamber),
- AAT is an adjacent interior zone air temperature (the temperature inside the laboratory housing both the climate and test chambers),
- Q_i is an internal heat load, and
- Q_c is the cooling rate (or heating rate) delivered through the radiant concrete floor.

The (t-n)th term is the measured value of each variable n time steps before the current time t. High thermal mass systems may require a large number of terms, N, in the time series to accurately predict temperature response. N corresponds to the order of the system and directly relates to the order of a corresponding thermal RC network derived state-space model as described in [Seem 1987] and [Jimenez and Madsen 2008]. The time-series of each variable is weighted by a set of coefficients which capture the thermal behavior of the zone.

As explained in [Armstrong et al 2006a], under steady-state conditions these coefficients must conform to a steady state heat transfer constraint, where time series of heat loads and temperatures are constant, given by:

$$(14) \qquad Q_{tot} = UA_1(OAT - T_i) + UA_2(AAT - T_i) = \sum_k UA_k(T_k - T_i)$$

In equation (14), Q_{tot} is the total heat load on the space, UA_i is a total heat transfer coefficient between two zones, including UA_1 between the climate chamber (exterior) and test chamber

(interior) and UA_2 between the adjacent zone (the laboratory) and the test chamber (interior). UA is measured in Watts per Kelvin. In a general form, k is the number of distinct zones bordering the internal zone being modeled and T_k is the temperature in each zone. In steady-state, equation (14) reduces to the following equation:

$$(15) \qquad QI\sum_{n=0}^{N} d_n + QC\sum_{n=0}^{N} e_n = iT\left(\sum_{n=1}^{N} a_n - 1\right) + OAT\sum_{n=0}^{N} b_n + AAT\sum_{n=0}^{N} c_n$$

By allowing the cooling rate Q_c or the internal heat rate Q_i to be zero at steady state condition, the following constraints are evident which can be applied in a constrained linear regression:

$$(16) \quad \text{i)} \quad \frac{-\left(\sum_{n=1}^{N} a_n - 1\right)}{\sum_{n=0}^{N} d_n} = UA_1 + UA_2 \qquad \text{ii)} \quad \frac{\sum_{n=0}^{N} b_n}{\sum_{n=0}^{N} d_n} = UA_1 \qquad \text{iii)} \quad \frac{\sum_{n=0}^{N} c_n}{\sum_{n=0}^{N} d_n} = UA_2$$

$$(17) \qquad -\left(\sum_{n=1}^{N} a_n - 1\right) = \sum_{n=0}^{N} b_n + \sum_{n=0}^{N} c_n$$

Applying these physical constraints ensures that the zone temperature response model will obey a steady-state heat transfer equation. Additional constraints on the poles of the temperature-CRTF when converted to a z-transform formulation are explained in [Armstrong et al 2006a] based on the work of [Hittle and Bishop 1983]. These constraints were not applied to allow for linear parameter estimation using simple constrained linear-regression to find the coefficients in equation (13).

4.3.1 Temperature-CRTF model testing

The temperature-CRTF model described above was first applied to a set of tests in which each mode of thermal input was varied separately to test the accuracy of temperature-CRTFs in identifying different temperatures subject to different types of loads for different model orders and sampling intervals.

The following interior temperatures were predicted using a temperature-CRTF: mean zone air temperature (ZAT), calculated as a mean of the head height or below air temperature measurements inside the chamber; mean radiant temperature (MRT) at the center point of the room calculated from the surface temperature measurements inside the chamber; and the operative temperature (OPT), calculated from the mean air temperature and mean radiant temperature.

[Seem 1987] showed that CRTFs can be formulated that include radiative heat transfer between interior surfaces using a linear approximation of called a star network, as shown in Figure 32 for a zone with three surfaces. The star network is an approximation of a view factor network of

linearized radiative heat transfer resistances. The T_{star} node is not a measurable temperature, but rather an imaginary, intermediate temperature between the surfaces of a room, represented by T_1, T_2 and T_3, and the room air temperature T_r. The loads q_1, q_2, and q_3 represent the net heat transfer across the exterior walls of a zone into each interior wall surface, calculated through conduction transfer functions (CTF). The resistances in the star network can be calculated from linearized radiative resistances in a view factor network as shown by Seem [1987]. Seem showed that CRTF models using this approximate star network can accurately, to within 0.7 percent, model cooling loads relative to a model that employs a more accurate view factor network.

A temperature-CRTF inverts the CRTF used by Seem to predict the room temperature T_r instead of cooling load q_{load}. Because the star network is a simple resistance network, it is straightforward to evaluate all of the surface temperatures, $T_{1\text{-}3}$, from a temperature-CRTF. Since both zone surface temperatures and air temperatures can be predicted from temperature-CRTF, the zone mean radiant temperature (MRT) and operative temperature (OPT) can also be predicted from temperature-CRTFs. MRT and OPT are simply linear combinations of surface and air temperatures. Steady state heat transfer constraints still apply, because the steady state temperatures and heat transfer into and out of each node in the star network must obey a steady state heat balance.

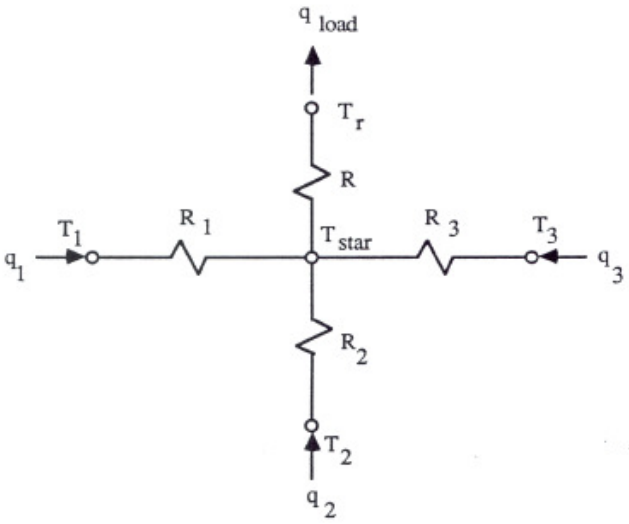

Figure 32 Star network for approximating radiative and convective heat transfer between wall surfaces and the zone air from [Seem 1987] where $T_{1\text{-}3}$ are wall surface temperatures, $q_{1\text{-}3}$ are net heat transfer rates into the wall surface calculated using each walls conduction transfer functions, $R_{1\text{-}3}$ are resistances to an intermediate temperature node T_{star}, R is the resistance between the intermediate temperature and the room temperature T_r and q_{load} is the zone cooling load

The coefficients of the temperature-CRTFs are derived from constrained linear regression using the code included in Appendix B.3. Because each mode of heat input was excited separately during model testing, training data from all of the excitation tests had to be used to generate

temperature-CRTF coefficients that capture every mode of excitation. As a result, around 20 days of training data were used to generate temperature-CRTF coefficients. It will be shown in the cooling test results that far less training data is required if the modes of thermal excitation are driven simultaneously.

A set of coefficients identified from inverse modeling the temperature responses ZAT, MRT, and OPT of the chamber for model testing with three layers of pavers are shown in Appendix B.4. A sample of the training data and the accuracy of the temperature-CRTF model predictions are shown in Figure 33. Six training data sets were used to identify the coefficients, spanning each of the four modes of excitation. Only one training data set, a radiant floor heating excitation, is shown in Figure 33, but the root mean square error (RMSE) shown is the error over *all* of the data sets. Temperature training data was averaged over five minute intervals to reduce measurement noise. Heat rate training data was averaged over the sampling interval. For the sample coefficients shown, four hours of data sampled every 30 minutes were used for model identification. This equates to N = 8 in equation (13) and an eighth order model. This is a high order model for a typical inverse building model, but is used here as an example that high order models can be identified that accurately represent zone temperature response. The accuracy of different model orders will be explored in detail below. The RMSE of the identified temperature-CRTF models in predicting all of the data in the training data sets was less than 0.1 K and less than 0.1 percent of the total temperature variation for all three output variables, ZAT, MRT and OPT.

The accuracy of the temperature-CRTF in performing one-step ahead prediction on two sets of validation data is presented in Figures 34 and 35. The validation data includes one internal convective heating excitation and one radiant floor heating excitation. The validation data show that the one-step ahead prediction RMSE for ZAT, MRT, and OPT are all near 1 percent or less of the total temperature variation. During testing of CRTF model identification methods, only the one-step-ahead prediction accuracy of temperature-CRTFs was evaluated. Later, in the next section on application of the temperature-CRTF models to a concrete floor cooling system, it will be shown that temperature-CRTF inverse modeling can provide simple and highly accurate predictions 24 hours in advance of ZAT, MRT and OPT useful for predictive control.

There are a few important points to note about the measured temperatures used for model identification. To the extent possible, single sensor measurements were used for model identification. This choice was made under the assumption that typically only a single sensor will be available in a real building. The adjacent zone temperature, AAT in equation (13), was measured from one TC along the East exterior wall of the chamber, xE2. This sensor is located in a zone bordering the North and East walls and the Roof of the test chamber. Any of the temperature sensors along the Roof, North or East walls may be substituted for this measurement.

The outside air temperature, OAT in equation (13), was measured with one TC on the exterior of the South wall of the test chamber, xS2. The adjacent zone temperatures along the West wall and below the floor were ignored because additional partition walls and the building's

floor provide additional insulation between the chamber and those adjacent zones. In a real building, either the entire building must be modeled or a multi-zonal model must be identified which capture the effects of inter-zonal heat transfer between all zones.

A number of questions arise in the process of selecting and identifying temperature-CRTF models of zone temperature response.

First, there is a question whether radiative and convective internal loads must be modeled separately. The radiant heating and convective heating inputs to the chamber have been treated as one set of internal heat loads with one set of temperature-CRTF coefficients. Separating the internal loads into convective and radiative terms with separate coefficients leads to model improvements of only a fraction of a percent of RMSE relative to both the training data and the validation data. This is fortunate because in practice it is difficult, if not impossible, to separate the convective and radiative part of internal load measurements. This conclusion may not hold for all systems as it may depend on internal convective and radiative heat transfer properties such as surface absorptivities. However, it is useful to observe that a net internal load measurement may be sufficient for accurately predicting zone temperature response when radiative and convective loads cannot be measured separately.

Another question that arises during the inverse modeling process is how frequently to sample data, how much history is necessary, and what model order is necessary to perform accurate model identification. A series of models was identified to test the importance of sampling interval and model order. Temperature-CRTFs were identified using data sampled at 15, 30, 45, 60, 90 and 120 minute intervals and for models of order zero through 24. A first order model includes only one previous measurement in each variable. A 24^{th} order model sampled with 30 minute averaging intervals would include 12 hours of past data for each variable sampled at 30 minute intervals. These models were compared on the basis of root mean square error (RMSE) in replicating the training data and in their one-step-ahead prediction accuracy for the validation data. The RMSE as a function of sample averaging interval and model order are shown in Figure 36.

The results show that increasing the model order and decreasing the sampling interval in general leads to more accurate models in replicating training data. However, the results also show that high model orders can lead to poor one-step ahead prediction of the validation data. In other words, including too many historic terms in exogenous variable time series can lead to an increase in the prediction RMSE, as shown in the bottom graph of Figure 36. One can conclude that, although high order models are better at replicating training data, they do not necessarily make better predictions. This may be a result of the temperature-CRTF identifying characteristics of the noise in the training data. A stochastic approach to model identification may address this problem. Furthermore, high order coefficients in the temperature-CRTF may not be representative of physical processes. Application of the additional constraints on the roots of the temperature-CRTFs identified by [Armstrong et al 2006a], which have not been applied in this work, may be useful in identifying more physically meaningful high order models.

Based on the relationship between validation data RMSE, model order and sample averaging interval, it is evident that at least a third or fourth order model is best for achieving accuracy. High order models may become less accurate, particularly at larger sampling intervals. Using relatively higher frequency sampling, over 15 to 30 minute intervals, leads to better prediction RMSEs but with diminishing returns. The local minima in the validation data RMSE surface at 60 minute sampling and third order is likely an artifact of the frequencies used to excite the chamber, where thermal inputs were varied in a round number of hours.

Changes in the types of internal loads, occupied periods, outdoor climate conditions, and other characteristics of a building or its use may cause previously identified models to become less accurate as the building changes or weather and loads deviate from previously observed conditions. These problems can be mitigated in part by careful selection of model order, sampling interval and model structure based on validation data RMSE and other goodness of fit metrics. Another approach is to perform continuous model identification from BAS data over time. The temperature-CRTF models can be updated continuously based on recent data to ensure that variations in loads, climate and other characteristics observed are used as new training data for the building. Continuous refinement will allow the temperature-CRTFs to improve over time.

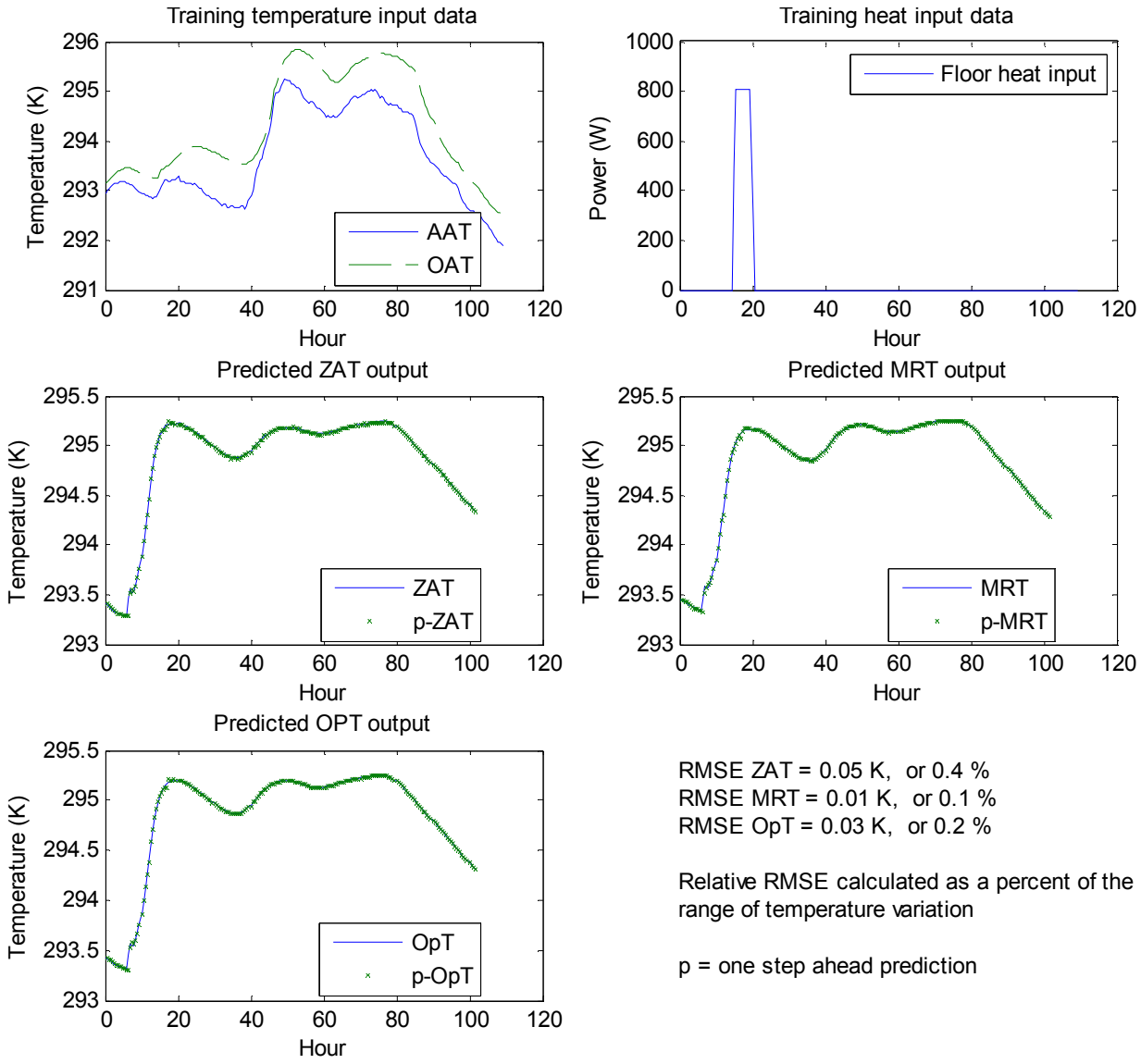

Figure 33 Accuracy of inverse model on training data. The top two graphs show a sample of training data for a floor heating test. The bottom three graphs show the inverse model's accuracy in predicting zone air temperature (ZAT), mean radiant temperature (MRT) and operative temperature (OPT). The RMSEs presented are for the entire training data set, including five sets of training data in addition to that shown

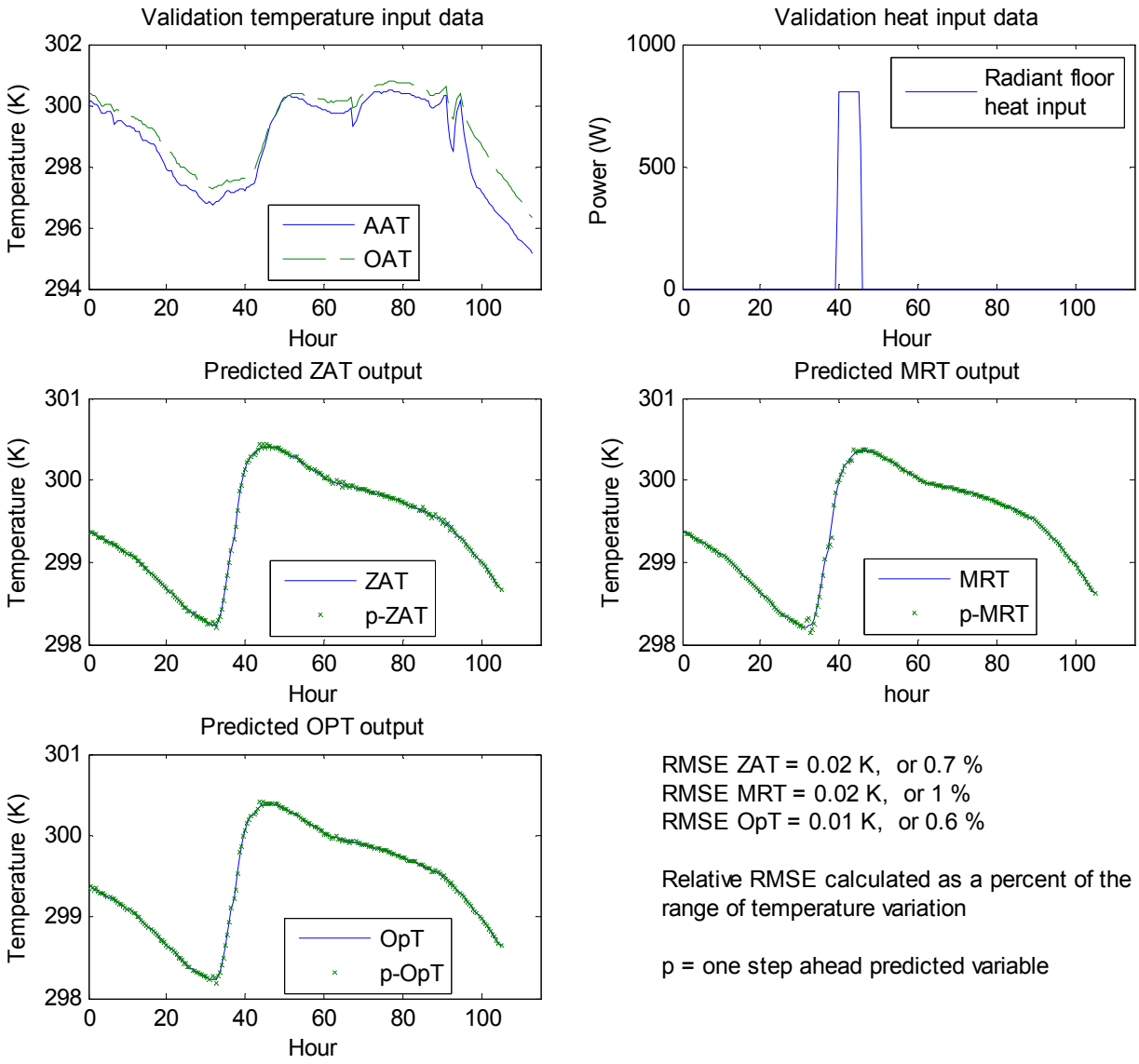

Figure 34 Accuracy of inverse model for floor heating validation data.

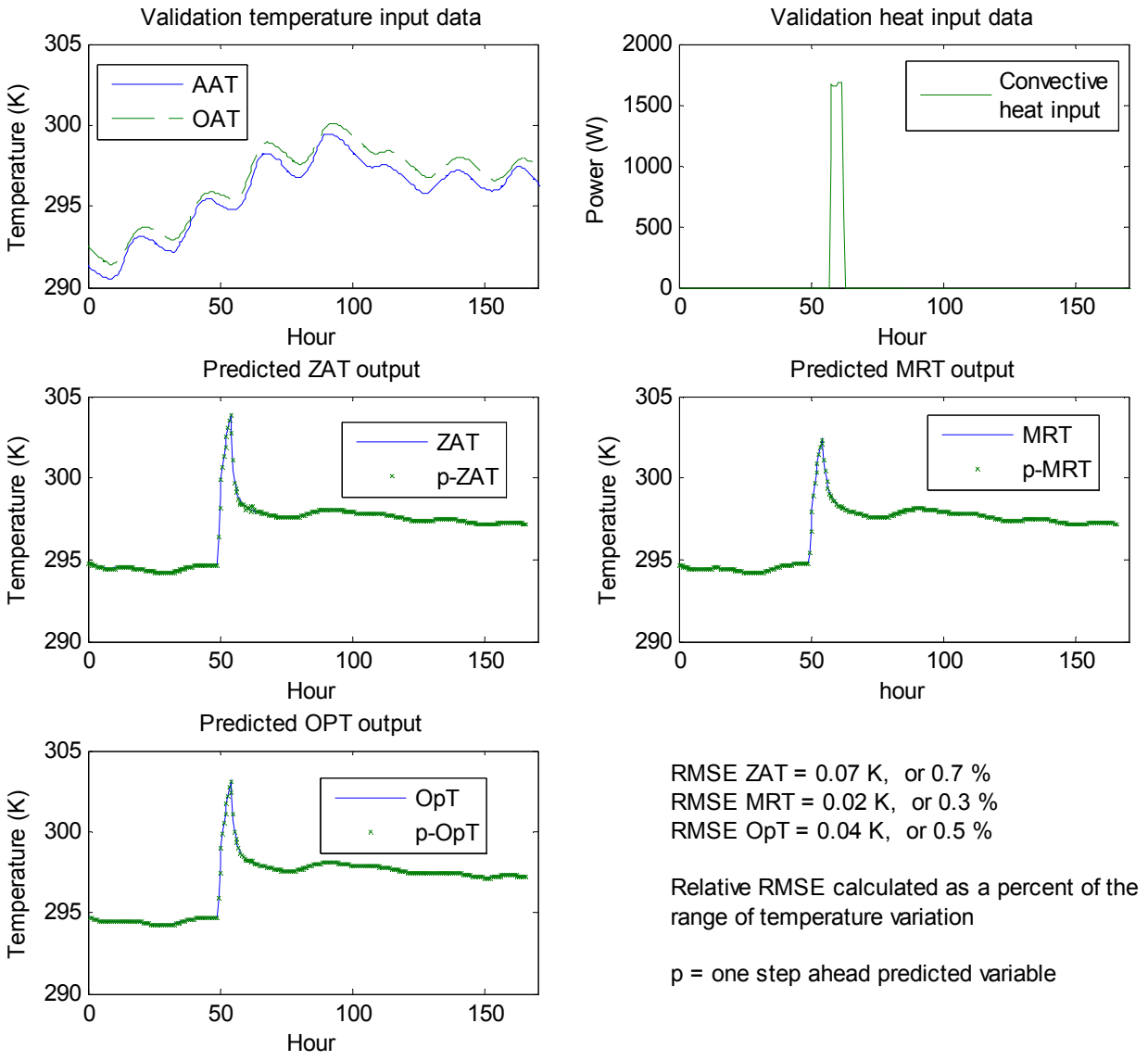

Figure 35 Accuracy of inverse model for convective heating validation data

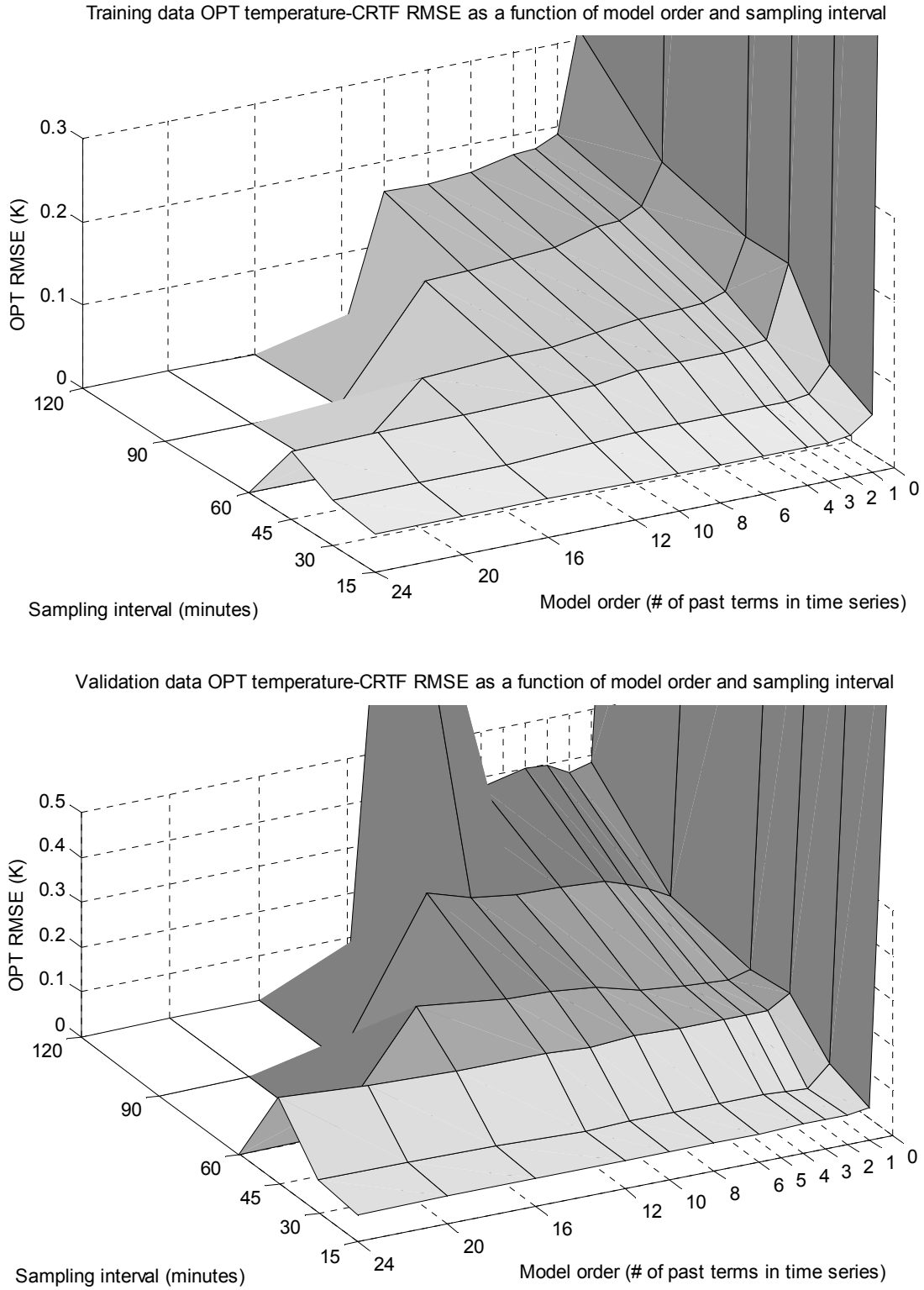

Figure 36 One-step ahead prediction RMSE for zone operative temperature (OPT) for training data (top) and validation data (bottom) as a function of the time interval for sampling data and the order of the temperature-CRTF model

4.3.2 Application of temperature-CRTFs to a zone with radiant concrete-core cooling

The temperature-CRTF models tested in the previous section were next applied to the test chamber after installation of a radiant concrete-core floor cooling system. In this case, the electrical resistance heaters underneath the concrete layers were replaced with a chilled water loop that provides cooling to the bottom of the concrete. This chilled water loop was supplied by an air-cooled chiller, created from the split-system air conditioner described in Chapter 3. This air-cooled chiller system will be described in detail in Chapter 6. The important point is that the cooling rate to the floor could be measured at the chilled water loop from the chilled water flow rate and the chilled water supply and return temperature difference. For purposes of this chapter, the cooling rate to the radiant concrete floor is the only important issue, the details of providing that cooling will be explained later.

In applying temperature-CRTFs to the chamber cooled with a radiant concrete floor, all modes of thermal excitation were implemented simultaneously on the chamber, as would be expected for a real building or zone. These include climate temperature variations due to diurnal cycles, internal heat loads, and radiant cooling from the floor. Solar loads were not simulated. Light bulbs were used to simulate internal loads from people, lights and equipment as described in the section 4.2 and in Appendix B.1. As before, temperature-CRTF models were identified to predict ZAT, MRT and OPT.

In addition to ZAT, MRT and OPT, a temperature underneath the slab (UST for under-slab temperature) and the chilled water return water temperature (RWT) were predicted. The UST is a measure of the pre-cooling of the concrete, and represents an energy state of the concrete-core TES. A temperature-CRTF identical to equation (13) is used to predict UST, where iT equals UST. In this case UST is a material temperature and the internal loads, outdoor temperature, and adjacent zone temperature impact UST through the temperature response of the zone and furthermore through the conduction transfer function of the concrete floor. As in the heating tests, the temperature below the floor is neglected, meaning that the chamber below the concrete floor and chilled water loop is assumed to be adiabatic.

The UST is a useful intermediate temperature for predicting the RWT. As will be explained in Chapter 5, the RWT is necessary to predict the power consumption of the chiller at future time steps, which is needed to minimize energy consumption over a 24 hour look-ahead period. Predicting the RWT could, in theory, be done with a temperature-CRTF using the same variables used to predict ZAT, MRT, and OPT. Outdoor air temperature, internal loads, and cooling rate are the only exogenous variables impacting RWT (at a fixed chilled water pump speed). However, in practice it is impractical and difficult, if not impossible, to predict RWT from these exogenous variables. In the test chamber, the temperature sensor measuring RWT is installed in the climate chamber. When the chilled water pump is off, the RWT approaches outdoor temperature. When the chilled water pump is on, the RWT is determined primarily by the UST and the cooling rate QC. The chilled water pump speed would also impact RWT, but for purposes of this research the pump speed has been held constant.

[Olesen et al 2003] and [Koschenz and Dorer 1999] show how thermal RC networks can be applied to relate chilled water loop temperatures to the temperature of a concrete-core radiant floor. From an inverse modeling perspective, any thermal RC network that can be represented in state-space form can be converted to a transfer function representation, as shown in [Jimenez and Madsen 2008]. Although the order of the thermal RC network relating RWT to the UST is unknown, it is sufficient to observe that a thermal RC network can be defined relating cooling rate, UST and RWT. Without a priori knowledge of the order of the system, transfer function models of increasing order can be identified until RMSE thresholds are met and any other goodness of fit metrics are satisfied. The following transfer function model was applied to model RWT:

$$RWT(t) = \sum_{m=1}^{M} a_m RWT(t-m) + \sum_{m=0}^{M} b_m UST(t-m) + \sum_{m=0}^{M} c_m QC(t-m) \quad (18)$$

RWT is chilled water return temperature, UST is under-slab temperature, QC is the cooling rate, and M is the number of historic terms in each time series. This is equivalent to stating that the chilled water temperature forms an Mth order thermal system affected by the cooling rate QC and the concrete temperature UST.

The training data used for temperature-CRTF model identification of ZAT, MRT, OPT, UST, and RWT were shown in the previous section in Figure 31. An eighth-order model with data sampled at 30 minute intervals was used for the ZAT, MRT, OPT and UST temperature-CRTFs with the same form as equation (13). A second-order model with data *averaged* over 30 minute intervals was applied for RWT. Averaging for RWT was performed because the transient response of the chilled water temperature was not of interest, but rather only the near-steady-state RWT for a given QC and UST. Sampling, rather than averaging, RWT results in very erratic predictions of RWT at times when the chilled water pump turns on or off. Averaging RWT over thirty minute intervals and modeling it only when the chilled water pump is on ensures that the model of RWT relative to UST and QC represents RWT temperature response and a steady operating condition.

The choice of order for these models will be explained below. Figure 37 shows the one-step-ahead prediction accuracy of the temperature-CRTF models identified from the training data. The RMSE for ZAT, MRT, OPT, and UST are within hundredths of a Kelvin, while the RMSE for RWT is much larger, around 0.8 K.

Validation data, which was not used to identify the temperature-CRTF coefficients, is shown in Figure 38. A sample of the 24-hour look-ahead accuracy of the temperature-CRTFs for a subset of the validation data is shown in Figure 39. The 24 hour prediction accuracy is important because the models will be used to predict zone temperature response 24 hours into the future in order to optimize chiller control and minimize system power consumption. The validation data show that the temperature-CRTF models are accurate to within a few tenths of a Kelvin for ZAT, MRT, OPT, and UST for 24 hour look ahead prediction. Prediction of RWT is noticeably less

accurate, with about a one degree Kelvin RMSE. Figure 40 shows the prediction RMSE for a sample of the validation data set for predicting further into the future, as far as 96 hours ahead. Beyond a few days the model predicted temperatures begin to drift away from measured validation data due to accumulated error.

The model order, eight, and sampling interval, 30-minutes, was selected based on an RMSE metric as described in the previous section. Figure 41 shows the OPT one-step ahead prediction RMSE for the training data and for the validation data as a function of model order and sampling interval. In looking at the one-step-ahead prediction RMSE, fourth order models or higher with sampling intervals of 15 or 30 minutes are reasonably accurate. However, the models must predict temperature 24 hours into the future.

Figure 42 shows the total *24-hour-ahead* RMSE for the complete validation data set as a function of model order and sampling interval. The total 24-hour-ahead RMSE is calculated from the validation data as follows. First, individual 24-hour-ahead RMSE are calculated beginning with a time series of length N, where N is the model order. These N measurements of each model input variable form the initial time series history for a 24-hour-ahead prediction of OPT, UST and RWT. An RMSE can be calculated for the 24 hours of predicted temperatures relative to the actual measured temperatures. This RMSE is for just one initial set of input variables. Multiple sets of input variables from the validation data, consisting of N samples of each input variable, can be used as the initial time series for a 24-hour-ahead prediction. To calculate the total 24-hour-ahead RMSE for the validation data set, 24-hour-ahead predictions are made beginning with subsets of validation data from time 1 to N, then 2 to N+1, and so on through the complete data set. The RMSE for all of the predictions made with all of these initial data sets are tallied for a complete 24-hour-ahead prediction RMSE for the temperature-CRTF model based on the validation data set.

The 24-hour-ahead RMSE show in general, as before, that lower RMSE can be achieved with higher frequency sampling, such as 15 or 30 minute intervals. However, the 24-hour-ahead RMSE show that somewhat higher model orders, above fifth order, are generally better than lower model orders at predicting 24 hours ahead. Overall, the best 24-hour-ahead RMSEs are in the range of 0.4 to 0.5 Kelvin with 15 or 30 minute sampling and a model order of five to eight. The 24-hour-ahead RMSE is significantly worse than the one-step-ahead RMSEs, which were closer to one tenth of a Kelvin. A balance must be maintained when selecting model order to achieve accuracy and reduce complexity and computational time required for simulation. Fifteen minute sampling would require predictions of 96 temperatures for each variable over a 24 hour prediction horizon, whereas 30 minute sampling requires half of that. To strike this balance an eighth order model with 30 minute sampling was elected, allowing for high accuracy 24 hour ahead prediction while maintaining a reasonable number of predicted temperatures in the prediction horizon.

A lower order model was applied for RWT prediction. The UST captures the higher order, slow thermal response of the concrete floor, whereas the transfer function model for RWT captures the faster temperature response between the UST, cooling rate QC, and RWT. Models of

increasing order for RWT were tested to identify an appropriate temperature response model for RWT. The RMSE for RWT prediction as a function of model order is shown in Figure 43 for one-step-ahead prediction of training data and validation data, and 24-hour-ahead prediction of the validation data. RWT has only been predicted when the chilled water pump is running. When the pump is off, the RWT is assumed to float back to the outdoor climate temperature because of the location of the RWT sensor. This has no impact on the thermal response of the room. Models of order greater than four show no improvement in predicting validation data. A second order model was elected for predicting RWT from UST and QC.

4.4 Thermal model identification for LLCS

A few observations can be made based on the analysis in this chapter relevant to applying thermal model identification and temperature-CRTFs to LLCS. First, transfer function models are well-suited for inverse modeling zone thermal dynamics for LLCS with radiant concrete-core floors where the thermal mass of the floor is used for energy storage. No a priori knowledge is necessary about building components or the order of the thermal system. Models of different system order and with different sampling intervals can be easily identified and compared based on validation data RMSE. Training data RMSE should not be used to elect model orders, because increasing RMSE may reflect better modeling of training data noise rather than the temperature response.

Accurate temperature-CRTF models for the primary temperatures of interest in radiant cooling can be identified from only a few days of training and validation data. These include air temperatures, mean radiant temperatures, and operative temperatures. Additional measurements such as slab temperatures and chilled water loop temperatures can also be predicted using such models. These temperatures will be important in a 24-hour-ahead predictive control algorithm, in which chiller power consumption depends on evaporating temperature, which in turn depends on chilled water temperature.

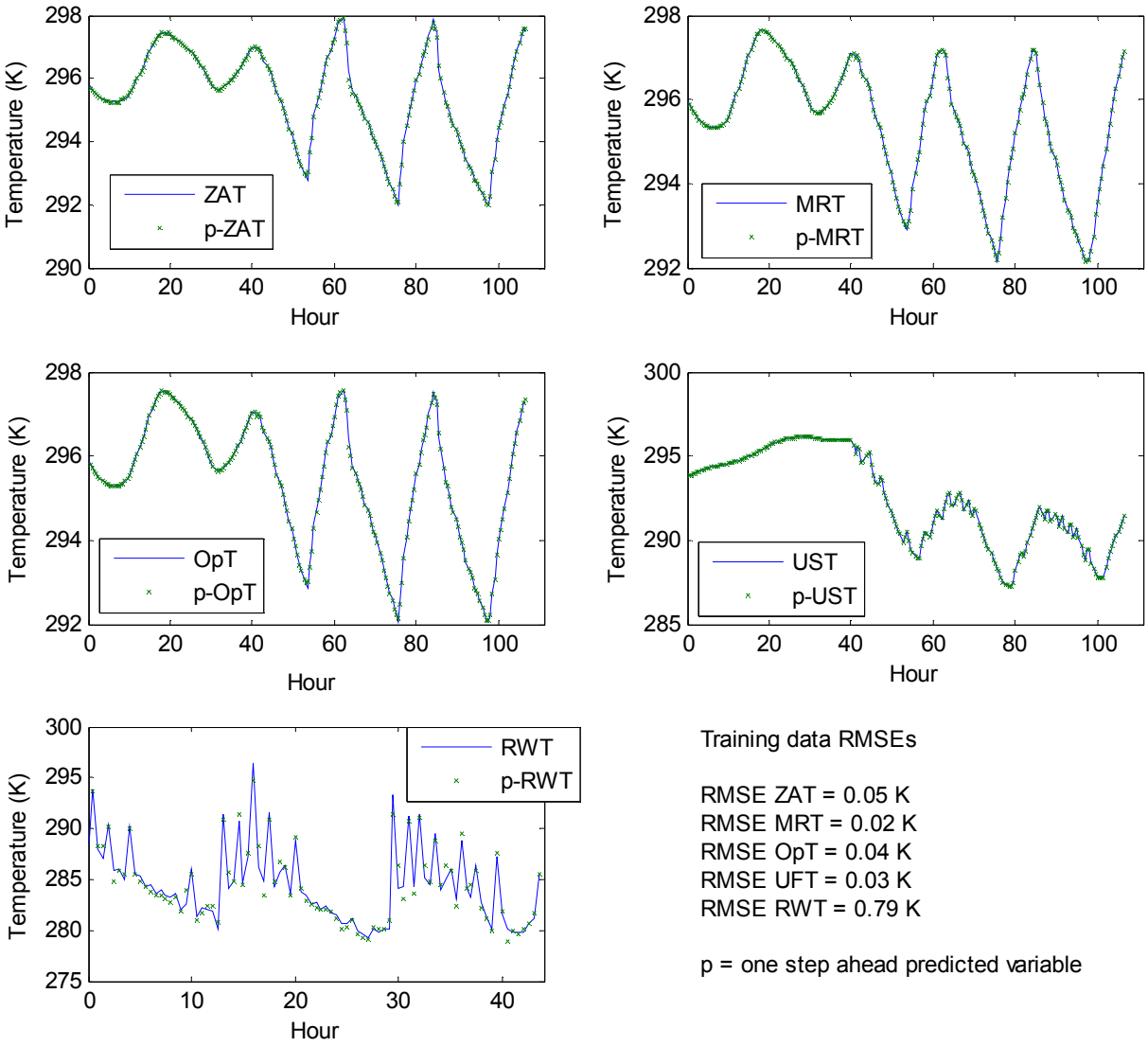

Figure 37 Concrete-core radiant floor cooling temperature-CRTF model one-step ahead training data prediction RMSE for ZAT, MRT, OPT, UST, and RWT

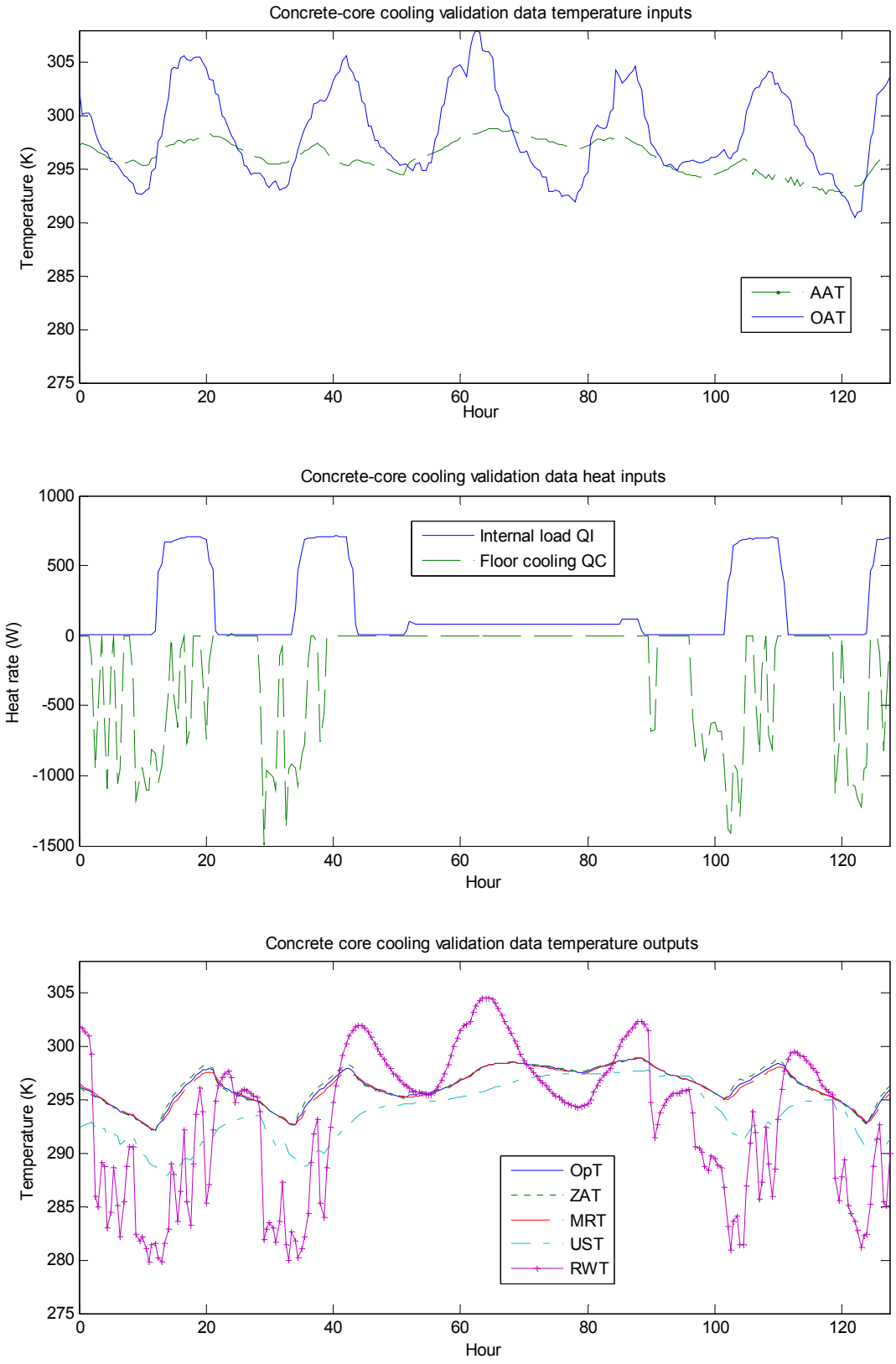

Figure 38 Concrete-core radiant floor sample validation data temperature inputs, thermal inputs, and temperature outputs

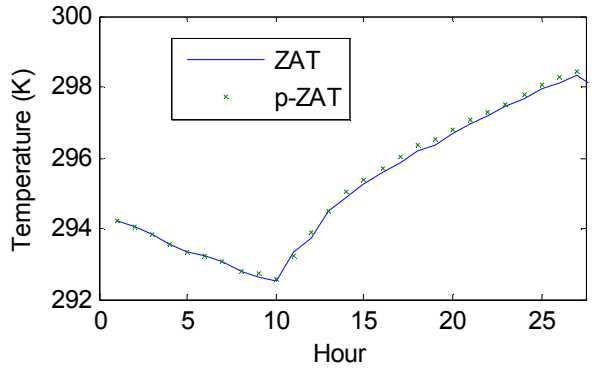

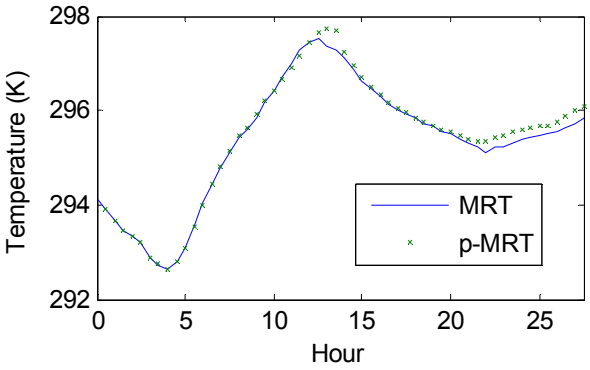

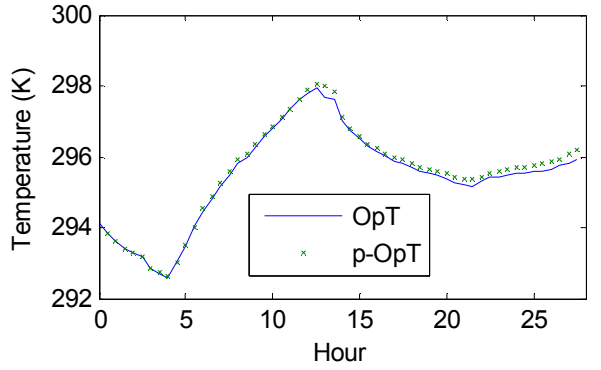

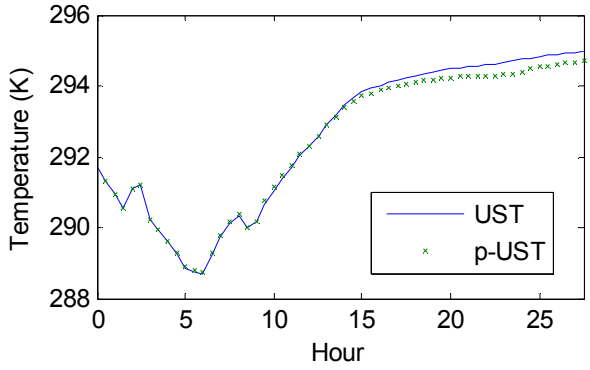

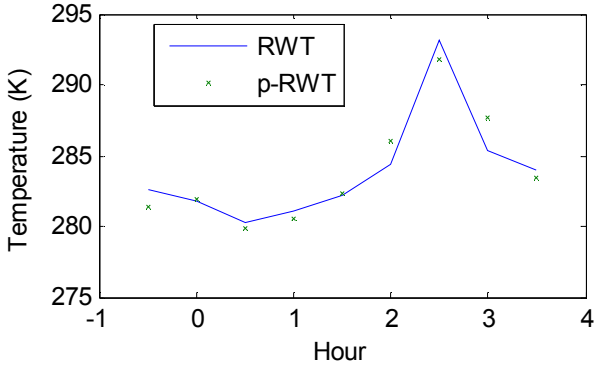

Validation data 24 hour look ahead RMSEs:

RMSE ZAT = 0.16 K
RMSE MRT = 0.14 K
RMSE OpT = 0.13 K
RMSE UFT = 0.18 K
RMSE RWT = 1.18 K

p = N step ahead predicted variable

Figure 39 Concrete-core radiant floor cooling temperature-CRTF model 24-hour-ahead validation data prediction RMSE for ZAT, MRT, OPT, UST, and RWT

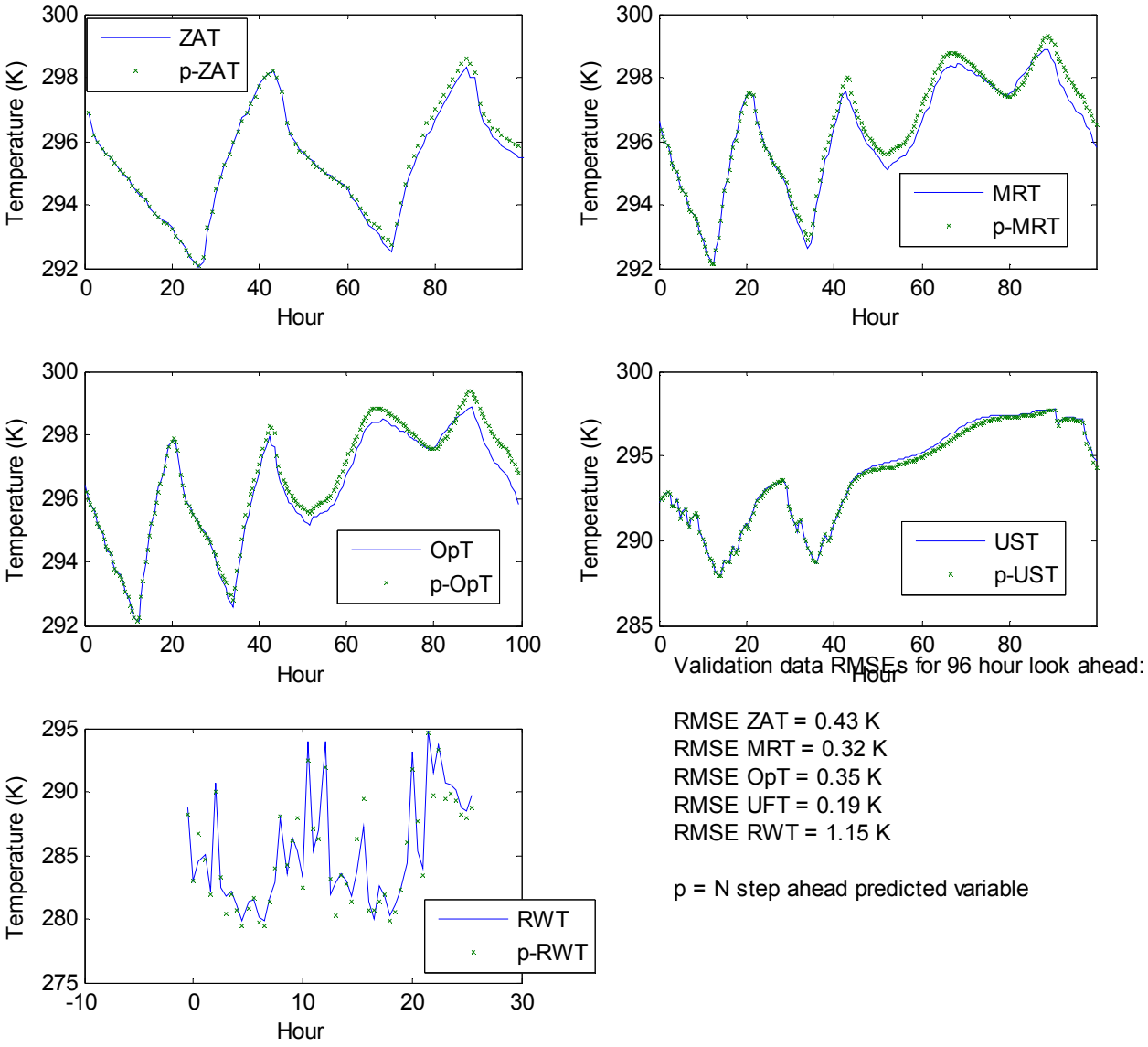

Figure 40 Concrete-core radiant floor cooling temperature-CRTF model 96-hour-ahead validation data prediction RMSE for ZAT, MRT, OPT, UST, and RWT

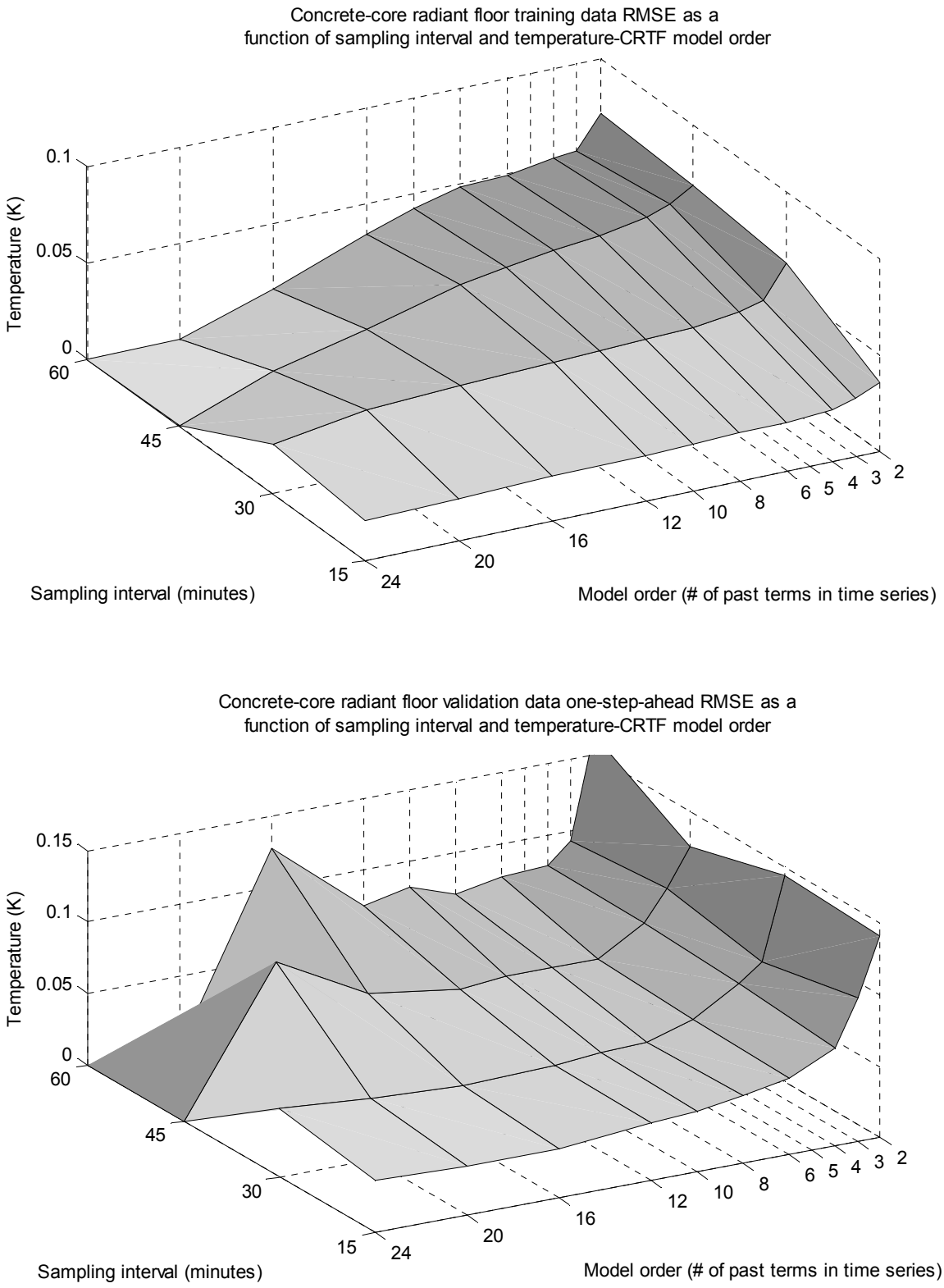

Figure 41 Concrete-core radiant floor OPT temperature-CRTF model one-step-ahead RMSE as a function of sampling interval and model order for training data (top) and validation data (bottom)

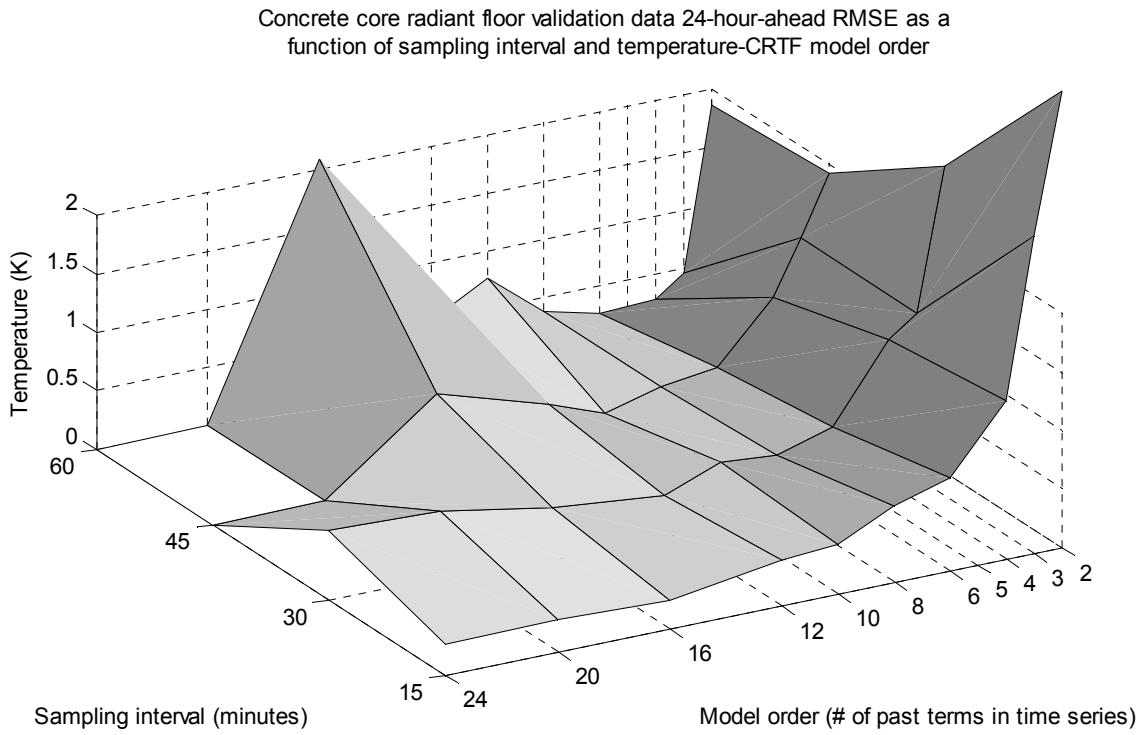

Figure 42 Concrete-core radiant floor OPT temperature-CRTF model 24-hour-ahead RMSE as a function of sampling interval and model order for validation data

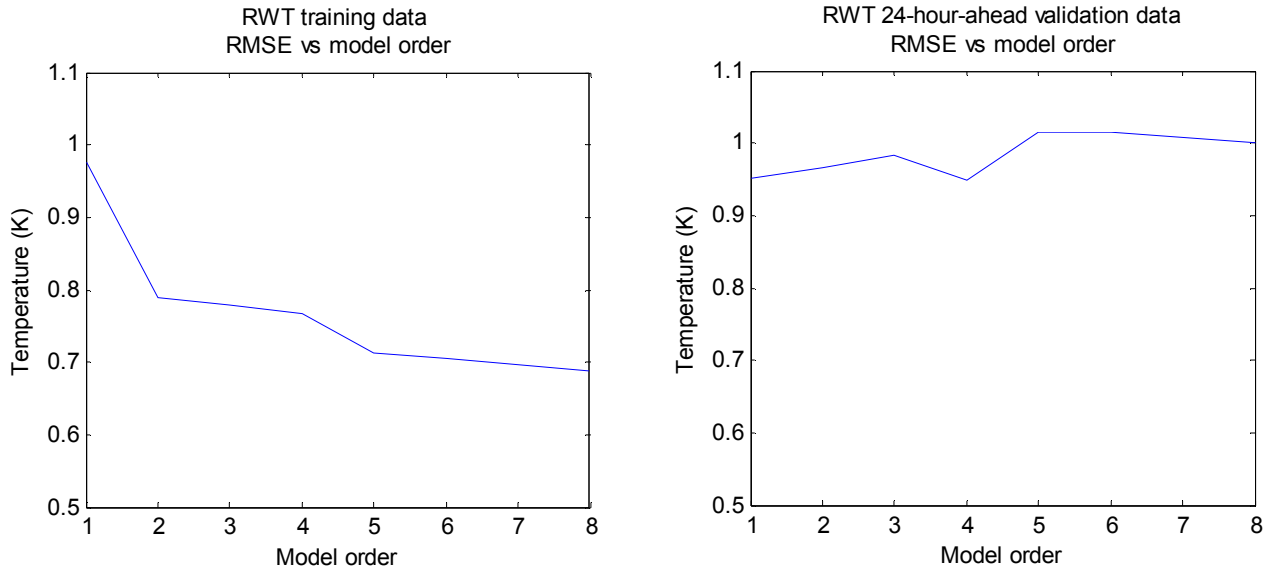

Figure 43 RWT prediction error with 30 minute sampling as a function of transfer function model order, corresponding to the order of the thermal network between the UST and RWT measurements.

Chapter 5 Pre-cooling control optimization

The ultimate goal of low-lift cooling is to achieve signficant cooling energy savings by operating a chiller at low pressure ratios more of the time to meet the daily cooling load. The key control element enabling low-lift cooling is a predictive pre-cooling control algorithm which optimizes the operation of a chiller over a 24 hour period by pre-cooling TES. This optimizer must minimize the power consumption of the chiller while providing enough cooling to maintain thermal comfort during occupied periods. The predictive control algorithm allows the chiller to operate at low part-loads more of the time by spreading out cooling load over more hours of the day and shifting the cooling load to night-time hours, when lower condensing temperatures are possible. Combined with a radiant cooling system which allows for higher evaporating temperatures, predictive pre-cooling control enables the low-lift chiller operation at the core of LLCS.

This Chapter will review previous work on predictive HVAC control algorithms relevant to this research. It will also describe the development of a chiller control optimization algorithm using the curve-fit low-lift heat pump model from Chapter 3 and the zone temperature response models from Chapter 4.

5.1 Predictive control with thermal energy storage and radiant systems

Predictive control of chillers has been used to reduce operating costs and, less frequently, energy consumption primarily by limiting peak cooling demand and shifting thermal loads. In some cases, inverse models of building cooling loads have been used simply to calculate the power consumption for an HVAC system with an assumed demand limiting, energy savings or cost reduction control strategy. In these cases, simple zone temperature setpoint schedules or other control schedules are proposed (not determined by an optimization algorithm) which will reduce energy consumption or operating costs [Braun et al 2001, Braun and Lee 2006, Lee and Braun 2008].

A more rigorous approach, though one that requires significantly more information, model complexity, and computational resources is to identify control schedules using an optimization algorithm. [Braun 1990] takes an approach similar to that developed in this research. An optimization algorithm is presented that includes: a temperature-CRTF model of zone temperature response similar to that described in chapter 4; a cooling plant power model as a function of chilled water loop load, the outdoor wet-bulb temperature, and supply air temperature difference; and an air handler power consumption model. An optimization is

performed to minimize the following objective function with respect to zone temperature set points T_z:

(19) $$J = \sum_{k=1}^{K} R(k) \times P^*(\vec{T}_z(k), \vec{f}(k)) \quad \text{subject to constraint} \quad T_{z,min}(k) \le T_z(k) \le T_{z,max}(k)$$

In equation (19), R(k) is an electricity rate at time k and P^* is the optimal cooling plant consumption at time k. The sum is over time k=1 through K where k can be 24 hours into the uure. P^*depends not only on current conditions at time k, but also on zone temperature setpoints and exogenous variables other times. As a consequence, P^* is a function of a vector of zone temperature setpoints $\vec{T}_z(k)$ and a vector of exogenous variables $\vec{f}(k)$. $\vec{f}(k)$ includes solar loads, internal loads and outdoor climate conditions at times k. An optimization over the vector of temperature setpoints $\vec{T}_z(k)$ is performed to minimize electricity cost (or energy consumption with R(k) = 1 for all k). The power consumption for HVAC equipment at each time k is calculated based on cooling loads, computed from a CRTF model, with fixed indoor temperature setpoints $\vec{T}_z(k)$.

The cooling loads at a given time k depend on current and past temperature setpoints. Consequently, calculation of cooling loads, power consumption, and costs at future time steps requires iteration of the CRTF using zone temperature set point history at each time step. For a given set point, the power consumption is a non-linear function depending on the operating state of the HVAC equipment and loads. Furthermore, the power consumption can be discontinuous as a result of changing operating states in HVAC equipment, such as when a chiller, pump or fan is on or off. [Braun 1990] applied a direct search method to optimize equation (19), solving for zone temperature set points that minimize electric costs due to HVAC power consumption over a 24 hour period.

[Henze et al 1997] develops an optimal pre-cooling control algorithm for ice-storage active TES under time-of-use (TOU) electricity pricing with a simplified chiller that has only two operating states. These two chiller operating states are modeled using one electric input ratio (EIR or 1/COP) while the chiller is chilling water and one, separate, lower EIR while the chiller is generating ice. An optimization is performed to minimize cooling costs by adjusting the time and duration over which the chiller produces ice for later use, or produces chilled water for immediate use to meet cooling loads not supplied by discharging the ice-storage. Dynamic programming is employed for optimization, which can be applied to problems where states are uniquely defined and do not depend on the path taken to reach a given state, such as the amount of ice stored in an ice storage system.

In [Henze et al 2004], an optimal chiller control algorithm is developed to minimize cooling costs for passive and active TES combined under a dynamic utility rate structure. However, the problem is greatly simplified by assuming, again, a constant chiller COP or EIR for chilled water and ice-making operation, independent of outdoor temperature and supply air or zone air temperature. The problem is thus split into two separate optimizations: one in which zone air

temperature set points are optimized to minimize cooling load (where power consumption is assumed to be directly proportional to cooling load); and another in which an optimal charging and discharging schedule for active TES is determined to meet a total daily cooling calculated from the passive storage optimization. By separating the passive and active TES optimization problems and treating chiller performance as a constant, the passive TES optimization remains a linear problem in which zone temperatures are adjusted to minimize cooling load under an assumed active TES charging and discharging schedule. This allows for the application of a quasi-Newton optimization method to the passive TES problem, coupled with a dynamic programming optimization for the active TES problem.

[Snyder and Newell 1990] use a 2R1C building model to find optimal control strategies for cooling cost minimization through load shifting and demand limiting. However, the problem is reduced to three variables: the pre-cooling start time; the duration of time the zone is allowed to float until it reaches maximum allowed temperature; and the thermal mass temperature at the start of the occupied period.

[Chen 2001, Chen 2002] develop a predictive control algorithm to minimize cost or energy consumption of a radiant floor heating system. Similar to [Henze et al 2003], the efficiency of the heating plant is not weather dependent or dependent on past heating rates. As a result, the optimization problem remains linear in thermal loads and temperature response.

[Wang and Ma 2008] provides an overview of supervisory and optimal control methods for HVAC systems. It includes a review of optimization methods employed for supervisory or predictive HVAC control such as direct search, sequential quadratic, conjugate gradient, simulated annealing, genetic algorithm, and others.

Drawing from this past research, a framework for a pre-cooling control optimization will be developed that determines on optimal chiller control schedule for each hour, 24 hours-ahead, that pre-cools a concrete-core radiant floor/TES system to maintain thermal comfort later in the day.

5.2 LLCS pre-cooling control objective function

The goal of the LLCS control is to minimize cooling energy consumption (or cost) of the LLCS over a 24-hour period by controlling cooling rate in a near optimal way. This near-optimal control function incorporates the performance map model of chiller power consumption from chapter 3, the temperature-CRTF models of the zone being controlled from chapter 4, and thermal comfort conditions desired in the zone. The optimization function can be described mathematically as follows:

$$\text{(20)} \qquad \operatorname{argmin}_{\omega} J = \sum_{t=1}^{24} \left(r_t P_t + \varphi \mathrm{PENOPT}_t + \mathrm{PENEVT}_t \right)$$

In equation (20), the objective function J is the sum over 24 hours of the cooling system power consumption, a penalty for operative temperatures outside of the comfort range, and a penalty for evaporating temperatures below a low temperature threshold. The variables are as follows:

- r_t is a weighting factor for system power consumption. r_t can be set to one for an energy consumption minimization or to a TOU pricing schedule for cost minimization (not including demand charges),
- P_t is the energy consumption of the cooling system over the hour t,
- φ is a weighting factor for the operative temperature penalty,
- $PENOPT_t$ is a penalty function for operative temperatures outside of a desired comfort range at time t,
- $PENEVT_t$ is a penalty function for evaporating temperatures below a low temperature threshold, which has been included to prevent control predictions that would cause the chiller to freeze.

The power consumption P_t is a non-linear function derived from the heat pump curve-fit models in Chapter 3, given by the following equation:

(21) $$P_t = P_{t,chwpump} + P_{t,air\_cooled\_chiller}(OAT_t, EVT_t, \omega_t, f(OAT_t, EVT_t, \omega_t))$$

- P_{t,chw_pump} is the energy consumption of the chilled water pump over the hour t. The chilled water pump is operated at constant speed while the chiller is on. Thus, its power consumption is either zero if the chiller is off or a constant while running.
- $P_{t,air\_cooled\_chiller}$ is a curve-fit model of the air-cooled chiller power as a function of outdoor air temperature OAT, evaporation temperature EVT, compressor speed ω, and fan speed f at hour t.

The curve fit model for the air-cooled chiller is derived in the same way as the heat pump model from Chapter 2, except that the zone air temperature in equation (10) is replaced with the refrigerant evaporating temperature EVT as an independent variable. This curve-fit model is shown in equation (22) with the independent variables evaporating temperature EVT, outdoor air temperature OAT, compressor speed ω, and fan speed f. The RMSEs for this curve-fit model with evaporating temperature as an independent variable are 5.8 percent or 29 Watts, similar to the accuracies found in chapter 3 for the air-cooled heat pump.

(22) $$P_{t,air\_cooled\_chiller} = \begin{pmatrix} C_1 + C_2 EVT + C_3 OAT + C_4 \omega + \\ C_5 EVT^2 + C_6 OAT^2 + C_7 \omega^2 + C_8 EVT \cdot OAT + C_9 EVT\omega + C_{10} OAT\omega + \\ C_{11} EVT^3 + C_{12} OAT^3 + C_{13} \omega^3 + \\ C_{14} EVT^2 OAT + C_{15} EVT^2 \omega + C_{16} OAT^2 EVT + C_{17} OAT^2 \omega + \\ C_{18} \omega^2 EVT + C_{19} \omega^2 OAT + C_{20} EVT \cdot OAT\omega + \\ C_{21} f + C_{22} f^2 + C_{23} f \cdot EVT + C_{24} f \cdot OAT + C_{25} f\omega \end{pmatrix}_t$$

Similar models with the same form as equation (22) have been identified for cooling capacity $Q_{t,air\_cooled\_chiller}$ and electric input ratio $EIR_{t,air\_cooled\_chiller}$ as a function of EVT, OAT, ω, and f. The RMSE for those models are 1.5 percent or 31 Watts and 4.4 percent or 0.01 kW_e /kW_{th} respectively. The coefficients for each of these curve-fit models are shown in Appendix A.4. Only two of these three curves, the cooling $Q_{t,air\_cooled\_chiller}$ and the power consumption of the chiller $P_{t,air\_cooled\_chiller}$ are used in the pre-cooling optimization. The cooling rate $Q_{t,air\_cooled\_chiller}$ at each time step is need to compute zone temperature response, shown below, where QC(t) equals $Q_{t,air\_cooled\_chiller}$. The power consumption, $P_{t,air\_cooled\_chiller}$, is needed to compute the power at time t, P_t, in equations (20) and (21).

The fan speed variable can be eliminated from equation (22) by choosing the optimal fan speed for a given EVT, OAT, and ω. By taking a partial derivative of the $EIR_{t,air\_cooled\_chiller}$ curve with respect to f, the optimal fan speed f_{opt} is seen to be as follows:

$$f_{opt} = \left(C_{21} + C_{23}EVT + C_{24}OAT + C_{25}\omega\right) / 2C_{22} \tag{23}$$

The presence of EVT in equation (22) requires that evaporating temperature be predicted, based on engineering calculations or data-driven models, from the chilled water supply or return temperatures and the chilled water flow rate. For a fixed water flow rate, EVT can be related directly to one water temperature if the chiller is operated with constant superheat control for a given compressor speed. The chilled water return temperature (RWT) will be used to predict EVT. Under steady state operation, the superheated refrigerant vapor temperature at the evaporator outlet approaches RWT and a closed loop superheat control algorithm relates evaporator outlet temperature to evaporating temperature EVT as a constant temperature difference for a given compressor speed. This will be discussed in more detail in chapter 6. Thus, EVT can be estimated from RWT. A model for RWT was developed in chapter 4 as a function of cooling rate QC history, RWT history, and under-slab temperature (UST) history:

$$RWT(t) = \sum_{n=1}^{N} a_n RWT(t-n) + \sum_{n=0}^{N} b_n UST(t-n) + \sum_{n=0}^{N} c_n QC(t-n) \tag{24}$$

As explained in chapter 4, UST is calculated from a temperature CRTF model of the form:

$$UST(t) = \sum_{n=1}^{N} a_n UST(t-n) + \sum_{n=0}^{N} b_n OAT(t-n) + \sum_{n=0}^{N} c_n AAT(t-n) + \sum_{n=0}^{N} d_n QI(t-n) + \sum_{n=0}^{N} e_n QC(t-n) \tag{25}$$

In equation (25), OAT is the outdoor (climate chamber) air temperature, AAT is an adjacent zone temperature, QI is the internal heat load, and QC is the cooling rate. At a given time, the evaporating temperature EVT can be calculated from the current return water temperature and the chiller power consumption and cooling rate can be calculated from equation (22) and a similar equation for $Q_{t,air\_cooled\_chiller}$. At a future time t, UST and RWT must be predicted from previous (both measured and predicted from the current time to future time t) cooling rates, forecast outdoor temperature, adjacent zone temperature, and internal loads up to time t.

The second term in equation (20) accounts for the operative temperature of the zone. Without this term the minimal power consumption would equal zero at all times. The operative temperature penalty function is given by the following equation:

$$\text{(26)} \qquad PENOPT_t = \begin{cases} ((OPT_{min} + 0.5) - OPT_t)^2 & OPT_t \le OPT_{min} + 0.5 \\ 0 & OPT_{min} + 0.5 < OPT_t < OPT_{max} - 0.5 \\ (OPT_t - (OPT_{max} - 0.5))^2 & OPT_t \ge OPT_{max} + 0.5 \end{cases}$$

OPT is calculated from a temperature-CRTF identified in chapter 4 as follows:

$$\text{(27)} \qquad OPT(t) = \sum_{n=1}^{N} a_n OPT(t-n) + \sum_{n=0}^{N} b_n OAT(t-n) + \sum_{n=0}^{N} c_n AAT(t-n) + \sum_{n=0}^{N} d_n QI(t-n) + \sum_{n=0}^{N} e_n QC(t-n)$$

The weight φ in the operative temperature penalty function equates temperature excursions outside the comfort range to power consumption. A good choice of φ is one for which the amount of energy consumption added to the penalty function for a operative temperature excursion just outside the comfort bounds is greater than the energy consumption required to run the chiller to prevent that excursion. For example, under most conditions the air-cooled chiller consumes less than 180 to 220 Watts at the slowest compressor speed. A φ of 300 Watts/K^2 results in a lower cost function with the compressor on than off under most conditions if the operative temperature begins to drift more than 0.25 to 0.5 K outside of the comfort region. The operative temperature range is chosen to be roughly 19 to 25 Celsius based on the summer (or 0.5 clo) operative temperature comfort range presented in [ASHRAE 2007a]. A graph of the operative temperature penalty term $\varphi PENOPT_t$ is shown in Figure 44.

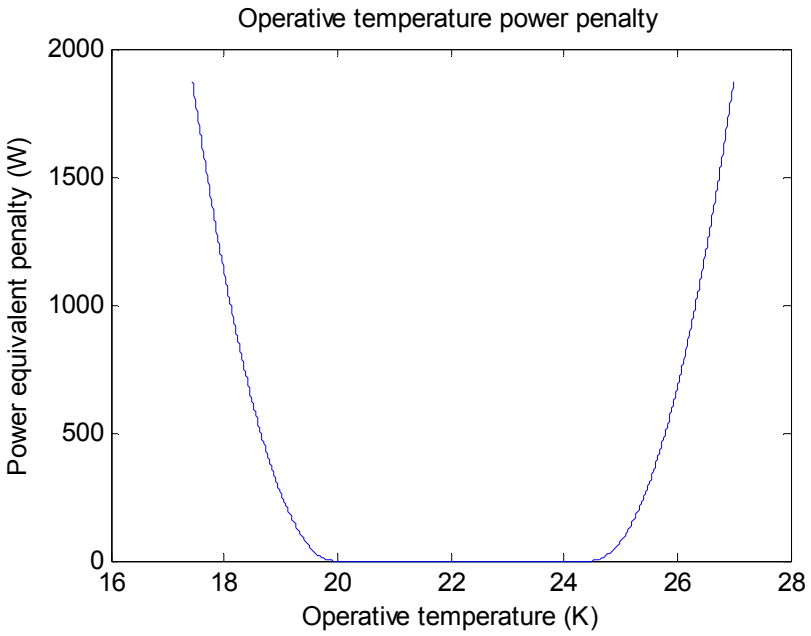

Figure 44 Operative temperature penalty term φPENOPT

The last term in the objective function, $PENEVT_t$ is a constraint on the evaporating temperature of the refrigerant EVT. EVT is constrained to prevent freezing of the chiller, or more precisely to prevent *predictions* of infeasible cooling rates at future time steps that would cause the chiller to freeze. The constraint on EVT was chosen conservatively to prevent EVT below one degree Celsius, with an infinite penalty for evaporating temperatures below the threshold (replaced by a very high penalty value in computer code). This choice was made to prevent any freezing, even if just locally on a heat exchanger surface, on the water-side of the chiller. The resulting evaporating temperature penalty function is as follows:

$$\text{(28)} \qquad PENEVT_t = \begin{cases} 0 & EVT(RWT_t) > 1 \\ INF & EVT(RWT_t) \le 1 \end{cases}$$

An alternative approach would be to apply the evaporating temperature constraint as a limitation on system operation. Penalizing the evaporating temperature in the objective function was convenient, because it eliminated the need to include additional constraints to the chiller curve-fit model. Furthermore, the OPT penalty function could have been incorporated as a constraint on operative temperatures. However, this approach does not allow for a simple tradeoff between comfortable temperatures and power consumption, which is useful for allowing some overheating as the optimization searches for the best chiller control schedule. If the OPT penalty was included as a constraint on OPT, or similarly if the weight φ for PENOPT was infinite, additional discontinuities in the search space would be introduced which would create many deep local minima at compressor speed schedules for which thermal comfort criteria was met.

5.3 LLCS pre-cooling control optimization

In the previous section, an objective function was defined for the pre-cooling control algorithm which contains penalties for power consumption of the cooling system, operative temperatures outside of a comfort region, and low evaporating temperatures. The goal of this section is describe how the objective function, equation (20) is minimized to optimize the chiller control over a 24 hour look ahead schedule.

Each hourly cost component of the objective function must be evaluated sequentially from hour one to 24. This is a result of the fact that P_t, $PENOPT_t$, and $PENEVT_t$ all depend on past values of both the independent and dependent variables. As the simulation moves into the future, the choice of compressor speed at simulation time t_{sim} depends on previous values of compressor speeds at times $t<t_{sim}$ and will affect the choice of future compressor speeds at times $t>t_{si,}$. A given compressor speed at time step t_{sim} will determine QC, and along with current outdoor air temperature OAT, adjacent zone air temperature AAT, and internal loads QI and their histories determine OPT, UST, RWT, and EVT at the next time step in the simulation.

The power consumption and cooling rate of the chiller are non-linear functions of OAT, EVT, and ω (with fan speed f_{opt} determined by these three variables). Consequently, the power consumption of the chiller at the current simulation time depends non-linearly both on the choice of compressor speed at the current time t_{sim} and previous choices of compressor speeds which determine the concrete slab temperature UST and EVT at t_{sim}. Furthermore, when the compressor speed is zero the cooling system is off and the power consumption and cooling rate become zero discontinuously, because the compressor cannot run at arbitrary speeds down to zero Hz.

As a result of these discontinuities and non-linearities in the objective function, an optimization method suitable for non-linear objective functions must be used. A simple form of direct search, called a pattern search was selected as an optimization method [Torczon 1997, Lewis et al 1999, Lewis et al 2000, Audit and Dennis 2003]. The pattern search seeks optimal compressor speeds for every hour t in a 24-hour-ahead schedule of chiller operation. Pattern search is essentially a grid search on the independent variable, where an initial guess is made and points in a grid around that guess are evaluated for a more optimal solution. Pattern search continues to search the grid until no more optimal solutions can be found, at which point it reduces the size of the grid and searches more locally around the optimal solution identified by the larger grid. What follow is a more detailed explanation of the pattern search algorithm employed in the experimental LLCS concrete-core radiant floor installation described in chapter 6.

As previously mentioned, the pattern search is essentially a grid search, where the grid size can change when more optimal solutions cannot be found using the current grid. Pattern search begins at an initial point in a grid that spans the entire search space. For this research, the search space is a 24-dimenstional space, where each dimension represents a possible chiller

compressor speed at each hour of a 24-hour-ahead schedule. The compressor speed at each hour can take the values of 0 Hz, or off, and anywhere between 19 Hz and 95 Hz. Some speeds will cause infinite penalties if the temperature-CRTF models determine that they will cause the chiller to freeze.

Beginning with a guess at an initial point in the 24-dimensional grid, pattern search evaluates the objective function at all of the grid points surrounding the initial guess. This is called a poll. All of these grid points are compared to identify the most optimal solution relative to each other and to the initial guess. If a more optimal grid point is identified, the pattern search continues by polling a grid around the new optimal solution. The grid size is increased, up to maximum selected by the user, each time a more optimal point in the grid is identified. If a more optimal grid point is not found, the pattern search continues around the current point with a smaller grid size, down to a minimum grid size. The pattern search continues searching the grid until no more optimal points can be found at the smallest grid size. For the pattern search implemented here, the starting grid size is 4 Hz, which is the difference between compressor speeds in each dimension of the 24-dimensional grid. The maximum grid size is four Hz and the minimum grid size is one Hz.

An optional step in a pattern search is the execution of a secondary optimization on the current grid point each time a new optimal solution is found around that point. Instead of immediately polling the grid around the new optimal solution, a search of the other dimensions of the grid (not the dimension in which a new optimal point has been found) is conducted to identify whether an even more optimal solution can be found. This allows the pattern search to perform faster, by moving in more than one-dimension of the grid at each iteration.

To summarize, pattern search is simply a grid search where the size of the grid changes. In its most basic implementation, pattern search starts with an initial guess in the grid, evaluates the objective function at all the adjacent grid points, proceeds to the most optimal point in the grid around the initial guess, then uses that new optimal point as the basis of a new pattern search. Adjusting the grid size and performing a secondary search on each grid point are simply methods for avoiding local minima and decreasing pattern search execution time.

A complete explanation of the pattern search algorithm is included Matlab's Global Optimization Toolbox: User's Guide [2010] and more information can be found in [Torczon 1997, Lewis et al 1999, Lewis et al 2000, Audit and Dennis 2003]. A flow chart of the pattern search implemented for the LLCS predictive pre-cooling control optimization is shown in Figure 46. This chart shows the process from the input, an initial guess of 24 compressor speeds at each hour of a 24-hour-ahead schedule, to the output, an optimal schedule of 24 compressor speeds. Each time the algorithm calls for the calculation of the objective function J in equation (20), equations (21) through (28) are applied to calculate the P_t, QC, OPT, UST, and RWT at each time step, from which the total value of J can be calculated by summing over all 24 future hours. Because a 30 minute temperature-CRTF model was elected for OPT, UST, and RWT in chapter 4, two values for each of these variables are calculated at every hour.

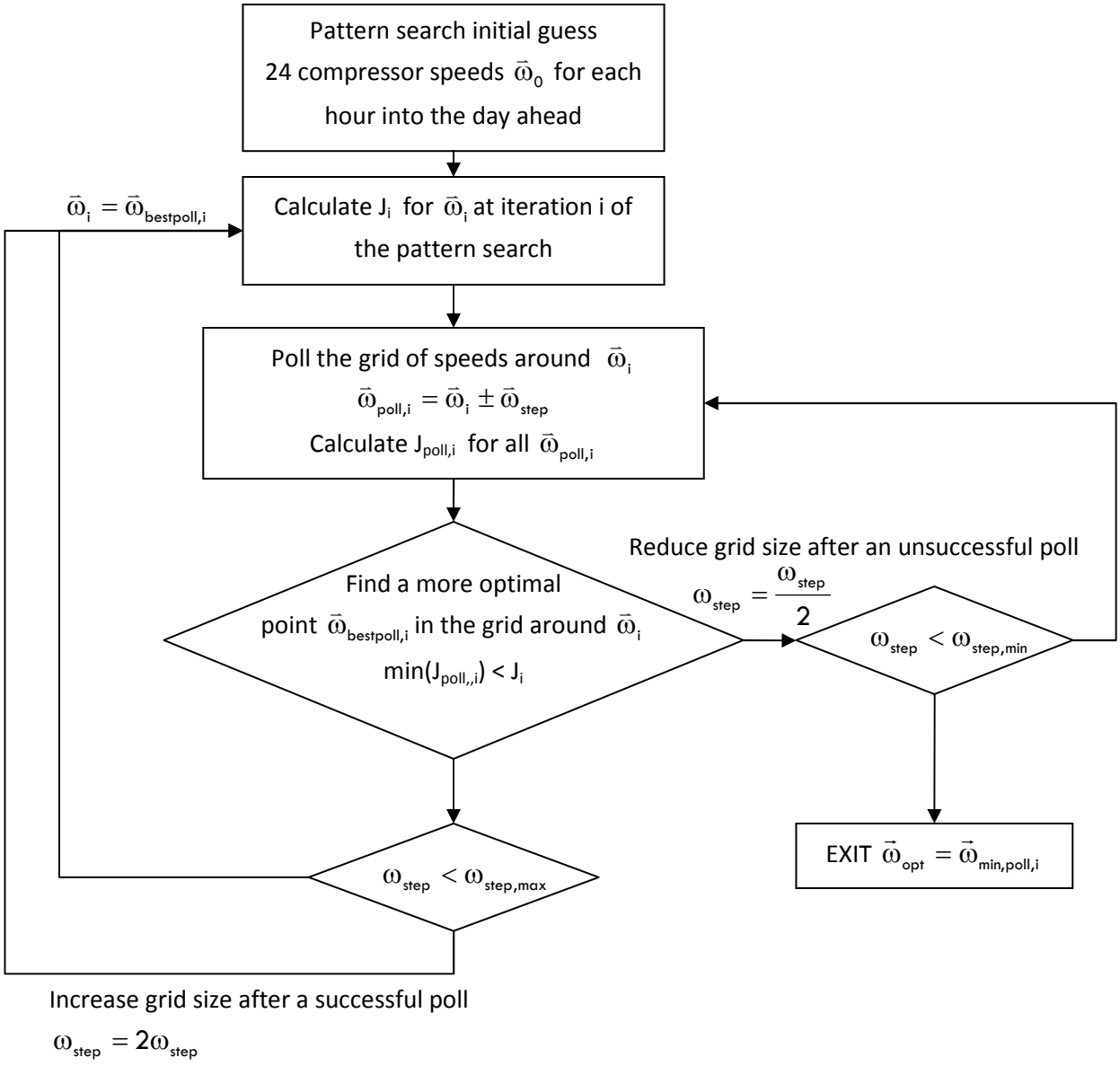

Figure 45 Pattern search optimization algorithm flow chart

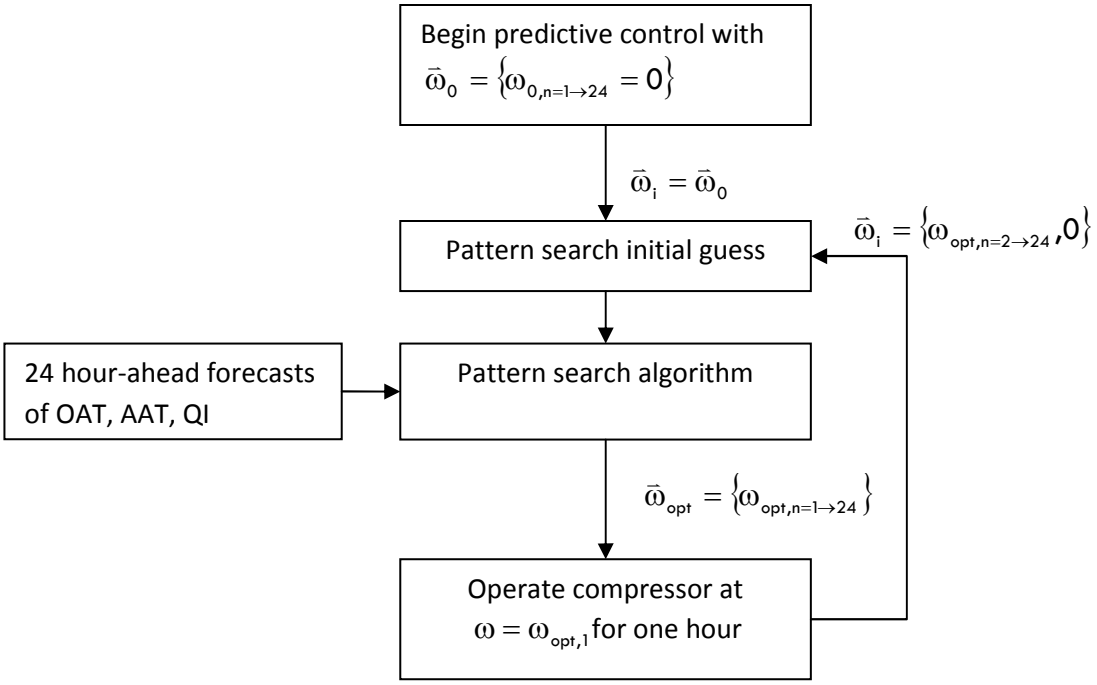

Figure 46 Closed loop optimization of compressor speed

The pattern search algorithm is employed at every hour to calculate a new set of optimal compressor speeds for the next 24 hours. This allows for the use of updated forecasts of outdoor air temperature OAT, adjacent zone air temperature AAT, and internal loads QI at each hour. Only the first compressor speed computed by the pattern search is used to set the compressor speed for the following hour. The remaining 23 compressor speeds are used as an initial guess for the new pattern search at the next hour, with the 24^{th} speed equal to zero. A new pattern search is then performed at the next hour to identify a new optimal set of 24 hour compressor speeds for the following 24 hours. This process is outlined in Figure 46. [Henze et al 2003] refers to this approach as closed loop optimization, where feedback from the previous time step (hour) and updated forecasts are used to determine a new optimal control schedule.

An alternative approach is consecutive time block optimization [Henze et al 2004], in which compressor speeds are predicted once at the beginning of a 24 hour time block. This approach is identical to closed loop optimization only in the case where model predictions and exogenous variable forecasts are perfect. In this research, although exogenous variables are being controlled, they are not being controlled perfectly and a closed loop optimization is more effective than consecutive time block optimization.

A sample result of the pattern search algorithm is shown in Figure 47. A predicted optimal compressor speed schedule, with a compressor speed for each of 24 hours into the future, is shown at the top schedule. For this schedule, the operative temperature OPT, underslab temperature UST, return water temperature RWT, evaporating temperature EVT, cooling rate QC, and chiller power consumption P are predicted for each half hour of the 24 hours ahead. At

the top right of Figure 47, the predicted OPT, UST, RWT, EVT for the 24 hour ahead period are shown along with the outdoor temperature OAT and the comfort constraint OPT_{max} and OPT_{min}. The chiller power at each time step and the cumulative energy consumption over the 24 hour period is shown at the bottom. The dependent variables are predicted at half hour increments because the temperature-CRTF models make predictions in half hour increments. For the hour following this optimization, the chiller is operated at the first predicted optimal compressor speed, which is 0 Hz, or off, in the case below.

The example below demonstrates certain important aspects of low-lift predictive pre-cooling control. First, the best time to perform most of the cooling is over night and during the early morning hours. The outdoor air temperature OAT is low and the chiller can run more efficiently. Second, the chiller runs at relatively low speed (19 Hz is its minimum) most of the time, and thus at low pressure ratios. Third, near the beginning of the scheduled operation of the compressor, at hours six, seven and eight, the compressor is scheduled to cycle on for an hour, then off for an hour, and then turn back on. The optimization has determined that it is more efficient not to run the compressor continuously for those three hours because it decrease UST, RWT, and most importantly EVT causing the chiller to run less efficiently at higher evaporating temperatures. Lastly, at the end of the scheduled pre-cooling the compressor turns off for an hour and then back on. This is the result of the evaporating temperature EVT approaching the low temperature threshold of one degree Celsius. The compressor is not allowed to run at hour 16 to prevent the chiller from freezing. This freezing constraint can be avoided by improving the design of the concrete-core radiant floor so that the difference between chilled water temperatures RWT and the concrete-core temperature UST is less.

The optimization is not especially sensitive to small changes in the compressor speed setpoint schedule. Adjusting the compressor speed by one Hz at a given hour will only marginally change the total energy consumption, by perhaps 10 to 50 Watt-hours or less than one percent of daily energy consumption. On the other hand, turning the compressor off for an hour or running it significantly faster may lead to a difference in energy consumption of a few hundred Watt-hours in the range of five to ten percent of daily energy consumption

Other optimization methods may be applicable to the LLCS predictive pre-cooling control problem and further research is necessary to evaluate the best optimization method for LLCS. For this research, however, pattern search was found to identify near-optimal solutions within a few minutes, whereas applying genetic algorithms or simulated annealing required hours of optimization time and did not always converge to a solution. Careful tuning and a comprehensive comparison of alternative optimization methods to the LLCS pre-cooling optimization problem may still yield a more appropriate optimization method than the pattern search employed here.

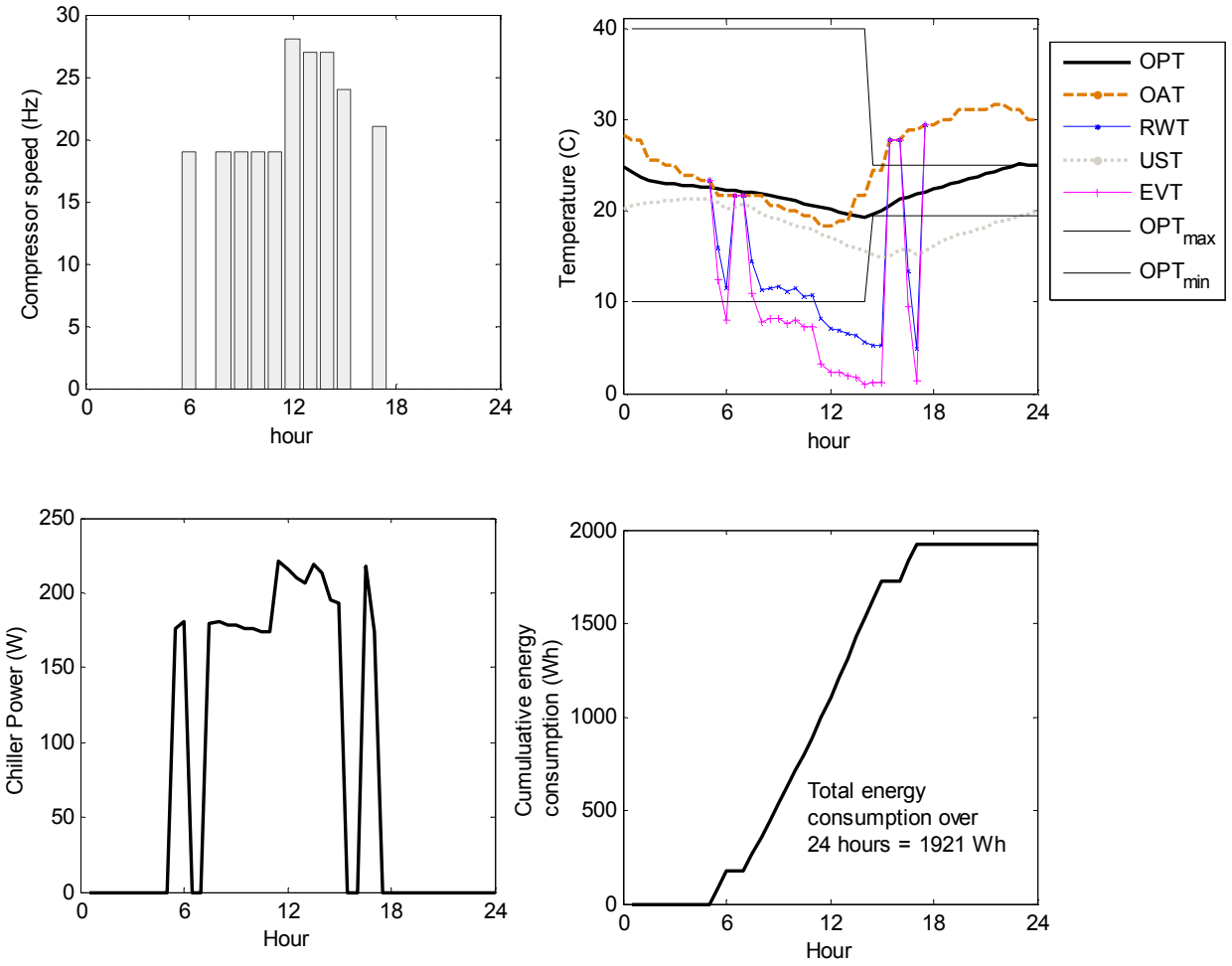

Figure 47 Sample pattern search results, including predicted OPT, RWT, and UST over a 24 hour look ahead (top left), cumulative energy consumption (top right), chiller power consumption at each half hour (bottom left), and predicted optimal compressor speed at each hour (bottom right)

Chapter 6 Low lift cooling experimental assessment

The primary objective of this thesis is to develop and *experimentally test* the performance of predictive pre-cooling control for low-lift cooling systems. To achieve this, a radiant concrete-core floor cooling system served by an air-cooled chiller was installed in the test chamber described in chapter 4. A concrete-core system was elected as the TES component of the LLCS because, in theory, it has high thermal storage efficiency. Furthermore, less research has been done on the coupling concrete- core system pre-cooling control and coupling with a predictive control of a chiller. Radiant concrete-core systems are also known as thermo-active building systems or TABS.

This chapter will describe the construction and performance of a concrete-core radiant floor cooling system (or TABS) in a near full scale experimental installation. This will include the design and installation of the system, instrumentation for measuring its performance, controls implemented for both local and supervisory predictive pre-cooling control, and installation of a split-system air conditioner (SSAC) used as a baseline. These two systems were tested subject to the same thermal inputs, a typical summer week for Atlanta, Georgia and typical standard efficiency internal loads. The energy and thermal comfort performance of the LLCS system will be compared to that of the SSAC under conventional thermostatic control.

6.1 Description of experimental systems

In order to test the performance of the LLCS, a near full-scale demonstration was constructed of a single-zone room served by an air-cooled chiller that provides chilled water to to a radiant concrete-core floor. This will be called the LLCS test chamber. The methods described in chapters 2 through 5 were applied to this system for predictive pre-cooling of the concrete floor. The LLCS test chamber allows for testing of an LLCS subject to different climates and under different loads. The system also enables comparison of LLCS energy consumption and thermal performance to a conventional, variable speed high-efficiency split-system air conditioner (SSAC) with a SEER rating of 16 Btu/Wh. The following sections will describe the cooling systems, the systems used to experimentally simulate climate and internal thermal loads, and the instrumentation installed for performance measurement and control.

6.1.1 Low-lift cooling system

The primary mechanical system for the demonstration LLCS is a variable capacity air-cooled chiller serving a concrete radiant floor. A Mitsubishi MUZ-A09NA-1 air conditioner/heat pump

outdoor unit, the same model characterized in chapter 3, was used to create the variable capacity chiller. The outdoor unit contains the compressor, condenser, condenser fan, expansion valve and electronics for the system. To chill water instead of cooling air, a separate refrigerant loop was created through a brazed plate heat exchanger (BPHX) between the stop valve exiting the expansion valve and the stop valve entering the compressor on the outdoor unit. The BPHX acts as a counter flow heat exchanger between the refrigerant loop and a water loop which serves the radiant floor. A schematic of the variable capacity chiller is shown in Figure 48 and a schematic of the water loop serving the concrete radiant floor is shown in Figure 49. Detailed information about the make and model of the equipment are shown in Appendix C.1.

Control over the compressor speed, condenser fan speed, and electronic expansion valve position was achieved through a manufacturer's interface to the Mitsubishi electronic control board. Serial commands from a desktop computer to this interface could adjust the compressor speed from 19 to 115 Hz, the condenser fan speed from 300 to 1200 RPM, and the expansion valve position from fully closed to fully open. The compressor speed and fan speed commands adjust the output from two separate inverters. The expansion valve commands control a stepper motor which moves the electronic expansion valve.

6. Low lift cooling experimental assessment

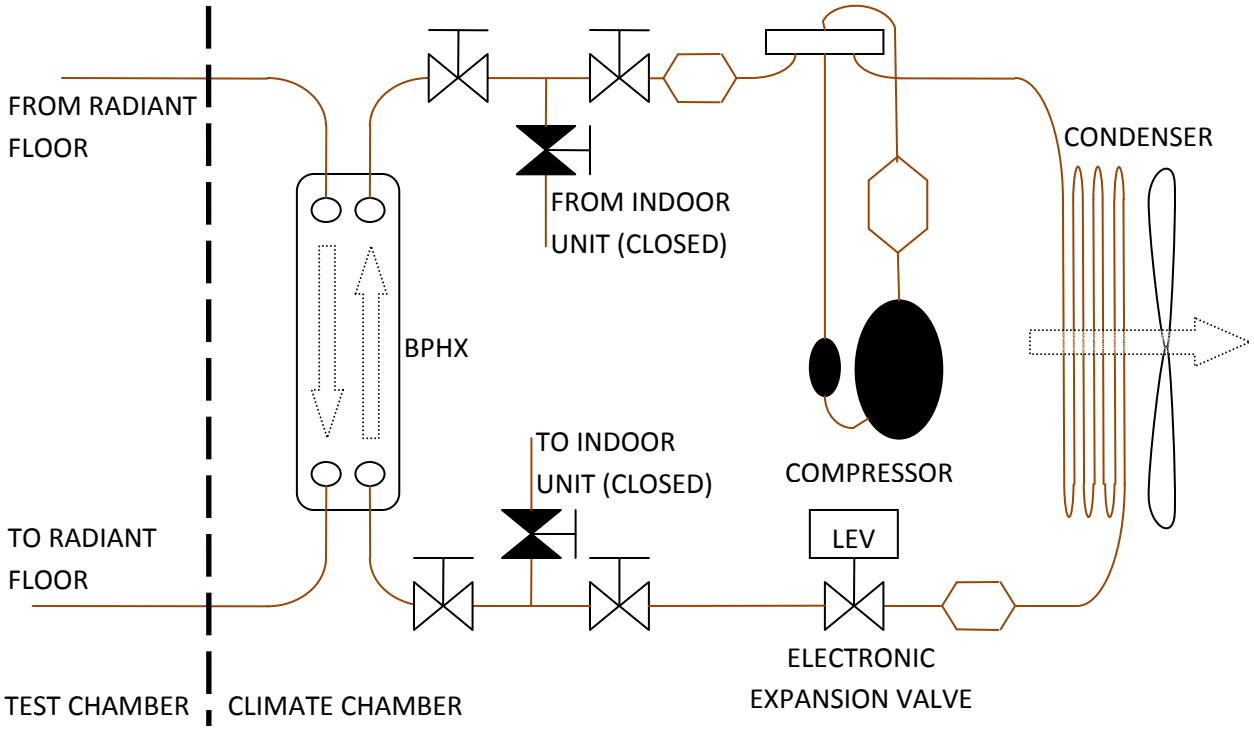

Figure 48 Low-lift cooling system: variable capacity chiller

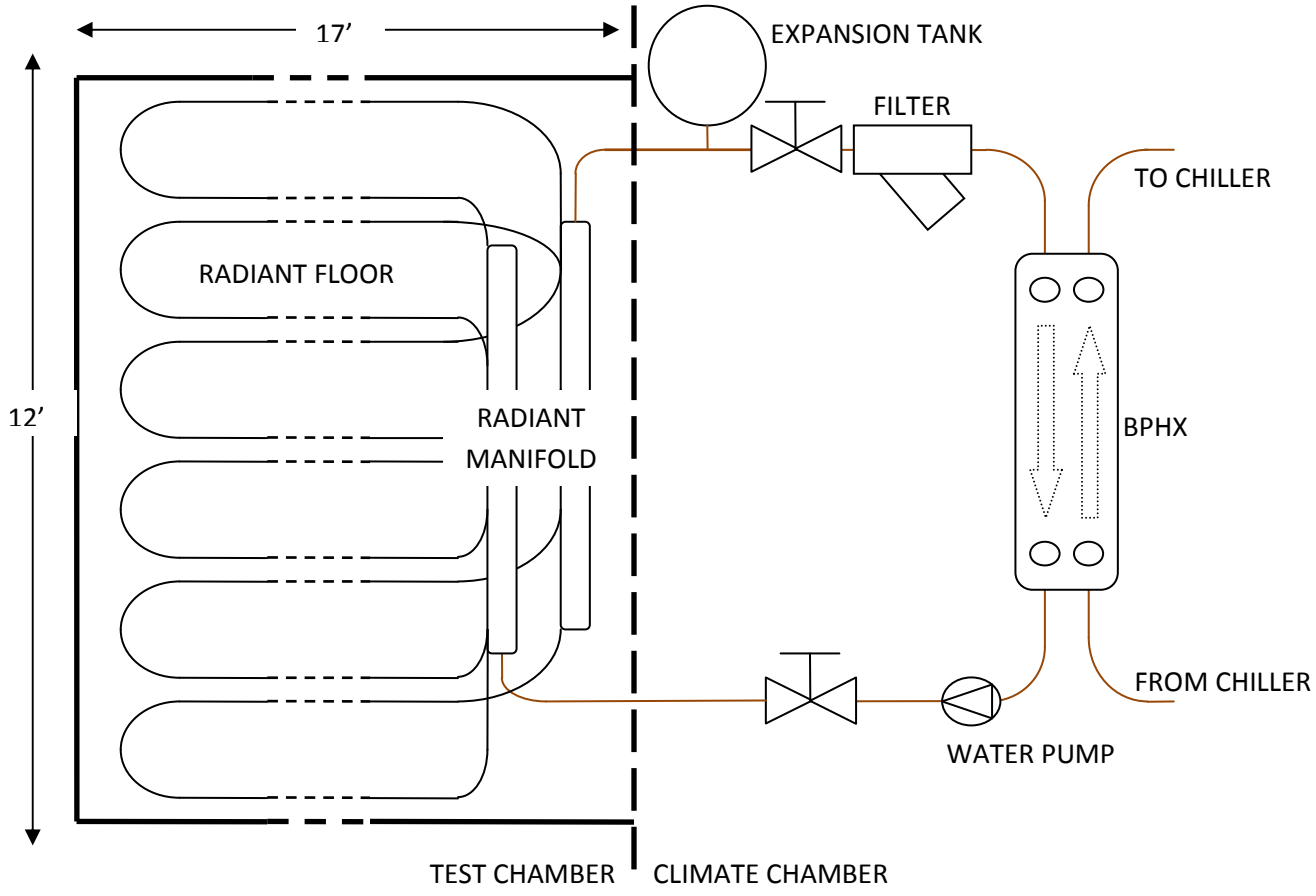

Figure 49 Low-lift cooling system: radiant floor water loop

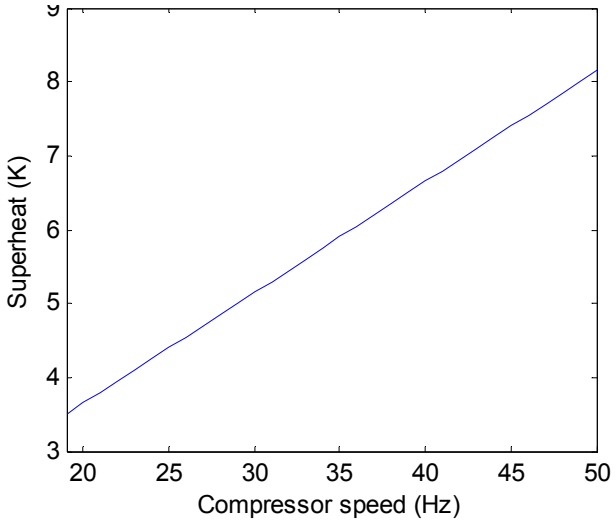

Figure 50 Superheat control set point vs compressor speed

Control over the expansion valve was customized for operation of the system as a chiller. A temperature difference provided by temperature sensors on the refrigerant inlet and outlet ports of the BPHX provided a measure of the refrigerant superheat across the BPHX evaporator. Constant superheat control could be implemented using this temperature difference. The superheat setpoint is a function of compressor speed, as shown in Figure 50. The superheat-compressor speed relationship was determined by observing the minimally stable superheat over a range of compressor speeds. The compressor speed was limited to less than 50 Hz under LLCS operation because higher speeds caused the BPHX temperatures to approach freezing rapidly. This limitation did not constrain LLCS chiller operation because the predictive control algorithm called for speeds below 50 Hz all of the time for the loads and climates tested, which will be described later. A proportional-integral-derivative (PID) control law was implemented for the electronic expansion valve to maintain constant superheat at a given compressor speed.

The radiant floor water loops in the schematic in Figure 49 lie embedded in Warmboard radiant subflooring underneath three layers of concrete pavers, as described in chapter 4. There are six parallel water loops each made of one half inch polyethylene (PEX) pipe. These six parallel loops were designed to minimize the pressure drop through the radiant floor and reduce pumping power. The pipes are spaced 12 inches apart center to center, with the aluminum surface of the Warmboard enhancing heat transfer between the pipe and bottom layer of the concrete layers. In a typical installation, the radiant loop piping would be more closely spaced (four to six inches) and embedded directly in poured concrete. However, pouring concrete was impractical in the lab setting in which the demonstration was built. Embedding pipe in Warmboard with an aluminum surface to enhance heat transfer to the concrete layer was a necessary compromise to mimic a poured concrete-core radiant floor.

The chilled water pump serving the radiant floor loops was operated at a constant speed of 2.1 gallons per minute (GPM). Ideally, an LLCS would include a variable speed chilled water pump which can be optimized to provide the highest COP under a given set of conditions. In this case,

because the chiller performance was measured as a function of compressor speed, condenser fan speed, outdoor temperature and evaporating temperature it was necessary to provide a simple relationship between water loop operation and the chiller evaporating temperature. The simplest method to achieve this was to operate the chilled water pump at a constant speed. This did not penalize chiller performance much because, even at the full speed of 2.1 GPM the specific pump power was very low, about 9 Watts per GPM, due to the low pressure drop across the radiant floor loops and the efficiency of the pump. The superheat set point as a function of compressor speed could be determined for fixed chilled water pump speed, and correspondingly the evaporating temperature EVT could be related directly to a return water temperature RWT.

Future research could test variable speed chilled water pumping by mapping the performance of the chiller, in terms of power, cooling capacity, and COP, as a function of chilled water pump speed in addition to compressor speed, condenser fan speed, outdoor air temperature, and evaporating temperature. More precisely the evaporating temperature could be replaced by two variables, chilled water pump speed/flowrate and return water temperature, both of which will affect evaporating temperature and subsequent chiller performance. This directly parallels the condenser side where outdoor air temperature and condenser fan speed relate to refrigerant condensing temperature. With this revised model of chiller performance the compressor speed, condenser fan speed, and chilled water pump speed can all be adjusted to optimize the performance of the chiller under 24-hour-ahead pre-cooling control [Armstrong et al 2009b].

Alternatively, a relationship between the chilled water distribution system operation and control and the evaporating temperature could be determined separately for any system served by the chiller. In that case, the chiller performance curves as a function of evaporating temperature could still be used with the predictive control algorithm, but a separate water distribution system model would be necessary to relate UST with the evaporating temperature of the chiller.

Although the chiller was constructed from a heat pump outdoor unit of the same model, Mitsubishi MUZ-A09NA-1, as that tested in chapter 3, it had slightly different performance curves. The new outdoor unit did not exhibit the exact same relationships between cooling rate QC, power consumption P, and electric input ratio EIR (or 1/COP) as the MUZ-A09NA-1 described in chapter 3. Modifications to the system for operation as an air-cooled chiller caused degradation in system performance. For a given set of conditions, the chiller was observed on average to achieve only 78 percent of the cooling rate predicted by the curve-fit model and measured previously while operated with an air-heated evaporator. With this reduced capacity, the power consumption also dropped to an average 89 percent of the model-predicted power consumption, and correspondingly the EIR increased, leading to a COP that was only 82 percent of the original outdoor unit's COP.

The reasons for this loss in performance are not entirely understood. Some differences in performance between the two outdoor units was expected because they contain different

parts, although they are of the same make and model. However, the magnitude of the differences in performance was larger than expected. Expectations were that the performance of the outdoor unit combined with the BPHX would be higher than that with the air-heated evaporator. The refrigerant-to-water counterflow BPHX should, in theory, be more effective than the cross-flow refrigerant-to-air finned tube heat exchanger. On the other hand, the finned tube heat exchanger has been designed by the manufacturer specifically for use with the MUZ-A09NA, whereas the BPHX has been generically matched to the outdoor unit's capacity. This may explain some of the difference in performance.

The observations of reduced capacity and efficiency may also relate to sub-optimal transient performance of the system. The performance models described in chapter 3 refer to the steady state power, cooling capacity, and 1/COP of the system, which is typically not reached until the system has been operating for over an hour. Furthermore, the curve-fit models of performance apply to the system when it is controlled for, approximately, a two to three Kelvin superheat across the air-heated evaporator for all compressor speeds. Under operation of the system with the BPHX a superheat of three Kelvin was only achievable at the slowest speeds. Superheat temperatures as high as six Kelvin were the lowest achievable for the highest compressor speeds. These higher superheats at high compressor speeds may cause some of the loss in capacity.

Data from which these observations were made are shown in Figure 51. Some of the spread in the data is a result of measurements being taken under transient operation and the chiller not reaching steady state. The cooling rate and power consumption predicted by the chiller model, equation (22), were scaled based on these results to ensure accurate prediction of cooling rate and power consumption for use in the temperature-CRTF models and the pre-cooling control optimization. It may be possible to get better performance out of the air-cooled chiller through better design of the BPHX and better expansion valve control. In theory, performance of the system with the BPHX should be at least as good as that of the air-heated evaporator.

Images of the chiller constructed from the modified Mitsubishi MUZ-A09NA-1 are shown in Figures 52-55. Figure 52 shows the condenser and condenser fan, housed in the original outdoor unit, along with the compressor and electronics which have been removed and heavily insulated at the bottom of the picture. The pre-insulation refrigerant and chilled water piping, including the branches that lead separately to the BPHX or to the air-side evaporator, are shown in Figure 53. The BPHX is located on the far left of the image. The chilled water flow meter and pump can be seen near the center and bottom of the image. Figure 54 shows the radiant floor system including the radiant floor manifold, the Warmboard subfloor, and the PEX pipe embedded in the Warmboard acting as the radiant floor chilled water loops. The six loops were balanced for equal flow using balancing valves on the radiant system manifold. The air-side evaporator served under conventional split-system air conditioner operation, described in the next section, is also shown. Figure 55 shows the completed LLCS test chamber with the concrete pavers installed.

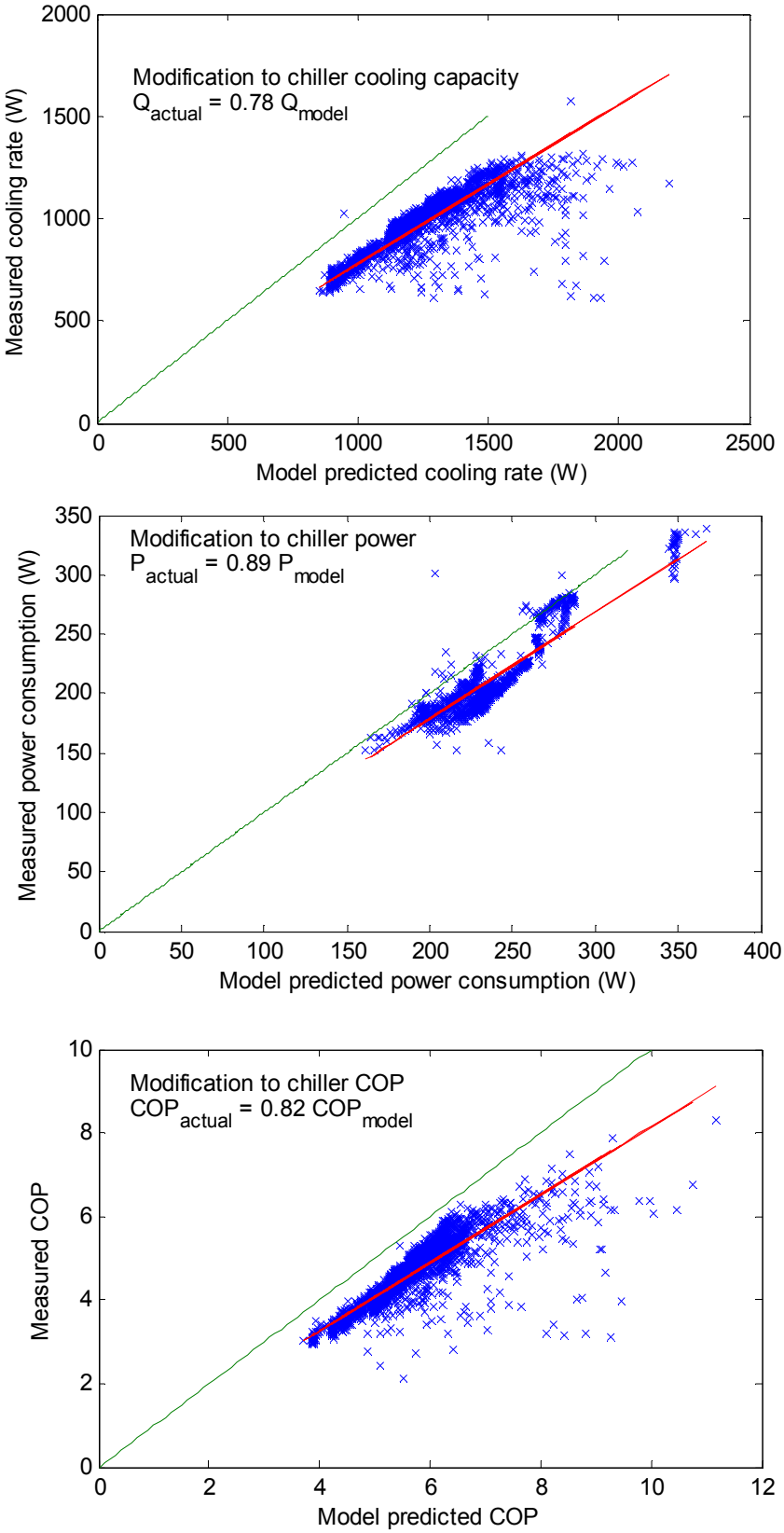

Figure 51 Offset in chiller capacity (top), power consumption (middle) and COP (bottom) for the modified chiller

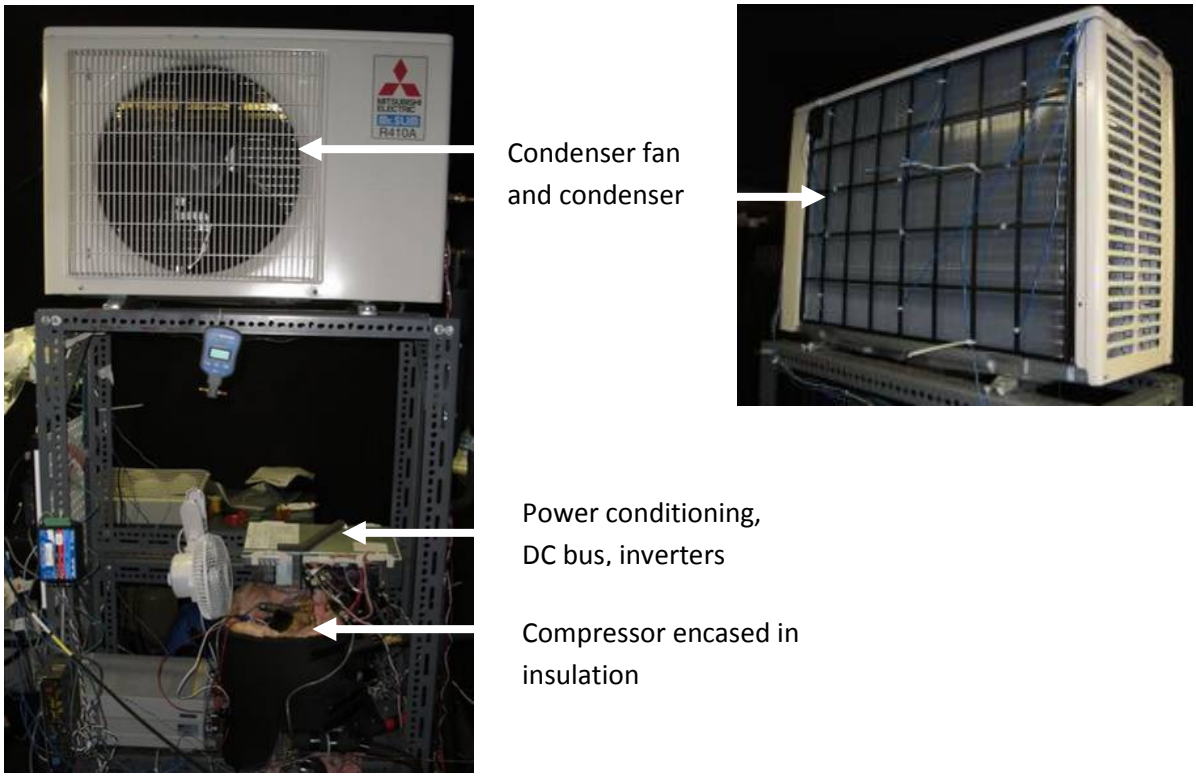

Figure 52 Condenser, condenser fan and compressor (normally the electronics, including the compressor inverter, is cooled by the condenser air stream)

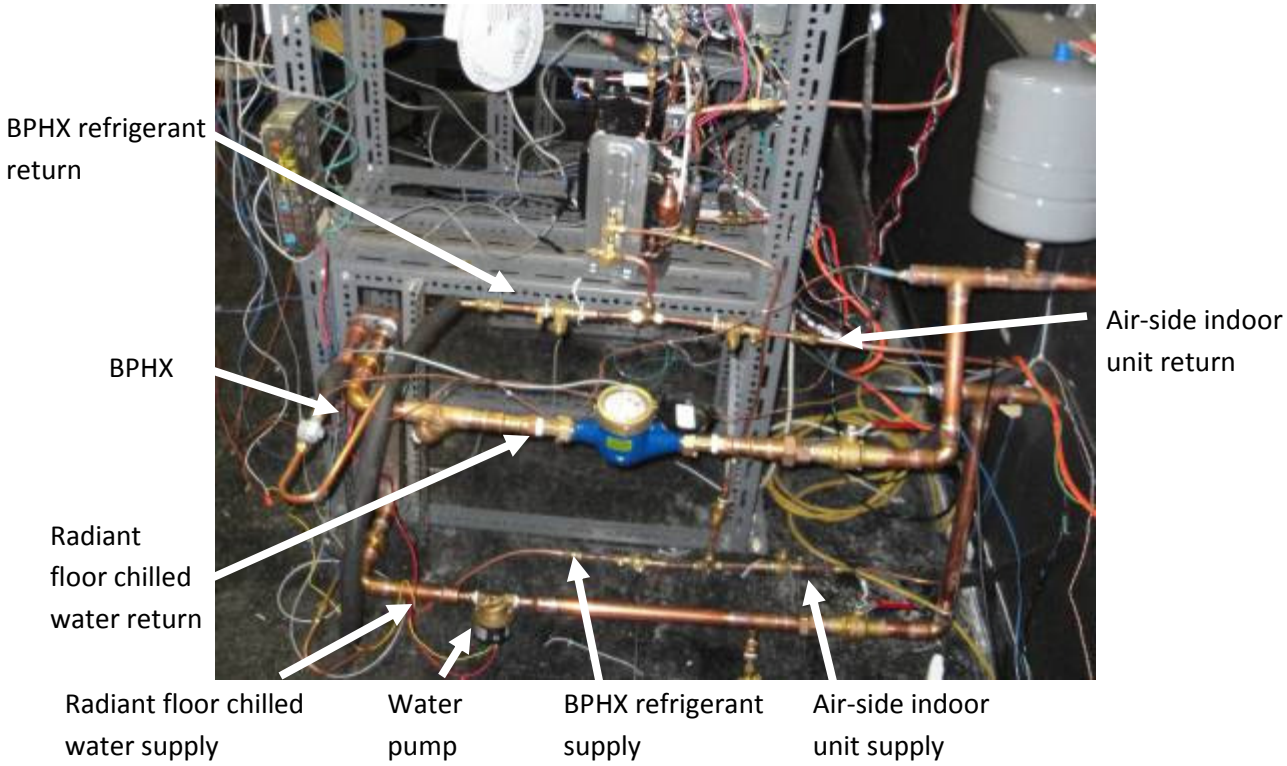

Figure 53 Two refrigerant loop branches serving the air -side indoor unit and the BPHX. The plant-side chilled water loop is also shown

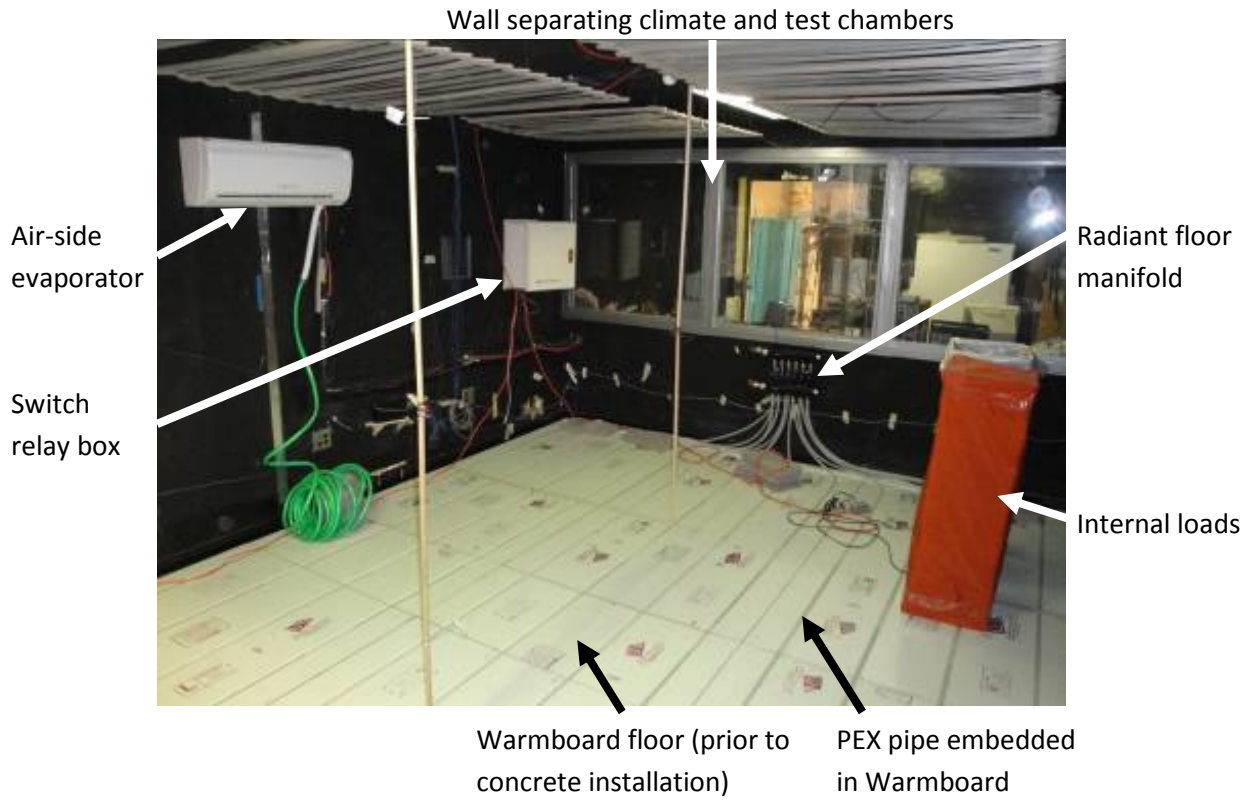

Figure 54 Chilled water loop distribution, including radiant floor manifold, PEX pipe loops, Warmboard sub-floor. The air-side indoor unit evaporator is also shown.

Figure 55 Complete LLCS radiant concrete-core floor test chamber

6.1.2 Conventional, variable capacity split-system air conditioner

A conventional split-system air conditioner (SSAC) was installed in the test chamber as a baseline comparison to the LLCS. This system consisted of an off-the-shelf Mitsubishi MUZ-A09NA-1 outdoor unit and an MSZ-A09NA indoor unit – an air-heated, finned-tube evaporator. The system is a high efficiency SSAC with a seasonal energy efficiency ratio (SEER) of 16 BTU/Wh [Mitsubishi 2006]. The same MUZ-A09NA-1 outdoor unit serves both the LLCS radiant concrete floor system and the conventional SSAC. This ensures that the performance of the two systems can be directly compared. The only differences between the systems are the evaporators and the controls. The SSAC used an air-heated evaporator, thermostatic control, and Mitsubishi's internal proprietary expansion valve, compressor speed and condenser fan speed controls. The LLCS uses a BPHX liquid evaporator, predictive pre-cooling control, and a constant superheat control over the expansion valve. All other components and aspects of the two systems are identical, including the variable speed compressor, variable speed condenser fan, their inverters and the corresponding efficiencies. Figure 56 shows the configuration of the SSAC. Under SSAC operation, the valves in the refrigerant lines serving the BPHX are closed and the valves to the air-heated evaporator are open.

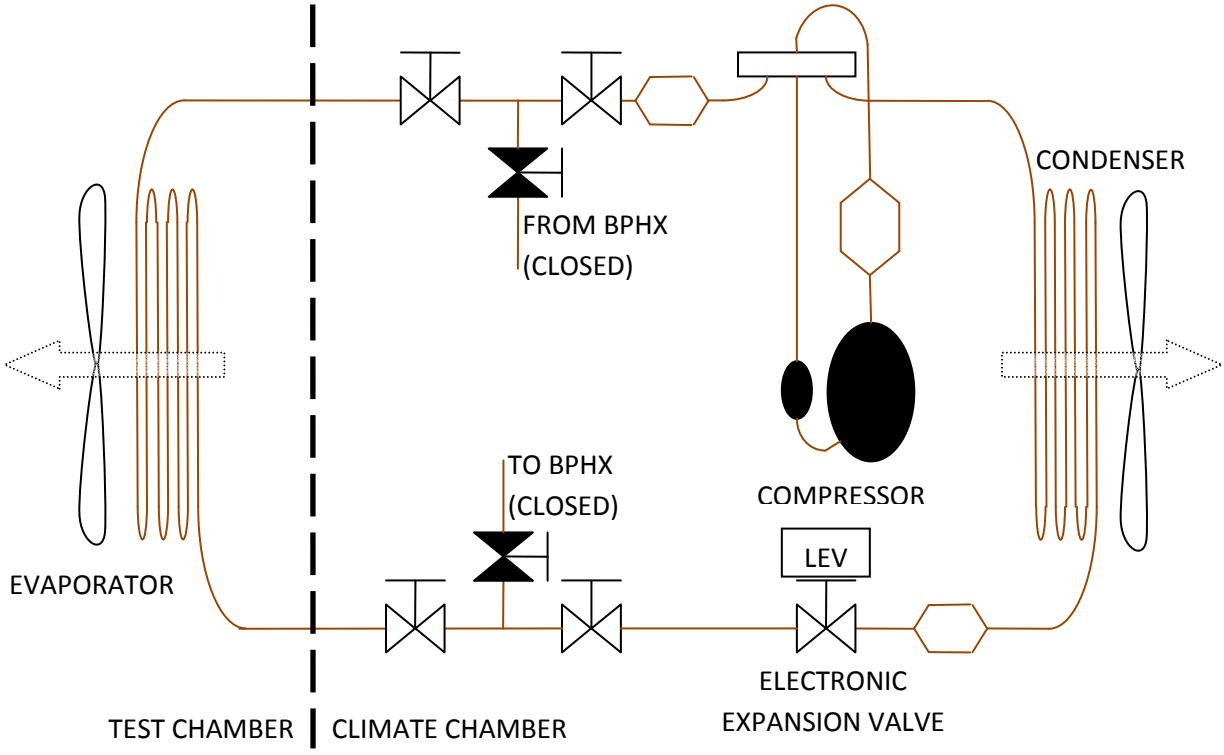

Figure 56 Split-system variable capacity air conditioner that uses the same outdoor unit as the LLCS

6.1.3 Thermal input systems: climate chamber and internal loads

Two other important systems for the LLCS test chamber include an HVAC system serving the climate chamber used to simulate outdoor temperature variations, and simulated internal thermal loads. These are described below.

The condenser (the same for both systems) is located in the climate chamber, adjacent to the test chamber, as described in chapter 4. The condenser air inlet temperature, a variable in the system performance, is equal to the climate chamber air temperature, the equivalent of outdoor air temperature (OAT) in the system models. To simulate the performance of the LLCS and SSAC in different climates, the climate chamber air temperature was controlled by a stand-alone constant volume HVAC system. A schematic of the climate chamber HVAC system from its Landis & Gyr control interface is shown in Appendix B.1.

This system controlled the return air temperature set point of air leaving the climate chamber. To ensure the return air temperature closely approximated climate chamber air temperature, fans were run continuously inside the climate chamber to mix the air. The return air temperature set point could be scheduled, through time-of-day schedules, to follow a desired hourly air temperature schedule. The control program for the climate chamber HVAC system was re-tuned to provide fast response to changes in climate temperature set point and disturbances, such as the chiller turning on and off and rejecting heat from the condenser. PID loops for the system cooling coil control valve, electric heating element, and supply air temperature set point were tuned to provide a stable response to disturbances within a few minutes. The control program for the climate chamber HVAC system, which was modified from an existing control program, is included in Appendix B.1.

Because it was impractical to perform year-long or even cooling season long tests of both systems, a choice of climate temperature control had to be made that would be representative of system performance over a period of time in a particular climate. Typical meteorological year (TMY) weather files are the standard for assessing building energy performance in a given climate. EnergyPlus weather (EPW) files are based on TMY data and supplemented with additional analysis. EnergyPlus contains a weather data conversion tool that can generate hourly weather data for a typical week over a selected period of time. This tool uses a heuristic, statistical method to compare the climate data statistics over the whole period to statistics of real, measured weeks within that period to identify a typical week [Crawley et al 1999].

Pre-processed data for seasonal typical and extreme weeks are included within EPW weather files for a given location, including typical weeks for summer (June-August), fall (September-November), winter (December-February) and spring (March-May). The EPW typical summer week for two climates was chosen as a basis for comparison of the LLCS to the split-system AC. The performance of the LLCS and SSAC was tested for the typical summer week in Atlanta, Georgia. The LLCS and SSAC will also be compared under a typical summer week for Phoenix, Arizona and possibly other climates, but this data is not yet available for publication. Testing in one climate requires two week-long tests, with a few days of advanced operation to achieve

steady-periodic temperature response, or one week for each combination of system and location. The climate chamber air temperature set points were taken directly from the EPW files for the typical summer week in Atlanta, Hartsfield-Jackson airport and Phoenix, Deer Valley airport. These week-long zone air temperature set points are shown in Figure 57.

For each of the two tests, programmed internal loads were placed inside the chamber to simulate sensible thermal loads from people, lights, and equipment. These thermal loads were constructed from incandescent light bulbs, in some cases installed inside opaque plastic enclosures. Two light bulbs were installed on the ceiling of the chamber to simulate lighting loads. One 75 Watt light bulb was placed in each of two opaque plastic enclosures to simulate the sensible thermal loads from two occupants. The bulbs were placed in the opaque plastic enclosure so that visible and near infrared light from the light bulb would be converted to infrared radiation and convective heat transferring from the surface of the enclosure. Light bulbs were placed in two additional plastic enclosures to simulate equipment loads. These enclosures were left open at the top to approximate a higher mix of convective load relative to radiative loads for electrical equipment. More information on these simulated internal loads is presented in Appendix B.1.

A ceiling fan was also installed in the chamber and measured as part of the internal loads. This fan was installed to create air movement inside the chamber and simulate the action of mixing created by the DOAS, equipment fans, and people moving around. It may be argued that this ceiling mixing fan should be considered as part of the LLCS because it causes air movement and improves the performance of the LLCS. On the other hand, an LLCS with a DOAS or with cooling from above may not need this ceiling mixing fan. The ceiling fan used for experiments was a very low efficiency fan, consuming around 30 Watts for as little as 200 CFM of flow. Because the fan should not be necessary for a typical radiant concrete-core cooling system, or TABS, its power consumption has not been included in the LLCS system power consumption. However, the fan is measured and counted as an internal load on the test chamber.

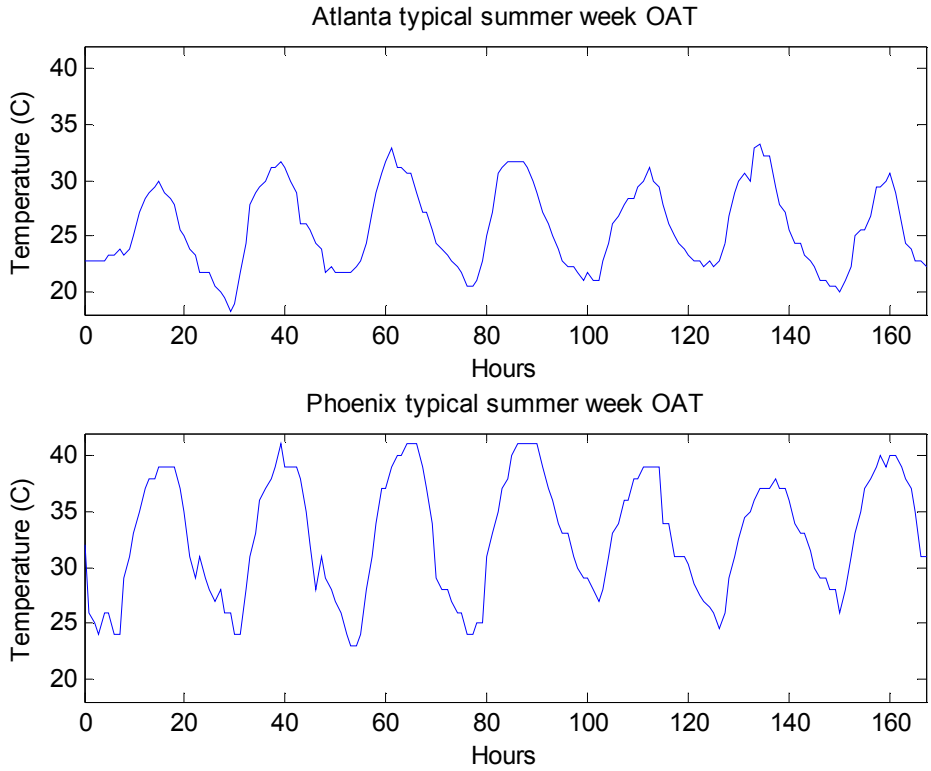

Figure 57 Typical summer week hourly outdoor air temperature (OAT) schedule for Atlanta and Phoenix

Two different types of internal load schedules were considered for testing, standard efficiency loads and high-efficiency loads. The equipment and lighting loads were selected based on the loads used in [Armstrong et al 2009b], and the occupant associated loads were chosen based on an assumption of two occupants with only sensible loads included. Light bulbs with different power consumption were installed in each of the three types of loads to create these two load schedules. Table 6 shows the break-down of internal loads by type - occupants, lighting and equipment - and the load densities. The loads are programmed such that at 8:00 am one occupant load, the lighting load, and half the equipment loads turn on, at 9:00 am all the loads turn on, at 5:00 pm one occupant load and half the equipment loads turn off, and at 6:00 pm all the loads turn off until the next day. Over weekends, the loads remain off. This schedule is meant to simulate a typical office weekly occupancy schedule in which two employees share the office, one arrives at 8:00 am and departs at 5:00 pm, one arrives at 9:00 am and departs at 6:00 pm, and both stay home on the weekends. The simulated internal loads are shown in Figure 58. The weekday load schedules for both the high efficiency and standard efficiency loads are shown in Figure 59.

Table 6 Internal load distribution and density

Load	Standard efficiency (W)	Standard efficiency (W/sqft)	High efficiency (W)	High efficiency (W/sqft)
2 People	160	0.8	160	0.8
Lights	220	1.1	120	0.6
Equipment	300	1.5	120	0.6

Figure 58 Lighting, simulated equipment and occupant loads

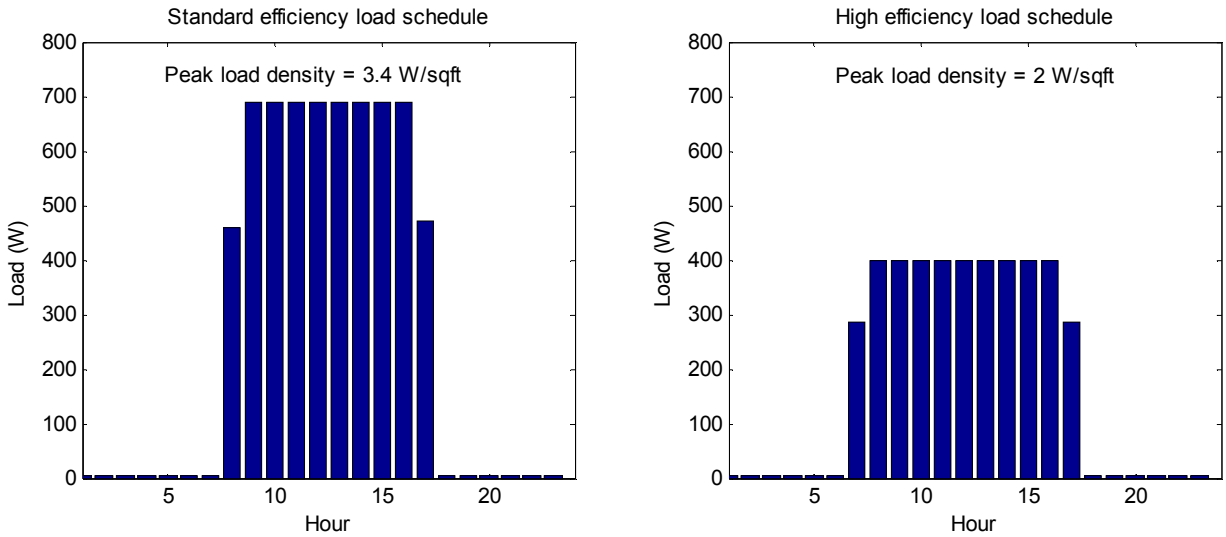

Figure 59 Internal load schedule for standard efficiency and high efficiency loads

The standard efficiency internal load schedule was applied to the tests for Atlanta climate conditions. This choice was made in part to match the capacity of the chiller, which is oversized for the LLCS test chamber when subjected to the high efficiency load schedule and the Atlanta typical summer week. The high efficiency internal load schedule will be applied to future testing under Phoenix climate conditions. For standard efficiency internal loads under Phoenix conditions the cooling capacity of the radiant floor – particularly the thermal storage capacity of the concrete slab – is undersized for the total thermal load. Working within the constraints of the installed systems and their capacities, comparative testing of the LLCS and SSAC was performed subject to Atlanta typical summer week climate conditions with standard efficiency internal loads.

There are two other important thermal inputs to the experimental system. First, the air temperature in the adjacent zone, referred to as AAT in chapters 4 and 5, also effects the zone temperature response. The adjacent zone refers to the laboratory in which the LLCS test chamber and climate chamber is built. The AAT was maintained around a constant 23 Celsius during the duration of the tests. This was done to ensure that the dominant heat transfer occurred between the test chamber zone and the climate chamber zone, and not the laboratory or adjacent zone. The heavily insulated surfaces separating the adjacent zone from the test chamber zone and the very low temperature differences between the zones limited the impact of the adjacent zone on the testing.

The second important thermal consideration is the relative humidity inside the test chamber. The radiant concrete floor cooling system is intended only to perform sensible cooling within the context of LLCS. A separate DOAS, as described in chapter 2, is necessary to perform latent cooling. Consequently, the experiments required that the relative humidity inside the chamber be kept as low as possible, with the dewpoint temperature well-below any surface temperature, to prevent latent cooling from occurring. The air inside the climate chamber and the air in the adjacent zone were continuously dehumidified to prevent moisture from entering the test chamber. No sources of moisture were present inside the chamber. This limited the amount of latent cooling that occurred. However, dewpoint temperature occasionally rose above certain surface temperature for both the LLCS and the SSAC, and both systems performed some latent cooling during testing.

For the SSAC, the condensate was collected and measured to account for latent cooling. After testing, the average measured COP of the unit from the test and the heat of vaporization of water was used to convert the mass of condensate water into an estimate of the SSAC energy consumption for latent cooling. Energy performance comparisons of the LLCS and SSAC will be made for the two systems with and without deducting this latent energy consumption from the SSAC energy consumption. Because the LLCS most likely performed some uncontrolled latent cooling as well, though immeasurable, it is not clear whether it is more fair for comparison to deduct the SSAC latent cooling energy consumption or not. Both approaches will be presented.

6.1.4 Performance measurement and instrumentation

Extensive monitoring equipment was installed on the experimental systems to measure thermal comfort and energy performance. The primary goal of these measurements was to compare the energy consumption and efficiency of the LLCS to the SSAC under the same set of thermal inputs. A secondary goal was to generate further data for improved physical modeling of variable capacity chillers and chiller components under low-lift conditions. The instrumentation for measurements on the systems is shown on the next page in Figure 61 and described in Table 7. Further details on the LLCS system instrumentation are presented in Appendix C.3.

The key measurements for comparing the performance of the systems include their total power consumption (P), the cooling rate (QC), the test chamber operative temperature (OPT), the climate chamber outdoor air temperature (OAT), and the internal load heat rate (QI). Additional important measurements, for control, are the adjacent zone air temperature (AAT), under-slab temperature (UST), return water temperature (RWT), evaporating temperature (EVT), and the superheat.

The power consumption of the LLCS was measured through Wattnode power meters on the outdoor unit, which includes power consumption of the compressor, condenser fan, and any electronics, and separately on the chilled water pump. Under SSAC operation, the Wattnode on the outdoor unit also measured the power consumption of the evaporator fan on the indoor unit.

Cooling rate for both systems was calculated from measurements of refrigerant mass flow rate and enthalpies on each side of the evaporators. A Coriolis mass flowmeter was installed on the condenser liquid line. Temperature and pressure measurements in the liquid and suctions lines were used to calculate enthalpies for whichever evaporator was in operation. On the LLCS, cooling rate was also calculated from a chilled water flow rate measurement and chilled water supply and return measurements. A comparison of these two measurements for the chiller under LLCS operation is shown in Figure 60.

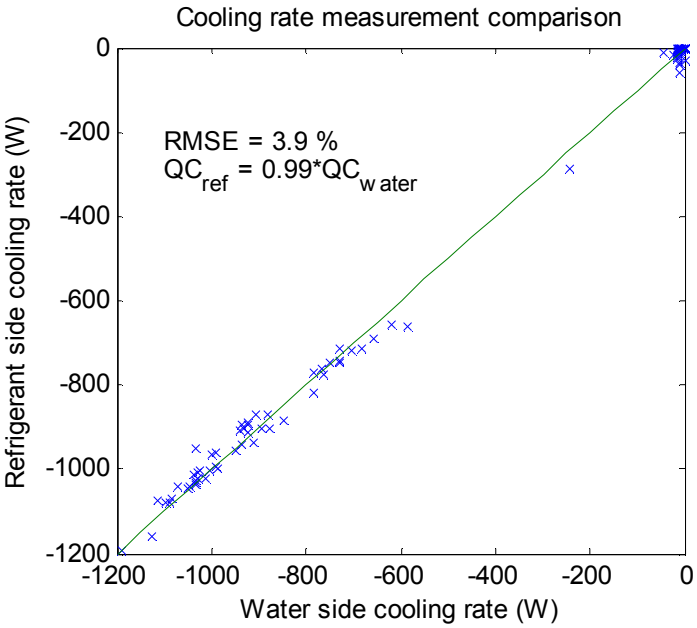

Figure 60 Comparison of refrigerant side and chilled water side cooling rate measurement CHANGE RMSE to CV-RMSE

6. Low lift cooling experimental assessment

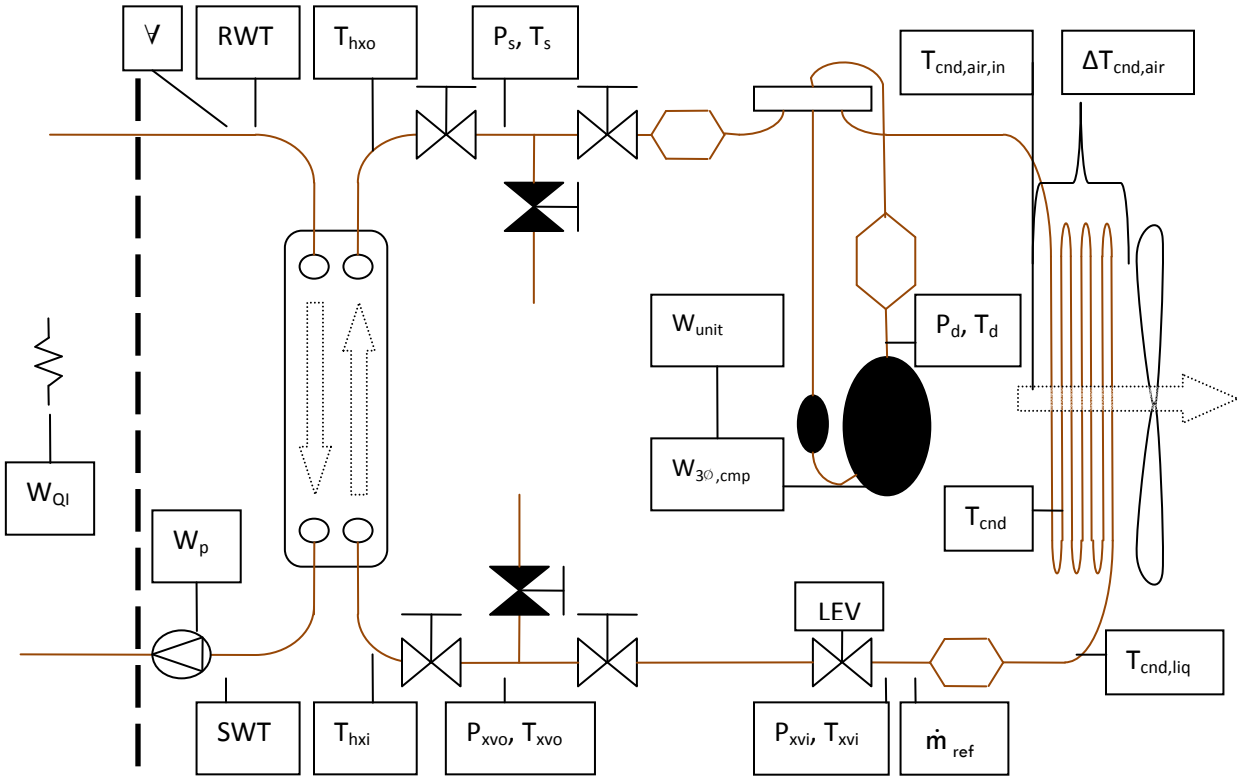

Figure 61 Low lift chiller system performance measurement instrumentation

Table 7 Low lift chiller system sensor labels

Label	Sensor description
T_s	Suction refrigerant temperature
T_d	Discharge refrigerant temperature
T_{cnd}	Refrigerant condensing temperature
$T_{cnd,liq}$	Condenser outlet liquid refrigerant temperature
T_{xvi}	Expansion valve inlet refrigerant temperature
T_{xvo}	Expansion valve outlet refrigerant temperature
T_{hxi}	Brazed plate heat exchanger inlet refrigerant temperature
T_{hxo}	Brazed plate heat exchanger outlet refrigerant temperature
$T_{cnd,air,in}$	Condenser inlet air temperature
T_{evp}	Refrigerant evaporating temperature (not shown, installed on indoor unit of split-system)
$\Delta T_{cnd,air}$	Condenser air temperature difference
P_s	Suction refrigerant pressure
P_d	Discharge refrigerant pressure
P_{xvi}	Expansion valve inlet refrigerant pressure
P_{xvo}	Expansion valve outlet refrigerant pressure
$\dot{m}_{ref}$	Refrigerant mass flowrate
W_{unit}	Total power to the outdoor unit, including inverters, condenser fan and compressor
$W_{3\varnothing,cmp}$	Three phase power from the inverter to the compressor
RWT	Chilled water return temperature
SWT	Chilled water supply temperature
∀	Chilled water volumetric flowrate
W_{QI}	Total power to the internal loads
W_p	Total power to the chilled water pump

The temperature measurements for the LLCS test chamber, including OPT, OAT, AAT, and UST were made using the same surface and air temperature measurements described in Chapter 4 and shown in Figure 29. For an installation in an occupied building, a globe temperature measurement may be substituted for the multiple air and surface temperature measurements as an approximation to OPT. However, for purposes of accurate and fair comparison of thermal performance, extensive monitoring of air and surface temperatures was performed for this research. A separate Wattnode power meter was used to measure the power consumption and thus heat dissipated by the simulated loads from people, lights and equipment.

Additional temperature sensors on the chilled water loop and the evaporator provided measurements of RWT and EVT. The refrigerant temperature at the inlet and outlet of the BPHX was measured from which the refrigerant superheat could be calculated for controlling the electronic expansion valve. Four pairs of pressure and temperatures at each of the key vapor compression cycle points were measured, at the suction port, discharge port, expansion valve inlet, and expansion valve outlet. Additional measurements included the refrigerant condensing and evaporating temperatures at the midpoints of the corresponding heat exchangers, three phase power consumption of the rolling-piston compressor, condenser air temperature, condenser air temperature difference, and evaporator inlet air temperature and humidity. The compressor speed, condenser fan speed, and expansion valve positions were set, and thus known, through the control system for the LLCS.

6.2 LLCS testing procedure

The following process was executed to generate performance data for the LLCS and the SSAC from which to compare energy consumption and thermal performance:

1. The outdoor climate chamber was continuously controlled to achieve an hourly air temperature schedule defined by a typical summer week for a selected climate as shown in Figure 57.

2. The internal loads were programmed to follow one of the daily load profiles shown in Figure 59 during weekdays. The internal loads remained off during the weekends.

3. The LLCS radiant concrete floor cooling system was operated for one week, including one weekend, after a three day initialization period. It was programmed to maintain operative temperature between 19.5 and 25 Fahrenheit, based on [ASHRAE 2007a] during an occupied period from 8:00 am to 6:00 pm. This required the following steps:

    a. A Matlab script implementing the predictive pre-cooling optimization algorithms shown in Figures 45 and 46 was initiated.

    b. At every hour, a pattern search predicted the near-optimal compressor speed and condenser fan speed schedules for the next 24 hours and set the

compressor speed and condenser fan speed to the optimal set point for the first hour.

c. The chilled water pump operated at a constant speed any time the compressor and condenser fan were running, otherwise it was shut off.

d. The predictive pre-cooling control of the LLCS radiant concrete floor cooling system was run for at least three days prior to gathering test data for comparison. This allowed the system to achieve a steady-periodic temperature response.

e. LLCS test data was gathered for one week. Data was recorded at one minute intervals for all of the sensors described in chapters 4 and 6. The week spanned a complete weekend so that the test included the energy required to cool down the concrete floor after a weekend of floating up to a higher temperature.

4. After completion of the LLCS test, the test chamber was allowed to achieve thermal equilibrium prior to conducting SSAC tests. Particularly, concrete temperatures were allowed to return to equilibrium with the zone air temperatures.

5. The refrigerant charge was balanced by observing the state of the refrigerant exiting the condenser into a receiver through two sight glasses. The valves on the entering side of the evaporator were left open, allowing refrigerant to be drawn from the other system, until the bottom of the receiver filled with liquid and the top of the receiver remained all or partially vapor over a wide range of compressor speeds. Thus, both systems operated under near zero sub-cooling for most compressor speeds.

6. The SSAC was operated for one week after an initialization period to achieve steady-periodic temperature response. The system was controlled to meet an average air temperature equal to the average operative temperature achieved by the LLCS for each corresponding day of operation. The off-the-shelf system could not be controlled to achieve operative temperature, because it operating under thermostatic control relative to its on-board air temperature sensor. However, the operative temperatures were compared after testing to ensure that a consistent level of comfort, based on daily mean operative temperature, was achieved in both cases.

This procedure was followed to test the LLCS and the SSAC under Atlanta typical summer week climate conditions with standard efficiency internal loads. In the near future, the systems will be tested under Phoenix typical summer week conditions with high efficiency internal loads. These two tests were chosen to sample the range of conditions under which LLCS may be applied and to provide appropriate thermal loads relative to the capacity of the systems. More testing will be performed with the chamber in future research.

6.3 LLCS energy and thermal performance assessment

This section will compare the sensible cooling energy and thermal comfort performance of the LLCS with predictive pre-cooling control to an SSAC subjected to the experimental tests described in section 6.1 and 6.2. As explained in chapter 2, simulations suggest that total cooling energy savings of LLCS, including sensible and latent cooling energy, relative to DOE benchmark building systems typically average around 60 percent of the total cooling energy consumption for medium office buildings.

The tests conducted for this research only investigate the *sensible* cooling energy savings provided by predictive control of the chiller pre-cooling the concrete radiant floor. The savings due to de-coupling of latent and sensible loads and more efficient dehumidification have not been investigated. Estimated latent cooling savings for an efficient DOAS vary by climate and building type. Mumma and Shank [2001] estimated only an 11 percent latent cooling energy savings per unit of outside air for a DOAS with enthalpy recovery and a run around heat exchanger relative to a conventional VAV system in Atlanta. However, they did not include (and noted it) that DOAS typically reduce outdoor air requirements relative to a VAV system. More research is necessary to evaluate potential latent cooling energy savings for different configurations of DOAS and dehumidification systems in combination with LLCS, by building and by climate.

The base line SSAC system to which the LLCS is compared is most similar to the VAV system with a variable speed chiller in [Armstrong et al 2009b, Katipamula et al 2010]. However, the VAV system from [Katipamula et al 2010] included an air-side economizer and larger specific fan power than the SSAC. In addition, the LLCS included a refrigerant side economizer, ideal TES, and a different chiller performance map.

Figures 62 and 63 show the results of testing the LLCS and the SSAC under Atlanta typical summer week climate conditions subject to standard efficiency internal loads. The figures show the temperature response, including outdoor air temperature (OAT), adjacent zone air temperature (AAT), operative temperature (OPT), under-slab temperature (UST) and return water temperature (RWT). Also shown are the internal load heat rate (QI), system cooling rate (QC), and system power (P).

In Figure 62, it may be observed that the LLCS runs for more hours but at lower power consumption, and in advance of the occupied period, than the SSAC, as shown in Figure 63. This is a key characteristic of low lift cooling. The cooling load is spread out over time and cooling is delivered to TES in advance, allowing the chiller to run at lower speeds and over night when lower condensing temperatures are possible. The displayed cooling rate under SSAC operation is not perfectly accurate. The cooling rate measurement does not include cooling during transient conditions, which are significant, because the refrigerant mass flow rate used for calculating QC was not measureable during transient conditions. This is a typical problem caused by two phase flow through the Coriolis mass flow meter used to measure mass flow rate.

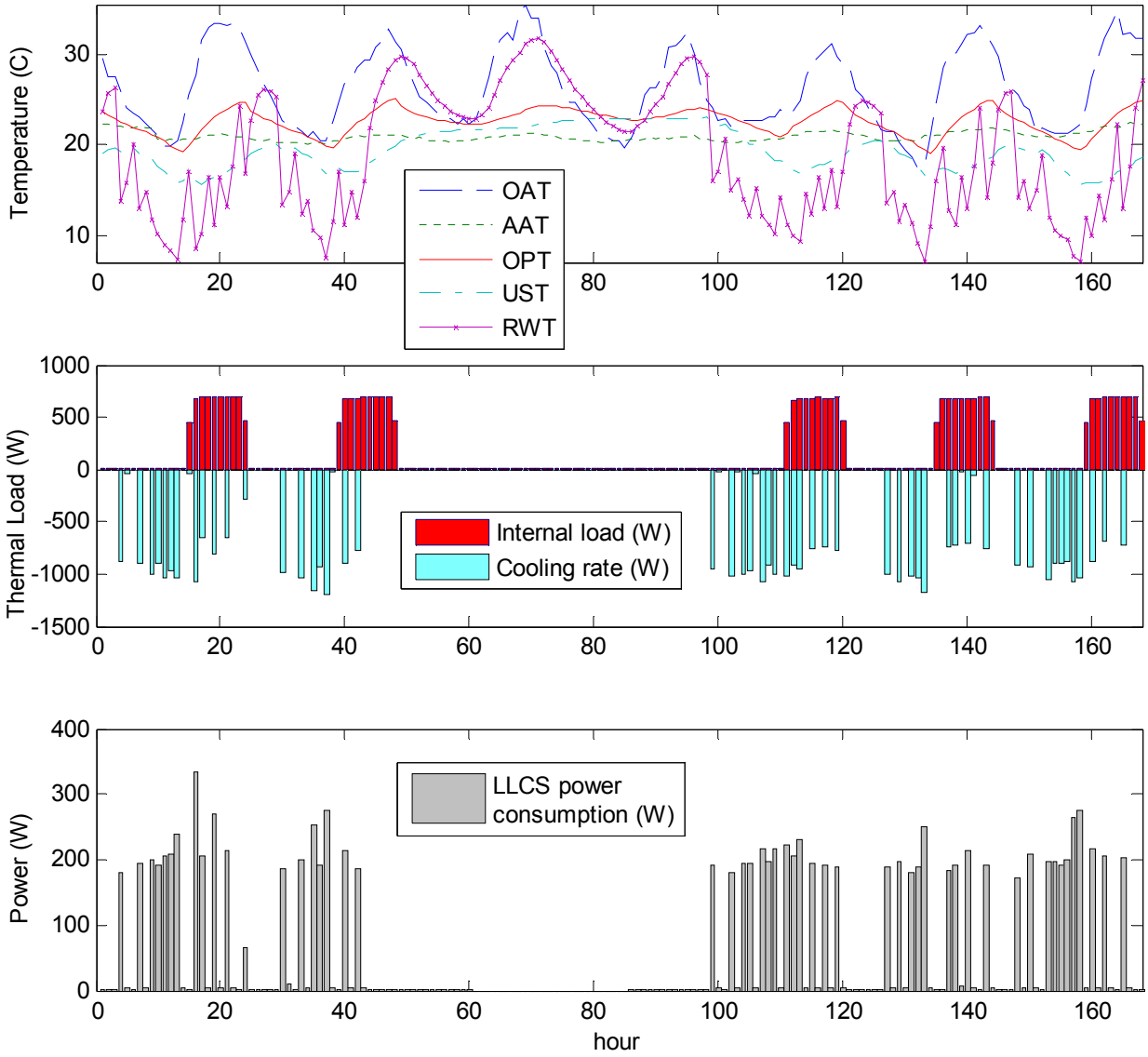

Figure 62 Results for the LLCS under Atlanta climate and standard loads. For the duration of the test, the top graph shows the outdoor air temperature (OAT), adjacent zone air temperature (AAT), zone operative temperature (OPT), under-slab temperature (UST) and return water temperature (RWT); the middle graph shows the internal load heat rate and the cooling rate; and the bottom graph shows the LLCS power consumption at each hour.

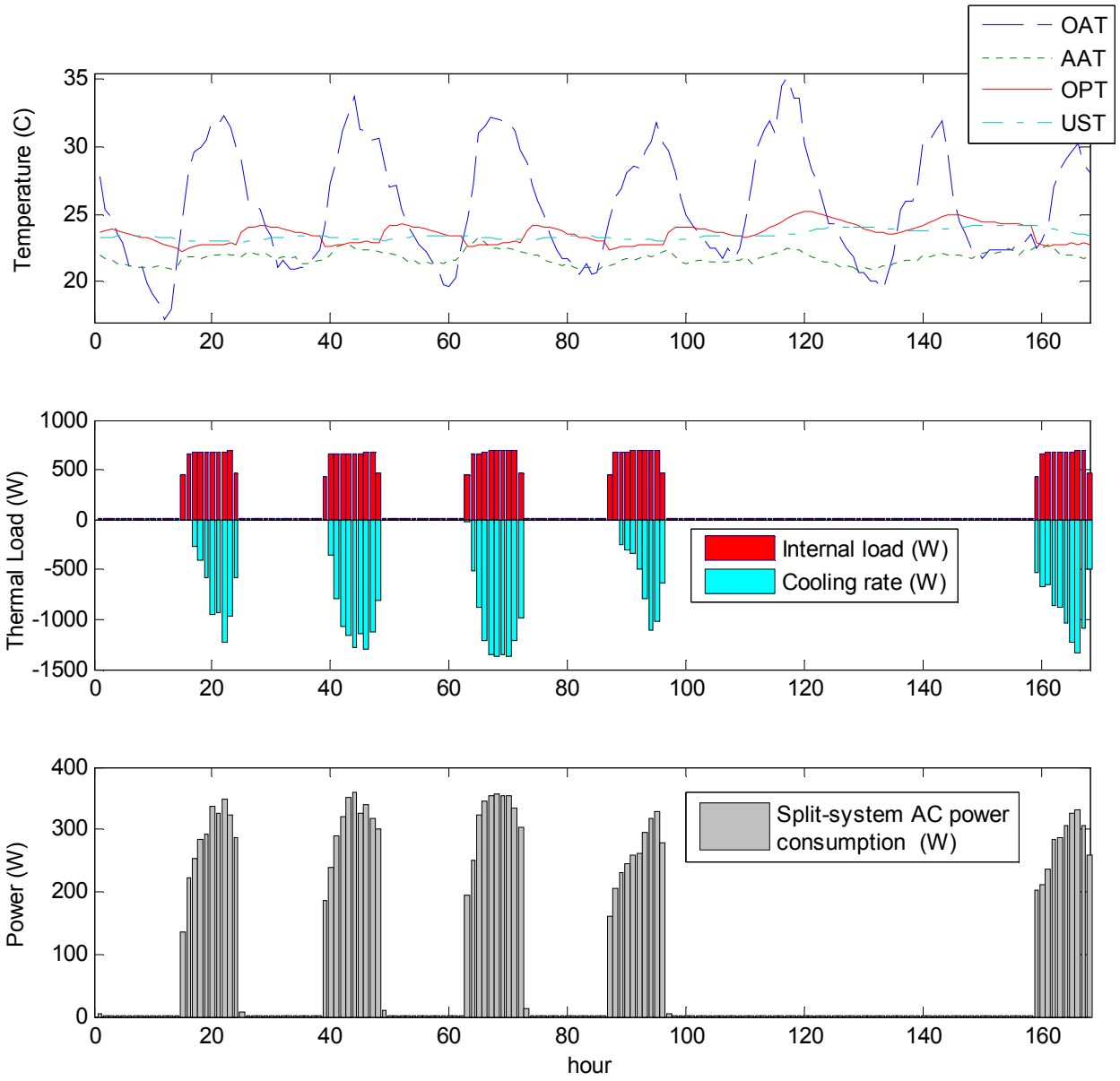

Figure 63 Results for the SSAC under Atlanta climate and standard loads. For the duration of the test, the top graph shows the outdoor air temperature (OAT), adjacent zone air temperature (AAT), zone operative temperature (OPT), under-slab temperature (UST) and return water temperature (RWT); the middle graph shows the internal load heat rate and the cooling rate; and the bottom graph shows the LLCS power consumption at each hour. Note: the cooling rate measurement does not include cooling during transient conditions, which are significant, because the refrigerant mass flow rate used for calculating QC was not measureable during transient conditions. (This is typical of Coriolis mass flow meters with significant two phase flow)

A comparison of the energy performance of the LLCS system to the SSAC is shown in Table 8. Table 8 presents the relative performance of the LLCS and SSAC with regard to cooling delivered, energy consumed, average COP and EER, and average pressure ratio over the duration of the test. The energy consumption data is reliable and accurate, based on simple power measurements. Comparing the other data requires caution. As previously mentioned, the cooling rate could not be measured continuously during the test due to the limitations of the refrigerant mass flow meter. Consequently, the total cooling delivered under SSAC operation is underestimated. The COP and EER estimates can be made in two ways. The average of the instantaneous COP during the test, while it was measurable, provides one estimate of average COP while the total measurable cooling delivered divided by the total energy consumed provides a second. The actual average COP of the SSAC during testing lies somewhere in between these two estimates. Therefore, only a range in percent improvement in COP and EER can be inferred.

Table 8 Comparison of SSAC and LLCS performance

	SSAC[a]	**LLCS**	**Percent difference**
Cooling delivered ($Wh_{th)}$	-38,927[a]	-48,002	23%[a]
Measured energy consumed (Wh_e)	14,645	10,982	-25%
Energy consumed after deducting latent cooling energy (Wh_e)	14,053[b]	10,982[b]	-22%
Average COP (W_{th} / W_e)	2.66-4.2[a]	4.7	12-77%[a]
Average EER (Btu/Wh)	9.1-14.3[a]	16.0	12-77%[a]
Average pressure ratio (kPa/kPa)	1.96	1.70	-13%

a. SSAC cooling rate is under-estimated due to limitations of the refrigerant mass flow meter
b. The latent energy consumption can only be estimated for SSAC operation based on measurement of condensate water. The LLCS also may have performed some latent cooling.

Two baseline SSAC cases are considered, one which includes the total measured energy consumption of the SSAC, and one for which the latent cooling energy associated with the measured condensate water has been deducted from the measured consumption. Both of these are compared to the measured energy consumption of the LLCS. The latent cooling energy consumption of the LLCS was not estimated, because it was not possible to measure, and thus it was not deducted from the LLCS power consumption.

The results in Table 8 show that LLCS sensible cooling energy savings are indeed significant. The actual measured energy consumption of the LLCS was 10,982 Wh for a typical summer week in Atlanta (based on the TMY data) subject to standard efficiency internal loads. The SSAC consumed 14,645 Wh for the same set of conditions. This is an energy savings of 25 percent. After deducting latent cooling energy from the SSAC consumption only, the energy savings is 22

percent. However, It may be argued that the deduction of latent cooling energy from only SSAC unfairly penalizes the LLCS. The LLCS may have performed latent cooling also though it could not be measured. Comparing the LLCS to SSAC energy consumption where latent cooling energy has been deducted from only the SSAC may result in bias favoring the latter.

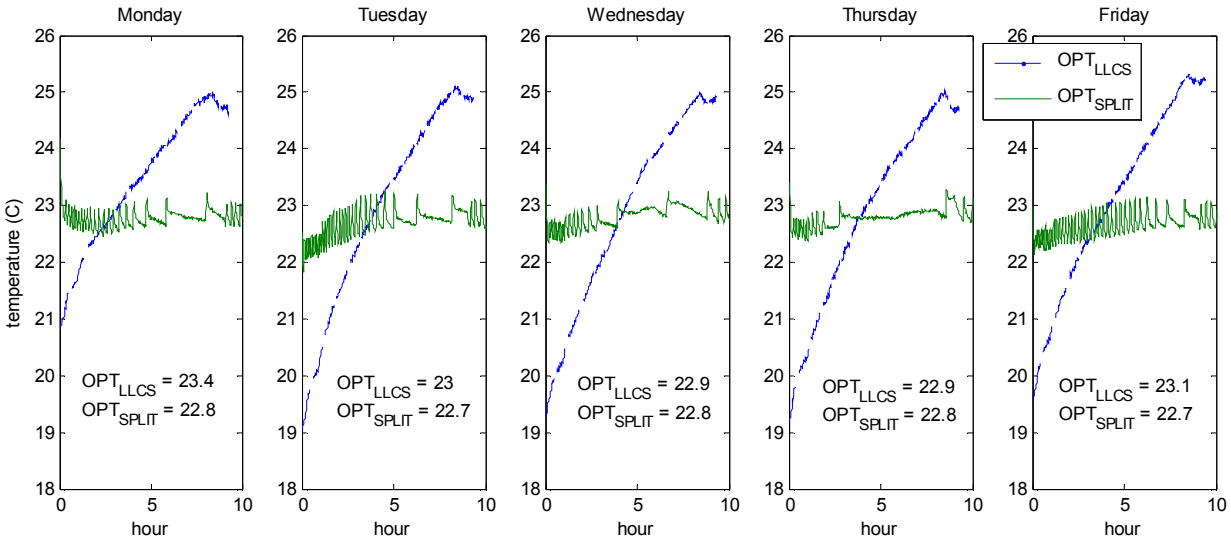

Figure 64 Comparing zone operative temperatures (OPT) for the LLCS and split system AC operation

Figure 64 shows the operative temperatures (OPT) for each day of the week under the SSAC and LLCS operation. The LLCS OPT rises dramatically over the course of a typical day. In the data for Tuesday, it rose from 19 Celsius at 8:00 am to 25 Celsius at 5:00 pm. This is below the limits for temperature variation over time in [ASHRAE 2007a], which allows a rise of 3.3 Celsius over four hours. However, some may argue that a six degree rise over the day is still too much, and that a three to four degree rise is the limit of acceptability based on HVAC designers' experience [Koschenz and Dorer 1999]. The vertical air temperature difference within the zone was less than one degree Celsius in both cases, in large part due to the presence of a ceiling mixing fan which was included to account for the effects of cooling from above and below in a full-scale concrete-core system and air movement cause by a DOAS.

The mean temperatures over the course of the full day are also shown in Figure 64 and are comparable for the LLCS and the SSAC over all of the days. Limitations on control over the SSAC made it impossible to exactly match the operative temperatures achieved by the LLCS and the SSAC. The SSAC is controlled by zone air temperature alone. An estimate of the average mean radiant temperature over a day had to be made from which a zone air set point could be chosen that would yield an operative temperature under SSAC operation comparable to the LLCS over each day.

The end result of the Atlanta tests are that the LLCS shows significant energy savings, around 25 percent, relative to the split system AC while still achieving comfortable operative temperatures between 19.4 and 25 Celsius over the day. The drift in operative temperature over a day is significant for the LLCS, and exacerbated by high internal loads, but is acceptable

for the standard efficiency internal loads tested. These results are comparable to the estimated annual energy savings, 28.8 percent, for the LLCS simulated in [Katipamula et al 2010] for Atlanta subject to standard efficiency internal loads.

However, the differences in the basis for these two savings estimates should be carefully noted. Most importantly, the savings presented in this research are based on the real life performance of an LLCS subject to a typical summer week in Atlanta. The savings in [Katipamula et al 2010] are based on simulations of a theoretical LLCS subject to a year of Atlanta conditions. y Furthermore, the base line VAV system in [Katipamula et al 2010] includes an air-side economizer and higher specific fan power, while the LLCS system includes a refrigerant side economizer, ideal TES, and a different chiller performance map.

The limitations of the LLCS test chamber must also be acknowledged in interpreting the energy performance results. Because the test chamber is quite small, the chiller is somewhat oversized for the test chamber loads. The internal loads were somewhat oversized in an attempt to match the chiller, but this also results in a mismatch between the concrete floor storage capacity, cooling capacity and the test chamber thermal loads. This mismatch inhibits the performance of the LLCS by requiring more cooling, and allowing less load shifting, than would be required for a well-matched system. Also, the test chamber is a single story zone, where cooling energy losses from the bottom of the slab do not contribute to cooling of a space below as they would in a multi-story concrete-core system. As a result, the LLCS provides more cooling to the LLCS test chamber concrete floor than it would in a multi-story application. Consequently, the LLCS system performance potential is somewhat constrained by the limitations of the LLCS test chamber, and the results presented here may underestimate the achievable sensible cooling energy savings.

6.4 Simulating LLCS predictive pre-cooling control applied to SSAC and RCP

In addition to measuring the actual system energy consumption of a conventionally controlled SSAC and an LLCS with a radiant concrete floor, simulations were performed of other possible LLCS configurations that use SSAC or radiant ceiling panels (RCP). The goal of these simulations were to identify how much energy savings could be achieved by applying predictive pre-cooling control for low-lift chiller or air conditioner operation without the use of the concrete-core radiant floor system. The as-built LLCS configuration with concrete radiant floor cooling will here be referred to as an LLCS thermo-active building system (TABS).

Five different system configurations, described below, were simulated to assess and compare predictive control to achieve low-lift cooling using the TABS system, the split-system air conditioner (SSAC), and a radiant ceiling panel (RCP). These simulations were performed in the Matlab environment using the modeling methods described in chapters 2 and 3 and the control algorithm from chapter 4. The temperature response of the zone for all of these cases was modeled using the same temperature-CRTFs, which are the same as those used for the experimental assessment previously described in chapter 4. The system models for each case were different. Calibrated data-driven models of the LLCS chiller performance, developed for

predictive control of the LLCS test chamber, were used for cases three through five. Un-calibrated data-driven models of the SSAC performance based on the data from chapter 3 were used for cases one and two, because calibration data was not collected for the SSAC. The five systems simulated are as follows:

1. Base case SSAC under thermostatic control (BASE-SSAC). The SSAC performance was modeled using the air conditioner performance described in chapter 3, but it was not calibrated to the as-built SSAC performance The SSAC studied in chapter 3 was the same make and model as that installed in the chamber, but not the same physical system. As a result, the actual performance of the SSAC in the test chamber differed from that of the curve-fit models from chapter 3. There is insufficient data to calibrate the SSAC model from chapter 3 to the as-built SSAC performance in the LLCS test chamber. Further data may be collected to calibrate the SSAC model, which would require more data on evaporator cooling rate, compressor speed and condenser fan speeds over a range of operating conditions. The zone air temperature setpoint for the thermostatic control was 23 Celsius, as in the experiments.

2. SSAC with predictive control (LLCS-SSAC). The SSAC performance was modeled as described above under BASE-SSAC. The same predictive pre-cooling control algorithm applied to the experimental LLCS-TABS system was used, as described in chapter 5.

3. TABS with predictive control (LLCS-TABS). The chiller system performance was modeled using the chiller performance map measured from the experimental test stand as described in chapter 3, but *calibrated* to the as-built performance of the chiller serving the concrete floor as described in chapter 6.

4. TABS with predictive control and a higher capacity radiant floor (LLCS-TABS+). This case was simulated to project the potential savings for an improved radiant concrete-core floor design, in which the floor had reduced pipe spacing, higher capacity, and less resistance between the bottom of the concrete and the chiller water loop. The temperature difference between the chilled water and the bottom of the concrete pavers was assumed to be half of that observed with the existing floor. Improvements to the thermal storage efficiency of the concrete floor, by adding insulation underneath, were not modeled. The chiller performance was modeled as described above under LLCS-TABS.

5. RCP with predictive control (LLCS-RCP). An RCP was modeled based on the radiant ceiling panel model described in [Armstrong et al 2009a]. The RCP total heat transfer coefficient was assumed to be 13.2 W/m^2-K based on the results of [Causone et al 2009]. The entire test chamber ceiling, 3.65 m by 5.2 m, was assumed to be covered with RCP. The return water temperature was calculated using equation 20a in [Armstrong et al 2009a], which is a simple heat exchanger effectiveness-NTU relation between the zone air and the chilled water, using a single air temperature on the zone air side. The evaporating temperature was calculated based on the superheat control law implemented in the as-built system instead of with the flooded evaporator model described in [Armstrong et al 2009a]. The

chiller performance was modeled as described above under LLCS-TABS, but using the return water temperature and subsequent evaporating temperature calculated for the RCP.

Each case was simulated under a typical summer week in Atlanta subject to standard efficiency internal loads. Forecasts of internal loads and outdoor temperature variations were perfect, because the forecasts rather than actual measured data from the experimental chamber were used for simulation. The total energy consumption over a typical summer week for each of these cases was calculated based on simulations of each system in Matlab. A summary of these findings is presented in Table 9.

Table 9 Energy consumption and relative savings from simulations of SSAC, TABS and RCP under with low-lift predictive pre-cooling control

	BASE-SSAC	LLCS-SSAC	LLCS-TABS	LLCS-TABS+	LLCS-RCP
Cooling delivered (Wh)	-47,940	-39,920	-53,200	-52,010	-39,420
Simulated energy (Wh)	11,110	8,038	11,072	10,824	5,285
Measured energy (Wh)	14,053	n/a	10,982	n/a	n/a
Error in simulation	20.9%	n/a	-0.8%	n/a	n/a
Savings relative to simulated base case	base	27.6%	base	2.2%	52.3%

The first important point about the results shown in Table 9 is that the simulated SSAC does not accurately model the as-built SSAC. There is a 20.9 percent difference between the *measured* SSAC system performance and the *simulated* SSAC system performance. This difference may have the following causes. First, the actual transient performance of the SSAC is not reflected in its steady-state performance map from chapter 3, which is the model used to simulate SSAC performance. Second, it is likely that the performance of the as-built SSAC is different from the SSAC tested in chapter 3, just as the as-built chiller performance was different from the performance map from chapter 3 and required the calibrations described in section 6.1.1. Currently, not enough information is available to calibrate the performance map model of the SSAC to its as-built performance. The same model structure should be applicable to the as-built SSAC, but the coefficients of the model may be somewhat different than the SSAC tested in chapter 3.

With these differences in system modeling in mind, the results of the simulations have only been compared when the same underlying cooling system model has been used for both cases. Thus, it is reasonable to compare the BASE-SSAC case to the LLCS-SSAC case because the exact same models were used for both simulations, only the control laws were changed. The same is true for the LLCS-TABS, LLCS-TABS+, and LLCS-RCP cases to the extent that the TABS+ and RCP assumptions are achievable and representative of a real system. The same calibrated chiller performance was used for those three cases.

The following conclusions can be drawn from the results in Table 9. First, by employing predictive pre-cooling control directly to the SSAC, simulations suggest over 27 percent energy savings relative to conventional control. These savings are comparable to the measured energy savings of the LLCS-TABS relative to the SSAC. However, it should not be taken at face value that an LLCS-SSAC could save the same energy as an LLCS-TABS in any situation. The ability of the SSAC to achieve the same savings as the TABS under predictive control for the modeled LLCS test chamber may be the result, in part, of low internal load densities relative to the chiller capacity. This mismatch results in less need for storing cooling energy in the concrete, and the SSAC can provide enough pre-cooling despite the fact that it is less effective than the TABS system at pre-cooling the concrete slab. It may also be affected by the thermal storage capacity of the slab, which is reduced by losses to below from the concrete-floor of the LLCS test chamber. This is evident in the amount of total cooling delivered by each case. The TABS systems provide far more cooling than required to meet the load due to losses from the floor. The cooling delivered by the TABS system in simulation is roughly 25 percent more than that of the RCP. This agrees, approximately with the results of a physical model of the concrete floor, which shows that the losses from the bottom of the floor may range from 15 to 30 percent depending on the actual thermal conductivity of the concrete, as described in Appendix B.1.

Second, improving the TABS system, represented by the LLCS-TABS+ case, to achieve higher chilled water temperatures may not achieve significantly greater savings than the LLCS-TABS case. Only an additional 2.2 percent savings was simulated for the LLCS-TABS+. This is likely because the chilled water temperatures and evaporating temperatures are only a few degrees warmer in the LLCS-TABS+ case than in the LLCS-TABS case.

Lastly, the LLCS-RCP system shows significant potential for energy savings over the LLCS-TABS case for the existing test chamber, with over 50 percent simulated savings relative to LLCS-TABS. This is primarily the result of significantly higher chilled water temperatures. However, again, the LLCS-RCP savings are skewed because of the mismatch between the chiller capacity and the internal loads, as well as the low thermal storage efficiency of the LLCS test chamber. Better matching of capacity and load and improved concrete-core thermal storage efficiency should result in more savings from the LLCS-TABS relative to the LLCS-RCP. In the LLCS-RCP simulated case, the RCP system runs primarily during occupied hours because it can efficiently meet the loads with higher chilled water temperatures without utilizing passive TES overnight.

In summary, the simulations show that predictive pre-cooling control for low-lift chiller or air conditioner operation has great potential for energy savings even without a TABS concrete radiant floor cooling system. Simply applying predictive pre-cooling control to the conventional SSAC resulted in 27 percent simulated energy savings. More research is needed to confirm and evaluate the actual energy savings achievable for each of these configurations and many other LLCS configurations beyond TABS, SSAC, or RCPs.

6.5 Experimental LLCS demonstration in Masdar City

One final component of this research is the construction of a larger LLCS test chamber exposed to real outdoor climate conditions at Masdar City in the United Arab Emirates (UAE). This demonstration project was constructed inside a portion of the Masdar field offices on the Masdar City construction site. Masdar City is a UAE sponsored project to build a net-zero energy city near Abu Dhabi, UAE. The Abu Dhabi Future Energy Company (ADFEC) has supported LLCS research with the possibility that, because of its low cooling energy intensity, it may help enable the development of a net-zero energy city. The need for efficient cooling is extremely important at Masdar City because cooling dominates electricity demand and daytime summer temperatures are frequently above 40 Celsius.

The Masdar LLCS test chamber was constructed from three modular building containers in the corner of the Masdar City field offices. Twenty five centimeters of foam insulation was installed on the floor of the modules and 15 centimeters of concrete was poured above the slab. Pex pipe with a pitch of 10 centimeters was embedded in the concrete slab. A system identical to the system described in Chapter 6 was constructed for the Masdar LLCS test chamber, but is still not operational. As part of this research, the radiant concrete floor, the low-lift chiller and base-case SSAC systems were constructed or assembled and sensors for measuring their performance were installed. Images of the Masdar City LLCS test chamber project are shown in Figure 65.

At the time of publication, researchers at the Masdar Institute of Science and Technology are continuing work on this LLCS demonstration project with the goal of making comparative assessments of LLCS and SSAC system performance. The project will require a number of advancements from this thesis. Solar loads will need to be inferred from irradiance measurements and incorporated into the CRTF models. The effects of wind and resulting variations in infiltration loads may need to be captured in the CRTF models. Real weather forecasts will be needed for the predictive pre-cooling control optimization. Results from these experiments are forthcoming.

Figure 65 Images of the Masdar City experimental LLCS demonstration project, including the underslab insulation and PEX chilled water pipe (top left), the variable capacity chiller (top right), the project site and the three LLCS modules (bottom left), and the poured concrete floor (bottom right).

Chapter 7 Conclusion

This chapter will summarize the original contributions presented in this research. This includes measured energy savings of a low lift cooling system (LLCS) with radiant concrete-core cooling relative to a split-system air conditioner (SSAC) in a near full scale LLCS test chamber. A summary of key technical contributions to develop LLCS model-based, predictive pre-cooling control algorithms will also be presented. The chapter will then describe alternative LLCS configurations and the barriers to and benefits of implementing LLCS on a large scale. Finally, future research directions stemming from this work will be explored.

7.1 Original contributions

This research significantly advances knowledge about the implementation, control and performance of LLCS. A specific LLCS configuration, a variable speed chiller serving a concrete radiant floor with near-optimal predictive pre-cooling control was implemented and tested. This included developing the data-driven models and controls necessary to support predictive pre-cooling control of LLCS based on measured building data. The following achievements are considered important original contributions of this research.

First, the sensible cooling energy savings of an LLCS concrete core radiant cooling system with predictive pre-cooling control relative to a high efficiency, variable speed SSAC was tested in an experimental test chamber for the typical summer week in Atlanta with standard efficiency internal loads. The measured LLCS sensible cooling energy savings relative to the SSAC was 25 percent of the SSAC typical summer week consumption. These results confirm previous estimates based on simple simulation models [Katipamula et al 2010] which found 28.8 percent *annual* energy savings for a *similar* (not identical) LLCS system relative to a *similar* base case system. Caveats in comparing these two savings estimates are discussed below.

A second major contribution of this work is a methodology for predictive pre-cooling control of a LLCS radiant concrete core cooling system that includes the thermal response of real building thermal mass. This methodology includes the use of chiller performance maps, or look-up tables, and building thermal response models, such as CRTFs, into a pre-cooling control optimization algorithm. Incorporating the thermal response of real concrete-core thermal mass into this optimization is a key contribution beyond prior research. This is necessary and important because the chiller efficiency depends on evaporating temperature, which in turn depends on chilled water temperature and thus on the state of the pre-cooled thermal mass.

A third contribution is a detailed data set on the performance of a rolling-piston compressor heat pump created from experimental measurements to support this and future research. The heat pump data was used to create curve-fit performance models of a low-lift chiller valid under low pressure ratios. The data has also been used by [Zakula 2010] to create detailed physical models of the steady state performance of heat pumps at low pressure ratios. There is ongoing research to use this data to validate physical models of heat pump and chiller components and perform a static optimization of chiller control variables under a given set of conditions.

The fourth contribution was to adapt transfer function models of operative temperature and concrete slab temperature transient response for LLCS control based on data from a test chamber highly instrumented with temperature, internal load, and cooling rate measurements.

These contributions have certain limitations that should be emphasized. The sensible cooling energy savings compare well to the savings estimated in [Katipamula et al 2010] for the most comparable base case mechanical system, a VAV system with a variable speed chiller. The savings for a medium office building in Atlanta subject to standard efficiency internal loads in [Katipamula et al 2010] were 28.8 percent, while the measured savings in this research were 25 percent.

Direct comparisons between the savings measured in this research and those simulated in [Katipamula et al 2010] should not be taken at face value. The savings are expected to be different for a variety of reasons. The base case system in [Katipamula et al 2010] most comparable to the SSAC is a VAV system with a variable speed chiller. These systems are not identical. The VAV system included an air-side economizer and larger specific fan power than the SSAC. In addition, the LLCS in [Katipamula et al 2010] included a refrigerant side economizer, ideal TES, and a different chiller performance map. Furthermore, the savings in [Katipamula et al 2010] are based on annual simulation, not a typical summer week. Most importantly, the savings estimated in [Katipamula et al 2010] are based on simulations, not on a real life system.

Limitations of the LLCS test chamber and the installed LLCS negatively impacted the achievable energy savings. Because of the small size of the chamber, even the smallest capacity variable speed compressor found was somewhat oversized for the test chamber. Additional internal load was added to match the cooling capacity of the chiller, which in turn meant the cooling and storage capacity of the concrete floor was somewhat undersized. Furthermore, the twelve inch pitch of the radiant water pipes was, in retrospect, too large and not made up for by the aluminum facing on the Warmboard. Finally, the insulation below the concrete floor, while significant, was not enough to prevent cooling energy losses from the bottom of the slab resulting in lower thermal storage efficiency. In a multi-story concrete-core system or TABS, the concrete slab would cool spaces both above and below and the thermal storage efficiency would be greater than the LLCS test chamber. All of these factors combine to cause lower evaporating temperatures, lower thermal storage efficiencies, lower radiant floor capacities, and overall less efficient performance of the LLCS.

A few important changes to the LLCS test chamber may lead to greater energy savings. Decreasing the chilled water pipe pitch and varying chilled water flow rate will lead to higher evaporating temperatures and should result in a reduction in chiller power at low part load. Optimizing the brazed plate heat exchanger evaporator for the air-cooled condenser may lead to higher chiller COPs, similar to those observed for the off-the-shelf heat pump in chapter 3. Better matching of the zone thermal loads, the capacity of the chiller, and the concrete-core storage along with increased under-floor insulation should improve the thermal storage capacity and efficiency relative to the cooling loads. All of these changes should result in greater savings, and a more accurate representation of right-sized LLCS performance when compared to a right-sized VAV system.

Another improvement over the existing methods involves the concrete slab temperature measurement, UST. The current pre-cooling control implementation requires a measurement of the concrete slab temperature and subsequently additional sensors in a BAS. While it is feasible that a control system could include a temperature sensor embedded in the concrete slab, it complicates installation and coordination of trades during construction. It may be possible to eliminate the slab temperature (UST) from the optimization, and relate chilled water return temperature (RWT) directly to the temperature response of the room air or operative temperature. Such an approach would be better suited for typical control systems, as a globe temperature sensor or air temperature sensor could be installed in each zone more easily than embedding a temperature sensor in the concrete core.

Relating RWT directly to zone air or operative temperatures may require the use of physical, forward modeling of the concrete slab which has been avoided in this thesis. For example, rather than applying transfer function modeling to both UST and RWT prediction, a heat exchanger model relating the RWT to an unmeasured UST coupled through a transfer function to OPT might be applied. This hybrid model would be, essentially, a high thermal mass gray-box heat exchanger model with its parameters identified from measured RWT and OPT data.

7.2 Alternative LLCS configurations

The LLCS radiant concrete core concept investigated in this research is not the only strategy for achieving low lift cooling and its potential energy savings. There are numerous configurations of the LLCS key strategies and systems that can also achieve low lift chiller operation for energy savings. Alternatives are available to the air-cooled chiller, radiant cooling, and the concrete-core TES investigated in this research. There are also multiple options for the dehumidification and ventilation systems, which have not been studied here. The following section investigates the potential for other LLCS configurations.

The predictive pre-cooling control algorithm developed in this research can be applied to a direct cooling system that passively charges building mass (without the use of embedded pipes). For example, the thermostatically controlled SSAC system used as a base case in chapter 6 could instead be predictively controlled to pre-cool the zone, passively pre-cooling the thermal mass. A simulation showed that applying the LLCS predictive pre-cooling control to

the SSAC system has the potential for roughly 27 percent savings relative to conventional thermostatic control of the SSAC in the LLCS test chamber.

LLCS controls could also be applied direct radiant cooling systems such as RCPs. Although the coupling between building thermal mass and RCPs is not as good as a concrete-core system, chillers serving RCPs can operate at higher evaporating temperatures than concrete-core systems. RCP chilled water temperatures are closer to zone air temperatures rather than pre-cooled concrete temperatures. A simulation of predictive pre-cooling control of RCPs in the LLCS test chamber resulted in 50 percent savings relative to the concrete core systems. This is unexpectedly large, but has highlighted a problem with the LLCS test chamber that needs to be fixed. The thermal storage efficiency of the chamber is low due to inadequate insulation below the concrete floor. Increasing the amount of insulation below the floor, so that the test chamber better represents a multi-story concrete-core system, will likely result in better performance of the concrete-core pre-cooling than pre-cooling with RCP.

There are many other LLCS configurations with potential that have not been investigated in detail, experimentally or through simulation, in this research. Different components for LLCS system configurations that merit further consideration include the following:

Thermal energy storage options:

- Radiant concrete-core (TABS): The building mass is pre-cooled through pipes (or ducts) embedded in building mass.
- Passive TES: The building mass is cooled indirectly, without embedded pipes, by direct cooling systems. Building mass might include concrete slabs and PCM wall or ceiling board.
- Active or discrete TES: A system separate from the building thermal mass, such as stratified-water or PCM tank storage, is utilized for TES. This approach requires additional pumping energy and may have lower thermal storage efficiencies.

Cooling distribution system options:

- Radiant concrete-core (TABS): In this case, the TES doubles as the cooling distribution system. TABS are actively charged but passively discharge cooling to spaces.
- Radiant ceiling panels: RCPs allow for high chiller evaporating temperatures, but must be combined with passive or active TES, which may be less effective than TABS.
- Chilled beams: Similar to RCPs, chilled beams allow for high chiller evaporating temperatures but again must be combined with passive or active TES.
- Efficient fan coil units (with low specific fan power, similar to the SSAC): Fan coil units with large heat exchangers and low fan power may be appropriate for LLCS, with caution to avoid offsetting LLCS energy savings by increased fan energy consumption.

Chiller/cooling source options:

- Air-cooled chiller: Lower condensing temperatures are achieved by night-time operation. Refrigerant side-economizers can provide additional savings.
- Water-cooled chiller: Lower condensing temperatures are achieved by night-time operation. Water-side economizers can provide additional savings.
- Ground source or water source heat pump: Lower condensing temperatures overall due to moderate condenser water temperatures. Additional savings due to load-spreading.
- Wet/dry water-cooled chiller: Condenser is installed inside a cooling tower and spray cooled above freezing, providing lower condensing temperatures and higher efficiencies overall.
- Evaporative dewpoint chiller: A variable speed evaporative cooling process can provide chilled water temperatures near dewpoint temperatures in dry climates, without the use of a compressor. Provides relatively high temperature chilled water suitable for radiant cooling systems.

Dedicated outdoor air system (DOAS) options:

- Enthalpy recovery: An enthalpy recovery wheel in the incoming and outgoing air streams can reduce the latent and sensible cooling requirements for outdoor air.
- Run-around heat exchanger: A run-around heat exchanger in the incoming air stream can reduce dehumidified air re-heating energy requirements.
- Desiccant dehumidification with solar thermal regeneration: Applying desiccant dehumidification to DOAS could eliminate the need for a separate direct expansion vapor compression system for the DOAS. Combined with solar thermal regeneration of the desiccant, energy consumption could be limited to DOAS fan and pump energy.

The components listed above may be combined in many different ways. Unfortunately, there is little research on the potential energy savings and costs for *all* the various combinations of these systems when LLCS predictive pre-cooling control is applied. However, a few observations can be made about system combinations that merit further research in particular building types.

In new commercial building construction, concrete-core TES and radiant cooling is appropriate and can provide energy and cost savings when buildings are designed to control infiltration, humidity and reduce internal loads. Pfafferott and Katz [2007] estimated that 60 concrete-core buildings had already been built in Germany by 2001, and that one third of planned new construction included concrete-core systems. Providing supplementary sensible cooling systems is also appropriate, through capillary tube radiant systems, RCPs, chilled beams or efficient fan coil units. These direct cooling systems allow better temperature control in response to uncertainties inherent to pre-cooling the concrete-core.

In existing buildings, concrete-core TABS systems are not impossible, but may be impractical. Some companies already offer products for slab-on-slab installation of concrete-core radiant cooling systems [Uponor 2010] that could be applied to existing buildings. However, this

approach decreases floor-to-floor height and the refurbishment may be too invasive. In many cases it may be more appropriate to use direct cooling systems which can be easily installed, such as RCPs, chilled beams and efficient fan coil units, along with passive or active TES. Active TES can be prohibitively costly, depending on the application and utility rates, and requires additional floor area dedicated to mechanical systems [Roth et al 2006b].

7.3 Implementing LLCS in real buildings

Ultimately, LLCS will only achieve significant energy savings if they are actually implemented in real buildings, and only then if they are widely-adopted. There are many barriers to scaling LLCS concepts, but there are also many benefits and opportunities. Katipamula et al [2010] discusses many of the barriers to and benefits of wide-scale application of LLCS in different markets.

One barrier to LLCS is the level of integration and complexity required in its systems and controls. Many building owners and developers want simple solutions, a more efficient rooftop unit (RTU) for example, without considering broader and coordinated retrofits or designs. LLCS requires owners, architects and engineers to be open to an integrated approach to cooling in which building automation systems (BAS) supervise control over mechanical equipment and passive LLCS components with a coordinated strategy. It also requires stakeholders to look beyond conventional practices in their region and their experience. In the U.S., systems such as RTUs or VAV systems are ubiquitous and familiar. Pursuing alternatives, such as radiant cooling and LLCS requires education and training of architects, engineers, owners and developers.

This first barrier will, in part, be overcome by time as emerging technologies become more familiar, building automation systems evolve, and the demand for energy efficient cooling increases. Radiant cooling has only recently been receiving greater attention and new development. Architects and engineers are still not generally aware of the potential for radiant cooling with LLCS, and the cost of radiant cooling technologies is still relatively high. NCI identified the cost of the radiant cooling system, especially the labor required for installation, as the major driver in the cost per square foot of LLCS. They estimate that 10 to 20 percent premiums are typically paid for emerging technologies such as radiant cooling systems, which may come down over time. They also estimate that around 15 percent cost premiums are paid for low-lift variable capacity chillers which are still relatively new to the market. Finally, BAS and their capabilities are changing rapidly, accommodating more measurements and supervisory controls.

The difficulties in retrofitting a building with TES and radiant cooling systems pose some barriers to applying LLCS to existing buildings. It is possible to lay pipe and pour concrete over existing floor structures, but it may not always be practical or economical. Consequently, direct cooling systems such as RCPs, efficient fan coil units, or chilled beams combined with passive or active TES may be more appropriate for existing buildings. With active TES, space must be allocated for the additional TES equipment. Roth et al [2006b] estimate that the paybacks for active TES suitable for LLCS are relatively quick, a few years for PCM storage systems and less

than a year for water-based storage (not ice). Thus, barriers to LLCS in existing buildings can be overcome with careful selection of LLCS components that complement the existing building configuration and climate.

Another barrier to LLCS is the perceived risk of condensation and maintenance challenges. It is crucial that appropriate care is given to sealing the building envelope to control latent loads and providing adequate latent cooling. Furthermore, provisions must be made to provide access to radiant piping systems so that repairs can be made. For concrete core systems, embedded piping must be designed to last the lifetime of the building, with maintenance access provided at any critical failure points. This may be easy at valves and pipe fittings, but ensuring that pipe embedded in concrete does not clog or fail over time may be difficult.

High costs of LLCS components, both real and perceived, are also a barrier. As previously, premiums paid for emerging technologies such as radiant cooling systems, TABS, and low-lift variable capacity chillers as well as higher costs for advanced controls increase the cost of LLCS. Over time, these costs are likely to come down. One potential cost benefit of LLCS is increased useable floor area. The use of radiant concrete-core systems require less space than conventional VAV systems for ductwork, freeing up rentable floor area. LLCS has significant cost savings potential in certain applications. Katipamula et al [2010] estimated the incremental costs per square foot for LLCS at -$0.58/sqft for medium office buildings, i.e. a cost *savings* relative to a total new construction cost of $7.91/sqft. They also estimate incremental costs of $0.70/sqft above total new construction costs of $7.63/sqft for large office buildings, $5.55/sqft over $17.59/sqft for supermarkets, and $2.61/sqft over $6.84/sqft for secondary schools. These estimates suggest medium and large office buildings are great candidates for wide-scale implementation of LLCS, with potential capital cost, life-cycle cost, and energy savings.

7.4 Future research

Understanding of LLCS and development for commercial application may be advanced through continued research. Areas of future research span the topics of low-lift chiller performance, thermal model identification methods, pre-cooling control optimization and implementation, demonstration LLCS projects and full-scale implementation of LLCS in real buildings.

Greater understanding of the performance of various types of chillers at low pressure ratios can be gleaned from further experimental testing and physics-based simulation. A chiller with a rolling-piston compressor was investigated in this research, but it would be useful to measure and create better models of the low-pressure ratio performance of chillers with reciprocating compressors, scroll compressors, and screw compressors. Manufacturers typically do not publish data on chillers and compressors at low-pressure ratios, although they may have it, and performance ratings for chillers are still limited to COP and IPLV. Greater transparency about the performance of chillers and compressors at low pressure ratios, particularly by

anufacturers of highly efficient equipment at part load, might lead to greater applications for their products.

Thermal model identification methods have long been an area of active research. Future research should focus particularly on implementation of these methods within existing and emerging BAS and energy management systems in real buildings. A few specific research directions include: determining how to inverse model internal loads, or how lack of information about internal loads may be overcome; developing multi-zonal models of thermal response with separately controlled zones that affect the cooling loads of adjacent zones; evaluating alternatives to using the concrete slab temperature UST by modeling RWT directly from more conventional measurements, such as zone air or operative temperatures; and developing better methods for identifying temperature-CRTF with physically meaningful parameters that can accurately make predictions 24 hours ahead.

Future research on pre-cooling control should focus on simplifying the underlying modeling, forecasts, and optimization methods to conform to what can be practically and affordably measured. For example, if only cooling rate and power consumption are measured, it may be possible to infer a predictive pre-cooling control schedule based on previous days of operation and current climate forecasts without additional inverse modeling of zone temperature response. Alternatively, the optimization might be reduced to a smaller set of variables, such as a handful of compressor speeds and a few times at which speeds change. This type of simplified pre-cooling control using start and stop times and set point schedules is more akin to the approaches taken by [Braun 2007] and [Henze et al 2010]. Integrating the pre-cooling control optimization, whether simplified or not, into real BAS is also an important area of future research.

The proper sizing of LLCS also needs to be addressed. In the work to date, it has been assumed that the LLCS and baseline systems under consideration have the same chiller size. Typical-year simulation results [Katipamula et al 2010] show that the maximum LLCS chiller cooling rate is less than the corresponding VAV chiller cooling rate. However downsizing on this basis will probably increase annual operating cost—the LLCS optimal size probably lies somewhere between the two extremes. A method is needed to determine the optimal LLCS size.

Finally, additional demonstration projects are needed to further validate LLCS performance and fine tune their design, control, and energy performance. The demonstration project at Masdar City will provide a test bed for addressing the complexities of solar loads, wind-driven infiltration, high outdoor humidities, and real-time weather forecasts. Full-scale implementation of LLCS in real buildings should also be pursued aggressively. The potential for LLCS in medium office buildings, in capital cost reductions but especially in energy and energy cost savings, motivate further research to implement LLCS in medium office buildings. Currently, a full scale LLCS is included in the plans for one academic office building at the Masdar Institute of Science and Technology. More full scale LLCS projects should be pursued.

7.5 Concluding remarks

Finding more efficient ways to cool buildings is becoming increasingly important. The need for efficient cooling is driven by global development, rising demand for cooling and thermal comfort, rising demand for energy, and the pressing need to address climate change. Low-lift cooling systems have tremendous potential for decreasing the energy consumption of buildings to help address these challenges. In developing economies, adopting LLCS has the potential to avoid large growth in energy consumption by "leapfrogging" to more efficient building technologies. The low cooling energy intensity of LLCS is well-suited for incorporation into high performance buildings, net-zero energy buildings, and buildings with integrated power generation. However, barriers such as LLCS complexity, lack of existing precedents, the need for smarter buildings with better BAS, and perceived costs and risks must be overcome for LLCS to be implemented at a large scale.

This research has sought to understand and work through the complexity of LLCS to create a real-life precedent from which further development of commercially viable LLCS can grow. It is the author's hope that from this research readers may understand the potential for LLCS, the methods involved in implementing LLCS, and the need for future research and full scale implementation in real buildings so that LLCS can be made simpler, more practical, and commercially viable at a large scale.

References

[Adlam 1948] Adlam T. 1948. Radiant Heating. The Industrial Press. New York, New York.

[Andersen et al 2000] Andersen KK, Madsen H, Hansen LH. 2000. Modeling the heat dynamics of a building using stochastic differential equations. Energy and Buildings 31: 13-24.

[Armstrong 2004] Armstrong PR. 2004. Model identification with application to building control and fault detection. Ph.D. Thesis. Massachusetts Institute of Technology.

[Armstrong et al 2006a] Armstrong PR, Leeb SB, Norford LK, Control with Building Mass – Part I: Thermal Response Model. ASHRAE Transactions Vol. 112(1)

[Armstrong et al 2006b] Armstrong PR, Leeb SB, Norford LK, Control with Building Mass – Part II: Simulation. ASHRAE Transactions Vol. 112(1)

[Armstrong et al 2009a] Armstrong PR, Jiang W, Katipamula S, Norford LK, Willingham R. 2009. Efficient Low Lift Cooling with Radiant Distribution, Thermal Storage, and Variable Speed Chiller Controls – Part I: Component and Subsystem Models. HVAC&R Research 15 (2): 402-432.

[Armstrong et al 2009b] Armstrong PR, Jiang W, Katipamula S, Norford LK. 2009. Efficient Low Lift Cooling with Radiant Distribution, Thermal Storage, and Variable Speed Chiller Controls – Part II: Annual Energy Use and Savings. HVAC&R Research 15 (2): 366-400

[ASHRAE 1971] American Society of Heating, Refrigerating, and Air-Conditioning Engineers. 1971. Procedures for Simulating the Performance of Components and Systems for Energy Calculations. Stoecker, W.F., ed., 2nd edition, American Society of Heating Refrigeration Air-conditioning Engineers, Atlanta, GA

[ASHRAE 2001] American Society for Heating, Refrigerating, and Air-Conditioning Engineers. 2001. 2001 ASHRAE Handbook – Fundamentals. American Society of Heating, Refrigerating, and Air-Conditioning Engineers, Atlanta, GA.

[ASHRAE 2004] American Society for Heating, Refrigerating, and Air-Conditioning Engineers. 2004. Energy Standard for Buildings Except Low-Rise Residential Buildings. ANSI/ASHRAE/IESNA Standard 90.1-2004. American Society of Heating, Refrigerating, and Air-Conditioning Engineers, Atlanta, GA.

[ASHRAE 2007a] American Society for Heating, Refrigerating, and Air-Conditioning Engineers. 2007. Thermal Environmental Conditions for Human Occupancy. ANSI/ASHRAE Standard 55-2007. American Society of Heating, Refrigerating, and Air-Conditioning Engineers, Atlanta, GA.

[ASHRAE 2007b] American Society for Heating, Refrigerating, and Air-Conditioning Engineers. 2007. Ventilation for Acceptable Indoor Air Quality. ANSI/ASHRAE Standard 62.1-2007. American Society of Heating, Refrigerating, and Air-Conditioning Engineers, Atlanta, GA.

[ASHRAE 2007c] American Society for Heating, Refrigerating, and Air-Conditioning Engineers. 2007. Energy Standard for Buildings Except Low-Rise Residential Buildings. ANSI/ASHRAE/IESNA Standard 90.1-2007. American Society of Heating, Refrigerating, and Air-Conditioning Engineers, Atlanta, GA.

[ASHRAE 2007d] American Society of Heating, Refrigerating, and Air-Conditioning Engineers. 1969. Procedures for Determining Heating and Cooling Loads for Computerized Energy Calculations: Algorithms for Building Heat Transfer Sub-routines. M. Lokmanhekim, ed., American Society of Heating Refrigeration Air-conditioning Engineers, Atlanta, GA.

[ASHRAE 2007e] American Society for Heating, Refrigerating, and Air-Conditioning Engineers. 2007. 2007 ASHRAE Handbook - HVAC Applications. American Society of Heating, Refrigerating, and Air-Conditioning Engineers, Atlanta, GA.

[ASHRAE 2009] American Society of Heating, Refrigerating, and Air-Conditioning Engineers. 2007. Standard for the Design of High-Performance Green Buildings Except Low-Rise Residential Buildings. ASHRAE Standard 189.1-2009. Atlanta, GA.

[Athienitis 1993] Athienitis AK. 1993. A Methodology for Integrated Building-HVAC System Thermal Analysis. Building and Environment 28(4): 483-496.

[Audin 2004] Audin, L. 2004. Slow Pace of HVAC Change Means Missed Gains. Building Operating Management 51 (1)

[Audit and Dennis 2003] Audet C, Dennis JE. 2003. Analysis of Generalized Pattern Searches, SIAM Journal on Optimization 13 (3): 889–903.

[Bahnfleth and Peyer 2004] Bahnfleth W, Peyer E. 2004. Variable Primary Flow Chilled Water Systems: Potential Benefits and Application Issues. Pennsylvania State University. March 2004. ARTI-21CR/611-20070-01.

[Balcomb 1983a] Balcomb JD. 1983. Thermal network reduction. Proc. Annual ASES Conf., Minneapolis, MN. LA-UR-83-869, LA-9694-MS.

[Balcomb 1983b] Balcomb JD. 1983. Heat storage and distribution inside passive-solar buildings. Proc. International Conference on Passive and Low Energy Architecture June 1983.

[Barakat 1987] Barakat SA. 1987. Experimental determination of the z-transfer function coefficients for houses. ASHRAE Transactions 93(1): 146–161.

[Benedict 1984] Benedict R. 1984. Fundamentals of Temperature, Pressure, and Flow Measurement. John Wiley and Sons, New York, N.Y., ISBN 0-471-89383-8.

[Brambley et al 2003] Brambley MR, Haves P, McDonald SC, Torcellini P, Hansen D, Holmberg DR, Roth KW. 2003. DOE Advanced Controls R&D Planning Workshop, June 11, 2003, Washington DC, Workshop Results. PNNL 15148.

[Brambley et al 2005] Brambley MR, Haves P, McDonald SC, Torcellini P, Hansen D, Holmberg DR, Roth KW. 2005. Advanced Sensors and Controls for Building Applications: Market Assessment and Potential R&D Pathways. PNNL 15149.

[Brandemuehl et al 1990] Brandemuehl MJ, Lepoer MJ, Kreider JF. 1990. Modeling and testing the interaction of conditioned air with building thermal mass. ASHRAE Transactions 96(2):871–875.

[Brandemuehl et al 1996] Brandemuehl M, Krarti M, Phelan J. 1996. 827-RP Final Report: Methodology Development to Measure In-Situ Chiller, Fan, and Pump Performance. American Society of Heating, Refrigerating, and Air-Conditioning Engineers, Atlanta, GA (March).

[Braun 1990] Braun JE. 1990. Reducing energy costs and peak electrical demand through optimal control of building thermal storage. ASHRAE Transactions 96(2): 876–888.

[Braun et al 2001] Braun J, Montgomery K, Chaturvedi N. Evaluating the Performance of Building Thermal Mass Control Strategies. HVAC&R Research, 7(4): 403-428

[Braun et al 2002] Braun JE, Lawrence TM, Klaassen CJ, and House JM. 2002. Demonstration of load shifting and peak load reduction with control of building thermal mass. Proceedings of the 2002 ACEEE Summer Study on Energy Efficiency in Buildings.

[Braun and Chaturvedi 2002] Braun J, Chaturvedi N. 2002. An Inverse Gray-Box Model for Transient Building Load Prediction. HVAC&R Research 8(1): 73-97.

[Brunello et al 2003] Brunello P, Carli MD, Tonon M, Zecchin R. 2003. Applications of Heating and Cooling Thermal Slabs for Different Buildings and Climates. ASHRAE Transactions: Symposia 2003: 637-646.

[Braun and Lee 2006] Braun JE, Lee KH. 2006. Assessment of Demand Limiting Using Building Thermal Mass in Small Commercial Buildings. ASHRAE Transactions 112(1): 547-558.

[Braun 2007] Braun JE. 2007. Impact of Control on Operating Costs for Cool Storage Systems with Dynamic Electric Rates. ASHRAE Transactions 113(2): 343-354.

[Brunner et al 2006] Brunner CU, Steinemann U, Jakob M. 2006. Adaptation of Commercial Buildings to Hotter Summer Climate in Europe. Improving Energy Efficiency of Commercial Buildings. Proceedings of the International Conference IEECB 2006.

[Burkhart 2004] Burkhart A. 2004. 7 Methods to Improving Performance of Existing Chiller Plants. HVAC Retrofit 2004. A Supplement to ASHRAE Journal.

[Capehart 2004] Capehart, B. 2004. Information Technology for Energy Managers. The Fairmont Press, Inc. Lilburn, GA.

[Casciaro and Thome 2001a] Casciaro S, Thome J. 2001. Thermal Performance of Flooded Evaporators, Part 1: Review of Boiling Heat Transfer Studies. ASHRAE Transactions: Symposia. 903-918.

[Casciaro and Thome 2001b] Casciaro S, Thome J. 2001. Thermal Performance of Flooded Evaporators, Part 2: Review of Void Fraction, Two –Phase Pressure Drop and Flow Pattern Studies. ASHRAE Transactions: Symposia. 919-930.

[Causone et al 2009] Causone F, Corgnati, S., Filippi M, Olesen B. 2009. Experimental evaluation of heat transfer coefficients between radiant ceiling and room. Energy and Buildings 41(6): 622-628.

[Chen 2001] Chen TY. 2001. Real-time predictive supervisory operation of building thermal systems with thermal mass. Energy and Buildings 33: 141-150

[Chen 2002] Chen TY. 2002. Application of adaptive predictive control to a floor heating system with a large thermal lag. Energy and Buildings 34: 45-51.

[CIBSE 2003] Chartered Institution of Building Services Engineers. 2003. The Energy Performance of Buildings Directive: A summary of its objectives and contents. CIBSE Briefing 6. Chartered Institution of Building Services Engineers, London, UK.

[Clarke et al 2002] Clarke JA, Cockroft J, Conner S, Hand JW, Kelly NJ, Moore R, O'Brien T, Strachan P. 2002. Simulation-assisted control in building energy management systems. Energy and Buildings 34: 933-943.

[Coley and Penman 1992] Coley DA, Penman JM. 1992. Second Order System Identification in the Thermal Response of Real Buildings. Paper II: Recursive Formulation for On-line Building Energy Management and Control. Building and Environment 27(3): 269-277.

[Coniff 1991] Conniff JP. 1991. Strategies for reducing peak air-conditioning loads by using heat storage in the building structure. *ASHRAE Transactions* 97(1): 704–709.

[Conry and Mumma 2001] Conroy CL, Mumma SA, 2001. Ceiling radiant cooling panels as a viable distributed parallel sensible cooling technology integrated with dedicated outdoor-air systems. ASHRAE Transactions 107(1)

[Crawford and Woods 1985] Crawford RR, Woods JE. 1985. A method for deriving a dynamic system model from actual building performance data. ASHRAE Transaction 91(2b).

[Crawley et al 2001] Crawley D, Hand J, Lawrie L. 1999. Improving the Weather Information Available to Simulation Programs. Building Simulation conference. September 1999.

[Crawley et al 2005] Crawley D, Hand J, Kummert M, Griffith B. 2005. Contrasting the Capabilities of Building Energy Performance Simulation Programs. Ninth International IBPSA Conference. Montreal, Canada. August 15-18, 2005

[Degelman 2002] Degelman LO. 2002. Which came first – building cooling loads or global warming? – a cause and effect examination. Building Serv. Eng. Res. Technol. 23(4): 259-267

[Dewson et al 1993] Dewson T, Day B, Irving AD. 1993. Least Squares Parameter Estimation of a Reduced Order Thermal Model of an Experimental Building. Building and Environment 28(2): 127-137

[Dieckmann et al 2003] Dieckmann J, Roth K, Brodrick J. 2003. Dedicated Outdoor Air Systems. ASHRAE Journal. March 2003.

[Dieckmann et al 2004] Dieckmann, J., K.W. Roth and J. Brodrick, 2004. Radiant Ceiling Cooling, EmergingTechnology report. ASHRAE Journal. June, 2004

[Dieckmann et al 2010] Dieckmann J, McKenney K, Guernsey M, Brodrick J. 2010. VFDs for Large Chillers. ASHRAE Journal. June 2010.

[Dincer 2002] Dincer I. 2002. On thermal energy storage systems and applications in buildings. Energy and Buildings 34: 377-388.

[Dunn et al 2005] Dunn GN, Knight IP, Hitchin ER. 2005. Measuring System Efficiencies of Liquid Chiller and Direct Expansion. ASHRAE Journal. February 2005.

[EnergyPlus 2009] EnergyPlus Engineering Reference. 2009. The Reference to EnergyPlus Calculations. University of Illinois and the Lawrence Berkeley National Laboratory.

[Engineered Systems 2002] Anonymous 2002. Reader's past experience: radiant cooling ultimately impractical – Letters to the Editor. Engineered Systems.

[Eto 1984] Eto, J.H. 1984. Cooling strategies based on indicators of thermal storage in commercial building mass. Annual Symp. on Improving Building Energy Efficiency 1984.

[Ferkl and Siroky 2010] Ferkl L, Siroky J. 2010. Ceiling radiant cooling: Comparison of ARMAX and subspace identification modeling methods. Building and Environment 45: 205-212.

[Feustel and Stetiu 1995] Feustel H, Stetiu C. 1995. Hydronic radiant cooling – preliminary assessment. Energy and Buildings 22: 193-205.

[Fracastoro and Lyberg 1983] Fracastoro GV, and Lyberg MD. 1983. Guiding Principles Concerning Design of Experiments, Instrumentation and Measuring Techniques. International Energy Agency and the Swedish Council for Building Research 1983. Stockholm, Sweden.

[Friere et al 2005] Friere RZ, Oliveira G, Mendes N. 2005. Development of single-zone predictive equations using linear regression for advanced controller synthesis. Proceedings of the Ninth International IBPSA Conference, Montreal, Canada. August 15-18, 2005.

[Forrester and Wepfer 1984] Forrester JR, and Wepfer WJ. 1984. Formulation of a load prediction algorithm for a large commercial building. *ASHRAE Transactions* 90(2b): 536–551.

[Geister and Thompson 2009] Geister WR, Thompson M. 2009. A Closer Look at Chiller Ratings. ASHRAE Journal. December 2009.

[Gillespie et al 2006] Gillespie KL, Haves P, Hitchcock RJ, Deringer J, Kinney K. 2006. A guide for specifying performance monitoring systems in commercial and institutional buildings. Proceedings of National Conference on Building Commissioning 2006.

[Goldstein 2007] Goldstein D. 2007. Saving energy, growing jobs: how environmental protection promotes economic growth, profitability, innovation, and competition. Bay Tree Publishing.

[Gonzalez and Zamarreno 2005] Gonzalez P, Zamarreno J. 2005. Prediction of hourly energy consumption in buildings based on a feedback artificial neural network. Energy and Buildings 37 (2005) 595-601.

[Gordon 1994] Gordon JM, Ng KC. 1994. Thermodynamic modeling of reciprocating chillers. Journal of Applied Physics 75(6): 2769-2774.

[Gordon 1995] Gordon JM Ng KC. 1995. Predictive and diagnostic aspects of a universal thermodynamic model for chillers. International Journal of Heat Mass Transfer 38(5): 807.

[Gorden et al 1995] Gordon JM, Ng KC, Chua HT. 1995. Centrifugal chillers: thermodynamic modeling and a diagnostic case study. International Journal of Refrigeration 18(4): 253.

[Granade et al 2009] Granade HC, Creyts J, Derkach A, Farese P, Nyquist S, Ostrowski K. 2009. Unlocking Energy Efficiency in the U.S. Economy. McKinsey & Company. July 2009.

[Griffith and Crawley 2006] Griffith B, Crawley D. 2006. Methodology for analyzing the technical potential for energy performance in the U.S. commercial buildings sector with detailed energy modeling. Proceedings of Simbuild 2006.

[Griffith et al 2006] Griffith B, Torcellini P, Long N, Crawley D, Ryan J. 2006 Assessment of the Technical Potential for Achieving Zero-Energy Commercial Buildings. ACEEE Summer Study on Energy Efficiency in Buildings.

[Haberl and Thamilseran 1996] Haberl J, Thamilseran S. 1996. Predicting Hourly Building Energy Use: The Great Energy Predictor Shootout II: Measuring Retrofit Savings -- Overview and Discussion of Results, ASHRAE Transactions: Research 102(2): 419 - 435 (June).

[Haberl and Bou-Saada 1998] Haberl J, Bou-Saada T. 1998. Procedures for calibrating hourly simulation models to measured building energy and environmental data. ASME Journal of Solar Energy Engineering 120:193-204 (August).

[Haberl et al 2003] Haberl J, Claridge D, Kissock K. 2003. Inverse model toolkit (1050RP): application and testing. ASHRAE Transactions 109(2): 435-448.

[Haghighat et al 1988] Haghighat F, Fazio P, Zmeureanu R. 1988. A systematic approach for derivation of transfer function coefficients of buildings from experimental data. Energy and Buildings 12: 101-111.

[Hatley et al 2005] Hatley DD, Meador RJ, Katipamula S, Brambley MR. 2005. Energy Management and Control System: Desired Capabilities and Functionality. Pacific Northwest National Laboratory. PNNL-15074.

[Hauser 2000] Hauser G, Kempkes C, Olesen BW, Liedelt DF. 2000. Computer simulation of the performance of a hydronic heating and cooling system with pipes embedded into the concrete slab between each floor. ASHRAE Transactions 106(1)

[He et al 1998] He XD, Liu S, Asada HH, Itoh H. 1998. Multivariable Control of Vapor Compression Systems. HVAC&R Research 4(3): 205-230

[Henze et al 1997] Henze G, Dodier RH, Krarti M. 1997. Development of a predictive optimal controller for thermal energy storage systems. Int'l. J. HVAC&R Research 3(3): 233–264.

[Henze and Krarti 1999] Henze G, Krarti M. 1999. The impact of forecasting uncertainty on performance of a predictive optimal controller for thermal energy storage systems. ASHRAE Transactions 105(1): 553–561.

[Henze et al 2004] Henze G, Felsmann C, Knabe G. 2004. Evaluation of optimal control for active and passive building thermal storage. International Journal of Thermal Sciences 43(2): 173-183.

[Henze et al 2008] Henze G, Felsmann C, Kalz D, Herkel S. 2008. Primary energy and comfort performance of ventilation assisted thermo-active building systems in continental climates. Energy and Buildings 40: 99-111.

[Henze et al 2010] Henze G, Florita A, Brandemuehl M, Felsmann C, Cheng H. 2010. Advances in Near-Optimal Control of Passive Building Thermal Storage. Journal of Solar Energy Engineering 132: 021009

[Hiller 1976] Hiller C. 1976. Improving Heat Pump Performance via Compressor Capacity Control, MIT Dept. Mechanical Engineering. PhD Thesis.

[Hittle and Bishop 1983] Hittle DC, Bishop R. 1983. An improved root-finding procedure for use in calculating transient heat flow through multilayered slabs. Int'l. J. Heat Mass Transfer 26(11): 1685–93.

[Holmes and Hacker 2007] Holmes MJ, Hacker JN. 2007. Climate change, thermal comfort and energy: Meeting the design challenges of the 21st century. Energy and Buildings 39: 802-814.

[Howell et al 2003] Howell R, Land D, Scheideman E. 2003. Air-Cooling Chillers for Hot, Dry Climates. ASHRAE Journal. December 2003.

[Hurley and Schooley 1984] Hurley CW, Schooley JF. 1984. Calibration of Temperature Measurement Systems Installed in Buildings. N.B.S. Building Science Series 153, January.

[Imanari et al 1999] Imanari T, Omori T, Bogaki K. 1999. Thermal comfort and energy consumption of the radiant ceiling panel system. Comparison with the conventional all-air system. Energy and Buildings 30: 167-175.

[Janargin et al 2006] Janargin RE, Liu B, Winiarski DW, McBride MF, Suharli L, Walden D. 2006. Technical support document: Development of the advanced energy design guide for small office buildings. PNNL-16250, Pacific Northwest National Laboratory, Richland, WA.

[Jeong et al 2003] Jeong JW, Mumma S, Bahnfleth W. 2003. Energy Conservation Benefits of a Dedicated Outdoor Air System with Parallel Sensible Cooling by Ceiling Radiant Panels. ASHRAE Transactions 109(2): 627-638

[Jiang et al 2007] Jiang W, Winiarski DW, Katipamula S, Armstrong PR. 2007. Cost Effective Integration of Low Lift Cooling Technologies. PNNL-17157. Pacific Northwest National Laboratory, Richland, WA.

[Jimenez and Heras 2005] Jimenez MJ, Heras MR. Application of multi-output ARX models for estimation of the U and g values of building components in outdoor testing. Solar Energy 79: 302-310.

[Jimenez and Madsen 2008] Jimenez MJ, Madsen H. 2008. Models for Describing The Thermal Characteristics of Building Components. Building and Environment 43: 152-162.

[Jimenez et al 2008] Jimenez MJ, Madsen H, Andersen KK. 2008. Identification of the main thermal characteristics of building components using MATLAB. Building and Environment 43: 170-180.

[Jin 2002] Jin H. 2002. Parameter estimation based models of water source heat pumps. PhD Thesis. Oklahoma State University. Stillwater, OK.

[Karatsou et al 2006] Karatsou S, Santamouris M, Geros V. Prediction of energy consumption in buildings with artificial intelligent techniques and Chaos time series analysis. Proceedings of the International Workshop on Energy Performance and Environmental Quality of Buildings. (July 2006) Milos Island, Greece.

[Katipamula et al 2010] Katipamula S, Armstrong PR, Wang W, Fernandez N, Cho H, Goetzler W, Burgos J, Radhakrishnan R, Ahlfeldt C. 2010. Cost-Effective Integration of Efficient Low-Lift Baseload Cooling Equipment FY08 Final Report. PNNL-19114. Pacific Northwest National Laboratory. Richland, WA.

[Keeney and Braun 1996] Keeney K, Braun J. 1996. A simplified method for determining optimal cooling control strategies for thermal storage in building mass. Int'l. J. HVAC&R Research 2(1): 59–78.

[Keeney and Braun 1997] Keeney KR, Braun JE. 1997. Application of building pre-cooling to reduce peak cooling requirements. ASHRAE Transactions 103(1): 463–469.

[Kim et al 2005] Kim T, Kato S, Murakami S, Rho Jw. 2005. Study on indoor thermal environment of office space controlled by cooling panel system using field measurement and the numerical simulation. Building and Environment 40: 301-310.

[Kintner-Meyer and Emery 1995] Kintner-Meyer M, Emery AF. 1995. Cost optimal analysis and load shifting potentials of cold storage equipment. ASHRAE Transactions 101(2): 539-548.

[Kissock et al 2003] Kissock, K., Haberl, J., and D. Claridge. 2003. Inverse model toolkit (1050RP): Numerical algorithms for best-fit variable-base degree-day and change-point models. ASHRAE Transactions 109(2): 425-434.

[Kitagawa et al 2009] Kitagawa K, Komoda N, Hayano H, Tanabe S. 1999. Effect of humidity and small air movement on thermal comfort under a radiant cooling ceiling by subjective experiments. Energy and Buildings 30: 185-193.

[Kobayashi 2001] Kobayashi N. 2001. Floor-Supply Displacement Ventilation System. Masters Thesis. Massachusetts Institute of Technology.

[Kolokotsa et al 2005] Kolokotsa D, Niachou K, Geros V, Kalaitzakis K, Stavrakakis GS, Santamouris M. 2005. Implementation of an integrated indoor environment and energy management system. Energy and Buildings 37: 93-99.

[Koschenz and Dorer 1999] Koschenz M, Dorer V. 1999. Interaction of an air system with concrete core conditioning. Energy and Buildings 30: 139–145.

[Krarti 2003] Krarti M. 2003. An Overview of Artificial Intelligence-Based Methods for Building Energy Systems. Journal of Solar Energy Engineering 125.

[Kreider and Haberl 1994a] Kreider J, Haberl J. 1994. Predicting hourly building energy usage: The great energy predictor shootout: Overview and discussion of results. ASHRAE Transactions 100(2): 1104-1118.

[Kreider and Haberl 1994b] Kreider J, Haberl J. 1994. Predicting hourly building energy usage: The results of the 1993 great energy predictor shootout identify the most accurate method for making hourly energy use predictions. ASHRAE Journal 35(3): 72-81.

[Kreider et al 1995] Kreider JF, Claridge DE, Curtiss P, Dodier R, Haberl JS, Krarti M. 1995. Building Energy Use Prediction and System Identification Using Recurrent Neural Networks. Journal of Solar Energy Engineering 117.

[Kumar et al 2008] Kumar M, Kar IN, Ray A. September 2008. State Space Based Modeling and Performance Evaluation of an Air Conditioning System. HVAR&R Research 14(5): 797-816

[Larranaga et al 2008] Larranaga M, Beruvides M, Holder HW, Karunasena E, Straus D. 2008. DOAS & Humidity Control. ASHRAE Journal May 2008.

[Lee and Braun 2006] Lee KH, Braun JE. 2006. An Experimental Evaluation of Demand Limiting Using Building Thermal Mass in a Small Commercial Building. ASHRAE Transactions 112 (21): 558-571

[Lee and Braun 2008] Lee KH, Braun JE. 2008. A Data-Driven Method for Determining Zone Temperature Trajectories that Minimize Peak Electrical Demand. ASHRAE Transactions 114 (2): 65-74.

[Lehman et al 2007] Lehmann B, Dorer V, Koschenz M. 2007. Application range of thermally activated buildings systems tabs. Energy and Buildings 39 (2007) 593-598.

[Leigh et al 2005] Leigh SB, Song DS, Hwang SH, Lee SY. 2005. A Study for Evaluating Performance of Radiant Floor Cooling Integrated with Controlled Ventilation. ASHRAE Transactions: Research: 72-81

[Levermore 2008] Levermore, GJ. A review of the IPCC Assessment Report Four, Part 2: Mitigation options for residential and commercial buildings. Building Serv. Eng. Res. Technol. 29(4): 363-374

[Levine et al 2007] Levine M, Ürge-Vorsatz D, Blok K, Geng L, Harvey D, Lang S, Levermore G, Mongameli Mehlwana A, Mirasgedis S, Novikova A, Rilling J, Yoshino H, 2007: Residential and commercial buildings. In Climate Change 2007: Mitigation. Contribution of Working Group III to the Fourth Assessment Report of the Intergovernmental Panel on Climate Change [B. Metz, O.R. Davidson, P.R. Bosch, R. Dave, L.A. Meyer (eds)], Cambridge University Press, Cambridge, United Kingdom and New York, NY, USA.

[Lewis et al 1999] Lewis RM, Torczon V. 1999. Pattern Search Algorithms for Bound Constrained Minimization. SIAM Journal on Optimization 9 (4): 1082–1099.

[Lewis et al 2000] Lewis RM, Torczon V. 2000. Pattern Search Methods for Linearly Constrained Minimization. SIAM Journal on Optimization 10(3): 917–941.

[Lewis 2004] Lewis M. 2004. Integrated Design for Sustainable Buildings. ASHRAE Journal September 2004.

[Lim et al 2006] Lim JH, Jo JH, Kim YY, Yeo MS, Kim KW. 2006. Application of control methods for radiant floor cooling system in residential buildings. Building and Environment 41: 60-73.

[Liu and Claridge 1998] Liu, M. and D.E. Claridge. 1998. Use of calibrated HVAC system models to optimize system operation. Journal of Solar Energy Engineering, May, Vol. 120.

[Ljung 1999] Ljung L. 1999. System Identification: Theory for the User. Prentice-Hall, Inc. Upper Saddle River, New Jersey.

[Lovins 1976] Lovins A. 1976. Energy Strategy: The Road Not Taken? Foreign Affairs.

[Lundin et al 2004] Lundin M, Andersson S, Ostin R. 2004. Development and validation of a method aimed at estimating building performance parameters, Energy and Buildings 36 (9): 905–914.

[Lundin et al 2005] Lundin M, Andersson S, Ostin R. 2005. Further validation of a method aimed to estimate building performance parameters. Energy and Buildings 37: 867-871.

[MacCracken 2004] MacCracken M. 2004. Thermal Energy Storage in Sustainable Buildings. ASHRAE Journal September 2004.

[MacCracken 2008] MacCracken M. 2008. Thermal Energy Storage Myths. ASHRAE Journal September 2008.

[MacDonald and Wasserman 1989] MacDonald JM, Wasserman DM. 1989. Investigation of Metered Data Analysis Methods for Commercial and Related Buildings. ORNL Report ORNL/CON-279. U.S. Department of Energy, Oak Ridge National Laboratory, Oak Ridge, TN.

[Mackensen et al 2002] Mackensen A, Klein SA, Reindl DT. 2002. Characterization of refrigerant system compressor performance. IRAC Conference Purdue University, West Lafayette, IN.

[Madsen and Holst 1995] Madsen H, Holst J. 1995. Estimation of continuous-time models for the heat dynamics of a building. Energy and Buildings 22: 67-79.

[Mahdavi 2001] Mahdavi A. 2001. Simulation-based control of buildings systems operation. Building and Environment 36: 789-796.

[Mathworks 2010] Mathworks. 2010. Matlab Global Optimization Toolbox 3: User's Guide. Natick, MA.

[McConahey 2008] McConahey E. 2008. Mixed Mode Ventilation: Finding the Right Mix. ASHRAE Journal September 2008.

[McKinsey 2007] Creyts J, Derkach A, Nyquist S, Ostrowski K, Stephenson J. 2007. Reducing U.S. Greenhouse Gas Emissions: How Much at What Cost? McKinsey and Company.

[Meierhans 1996] Meierhans RA. 1996. Room air-conditioning by means of overnight cooling of the concrete ceiling. ASHRAE Transactions 102(1): 693-697

[Michel 2000] Michel E, Isoardi JP. 1993. Cooling floor, Proceedings of Clima2000, London, UK.

[Mitalas and Stephenson 1967] Mitalas GP, Stephenson DG. 1967. Room Thermal Response Factors. ASHRAE Transactions 73(1)

[Mitsubishi 2006] Mitsubishi Electric. 2006. Submittal Data: MSZ-A09NA & MUZ-A09NA. Mitsubishi Electric HVAC Advanced Products Division. Suwanee, GA.

[Motegi and Piette 2002] Motegi M, Piette MA. 2002. Web-based Energy Information Systems for Large Commercial Buildings. National Conference on Building Commissioning, May 8-10 2002.

[Motegi et al 2003] Motegi N, Piette MA, Kinney S, Herter K. 2003. Web-based energy information systems for energy management and demand response in commercial buildings. LBNL-52510. Lawrence Berkeley National Laboratory.

[Mui et al 2006] Mui KW, Wong LT, Ho WL. 2006. Evaluation on sampling point densities for assessing indoor air quality. Building and Environment 41: 1515-1521.

[Mumma 2001] Mumma S. 2001. Ceiling Panel Cooling Systems. ASHRAE Journal November 2001.

[Mumma and Shank 2001] Mumma S, Shank K. 2001. Achieving Dry Outside Air in an Energy-Efficient Manner. ASHRAE Transactions 107(1): 1-9

[Mustafaraj et al 2009] Mustafaraj G, Chen, J, Lowry G. 2009. Thermal behavior model identification for an office space using BMS data. Building Serv. Eng. Res. Technol. 30(4): 329-341

[Nielsen and Madsen 1998] Nielsen B, Madsen H. 1998. Identification of a Linear Continuous Time Stochastic Model of the Heat Dynamics of a Greenhouse. J. Agric. Engng. Res. 71: 249-256.

[NIST 2009] NIST. NIST Reference Fluid Thermodynamic and Transport Properties Database (REFPROP): Version 8.0. NIST Standard Reference Database 23.

[Niu et al 1995] Niu J, Kooi Jvd, Ree Hvd. 1995. Energy saving possibilities with cooled-ceiling systems. Energy and Buildings 23: 147-158.

[Norford et al 1985] Norford LK, Rabl A, Socolow RH, Persily AK. 1985. Measurement of thermal characteristics of office buildings. Proc. BTECC III Conf., ASHRAE SP 49: 272–288.

[Olesen 1997] Olesen BW. 1997. Possibilities and limitations of radiant floor cooling. ASHRAE Transactions 103(1): 42-48.

[Olesen 2000a] Olesen BW, Liedelt DF, Michel E, Bonnefoi F, De Carli M. 2000. Heat exchange coefficient between floor surface and space by floor cooling: theory or a question of definition, ASHRAE Transactions 106(1).

[Olesen 2000b] Olesen BW. 2000. Hydronic radiant heating and cooling of buildings using pipes embedded in the building structure. Conference proceedings of AICARR 41.

[Olesen et al 2003] Olesen B, Koschenz M, Johansson C. 2003. New European Standard Proposal for Design and Dimensioning of Embedded Radiant Surface Heating and Cooling Systems. ASHRAE Transactions KC-03-7-4.

[Olesen 2008] Olesen B. 2008. Radiant Floor Cooling Systems. ASHRAE Journal Journal 2008.

[Oxizidis and Papadopolous 2008] Oxizidis S, Papadopoulos AM. 2008. Solar Air Conditioning: A Review of Technological and Market Perspectives. Advances in Buildings Energy Research 2: 123-157.

[Paksoy 2002] Paksoy H. 2002. Advanced thermal energy storage through phase change materials and chemical reactions – feasibility studies and demonstration projects. IEA, ECES IA Annex 17. 3rd Workshop, 1-2 October 2002. Tokyo, Japan.

[Penman 1990] Penman JM. 1990. Second Order System Identification in the Thermal Response of a Working School. Building and Environment 25(2): 105-110.

[Perez-Lombard et al 2007] Perez-Lombard L, Ortiz J, Pout C. 2007. A review on buildings energy consumption information. Energy and Buildings 40(3): 394-398.

[Pfafferott and Katz 2007] Pfafferott J, Katz D. 2007. Thermo-active building systems. BINE Themeninfo 2007.

[Pieete et al 2001] Piette MA, Khalsa S, Haves P. 2001. Analysis of an Information Monitoring and Diagnostic System to Improve Building Operations. Energy and Buildings, 33(8): 783-792.

[Pryor and Winn 1982] Pryor DV, Winn C.B. 1982. A Sequential Filter Used for Parameter Estimation in a Passive Solar System. *Solar Energy* 28: 65.

[Quartararo et al 2006] Quartararo L, Roth K, Brodrick J. 2006. Optimal Whole Building Control Systems. ASHRAE Journal March 2006.

[Rabl 1988] Rabl A. 1988. Parameter estimation in buildings: Methods for dynamic analysis of measured energy use. Journal of Solar Energy Engineering 110: 52-66.

[Rabl and Norford 1991] Rabl A, Norford LK. 1991. Peak load reduction by preconditioning buildings at night. Int'l. J. Energy Res. 15: 781–798.

[Reddy 1989] Reddy TA. 1989. Application of dynamic building inverse models to three occupied residences monitored non-intrusively. Proceedings of the Thermal Performance of the Exterior Envelopes of Buildings IV, ASHRAE/DOE/BTECC/CIBSE, Orlando, Florida, December.

[Reddy et al 2002] Reddy TA, Elleson, J, Haberl J. 2002. Methodology development for determining long-term performance of cool storage systems from short term tests. ASHRAE Transactions 108(1): 1085-1103.

[Richalet and Neirac 1991] Richalet V, Neirac F. 1991. On Site Identification of Building Energy Performances. Conference Proceedings of Building Simulation 1991, Nice, France, 578-583.

[Roth et al 2005] Roth K, Westphalen D, Feng M, Llana P, Quartararo L. 2005. Energy Impact of Commercial Buildings Controls and Performance Diagnostics: Market Characterization, Energy Impact of Buildings Faults and Energy Savings Potential. TIAX LLC.

[Roth et al 2006a] Roth K, Westphalen D, Brodrick J. 2006. Ductless Split Systems. ASHRAE Journal July 2006.

[Roth et al 2006b] Roth K, Zogg R, Brodrick J. 2006. Cool Thermal Energy Storage. ASHRAE Journal September 2006.

[Roth et al 2007] Roth K, Dieckmann J, Zogg R, Brodrick J. 2007. Chilled Beam Cooling. ASHRAE Journal September 2007.

[Roth et al 2009] Roth K, Dieckmann J, Brodrick J. 2009. Using Off-Peak Precooling. ASHRAE Journal March 2009.

[Ruano et al 2006] Ruano AE, Crispim EM, Conceicao EZE, Lucio MMJR. 2006. Prediction of buildings' temperature using neural networks models. Energy and Buildings 38: 682-694.

[Ruud et al 1990] Ruud MD, Mitchell JW, Klein SA. 1990. Use of building thermal mass to offset cooling loads. ASHRAE Transactions 96(2): 820–829.

[Ryu et al 2004] Ryu SR, Lim JH, Yeo MS, Kim KW. 2004. A Study on the Control Methods for Radiant Floor Heating and Cooling System in Residential Building. ASHRAE Transactions: Research 2004: 106-116.

[Santamouris and Georgakis 2003] Santamouris M, Georgakis C. 2003. Energy and indoor climate in urban built environments: recent trends. Building Serv. Eng. Res. Technol. 24(2): 69–81.

[Scheatzle 2006] Scheatzle D. 2006. Combining Radiant and Convective Systems with Thermal Mass for a More Comfortable Home. ASHRAE Transactions 112(1): 253-268.

[Seem and Hancock 1985] Seem JE, Hancock CE. 1985. A method for characterizing the performance of a thermal storage wall from measured data. Thermal Performance of the Exterior Envelopes of Buildings III, ASHRAE/DOE/BTECC, Clearwater Beach, FL.

[Seem 1987] Seem JE. 1987 Modeling of heat transfer in buildings. PhD Thesis, University of Wisconsin, Madison.

[Shao et al 2004] Shao S, Shi W, Li X, Chen H. 2004. Performance representation of variable-speed compressor for inverter air conditioners based on experimental data. International Journal of Refrigeration 27: 805-815.

[Simmonds 1994] Simmonds P. 1994. Control strategies for combined heating and cooling radiant systems, ASHRAE Transactions 100(1): 1031-1039.

[Simmonds et al 2000] Simmonds P, Holst S, Reuss S, Gaw W. 2000. Using radiant cooled floors to condition large spaces and maintain comfort conditions, ASHRAE Transactions 106(1): 695-701

[Simmonds et al 2006] Simmonds P, Chambers I, Mehlomakulu B, Simmonds C. 2006. Applied Performance of Radiant Ceiling Panels for Cooling. ASHRAE Transactions 112(1): 368-376

[Sivak 2009] Sivak M. 2009. Potential energy demand for cooling in the 50 largest metropolitan areas of the world: Implications for developing countries. Energy Policy 37: 1382-1384.

[Snyder and Newell 1990] Snyder ME, Newell TA. 1990. Cooling Cost Minimization Using Building Mass for Thermal Storage. ASHRAE Transactions: Research. SL-90-14-3.

[Sodec 1999] Sodec F. 1999. Economic viability of cooling ceiling systems. Energy and Buildings 30: 195-201.

[Sonderegger 1977] Sonderegger R. 1977. Dynamic Models of House Heating Based on Equivalent Thermal Parameters. Ph.D. Thesis, Center for Energy and Environmental Studies, Report No. 57, Princeton University.

[Sonderreger 1978] Sonderegger R. 1978. Diagnostic tests determining the thermal response of a house. ASHRAE Transactions 84(1): 691-702.

[Spasokukotskiy 2003] Spasokukotskiy K, Trankler H, Lukasheva K. 2003. Model-based method to measure thermal comfort in buildings. IEEE International Workshop on Intelligent Data Acquisition and Advanced Computing Systems: Technology and Applications 8-10 Sept. 2003, Lviev, Ukraine.

[Spindler and Norford 2009] Spindler H, Norford LK. 2009. Naturally ventilated and mixed-mode buildings – Part I: Thermal modeling. Building and Environment 44: 736-740.

[Stephenson and Mitalas 1967] Stephenson DG, Mitalas GP. 1967. Cooling Load Calculations by Thermal Reponse Factor Method. ASHRAE Transactions 73(1)

[Stephenson and Mitalas 1971] Stephenson DG, Mitalas GP. 1971. Calculation of heat conduction transfer functions for multi-layer slabs. ASHRAE Transactions 77(2):117–126.

[Stetiu 1999] Stetiu C. 1999. Energy and peak power savings potential of radiant cooling systems in US commercial buildings. Energy and Buildings 30: 127-138.

[Strand 1997] Strand, R.K. and C.O. Pedersen. 1997. Implementation of a radiant heating and cooling model into an integrated building energy analysis program, ASHRAE Transactions 103(1): 949-958.

[Subbarao 1985] Subbarao K. 1985. Thermal parameters for single and multizone buildings and their determination from performance data. Golden, CO: Solar Energy Research Institute Report SERI/TR-253-2617.

[Subbarao et al 1990] Subbarao K, Burch J, Hancock CE. 1990 How to accurately measure the load coefficient of a residential building. Sol Eng 1990 Twelfth Annu Int Sol Energ Conf 1990: 419–25.

[Takebayashi et al 1994] Takebayashi M, Kohsokabe H, Sekigami K, Suefuji K, Tsubono I, Inaba K. 1994. Performance Improvement of a variable-speed controlled scroll compressor for household air conditioners. ASHRAE Transactions 100(1): 471-475.

[Tian and Love 2009] Tian Z, Love J. 2009. Energy performance optimization of radiant slab cooling using building simulation and field measurements. Energy and Buildings 41: 320-330.

[Todesco 2004] Todesco G. 2004. Integrated Designs and HVAC Equipment Sizing. ASHRAE Journal September 2004.

[Torczon 1997] Torczon, V. 1997. On the Convergence of Pattern Search Algorithms. SIAM Journal on Optimization 7(1): 1–25

[UNEP 2007] United Nations Environment Programme. 2007. Buildings and Climate Change: Status, Challenges and Opportunities. ISBN: 978-92-807-2795-1.

[USDOE 2006] USDOE. 2006. U.S. Residential and Commercial Buildings Total Primary Energy Consumption. Buildings Energy Data Book.

[Uponor 2010] Uponor. 2010. Radiant Cooling Systems. http://www.uponor-usa.com/en/Misc/Applications/Radiant-Cooling.aspx (accessed July 31, 2010).

[Vangtook and Chirarattananon 2006] Vangtook P, Chirarattananon S. 2006. An experimental investigation of application of radiant cooling in hot humid climates. Energy and Building 38: 273-285.

[Wang and Xu 2003] Wang S, Xinhua X. 2003. Hybrid model for building performance diagnosis and optimal control. Proceedings of the International Conference for Enhanced Building Operations 2003.

[Wang and Ma 2008] Wang S, Ma Z. 2008. Supervisory and Optimal Control of Building HVAC Systems: A Review. HVAC&R Research 14 (1): 3-32.

[Watson et al 1996] Watson RT, Zinyowera MC, and Moss RH. 1996. Technologies, Policies and Measures for Mitigating Climate Change. Intergovernmental Panel on Climate Change.

[Willingham 2009] Willingham R. 2009. Testing and Modeling of Compressors for Low-Lift Cooling Applications. Masters Thesis. Massachusetts Institute of Technology.

[Wilson et al 1985] Wilson NW, Wagner BS, Colbourne WG. 1985. Equivalent Thermal Parameters for an Occupied Gas-Heated House. ASHRAE Transactions 91(2)

[Xu and Haves 2005] Xu P, Haves P. 2006. Case Study of Demand Shifting with Thermal Mass in Two Large Commercial Buildings. ASHRAE Transactions 112(1): 572-580

[Yang 1999] Yang X. 1999. Study of Building Material Emissions and Indoor Air Quality. PhD Thesis. Massachusetts Institute of Technology.

[Zakula 2010] Zakula, T. 2007. Heat Pump Simulation Model and Optimal Variable-Speed Control for a Wide Range of Cooling Conditions. Masters Thesis. Massachusetts Institute of Technology.

[Zhou et al 2008] Zhou J, Wei G, Turner WD, Deng S, Claridge D, Contreras O. 2005. Control Optimization for a Chilled Water Thermal Storage System Under a Complicated Time-of-Use Electricity Rate Schedule. ASHRAE Transactions: Research 2005.

Appendix A. Low lift heat pump performance testing

A.1 Heat pump test stand sensors and instrumentation

A.1.1 Table of sensors on heat pump test stand

Label	Sensor description	Sensor Make/Model	Installation notes	Accuracy
T_s	Suction refrigerant temperature	Omega/PR-T-24-SLE	Insulated refrigerant pipe surface temperature, would to prevent stem loss	0.5 C
T_d	Discharge refrigerant temperature	Omega/PR-T-24-SLE	Insulated refrigerant pipe surface temperature, would to prevent stem loss	0.5 C
$T_{cnd,liq}$	Condenser outlet liquid refrigerant temperature	Omega/PR-T-24-SLE	Insulated refrigerant pipe surface temperature, would to prevent stem loss	0.5 C (rated)
T_{xvo}	Expansion valve outlet refrigerant temperature	Omega/PR-T-24-SLE	Insulated refrigerant pipe surface temperature, would to prevent stem loss	0.5 C (rated)
$T_{air,zone}$	Evaporator zone air temperature	Omega/PR-T-24-SLE	In center of zone control volume	0.5 C (rated)
$T_{evp,air,in}$	Evaporator inlet air temperature	Omega/PR-T-24-SLE	In center of evaporator inlet air stream	0.5 C (rated)
$T_{air,amb}$	Ambient air temperature	Omega/PR-T-24-SLE	At one foot away from condenser inlet	0.5 C (rated)
$\Delta T_{evp,air}$	Evaporator air temperature difference	Omega/PR-T-24-SLE	Average temperature difference across the evaporator using a 9x2 junction thermopile	0.5 C (rated)
$T_{cnd,air,in}$	Condenser inlet air temperature	Omega/PR-T-24-SLE	In center of condenser inlet air stream	0.5 C (rated)
$T_{cnd,air,out}$	Condenser outlet air temperature	Omega/PR-T-24-SLE	In center of condenser outlet air stream	0.5 C (rated)
$\Delta T_{cnd,air}$	Condenser air temperature difference	Omega/PR-T-24-SLE	Average temperature difference across the evaporator using a 16x2 junction thermopile	0.5 C (rated)
P_s	Suction refrigerant pressure	MEAS, INC. MSP-300-500-P2-N1	Installed at the outdoor unit stop valve in a 1/4" NPT fitting	1% of span
P_d	Discharge refrigerant pressure	MEAS, INC. MSP-300-1000-P2-N1	Installed at the discharge service port	1% of span
P_{xvo}	Expansion valve outlet pressure	MEAS, INC. MSP-300-500-P2-N1	Installed at the outdoor unit stop valve in a 1/4" NPT fitting	1% of span
P_{amb}	Ambient air pressure measured at local weather station	Measured at time of test from weather station KMACAMBR9. Data listed at http://www.wunderground.com		
$\forall$	Volumetric condenser air flowrate	Correlated to condenser fan speed through the measurements shown in Appendix A.1.2		

W_{box}	Total power to the zone control volume, including fan and heaters	Wattnode WNB-3D-240-P	Installed on the 208 VAC input to the evaporator fan and electrical heaters installed inside the zone control volume. Primary component of	0.5% of reading
W_{unit}	Total power to the outdoor unit, including inverters, fan and compressor	Wattnode WNB-3D-240-P	Installed on the 208 VAC input to the outdoor unit. Does not include evaporator fan power which was measured separately along with the zone heat load	0.5% of reading
$W_{DC,fan}$	DC power to the condenser fan inverter	Yokogawa WT230 3-input Digital Power Meter	Installed on the primary side of the condenser fan inverter	0.1% of reading
$W_{DC,cmp}$	DC power to the compressor inverter	Yokogawa WT230 3-input Digital Power Meter	Installed on the primary side of the compressor's inverter	0.1% of reading
$W_{3\varnothing,fan}$	Three phase power from the inverter to the condenser fan	Yokogawa WT230 3-input Digital Power Meter	Installed on the secondary side of the condenser fan inverter, between the inverter and the fan motor	0.1% of reading
$W_{3\varnothing,cmp}$	Three phase power from the inverter to the compressor	Yokogawa WT230 3-input Digital Power Meter	Installed on the secondary side of the compressor inverter, between the inverter and the compressor motor	0.1% of reading
UA_{box}	Thermal conductance of the insulated zone control volume	Calculated based on W_{box}, $T_{air,zone}$, $T_{air,amb}$	UA_{box} is calculated based on repeated experiments in which a constant heat input W_{box} was applied to the zone control volume until a steady state temperature difference was achieved, $(T_{air,zone}-T_{air,amb})$. $UA_{box} = W_{box}/(T_{air,zone}-T_{air,amb})$ ~1.9 W/K	

All data was logged using a Campbell Scientific CR10X data logger, with a slave Campbell Scientific AM25T 25-channel-multiplexer for thermocouple measurements. The data logging code for the CR10X logger, in the Campbell Scientific EdLog 32 format, is shown below

Heat pump test stand CR10X EdLog32 data-logging code(written in part by P.R. Armstrong)

```
;{CR10X}
*Table 1 Program
  01: 2.5       Execution Interval (seconds)

1:  Batt Voltage (P10)
  1: 1        Loc [ Batt_Volt ]
2:  If time is (P92)
  1: 0        Minutes (Seconds --) into a
  2: 1440     Interval (same units as above)
  3: 30       Then Do
    3:  Signature (P19)
      1: 2        Loc [ Prog_Sig  ]
4:  End (P95)

5:  Do (P86)
  1: 41       Set Port 1 High

6:  Full Bridge (P6)
  1: 1        Reps
  2: 23       25 mV 60 Hz Rejection Range
  3: 1        DIFF Channel
  4: 1        Excite all reps w/Exchan 1
  5: 1200     mV Excitation
  6: 3        Loc [ RTemp_C   ]
  7: -0.001   Multiplier
  8: 0.09707  Offset

7:  BR Transform Rf[X/(1-X)] (P59)
  1: 1        Reps
  2: 3        Loc [ RTemp_C   ]
  3: 10.025   Multiplier (Rf)

8:  Temperature RTD (P16)
  1: 1        Reps
  2: 3        R/R0 Loc [ RTemp_C   ]
  3: 3        Loc [ RTemp_C   ]
  4: 1        Multiplier
  5: 0        Offset

; ------------Temperatures, AM25T Chn:1-11----------
```

```
9:  Beginning of Loop (P87)
 1: 0       Delay
 2: 11      Loop Count

   10:  Do (P86)
    1: 72      Pulse Port 2
   11:  Excitation with Delay (P22)
    1: 1       Ex Channel
    2: 0       Delay W/Ex (0.01 sec units)
    3: 1       Delay After Ex (0.01 sec units)
    4: 0       mV Excitation
   12:  Do (P86)
    1: 72      Pulse Port 2
   13:  Excitation with Delay (P22)
    1: 1       Ex Channel
    2: 0       Delay W/Ex (0.01 sec units)
    3: 1       Delay After Ex (0.01 sec units)
    4: 0       mV Excitation
   14:  Thermocouple Temp (DIFF) (P14)
    1: 1       Reps
    2: 0       Auto Slow Range (OS>1.09)
    3: 1       DIFF Channel
    4: 1       Type T (Copper-Constantan)
    5: 3       Ref Temp (Deg. C) Loc [ RTemp_C   ]
    6: 4     -- Loc [ Tsuc     ]
    7: 1       Multiplier
    8: 0       Offset
15:  End (P95)

;-------------Yokogawa phase to phase powers Chn:12-13--------------
   16:  Do (P86)
    1: 72      Pulse Port 2
   17:  Excitation with Delay (P22)
    1: 1       Ex Channel
    2: 0       Delay W/Ex (0.01 sec units)
    3: 1       Delay After Ex (0.01 sec units)
    4: 0       mV Excitation
   18:  Do (P86)
    1: 72      Pulse Port 2
   19:  Excitation with Delay (P22)
    1: 1       Ex Channel
    2: 0       Delay W/Ex (0.01 sec units)
    3: 1       Delay After Ex (0.01 sec units)
    4: 0       mV Excitation
   20:  Volt (Diff) (P2)
    1: 1       Reps
    2: 15      2500 mV Fast Range
    3: 1       DIFF Channel
    4: 50      Loc [ ACYoko    ]
    5: 0.6     Multiplier
    6: 0.0     Offset

;Yokogawa power measurement, 300 Volts, 10 Amps, 6000 kW, 5
VDC output
   21:  Do (P86)
    1: 72      Pulse Port 2
   22:  Excitation with Delay (P22)
    1: 1       Ex Channel
    2: 0       Delay W/Ex (0.01 sec units)
    3: 1       Delay After Ex (0.01 sec units)
    4: 0       mV Excitation
   23:  Do (P86)
    1: 72      Pulse Port 2
   24:  Excitation with Delay (P22)
    1: 1       Ex Channel
    2: 0       Delay W/Ex (0.01 sec units)
    3: 1       Delay After Ex (0.01 sec units)
    4: 0       mV Excitation
   25:  Volt (Diff) (P2)
    1: 1       Reps
    2: 15      2500 mV Fast Range
    3: 1       DIFF Channel
    4: 51      Loc [ ABYoko    ]
    5: 0.6     Multiplier
    6: 0.0     Offset

; ------------Pressure Drops 1/1000 inches water column, AM25T
Chn:14-15--------------
26:  Beginning of Loop (P87)
 1: 0       Delay
 2: 2       Loop Count
   27:  Do (P86)
    1: 72      Pulse Port 2
   28:  Excitation with Delay (P22)
    1: 1       Ex Channel
    2: 0       Delay W/Ex (0.01 sec units)
    3: 1       Delay After Ex (0.01 sec units)
    4: 0       mV Excitation
   29:  Do (P86)
    1: 72      Pulse Port 2
   30:  Excitation with Delay (P22)
    1: 1       Ex Channel
    2: 0       Delay W/Ex (0.01 sec units)
    3: 1       Delay After Ex (0.01 sec units)
    4: 0       mV Excitation
   31:  Volt (Diff) (P2)
    1: 1       Reps
    2: 25      2500 mV 60 Hz Rejection Range
    3: 1       DIFF Channel
    4: 17    -- Loc [ delPHx    ]
    5: 0.1     Multiplier
    6: 0.0     Offset
;  0-5 VDC output with 11K-11K voltage divider (0-2500 mV), 0 to
0.25 in WC full scale = 0.0001 inches water column/mV
32:  End (P95)

; ------------Yoko DC Power, AM25T Chn:16--------------
33:  Do (P86)
 1: 72      Pulse Port 2
34:  Excitation with Delay (P22)
 1: 1       Ex Channel
 2: 0       Delay W/Ex (0.01 sec units)
 3: 1       Delay After Ex (0.01 sec units)
 4: 0       mV Excitation
35:  Do (P86)
 1: 72      Pulse Port 2
36:  Excitation with Delay (P22)
 1: 1       Ex Channel
 2: 0       Delay W/Ex (0.01 sec units)
 3: 1       Delay After Ex (0.01 sec units)
 4: 0       mV Excitation
37:  Volt (Diff) (P2)
 1: 1       Reps
 2: 15      2500 mV Fast Range
 3: 1       DIFF Channel
 4: 49    -- Loc [ DCYoko    ]
 5: 0.6     Multiplier
 6: 0.0     Offset

; ------------Air-Side dT, AM25T Chn:17-19--------------
38:  Do (P86)
 1: 72      Pulse Port 2
```

```
39:  Excitation with Delay (P22)
 1: 1       Ex Channel
 2: 0       Delay W/Ex (0.01 sec units)
 3: 1       Delay After Ex (0.01 sec units)
 4: 0       mV Excitation
40:  Do (P86)
 1: 72      Pulse Port 2
41:  Excitation with Delay (P22)
 1: 1       Ex Channel
 2: 0       Delay W/Ex (0.01 sec units)
 3: 1       Delay After Ex (0.01 sec units)
 4: 0       mV Excitation
42:  Volt (Diff) (P2)
 1: 1       Reps
 2: 23      25 mV 60 Hz Rejection Range
 3: 1       DIFF Channel
 4: 20    -- Loc [ dTcndair  ]
 5: 1.0     Multiplier
 6: 0.0     Offset

;----------dTcndcalcs----------
43:  Z=X*F (P37)
 1: 20      X Loc [ dTcndair  ]
 2: .111111  F
 3: 20      Z Loc [ dTcndair  ]
;mV per thermopile cell from 9 cells in series
44:  Z=X (P31)
 1: 20      X Loc [ dTcndair  ]
 2: 38      Z Loc [ delta_e   ]
45:  Z=X (P31)
 1: 8       X Loc [ TcndAirIn ]
 2: 39      Z Loc [ TPref     ]
46:  Do (P86)
 1: 1       Call Subroutine 1
47:  Z=X (P31)
 1: 42      X Loc [ TPresult  ]
 2: 20      Z Loc [ dTcndair  ] ;

;----------dtevp----------
48:  Do (P86)
 1: 72      Pulse Port 2
49:  Excitation with Delay (P22)
 1: 1       Ex Channel
 2: 0       Delay W/Ex (0.01 sec units)
 3: 1       Delay After Ex (0.01 sec units)
 4: 0       mV Excitation
50:  Do (P86)
 1: 72      Pulse Port 2
51:  Excitation with Delay (P22)
 1: 1       Ex Channel
 2: 0       Delay W/Ex (0.01 sec units)
 3: 1       Delay After Ex (0.01 sec units)
 4: 0       mV Excitation
52:  Volt (Diff) (P2)
 1: 1       Reps
 2: 23      25 mV 60 Hz Rejection Range
 3: 1       DIFF Channel
 4: 21    -- Loc [ dTevpair  ]
 5: 1.0     Multiplier
 6: 0.0     Offset

;----------dTevpcalcs----------
53:  Z=X*F (P37)
 1: 21      X Loc [ dTevpair  ]
 2: 0.125   F
 3: 21      Z Loc [ dTevpair  ]
;mV per thermopile cell from 8 cells in series
54:  Z=X (P31)
 1: 21      X Loc [ dTevpair  ]
 2: 38      Z Loc [ delta_e   ]
55:  Z=X (P31)
 1: 9       X Loc [ TevpAirIn ]
 2: 39      Z Loc [ TPref     ]
56:  Do (P86)
 1: 1       Call Subroutine 1
57:  Z=X (P31)
 1: 42      X Loc [ TPresult  ]
 2: 21      Z Loc [ dTevpair  ] ;

;----------dT fanfin----------
58:  Do (P86)
 1: 72      Pulse Port 2
59:  Excitation with Delay (P22)
 1: 1       Ex Channel
 2: 0       Delay W/Ex (0.01 sec units)
 3: 1       Delay After Ex (0.01 sec units)
 4: 0       mV Excitation
60:  Do (P86)
 1: 72      Pulse Port 2
61:  Excitation with Delay (P22)
 1: 1       Ex Channel
 2: 0       Delay W/Ex (0.01 sec units)
 3: 1       Delay After Ex (0.01 sec units)
 4: 0       mV Excitation
62:  Volt (Diff) (P2)
 1: 1       Reps
 2: 23      25 mV 60 Hz Rejection Range
 3: 1       DIFF Channel
 4: 22    -- Loc [ dTfanfin  ]
 5: 1.0     Multiplier
 6: 0.0     Offset

;----------dTfanfin calcs----------
63:  Z=X*F (P37)
 1: 22      X Loc [ dTfanfin  ]
 2: .111111  F
 3: 22      Z Loc [ dTfanfin  ]
;mV per thermopile cell from 9 cells in series
64:  Z=X (P31)
 1: 22      X Loc [ dTfanfin  ]
 2: 38      Z Loc [ delta_e   ]
65:  Z=X (P31)
 1: 10      X Loc [ TcndAirOu ]
 2: 39      Z Loc [ TPref     ]
66:  Do (P86)
 1: 1       Call Subroutine 1
67:  Z=X (P31)
 1: 42      X Loc [ TPresult  ]
 2: 22      Z Loc [ dTfanfin  ] ;

; ----------Air-Side dT across condenser rake, AM25T Chn:20--------
68:  Do (P86)
 1: 72      Pulse Port 2
69:  Excitation with Delay (P22)
 1: 1       Ex Channel
 2: 0       Delay W/Ex (0.01 sec units)
 3: 1       Delay After Ex (0.01 sec units)
 4: 0       mV Excitation
70:  Do (P86)
 1: 72      Pulse Port 2
71:  Excitation with Delay (P22)
 1: 1       Ex Channel
```

```
 2: 0       Delay W/Ex (0.01 sec units)
 3: 1       Delay After Ex (0.01 sec units)
 4: 0       mV Excitation
72:  Volt (Diff) (P2)
 1: 1       Reps
 2: 24      250 mV 60 Hz Rejection Range
 3: 1       DIFF Channel
 4: 23    -- Loc [ dTrakeAir ]
 5: 1.0     Multiplier
 6: 0.0     Offset

;-----------------------------------------
73:  Z=X*F (P37)
 1: 23      X Loc [ dTrakeAir ]
 2: .015151  F
 3: 23      Z Loc [ dTrakeAir ]
;mV per thermopile cell from 66 cells in series
74:  Z=X (P31)
 1: 23      X Loc [ dTrakeAir ]
 2: 38      Z Loc [ delta_e   ]
75:  Z=X (P31)
 1: 8       X Loc [ TcndAirIn ]
 2: 39      Z Loc [ TPref     ]
76:  Do (P86)
 1: 2       Call Subroutine 2
77:  Z=X (P31)
 1: 42      X Loc [ TPresult  ]
 2: 23      Z Loc [ dTrakeAir ] ;

; ------------Temperatures, AM25T Chn:21-23--------------
78:  Beginning of Loop (P87)
 1: 0       Delay
 2: 3       Loop Count
    79:  Do (P86)
     1: 72      Pulse Port 2
    80:  Excitation with Delay (P22)
     1: 1       Ex Channel
     2: 0       Delay W/Ex (0.01 sec units)
     3: 1       Delay After Ex (0.01 sec units)
     4: 0       mV Excitation
    81:  Do (P86)
     1: 72      Pulse Port 2
    82:  Excitation with Delay (P22)
     1: 1       Ex Channel
     2: 0       Delay W/Ex (0.01 sec units)
     3: 1       Delay After Ex (0.01 sec units)
     4: 0       mV Excitation
    83:  Thermocouple Temp (DIFF) (P14)
     1: 1       Reps
     2: 0       Auto Slow Range (OS>1.09)
     3: 1       DIFF Channel
     4: 1       Type T (Copper-Constantan)
     5: 3       Ref Temp (Deg. C) Loc [ RTemp_C   ]
     6: 24    -- Loc [ Tcndtop   ]
     7: 1       Multiplier
     8: 0       Offset
84:  End (P95)

; -----------Vaisala temperature C, AM25T Chn:24--------------
85:  Do (P86)
 1: 72      Pulse Port 2
86:  Excitation with Delay (P22)
 1: 1       Ex Channel
 2: 0       Delay W/Ex (0.01 sec units)
 3: 1       Delay After Ex (0.01 sec units)
 4: 0       mV Excitation
87:  Do (P86)
 1: 72      Pulse Port 2
88:  Excitation with Delay (P22)
 1: 1       Ex Channel
 2: 0       Delay W/Ex (0.01 sec units)
 3: 1       Delay After Ex (0.01 sec units)
 4: 0       mV Excitation
89:  Volt (Diff) (P2)
 1: 1       Reps
 2: 5       2500 mV Slow Range
 3: 1       DIFF Channel
 4: 27    -- Loc [ VaisT     ]
 5: 0.1     Multiplier
 6: -40     Offset

; -----------Vaisala RH percent, AM25T Chn:25--------------
90:  Do (P86)
 1: 72      Pulse Port 2
91:  Excitation with Delay (P22)
 1: 1       Ex Channel
 2: 0       Delay W/Ex (0.01 sec units)
 3: 1       Delay After Ex (0.01 sec units)
 4: 0       mV Excitation
92:  Do (P86)
 1: 72      Pulse Port 2
93:  Excitation with Delay (P22)
 1: 1       Ex Channel
 2: 0       Delay W/Ex (0.01 sec units)
 3: 1       Delay After Ex (0.01 sec units)
 4: 0       mV Excitation
94:  Volt (Diff) (P2)
 1: 1       Reps
 2: 5       2500 mV Slow Range
 3: 1       DIFF Channel
 4: 28    -- Loc [ VaisRH    ]
 5: 0.1     Multiplier
 6: 0       Offset
95:  Z=X-Y (P35)
 1: 12      X Loc [ Tevapgas  ]
 2: 13      Y Loc [ Tevapliq  ]
 3: 44      Z Loc [ Tsucsuph  ]
96:  Do (P86)
 1: 51      Set Port 1 Low

;-----END OF AM25 VOLTAGE INPUTS---NOW  CR10X INPUTS-----
97:  Volt (Diff) (P2)
 1: 1       Reps
 2: 4       250 mV Slow Range
 3: 2       DIFF Channel
 4: 29      Loc [ DCBusV    ]
 5: 1.5     Multiplier
 6: 0.0     Offset
;450:0.3k voltage divider
98:  Volt (Diff) (P2)
 1: 1       Reps
 2: 4       250 mV Slow Range
 3: 4       DIFF Channel
 4: 30      Loc [ Psuc      ]
 5: 5.0     Multiplier
 6: 0.0     Offset
;100mV at 500psig
99:  Volt (Diff) (P2)
 1: 1       Reps
 2: 4       250 mV Slow Range
 3: 5       DIFF Channel
 4: 31      Loc [ PTXV      ]
```

```
 5: 10.0    Multiplier
 6: 0       Offset
;100mV at 1000psig
100:  Volt (Diff) (P2)
 1: 1       Reps
 2: 4       250 mV Slow Range
 3: 6       DIFF Channel
 4: 32      Loc [ Pdis     ]
 5: 10.0    Multiplier
 6: 0.0     Offset
;100mV at 1000psig
101:  Volt (Diff) (P2)
 1: 1       Reps
 2: 24      250 mV 60 Hz Rejection Range
 3: 3       DIFF Channel
 4: 16      Loc [ DCfanAmp  ]
 5: .00146  Multiplier
 6: 0       O
;2 A/ma divided by 31 turns thru 29.6 ohm sense resistor.
;
;98:  Volt (Diff) (P2)
; 1: 1       Reps
; 2: 5       2500 mV Slow Range
; 3: 3       DIFF Channel
; 4: 45      Loc [ YokoPower ]
; 5: 1.2     Multiplier
; 6: 0       O
102:  Pulse (P3)
 1: 1       Reps
 2: 1       Pulse Channel 1
 3: 20      High Frequency, Output Hz
 4: 33      Loc [ WNoutdoor ]
 5: 6       Multiplier
 6: 0.0     Offset
;0.0001667 Wh/pulse per CTratedAmp = 0.6 W/Hz per CT rated
Amp with 10-Amp CTs = 6x (9x for 15 AMP) (3x for 5 AMP)
103:  Pulse (P3)
 1: 1       Reps
 2: 2       Pulse Channel 2
 3: 20      High Frequency, Output Hz
 4: 34      Loc [ WNevap    ]
 5: 9       Multiplier
 6: 0.0     Offset
;0.0001667 Wh/pulse per CTratedAmp = 0.6 W/Hz per CT rated
Amp with 15-Amp CTs
104:  Z=X*Y (P36)
 1: 29      X Loc [ DCBusV    ]
 2: 15      Y Loc [ DCcmpAmp  ]
 3: 35      Z Loc [ DCcmprW   ]
105:  Z=X*Y (P36)
 1: 29      X Loc [ DCBusV    ]
 2: 16      Y Loc [ DCfanAmp  ]
 3: 36      Z Loc [ DCfanW    ]
106:  Z=X+Y (P33)
 1: 35      X Loc [ DCcmprW   ]
 2: 36      Y Loc [ DCfanW    ]
 3: 37      Z Loc [ DCTotW    ]
107:  Z=X-Y (P35)
 1: 12      X Loc [ Tevapgas  ]
 2: 13      Y Loc [ Tevapliq  ]
 3: 46      Z Loc [ Tsupheat  ]

108:  Do (P86)
 1: 10      Set Output Flag High (Flag 0)
109:  Set Active Storage Area (P80)^26549
 1: 1       Final Storage Area 1
 2: 101     Array ID
110:  Real Time (P77)^1071
 1: 1221    Year,Day,Hour/Minute,Seconds (midnight = 2400)
111:  Average (P71)^21732
 1: 1       Reps
 2: 3       Loc [ RTemp_C   ]
112:  Average (P71)^31376
 1: 1       Reps
 2: 4       Loc [ Tsuc      ]
113:  Average (P71)^11451
 1: 1       Reps
 2: 5       Loc [ Tdis      ]
114:  Average (P71)^7271
 1: 1       Reps
 2: 6       Loc [ TcndLqo   ]
115:  Average (P71)^31196
 1: 1       Reps
 2: 7       Loc [ TXVo      ]
116:  Average (P71)^23337
 1: 1       Reps
 2: 8       Loc [ TcndAirIn ]
117:  Average (P71)^21595
 1: 1       Reps
 2: 9       Loc [ TevpAirIn ]
118:  Average (P71)^12054
 1: 1       Reps
 2: 10      Loc [ TcndAirOu ]
119:  Average (P71)^11086
 1: 1       Reps
 2: 11      Loc [ Tevapbox  ]
120:  Average (P71)^8418
 1: 1       Reps
 2: 12      Loc [ Tevapgas  ]
121:  Average (P71)^1191
 1: 1       Reps
 2: 13      Loc [ Tevapliq  ]
122:  Average (P71)^29608
 1: 1       Reps
 2: 14      Loc [ Tambient  ]
123:  Average (P71)^21454
 1: 1       Reps
 2: 15      Loc [ DCcmpAmp  ]
124:  Average (P71)^11870
 1: 1       Reps
 2: 16      Loc [ DCfanAmp  ]
125:  Average (P71)^18522
 1: 1       Reps
 2: 17      Loc [ delPHx    ]
126:  Average (P71)^17941
 1: 1       Reps
 2: 18      Loc [ delPfan   ]
127:  Average (P71)^12984
 1: 1       Reps
 2: 19      Loc [ HXflow    ]
128:  Average (P71)^1637
 1: 1       Reps
 2: 20      Loc [ dTcndair  ]
129:  Average (P71)^20142
 1: 1       Reps
 2: 21      Loc [ dTevpair  ]
130:  Average (P71)^12993
 1: 1       Reps
 2: 22      Loc [ dTfanfin  ]
131:  Average (P71)^32511
 1: 1       Reps
 2: 23      Loc [ dTrakeAir ]
```

```
132:  Average (P71)^28679
 1: 1       Reps
 2: 27      Loc [ VaisT    ]
133:  Average (P71)^10793
 1: 1       Reps
 2: 28      Loc [ VaisRH   ]
134:  Average (P71)^18513
 1: 1       Reps
 2: 29      Loc [ DCBusV   ]
135:  Average (P71)^4599
 1: 1       Reps
 2: 30      Loc [ Psuc     ]
136:  Average (P71)^19828
 1: 1       Reps
 2: 31      Loc [ PTXV     ]
137:  Average (P71)^30326
 1: 1       Reps
 2: 32      Loc [ Pdis     ]
138:  Average (P71)^28626
 1: 1       Reps
 2: 33      Loc [ WNoutdoor ]
139:  Average (P71)^4420
 1: 1       Reps
 2: 34      Loc [ WNevap   ]
140:  Average (P71)^22397
 1: 1       Reps
 2: 35      Loc [ DCcmprW  ]
141:  Average (P71)^25983
 1: 1       Reps
 2: 36      Loc [ DCfanW   ]
142:  Average (P71)^6196
 1: 1       Reps
 2: 24      Loc [ Tcndtop  ]
143:  Average (P71)^10541
 1: 1       Reps
 2: 25      Loc [ Tcndbot  ]
144:  Average (P71)^28189
 1: 1       Reps
 2: 26      Loc [ Tcndmix  ]
145:  Average (P71)^25586
 1: 1       Reps
 2: 37      Loc [ DCTotW   ]
146:  Average (P71)^24896
 1: 1       Reps
 2: 44      Loc [ Tsucsuph ]
147:  Average (P71)^1341
 1: 1       Reps
 2: 49      Loc [ DCYoko   ]
148:  Average (P71)^11257
 1: 1       Reps
 2: 50      Loc [ ACYoko   ]
149:  Average (P71)^729
 1: 1       Reps
 2: 51      Loc [ ABYoko   ]
150:  Average (P71)^16001
 1: 1       Reps
 2: 46      Loc [ Tsupheat ]
*Table 2 Program
 01: 10.0000   Execution Interval (seconds)

*Table 3 Subroutines
1:  Beginning of Subroutine (P85)
 1: 1       Subroutine 1
   2:  Z=X*F (P37)
    1: 38      X Loc [ delta_e   ]
    2: .1      F
    3: 38      Z Loc [ delta_e   ]
   3:  Z=X*F (P37)
    1: 39      X Loc [ TPref     ]
    2: .01     F
    3: 39      Z Loc [ TPref     ]
   4:  Z=X*Y (P36)
    1: 38      X Loc [ delta_e   ]
    2: 39      Y Loc [ TPref     ]
    3: 40      Z Loc [ e_TPref   ]
   5:  Polynomial (P55)
    1: 1       Reps
    2: 38      X Loc [ delta_e   ]
    3: 41      F(X) Loc [ TPsensitv ]
    4: 25.89   C0
    5: -7.447  C1
    6: 4.654   C2
    7: -2.188  C3
    8: 0.0000  C4
    9: 0.0000  C5

   6:  Polynomial (P55)
    1: 1       Reps
    2: 39      X Loc [ TPref     ]
    3: 42      F(X) Loc [ TPresult  ]
    4: 0.0000  C0
    5: -5.749  C1
    6: 1.635   C2
    7: -0.4475 C3
    8: 0.0000  C4
    9: 0.0000  C5
   7:  Z=X+Y (P33)
    1: 41      X Loc [ TPsensitv ]
    2: 42      Y Loc [ TPresult  ]
    3: 41      Z Loc [ TPsensitv ]
   8:  Z=X*F (P37)
    1: 40      X Loc [ e_TPref   ]
    2: 5.557   F
    3: 42      Z Loc [ TPresult  ]
   9:  Z=X+Y (P33)
    1: 41      X Loc [ TPsensitv ]
    2: 42      Y Loc [ TPresult  ]
    3: 41      Z Loc [ TPsensitv ]
   10:  Z=X*Y (P36)
    1: 39      X Loc [ TPref     ]
    2: 40      Y Loc [ e_TPref   ]
    3: 42      Z Loc [ TPresult  ]
   11:  Z=X*F (P37)
    1: 42      X Loc [ TPresult  ]
    2: -2.107  F
    3: 42      Z Loc [ TPresult  ]
   12:  Z=X+Y (P33)
    1: 41      X Loc [ TPsensitv ]
    2: 42      Y Loc [ TPresult  ]
    3: 41      Z Loc [ TPsensitv ]
   13:  Z=X*Y (P36)
    1: 38      X Loc [ delta_e   ]
    2: 40      Y Loc [ e_TPref   ]
    3: 42      Z Loc [ TPresult  ]
   14:  Z=X*F (P37)
    1: 42      X Loc [ TPresult  ]
    2: -3.793  F
    3: 42      Z Loc [ TPresult  ]
   15:  Z=X+Y (P33)
    1: 41      X Loc [ TPsensitv ]
    2: 42      Y Loc [ TPresult  ]
    3: 41      Z Loc [ TPsensitv ]
```

```
   16:  Z=X*F (P37)
    1: 38      X Loc [ delta_e   ]
    2: 10      F
    3: 38      Z Loc [ delta_e   ]
   17:  Z=X*Y (P36)
    1: 41      X Loc [ TPsensitv ]
    2: 38      Y Loc [ delta_e   ]
    3: 42      Z Loc [ TPresult  ]
   18:  Z=X*F (P37)
    1: 39      X Loc [ TPref     ]
    2: 100     F
    3: 39      Z Loc [ TPref     ]
19:  End (P95)

; ------------Type J subroutine----------------
; delta_e is the thermopile voltage difference
; Tref is the reference temperature
; the fit is valid for reference temperatures between 0 and 40
degrees C
; and temperature differences between -40 and +40 C

20:  Beginning of Subroutine (P85)
 1: 2       Subroutine 2
   21:  Z=X*F (P37)
    1: 38      X Loc [ delta_e   ]
    2: 0.1     F
    3: 47      Z Loc [ del_e_sca ]
   22:  Polynomial (P55)
    1: 1       Reps
    2: 47      X Loc [ del_e_sca ]
    3: 41      F(X) Loc [ TPsensitv ]
    4: 19.7843  C0
    5: -2.00106 C1
    6: 1.03148  C2
    7: -.22977  C3
    8: 0.0000   C4
    9: 0.0000   C5
   23:  Z=X*F (P37)
    1: 39      X Loc [ TPref     ]
    2: 0.01    F
    3: 48      Z Loc [ Tref_scal ]
   24:  Polynomial (P55)
    1: 1       Reps
    2: 48      X Loc [ Tref_scal ]
    3: 42      F(X) Loc [ TPresult  ]
    4: 0       C0
    5: -2.02409 C1
    6: .698583  C2
    7: -.052860 C3
    8: 0.0000   C4
    9: 0.0000   C5
   25:  Z=X+Y (P33)
    1: 41      X Loc [ TPsensitv ]
    2: 42      Y Loc [ TPresult  ]
    3: 41      Z Loc [ TPsensitv ]
   26:  Z=X*Y (P36)
    1: 38      X Loc [ delta_e   ]
    2: 39      Y Loc [ TPref     ]
    3: 40      Z Loc [ e_TPref   ]
   27:  Z=X*F (P37)
    1: 40      X Loc [ e_TPref   ]
    2: .001572  F
    3: 42      Z Loc [ TPresult  ]
   28:  Z=X+Y (P33)
    1: 41      X Loc [ TPsensitv ]
    2: 42      Y Loc [ TPresult  ]
    3: 41      Z Loc [ TPsensitv ]
   29:  Z=X*Y (P36)
    1: 39      X Loc [ TPref     ]
    2: 40      Y Loc [ e_TPref   ]
    3: 42      Z Loc [ TPresult  ]
   30:  Z=X*F (P37)
    1: 42      X Loc [ TPresult  ]
    2: .0001   F
    3: 42      Z Loc [ TPresult  ]
   31:  Z=X*F (P37)
    1: 42      X Loc [ TPresult  ]
    2: -.031249 F
    3: 42      Z Loc [ TPresult  ]
   32:  Z=X+Y (P33)
    1: 41      X Loc [ TPsensitv ]
    2: 42      Y Loc [ TPresult  ]
    3: 41      Z Loc [ TPsensitv ]
   33:  Z=X*Y (P36)
    1: 38      X Loc [ delta_e   ]
    2: 40      Y Loc [ e_TPref   ]
    3: 42      Z Loc [ TPresult  ]
   34:  Z=X*F (P37)
    1: 42      X Loc [ TPresult  ]
    2: .0001   F
    3: 42      Z Loc [ TPresult  ]
   35:  Z=X*F (P37)
    1: 42      X Loc [ TPresult  ]
    2: -.477042 F
    3: 42      Z Loc [ TPresult  ]
   36:  Z=X+Y (P33)
    1: 41      X Loc [ TPsensitv ]
    2: 42      Y Loc [ TPresult  ]
    3: 41      Z Loc [ TPsensitv ]
   37:  Z=X*Y (P36)
    1: 41      X Loc [ TPsensitv ]
    2: 38      Y Loc [ delta_e   ]
    3: 42      Z Loc [ TPresult  ]

38:  End (P95)
End Program
```

A.1.2 Condenser airflow rate measurement

The condenser airflow rate for different condenser fan speeds was measured using an eight point per radii traverse following the methods described in the section on measuring flow in ducts in ASHRAE Fundamentals, Chapter 14 Measurement and Instruments [ASHRAE 2001]. The eight sampling points were chosen based on the log-linear rule for circular ducts. A flow straightener and circular duct was installed on the outlet of the condenser air stream as shown below. The average of the data from these airflow traverse measurements, along with selected data recorded using sensors listed in Appendix A.1.1 are shown in the table below.

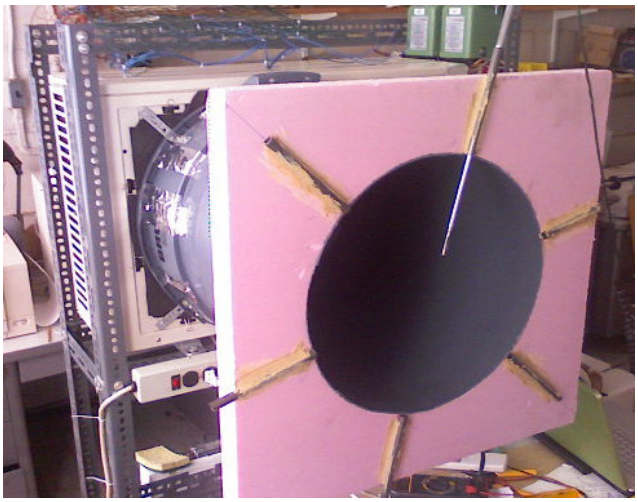

Condenser airflow rate measurements

Fan Speed (RPM)	Flow rate (CFM)	3-phase power (W)	DC power (W)	DC bus voltage (V)	DC current (A)
300	318	1.5	2.5	283	0.009
400	465	3.5	4.6	282	0.016
500	585	6.2	6.9	281	0.025
600	727	10.9	11.6	277	0.042
700	861	16.8	18.1	274	0.066
800	992	24.5	25.9	271	0.096
900	1124	34.0	36.4	267	0.136
1000	1256	46.8	49.4	264	0.187
1100	1392	61.8	66.6	259	0.257

A.2 Compressor inverter model

The efficiency of the inverter, or intelligent power module (IPM), providing three phase power to the compressor is an important consideration in assessing the improved efficiency of the heat pump or chiller with a variable speed compressor. Significant IPM losses will reduce the total efficiency of the variable capacity chiller or heat pump relative to a constant speed system operating at the same frequency. A model of the IPM losses is shown below. The IPM converts direct current (DC) power into three-phase alternating-current (AC) power at different frequencies to drive the compressor. The power losses at the IPM depend strongly on the total three phase power consumption of the compressor, and have a weaker dependence on the compressor speed.

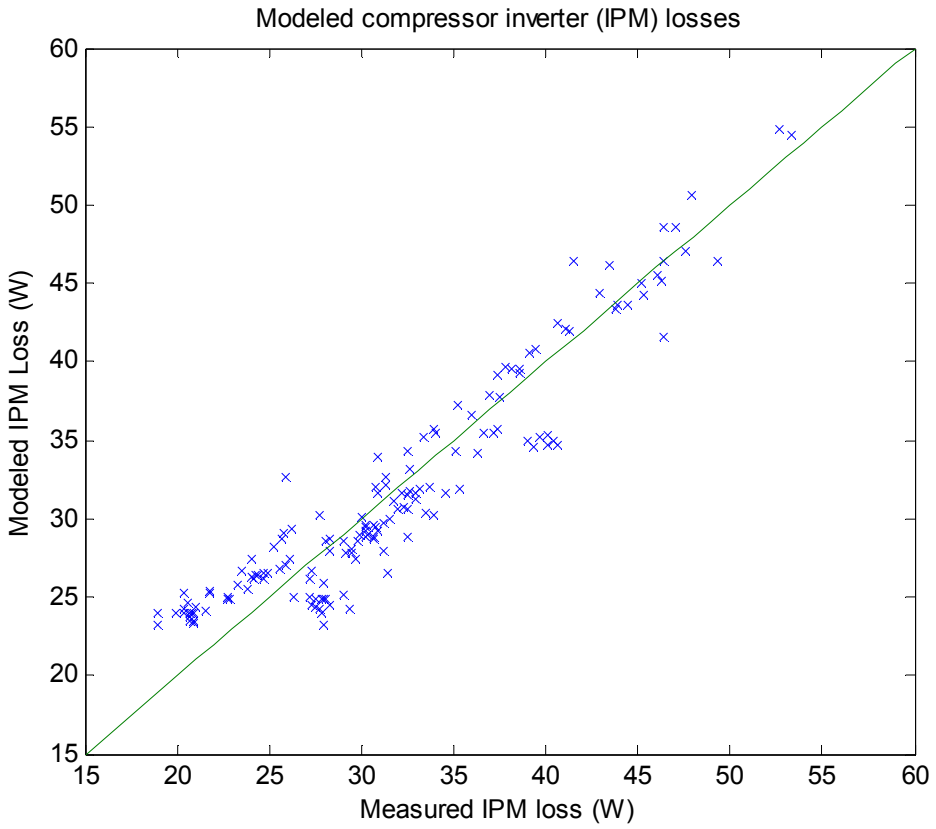

RMSE = 2.6 W

Relative RMSE = 9.5 %

IPM Loss (W) = $24 + 0.046W_{3\phi comp} - 0.24\omega_{comp} - 0.0026\omega_{comp}^2$ +/- 2.6 W

A.3 Low lift heat pump performance data

Test conditions					Refrigerant Temperatures					Refrigerant pressures			
Test point	Comp-ressor Speed (Hz)	Condenser fan speed (RPM)	Zone Air Temp (C)	Outdoor Air Temp (C)	Suction Temp (C)	Discharge Temp (C)	Condenser Outlet Temp (C)	EXV Outlet Temp (C)	Evaporator Inlet Temp (C)	Ambient Pressure (kPa)	Suction pressure (psig)	Post-EXV pressure (psig)	Discharge pressure (psig)
1	19	750	23.93	22.75	15.65	39.42	24.36	15.13	15.01	102.91	164	166	248
2	60	750	23.96	22.61	4.67	56.94	25.54	7.18	6.80	101.66	112	125	300
3	30	750	23.85	22.32	12.06	44.95	26.22	12.03	11.81	102.47	145	150	260
4	60	750	34.07	22.55	10.36	57.85	26.79	12.71	12.31	101.59	137	152	319
5	30	750	34.14	22.76	22.60	47.40	24.85	18.12	18.00	102.74	178	183	272
6	19	750	33.93	30.22	24.83	46.90	32.69	23.41	23.26	101.52	211	214	306
7	30	750	34.22	30.40	20.81	50.00	34.68	21.22	21.01	101.76	194	200	327
8	19	750	34.07	37.47	25.11	54.48	40.42	25.14	24.91	102.44	220	224	364
9	30	750	33.98	37.73	21.84	59.33	41.37	22.38	22.16	101.66	199	206	384
10	30	750	34.16	45.10	23.48	69.24	50.11	24.29	23.89	101.52	208	217	454
11	30	750	14.85	18.09	4.79	36.85	20.67	5.03	4.85	101.49	114	117	217
12	60	750	24.11	18.76	6.70	56.21	22.26	5.45	5.07	101.59	105	118	263
13	60	750	33.93	18.54	14.92	59.72	21.42	10.62	10.26	101.56	130	142	288
14	19	750	14.12	16.70	8.33	35.02	17.19	6.71	6.59	101.22	123	125	200
15	30	750	14.03	16.57	4.42	36.31	18.55	4.53	4.38	101.22	112	115	208
16	60	750	23.84	17.71	7.51	56.97	20.79	4.95	4.60	101.42	104	116	256
17	30	750	24.01	16.63	15.46	44.48	17.41	9.68	9.51	101.19	135	138	223
18	19	750	13.98	15.42	7.99	33.28	16.30	5.95	5.86	102.44	120	121	192
19	19	750	13.89	15.42	7.90	33.25	16.33	5.91	5.81	102.44	120	121	191
20	19	750	13.93	15.46	7.95	33.22	16.41	5.93	5.83	102.44	120	121	191
21	95	750	14.12	16.28	-1.16	84.57	17.85	-3.19	-3.83	102.44	64	82	284
22	95	750	24.09	16.73	4.28	81.36	19.35	2.47	1.91	102.44	82	104	306

Test conditions					Refrigerant Temperatures					Refrigerant pressures			
Test point	Comp-ressor Speed (Hz)	Condenser fan speed (RPM)	Zone Air Temp (C)	Outdoor Air Temp (C)	Suction Temp (C)	Discharge Temp (C)	Condenser Outlet Temp (C)	EXV Outlet Temp (C)	Evaporator Inlet Temp (C)	Ambient Pressure (kPa)	Suction pressure (psig)	Post-EXV pressure (psig)	Discharge pressure (psig)
23	95	750	34.03	17.13	9.10	80.04	21.22	7.62	7.10	102.44	101	126	331
24	95	750	34.22	17.35	9.18	80.34	21.49	7.78	7.25	102.44	101	127	333
25	95	750	33.96	17.28	8.63	80.10	21.40	7.65	7.12	102.44	101	126	332
26	95	750	34.01	17.22	8.94	80.03	21.32	7.65	7.14	102.44	101	126	332
27	19	750	13.79	22.18	8.22	41.46	23.73	7.26	7.10	100.85	124	123	229
28	30	750	14.11	22.51	5.76	49.77	23.51	4.91	4.69	101.25	113	115	252
29	60	750	14.10	22.57	1.92	68.44	23.55	1.15	0.68	100.88	90	99	299
30	95	750	13.97	22.39	-0.22	96.10	24.41	-1.72	-2.53	102.30	67	87	335
31	95	750	24.05	22.49	5.21	91.36	25.62	3.92	3.21	102.27	86	109	358
32	30	300	14.08	30.01	8.48	74.70	33.19	6.75	6.20	101.83	119	121	359
33	30	450	13.97	30.06	8.41	69.74	31.63	6.22	5.75	101.86	117	120	330
34	30	600	14.03	29.78	7.59	66.00	30.87	6.37	5.95	101.93	118	120	319
35	30	600	14.09	29.97	7.69	65.54	31.04	6.37	5.96	101.93	118	120	320
36	30	600	13.98	30.13	7.56	66.42	31.22	6.40	6.01	101.56	118	120	322
37	30	750	14.04	30.20	8.06	65.29	30.49	6.09	5.84	101.29	117	120	314
38	30	900	13.87	29.82	7.52	63.29	30.27	6.14	5.87	101.29	117	120	304
39	30	1050	14.20	30.30	8.10	63.25	30.53	6.28	6.03	101.29	118	120	305
40	30	1200	13.96	30.42	6.79	63.09	31.19	6.41	6.09	101.29	119	121	310
41	60	450	14.05	30.41	3.48	90.43	32.59	2.35	1.84	101.25	94	103	405
42	60	600	14.09	29.77	3.15	84.66	31.39	2.29	1.62	101.29	94	103	378
43	60	750	14.12	30.09	3.12	81.39	31.20	2.23	1.73	99.97	93	103	361
44	60	900	14.04	29.81	3.04	78.75	30.14	1.99	1.49	101.19	93	102	347
45	60	1050	14.11	30.31	3.77	78.15	30.86	1.96	1.53	101.83	92	101	339
46	60	1200	14.11	30.14	3.66	78.05	30.78	1.93	1.42	101.83	92	101	337
47	80	450	14.04	29.87	1.77	106.57	34.32	1.37	0.39	101.90	83	98	442

Test conditions					Refrigerant Temperatures					Refrigerant pressures			
Test point	Comp-ressor Speed (Hz)	Condenser fan speed (RPM)	Zone Air Temp (C)	Outdoor Air Temp (C)	Suction Temp (C)	Discharge Temp (C)	Condenser Outlet Temp (C)	EXV Outlet Temp (C)	Evaporator Inlet Temp (C)	Ambient Pressure (kPa)	Suction pressure (psig)	Post-EXV pressure (psig)	Discharge pressure (psig)
48	89	600	13.97	29.76	0.99	108.13	33.14	0.43	-0.52	101.90	76	95	422
49	93	750	14.08	30.20	0.13	106.92	33.06	0.40	-0.59	101.90	75	94	412
50	93	900	13.96	30.11	0.45	104.71	32.37	0.12	-0.83	101.86	74	93	395
51	93	1050	14.01	30.21	0.98	103.98	32.05	-0.12	-1.03	101.86	73	93	385
52	93	1200	13.93	29.97	1.16	103.33	31.44	-0.51	-1.33	101.83	72	91	375
53	19	300	23.97	30.23	18.13	59.26	34.22	16.62	16.38	101.69	170	172	336
54	19	450	24.05	30.16	18.00	54.43	32.20	16.29	16.16	101.69	169	170	314
55	19	600	23.94	30.29	17.88	53.64	31.98	16.16	16.00	101.69	168	170	308
56	19	750	24.15	30.26	18.15	52.15	31.58	16.22	16.07	101.76	168	170	301
57	19	900	24.04	30.22	18.09	51.62	31.32	16.05	15.88	101.76	168	169	297
58	19	1050	24.01	30.06	18.32	51.49	30.96	15.87	15.72	101.83	167	168	294
59	19	1200	24.01	29.98	17.65	49.47	31.06	16.10	15.92	101.86	168	170	291
60	30	1050	14.14	30.03	8.30	63.21	30.44	6.09	5.82	102.10	117	119	301
61	30	1200	14.07	30.16	8.29	63.21	30.48	6.05	5.79	102.10	117	119	301
62	60	450	24.02	29.90	10.00	85.97	35.75	9.14	8.48	101.42	120	132	432
63	60	600	23.98	29.78	9.56	77.35	34.55	8.78	8.10	101.32	119	131	381
64	60	750	24.07	30.07	9.45	74.76	33.73	8.68	8.07	101.49	118	131	368
65	60	900	24.19	29.93	9.62	72.82	32.44	8.34	7.81	101.52	117	129	352
66	60	1050	23.98	30.22	9.39	71.93	32.36	8.31	7.77	101.59	117	129	348
67	60	1200	24.00	29.81	10.00	71.16	31.43	7.68	7.09	101.35	114	126	335
68	84	450	24.00	29.83	7.98	107.08	36.51	6.58	5.67	102.64	101	120	480
69	88	600	24.07	29.57	7.36	103.15	33.53	5.55	4.75	102.68	95	115	438
70	93	750	23.92	30.30	6.40	102.38	32.92	5.30	4.53	102.68	91	115	423
71	95	900	23.99	30.01	5.35	100.00	32.27	5.05	4.21	102.74	89	113	408
72	95	1050	24.05	29.87	6.04	98.98	31.63	4.96	4.05	102.74	89	113	397

Test conditions					Refrigerant Temperatures					Refrigerant pressures			
Test point	Comp-ressor Speed (Hz)	Condenser fan speed (RPM)	Zone Air Temp (C)	Outdoor Air Temp (C)	Suction Temp (C)	Discharge Temp (C)	Condenser Outlet Temp (C)	EXV Outlet Temp (C)	Evaporator Inlet Temp (C)	Ambient Pressure (kPa)	Suction pressure (psig)	Post-EXV pressure (psig)	Discharge pressure (psig)
73	95	1200	23.98	30.01	5.45	96.77	30.90	4.86	4.03	102.74	88	112	387
74	60	750	34.03	30.04	16.25	74.97	33.81	13.96	13.44	102.61	142	156	389
75	89	750	34.23	30.14	13.75	98.08	34.71	10.99	10.15	102.64	115	140	443
76	50	750	26.79	35.30	13.56	75.34	38.23	13.16	12.59	101.96	142	152	403
77	50	750	26.94	35.20	14.09	75.35	38.70	13.23	12.54	101.96	142	153	399
78	30	750	14.03	37.33	9.51	78.90	38.03	6.94	6.51	102.00	119	123	371
79	60	750	13.98	37.93	4.55	94.57	39.66	3.83	2.98	101.19	97	108	434
80	79	750	14.05	37.51	3.29	110.48	39.44	1.60	0.70	100.88	84	99	456
81	60	750	24.06	37.21	11.43	88.13	38.93	9.28	8.58	100.78	120	132	431
82	95	750	24.10	37.21	8.03	104.65	40.61	7.82	6.77	102.61	104	125	476
83	60	750	33.91	37.45	16.28	84.34	42.53	16.09	15.14	102.64	151	167	463
84	81	750	34.00	37.27	14.10	98.08	42.63	13.84	12.92	102.44	131	154	495
85	30	750	14.11	45.02	10.15	90.48	45.58	8.42	7.89	102.51	125	128	443
86	30	900	14.11	45.05	9.79	90.18	45.45	8.49	7.98	102.51	125	129	437
87	30	1050	13.92	45.19	9.91	90.93	45.69	8.45	7.77	102.51	125	128	437
88	30	1200	14.21	45.25	10.64	90.57	45.62	8.39	7.72	102.51	125	128	435
89	60	600	14.07	44.77	6.10	110.83	46.82	5.20	4.38	102.47	102	113	522
90	60	750	14.15	45.06	5.93	106.91	46.69	5.46	4.51	102.44	102	114	507
91	60	900	13.99	45.10	5.83	105.80	46.40	5.27	4.27	102.47	101	113	497
92	60	1050	14.04	44.95	5.63	103.87	46.02	5.29	4.32	102.47	102	113	488
93	60	1200	14.09	44.94	5.59	102.66	46.06	5.36	4.27	102.51	102	113	485
94	68	900	14.04	45.10	5.16	111.75	46.64	4.41	3.37	101.52	96	110	509
95	68	1050	13.85	45.10	5.17	111.10	46.24	4.08	3.03	101.52	95	108	500
96	68	1200	14.13	45.16	5.71	110.76	46.01	3.99	3.03	101.52	94	108	493
97	30	750	23.98	45.37	17.99	83.64	46.71	15.97	15.50	102.64	162	166	457

Test conditions					Refrigerant Temperatures					Refrigerant pressures			
Test point	Comp-ressor Speed (Hz)	Condenser fan speed (RPM)	Zone Air Temp (C)	Outdoor Air Temp (C)	Suction Temp (C)	Discharge Temp (C)	Condenser Outlet Temp (C)	EXV Outlet Temp (C)	Evaporator Inlet Temp (C)	Ambient Pressure (kPa)	Suction pressure (psig)	Post-EXV pressure (psig)	Discharge pressure (psig)
98	30	750	24.02	45.37	17.32	82.27	46.86	16.28	15.81	102.64	163	168	457
99	60	750	23.93	45.01	12.00	99.48	48.02	11.77	10.86	102.61	129	144	523
100	75	750	24.16	45.18	11.43	111.20	48.45	10.60	9.57	102.64	118	137	548
101	19	750	34.05	45.07	28.03	69.80	46.97	26.06	25.73	102.03	225	228	436
102	74	750	33.92	44.54	15.86	102.25	49.16	16.21	15.17	102.44	144	166	548
103	19	750	14.02	14.76	7.67	32.71	15.42	6.09	6.02	99.32	122	122	190
104	30	750	13.89	17.60	5.61	43.07	18.56	3.92	3.74	101.90	110	111	216
105	60	750	13.86	19.21	1.17	63.96	20.02	-0.46	-0.88	101.86	85	93	265
106	95	750	13.96	19.10	-1.44	92.37	20.62	-3.81	-4.55	100.78	62	80	306
107	19	750	24.10	17.11	16.51	31.97	19.31	13.68	13.63	101.86	158	160	207
108	30	750	23.86	17.26	13.10	40.90	18.20	10.40	10.27	101.90	139	142	225
109	60	750	24.06	17.84	7.40	60.26	19.72	4.66	4.32	100.85	104	114	270
110	95	750	24.61	19.14	4.19	87.60	21.63	2.02	1.38	100.81	80	102	326
111	30	750	34.02	17.98	20.12	39.22	20.20	16.81	16.73	101.86	173	177	238
112	60	750	34.22	17.28	12.85	56.52	20.32	10.01	9.75	100.85	128	139	278
113	19	750	24.05	22.80	16.08	38.45	23.57	14.60	14.50	103.08	162	163	239
114	30	750	24.03	22.68	14.01	49.19	23.93	11.57	11.38	100.95	144	147	265
115	60	750	24.28	23.09	8.61	69.42	25.39	5.76	5.22	100.95	108	118	315
116	19	750	34.01	22.68	23.70	36.81	26.82	21.83	21.73	100.24	204	206	253
117	30	750	34.13	22.62	20.55	45.41	25.62	18.31	18.11	101.15	180	184	274
118	30	300	23.93	29.84	14.83	69.09	35.49	13.93	13.51	102.47	153	157	377
119	30	450	24.06	30.01	15.56	64.55	32.63	13.13	12.73	102.44	149	153	341
120	30	600	23.78	30.10	14.78	61.86	32.29	13.13	12.77	102.47	150	153	331
121	30	750	24.07	30.26	15.29	62.30	32.38	13.24	12.91	102.54	150	153	332
122	30	900	23.93	30.46	14.64	60.26	32.39	13.36	13.02	102.98	151	154	326

Test conditions					Refrigerant Temperatures					Refrigerant pressures			
Test point	Comp-ressor Speed (Hz)	Condenser fan speed (RPM)	Zone Air Temp (C)	Outdoor Air Temp (C)	Suction Temp (C)	Discharge Temp (C)	Condenser Outlet Temp (C)	EXV Outlet Temp (C)	Evaporator Inlet Temp (C)	Ambient Pressure (kPa)	Suction pressure (psig)	Post-EXV pressure (psig)	Discharge pressure (psig)
123	19	750	34.04	29.93	25.09	47.89	32.15	22.82	22.69	99.93	207	210	304
124	30	750	34.16	29.79	22.05	55.78	32.60	19.37	19.11	99.90	184	188	324
125	19	750	24.01	37.60	18.57	64.23	38.38	16.74	16.43	100.10	170	172	359
126	30	750	23.98	37.54	15.76	70.97	38.84	14.32	13.83	101.08	155	158	382
127	19	750	34.02	37.41	25.81	57.10	41.01	24.43	24.09	100.07	216	219	363
128	30	750	34.19	37.57	23.65	68.25	39.92	20.88	20.48	101.05	191	195	395
129	30	750	33.77	45.15	23.96	76.81	47.93	22.80	22.19	101.12	200	206	464
130	60	750	33.59	44.85	17.87	98.30	48.24	16.22	15.24	101.15	150	166	532
131	19	750	24.13	30.08	17.59	51.98	31.69	16.09	15.75	103.01	168	169	301

	Condenser conditions				Evaporator conditions				Power measurements		
Test point	Condenser Air Inlet Temp (C)	Condenser Air Temp Difference (C)	Condenser Air Mass Flowrate (kg/s)	Condenser Air Total Heat Rate (W)	Evaporator Air Inlet Temp (C)	Evaporator Air Temp Difference (C)	Zone Electrical Input (W)	Total cooling load (W)	Outdoor unit power (W)	Compressor Inverter DC Power (W)	Compressor three phase power (W)
1	23.15	2.65	0.530	1412	25.25	-8.51	1422	1419	156	129	109
2	22.86	6.55	0.523	3449	26.68	-19.00	3073	3070	647	606	581
3	23.17	3.89	0.528	2066	25.90	-11.62	1938	1934	271	241	213
4	22.73	7.84	0.523	4126	37.15	-23.28	3692	3670	661	621	594
5	22.73	4.55	0.529	2419	36.61	-14.82	2441	2415	251	221	193
6	30.32	3.41	0.510	1751	35.70	-10.33	1691	1683	170	143	121
7	30.70	4.90	0.510	2518	36.86	-14.18	2354	2346	305	275	245
8	37.72	3.25	0.502	1643	35.63	-9.27	1548	1555	216	188	164
9	36.72	4.78	0.498	2398	36.37	-13.05	2145	2153	374	343	311
10	45.28	4.62	0.486	2259	36.26	-11.51	1894	1919	455	422	385
11	18.03	3.24	0.531	1730	16.26	-9.42	1530	1536	250	221	194
12	18.69	6.23	0.530	3325	26.56	-18.61	2995	2985	576	536	512
13	18.45	7.58	0.530	4046	37.35	-22.92	3715	3686	600	561	536
14	16.60	2.15	0.532	1152	15.07	-6.77	1135	1140	146	120	99
15	16.48	3.17	0.532	1699	15.36	-9.44	1570	1575	242	213	186
16	17.65	6.16	0.531	3293	26.69	-18.66	3017	3005	563	524	501
17	16.56	3.76	0.532	2011	25.85	-11.89	1954	1940	237	208	180
18	15.39	2.10	0.541	1144	14.91	-6.70	1119	1121	142	114	94
19	15.36	2.10	0.541	1144	14.79	-6.65	1107	1110	141	114	94
20	15.42	2.11	0.540	1145	14.84	-6.65	1108	1111	142	115	94
21	16.31	7.43	0.539	4031	17.39	-18.68	3066	3070	1049	990	961
22	16.74	8.50	0.538	4602	28.08	-23.49	3787	3774	1132	1071	1040
23	17.12	10.03	0.537	5426	38.53	-28.16	4101	4069	1214	1148	1116
24	17.33	10.09	0.537	5450	38.58	-28.11	4108	4076	1221	1156	1122

	Condenser conditions				Evaporator conditions				Power measurements		
Test point	Condenser Air Inlet Temp (C)	Condenser Air Temp Difference (C)	Condenser Air Mass Flowrate (kg/s)	Condenser Air Total Heat Rate (W)	Evaporator Air Inlet Temp (C)	Evaporator Air Temp Difference (C)	Zone Electrical Input (W)	Total cooling load (W)	Outdoor unit power (W)	Compressor Inverter DC Power (W)	Compressor three phase power (W)
25	17.26	10.07	0.537	5441	38.13	-27.88	4078	4048	1218	1152	1119
26	17.20	10.03	0.537	5422	38.51	-28.15	4101	4070	1217	1151	1118
27	24.26	2.07	0.520	1085	14.87	-6.16	1012	1027	168	142	121
28	22.71	3.14	0.521	1646	15.57	-8.89	1471	1486	288	258	230
29	22.42	5.93	0.519	3101	17.04	-15.25	2463	2479	654	613	588
30	22.65	7.39	0.527	3919	17.04	-17.36	2886	2901	1179	1119	1085
31	22.78	8.76	0.527	4643	27.95	-22.16	3657	3654	1273	1208	1173
32	30.00	8.53	0.189	1625	15.44	-7.82	1285	1313	372	359	326
33	30.22	5.27	0.294	1559	15.37	-8.02	1315	1344	348	332	302
34	30.34	3.82	0.402	1548	15.46	-8.22	1343	1371	343	322	291
35	30.46	3.82	0.402	1546	15.57	-8.22	1349	1378	344	322	292
36	30.40	3.83	0.400	1542	15.36	-8.10	1333	1362	346	324	293
37	30.70	3.02	0.508	1546	15.43	-8.14	1343	1372	347	304	273
38	29.95	2.59	0.620	1615	15.22	-8.14	1345	1374	351	307	277
39	30.27	2.28	0.732	1677	15.57	-8.18	1360	1389	373	307	277
40	30.93	1.96	0.846	1672	15.30	-8.12	1346	1375	405	313	283
41	30.56	9.86	0.292	2896	16.56	-13.62	2202	2231	822	791	756
42	30.53	6.96	0.400	2799	16.75	-13.95	2253	2281	783	748	715
43	30.20	6.04	0.502	3051	16.74	-14.23	2267	2295	763	719	688
44	30.09	4.63	0.620	2889	16.72	-14.17	2304	2333	752	691	665
45	29.77	3.95	0.736	2926	16.65	-14.12	2277	2306	757	681	649
46	30.06	3.46	0.851	2964	16.64	-14.12	2272	2301	782	678	647
47	30.08	12.65	0.294	3746	16.92	-15.71	2507	2535	1197	1152	1111
48	29.93	9.84	0.402	3984	17.08	-16.60	2654	2682	1313	1256	1217
49	30.00	7.76	0.511	3995	17.25	-17.03	2728	2757	1359	1293	1255

	Condenser conditions				Evaporator conditions				Power measurements		
Test point	Condenser Air Inlet Temp (C)	Condenser Air Temp Difference (C)	Condenser Air Mass Flowrate (kg/s)	Condenser Air Total Heat Rate (W)	Evaporator Air Inlet Temp (C)	Evaporator Air Temp Difference (C)	Zone Electrical Input (W)	Total cooling load (W)	Outdoor unit power (W)	Compressor Inverter DC Power (W)	Compressor three phase power (W)
50	30.13	6.30	0.623	3952	17.22	-17.07	2738	2767	1332	1252	1215
51	30.20	5.35	0.736	3963	17.24	-17.01	2727	2757	1327	1227	1191
52	30.00	4.64	0.852	3977	17.14	-16.89	2713	2742	1327	1201	1165
53	30.03	7.54	0.189	1435	25.15	-7.31	1209	1220	208	200	171
54	30.14	4.60	0.293	1357	25.28	-7.66	1260	1271	192	181	155
55	30.07	3.34	0.401	1347	25.17	-7.68	1256	1268	193	176	151
56	29.86	2.61	0.511	1340	25.46	-7.79	1281	1292	198	171	146
57	29.85	2.16	0.622	1354	25.34	-7.80	1279	1290	209	167	143
58	29.98	1.81	0.737	1341	25.30	-7.75	1279	1290	227	166	142
59	30.12	1.60	0.852	1372	25.33	-7.83	1300	1311	251	163	138
60	29.65	2.24	0.739	1668	15.53	-8.21	1350	1379	369	305	274
61	30.04	1.94	0.853	1666	15.47	-8.21	1346	1375	396	305	273
62	30.39	11.84	0.293	3491	26.91	-17.14	2867	2877	788	840	802
63	30.24	8.45	0.400	3400	26.95	-17.59	2885	2895	771	752	718
64	30.58	6.55	0.510	3363	27.03	-17.72	2885	2896	771	728	695
65	30.11	5.36	0.622	3354	27.08	-17.91	2885	2895	771	701	669
66	30.61	4.58	0.734	3387	26.98	-17.90	2885	2896	771	692	661
67	29.72	3.88	0.848	3308	26.93	-17.87	2777	2788	873	669	638
68	30.48	15.26	0.296	4555	26.96	-19.77	3164	3175	1407	1352	1306
69	29.95	11.06	0.405	4513	27.12	-20.63	3288	3298	1380	1319	1277
70	30.62	8.58	0.515	4453	27.06	-20.85	3334	3345	1426	1353	1313
71	30.32	7.07	0.629	4475	27.10	-21.04	3381	3392	1427	1342	1303
72	30.01	6.07	0.744	4545	27.33	-21.21	3392	3402	1417	1312	1274
73	29.86	5.23	0.859	4521	27.18	-21.28	3418	3429	1417	1285	1248
74	30.11	7.89	0.515	4093	37.24	-21.60	3504	3497	804	758	724

	Condenser conditions				Evaporator conditions				Power measurements		
Test point	Condenser Air Inlet Temp (C)	Condenser Air Temp Difference (C)	Condenser Air Mass Flowrate (kg/s)	Condenser Air Total Heat Rate (W)	Evaporator Air Inlet Temp (C)	Evaporator Air Temp Difference (C)	Zone Electrical Input (W)	Total cooling load (W)	Outdoor unit power (W)	Compressor Inverter DC Power (W)	Compressor three phase power (W)
75	30.51	10.14	0.515	5260	38.10	-24.98	3904	3897	1445	1372	1329
76	34.85	5.99	0.503	3036	29.96	-16.14	2602	2618	687	646	609
77	34.88	5.95	0.503	3016	30.20	-16.14	2614	2629	680	640	603
78	37.27	3.05	0.500	1534	15.04	-7.21	1176	1218	403	372	337
79	37.47	5.74	0.495	2863	16.47	-12.89	2061	2104	882	835	796
80	37.94	7.00	0.494	3483	16.70	-14.70	2331	2373	1233	1173	1129
81	37.01	7.03	0.494	3498	27.05	-16.64	2644	2668	889	842	804
82	37.64	8.63	0.503	4376	27.20	-19.46	3127	3150	1435	1365	1318
83	38.02	7.63	0.503	3865	36.92	-20.01	3236	3243	946	897	855
84	37.69	9.42	0.502	4768	37.49	-23.13	3686	3692	1420	1351	1304
85	44.94	2.99	0.490	1476	15.00	-6.31	1025	1081	470	437	397
86	44.93	2.44	0.598	1471	15.06	-6.37	1042	1098	480	433	393
87	45.21	2.08	0.706	1481	14.86	-6.28	1017	1074	500	433	393
88	45.21	1.83	0.816	1504	15.14	-6.37	1036	1092	524	431	391
89	45.01	7.18	0.385	2788	16.12	-11.46	1841	1896	1031	991	941
90	45.22	5.71	0.490	2821	16.30	-11.66	1885	1941	1012	962	916
91	45.29	4.66	0.597	2806	16.07	-11.59	1871	1927	1007	944	899
92	45.22	3.97	0.706	2822	16.13	-11.73	1889	1945	1012	929	885
93	45.49	3.46	0.817	2847	16.27	-11.79	1904	1959	1032	924	880
94	44.96	5.26	0.592	3138	16.31	-12.50	1988	2044	1155	1088	1041
95	44.84	4.42	0.700	3118	16.09	-12.48	1973	2029	1152	1067	1021
96	44.94	3.82	0.808	3115	16.40	-12.49	1983	2039	1168	1057	1012
97	45.06	3.59	0.491	1772	25.46	-8.70	1432	1471	481	446	406
98	45.08	3.60	0.491	1780	25.50	-8.79	1447	1485	480	445	405
99	44.69	6.64	0.491	3285	26.73	-14.88	2399	2437	1057	1005	957

	Condenser conditions				Evaporator conditions				Power measurements		
Test point	Condenser Air Inlet Temp (C)	Condenser Air Temp Difference (C)	Condenser Air Mass Flowrate (kg/s)	Condenser Air Total Heat Rate (W)	Evaporator Air Inlet Temp (C)	Evaporator Air Temp Difference (C)	Zone Electrical Input (W)	Total cooling load (W)	Outdoor unit power (W)	Compressor Inverter DC Power (W)	Compressor three phase power (W)
100	44.88	8.07	0.491	3990	27.31	-16.94	2717	2755	1419	1353	1300
101	45.07	3.07	0.488	1509	35.58	-8.19	1355	1375	279	252	218
102	44.70	9.17	0.491	4535	36.93	-20.63	3284	3303	1415	1346	1294
103	14.83	2.09	0.525	1106	14.58	-6.89	1131	1132	148	114	95
104	17.58	2.94	0.534	1578	14.67	-9.18	1543	1550	322	224	197
105	19.15	5.48	0.531	2928	15.19	-14.72	2411	2421	624	555	531
106	19.10	7.39	0.525	3906	15.18	-17.71	2834	2843	1181	1040	1008
107	17.11	2.66	0.534	1433	24.79	-8.79	1476	1464	164	98	79
108	17.26	3.75	0.534	2015	25.08	-12.19	2038	2026	325	208	180
109	17.80	6.76	0.528	3587	25.41	-18.78	3008	2997	643	552	528
110	19.18	8.72	0.525	4610	26.26	-22.54	3614	3604	1280	1127	1095
111	18.04	4.65	0.533	2495	35.50	-15.30	2549	2521	271	185	157
112	17.24	7.80	0.529	4149	36.02	-23.40	3732	3702	633	542	518
113	21.84	2.87	0.530	1530	24.81	-8.46	1418	1415	157	124	103
114	22.47	4.24	0.520	2217	25.14	-11.52	1905	1903	286	249	221
115	23.30	6.99	0.519	3650	25.61	-18.02	2910	2908	715	638	610
116	22.81	3.86	0.516	2004	35.09	-10.98	1807	1786	132	101	80
117	22.97	5.04	0.521	2642	35.53	-14.81	2444	2424	261	225	196
118	30.16	10.52	0.191	2018	24.89	-10.00	1686	1696	386	367	334
119	30.04	6.39	0.296	1901	25.08	-10.28	1733	1744	352	331	299
120	30.56	4.77	0.404	1938	24.80	-10.43	1744	1755	346	320	289
121	31.45	3.62	0.515	1874	25.10	-10.43	1750	1761	357	320	290
122	31.60	3.02	0.629	1910	24.95	-10.44	1756	1767	364	314	284
123	30.18	3.36	0.502	1699	34.90	-10.10	1659	1652	175	144	123
124	30.11	4.65	0.502	2351	35.47	-13.89	2241	2233	318	283	253

	Condenser conditions				Evaporator conditions				Power measurements		
Test point	Condenser Air Inlet Temp (C)	Condenser Air Temp Difference (C)	Condenser Air Mass Flowrate (kg/s)	Condenser Air Total Heat Rate (W)	Evaporator Air Inlet Temp (C)	Evaporator Air Temp Difference (C)	Zone Electrical Input (W)	Total cooling load (W)	Outdoor unit power (W)	Compressor Inverter DC Power (W)	Compressor three phase power (W)
125	37.59	2.47	0.490	1220	24.56	-6.81	1098	1122	249	216	188
126	37.62	3.63	0.495	1812	24.92	-9.78	1603	1627	410	373	340
127	37.52	3.31	0.491	1633	34.88	-9.15	1479	1485	222	190	164
128	37.48	4.47	0.495	2227	35.49	-12.67	2081	2087	402	366	332
129	45.33	4.43	0.484	2161	34.96	-11.58	1876	1897	479	439	400
130	44.89	7.68	0.484	3746	35.12	-17.91	2838	2858	1093	1036	989
131	30.49	2.53	0.517	1319	24.82	-7.46	1269	1280	204	172	148

A.4 Heat pump/chiller curve-fit model coefficients

A.4.1 Heat pump curve fit model coefficients

Heat pump model coefficients (cooling only)

Term	EIR coefficients	Q coefficients	P coefficients
1	2.72E-01	-6.10E+02	-1.59E+02
ZAT	-2.78E-02	1.11E+02	3.09E+01
OAT	5.89E-03	3.71E+00	1.33E+01
ω	6.08E-03	1.80E+01	-1.40E+00
ZAT^2	1.36E-03	-4.76E+00	-7.76E-01
OAT^2	3.22E-05	-3.80E-01	-5.13E-01
ω^2	-5.05E-05	3.52E-02	1.34E-01
ZAT*OAT	-4.03E-04	-2.71E-02	-6.42E-01
ZAT*ω	-1.25E-04	1.81E+00	-2.66E-01
OAT*ω	4.94E-05	1.93E-01	5.57E-01
ZAT^3	-2.18E-05	7.68E-02	5.54E-03
OAT^3	2.75E-06	4.49E-03	7.15E-03
ω^3	3.93E-07	-8.15E-04	-3.17E-04
ZAT^2*OAT	6.49E-06	2.17E-03	7.44E-03
ZAT^2*ω	2.71E-06	-1.60E-02	3.07E-03
OAT^2 *ZAT	-2.50E-06	-7.49E-03	3.61E-03
OAT^2 *ω	-1.05E-06	-5.14E-03	-3.00E-03
ω^2*ZAT	-2.39E-07	-7.94E-03	1.33E-03
ω^2*OAT	3.64E-07	-9.85E-04	-1.87E-03
ZAT*OAT*ω	1.13E-06	4.04E-03	3.16E-03
f	-2.23E-04	3.89E-01	-2.78E-01
f^2	1.95E-07	-2.35E-04	3.10E-04
f*OAT	9.92E-07	-8.90E-04	4.31E-05
f*ZAT	-6.02E-07	-2.04E-05	-1.99E-03
f*ω	-2.07E-06	1.79E-03	-3.59E-03

ZAT = Zone air temperature (C)

OAT = Outdoor air temperature (C)

ω = compressor speed (Hz)

f = condenser fan speed (RPM)

A.4.2 Chiller curve fit model coefficients

Chiller model coefficients

Term	EIR coefficients	Q coefficients	P coefficients
1	2.31E-02	7.55E+02	1.30E+01
EVT	1.28E-02	-1.65E+02	2.61E+01
OAT	5.83E-03	1.98E+01	1.03E+01
ω	5.77E-03	6.87E+00	-2.11E+00
EVT^2	-1.34E-03	1.52E+01	-1.49E+00
OAT^2	-1.37E-04	1.01E+00	-6.48E-01
ω^2	-6.89E-05	8.61E-01	1.31E-01
EVT*OAT	2.66E-04	-6.51E+00	2.21E-02
EVT*ω	-4.64E-04	7.83E+00	-6.93E-01
OAT*ω	7.30E-05	-1.66E+00	6.06E-01
EVT^3	3.05E-05	-3.84E-01	2.63E-02
OAT^3	4.28E-06	1.33E-03	8.35E-03
ω^3	4.29E-07	-6.40E-03	-1.66E-04
EVT^2*OAT	-1.24E-05	2.49E-01	-6.90E-03
EVT^2*ω	2.15E-05	-2.21E-01	1.83E-02
OAT^2 *EVT	-1.04E-06	-5.99E-02	4.23E-03
OAT^2 *ω	-4.74E-07	-1.40E-02	-2.24E-03
ω^2*EVT	3.11E-06	-5.42E-02	5.26E-03
ω^2*OAT	2.05E-07	1.15E-02	-2.30E-03
EVT*OAT*ω	-6.67E-06	9.39E-02	-2.94E-04
f	-1.97E-04	3.43E-01	-2.76E-01
f^2	2.00E-07	-2.90E-04	3.05E-04
f*OAT	2.69E-07	9.06E-03	-3.39E-04
f*EVT	-1.11E-06	-2.02E-03	-1.79E-03
f*ω	-2.20E-06	5.41E-03	-3.48E-03

EVT = Refrigerant evaporating temperature (C)

OAT = Outdoor air temperature (C)

ω = compressor speed (Hz)

f = condenser fan speed (RPM)

A.4.3 Curve fit model linear regression code

The following Matlab codes identify the coefficients of curve-fit multivariable polynomial models of the power consumption, cooling capacity, and the reciprocal of the coefficient of performance (or electric input ratio EIR) of the split system air conditioner as a function of outdoor air temperature, zone air temperature, compressor speed and condenser fan speed and the chiller as a function of outdoor air temperature, evaporating temperature, compressor speed and condenser fan speed.

```
function IdentifyACcurves()
%% function identifies the coefficients of the air conditioner's EIR model,
% cooling rate Q model, and power P model
% a 4-variable polynomial in compressor speed w, condenser fan speed f,
% outdoor air temperature x, and indoor zone air temperature z
format long
load CompMapData % load measured heat pump/chiller performanace data

% convert data structure objects to matlab matrices
for i=1:length(CompMapData)
   z(i) = CompMapData(i).averages(14); % zone air temperature
   x(i) = CompMapData(i).averages(17); % outdoor air temperature
   w(i) = CompMapData(i).averages(56); % compressor speed
   f(i) = CompMapData(i).averages(57); % condenser fan speed
   p(i) = CompMapData(i).averages(33); % outdoor unit power consumption
   q(i) = CompMapData(i).averages(50); % cooling load on the evaporator
end
z = z'; x = x'; q = q'; w = w'; f = f'; p = p'; % create column vectors

eir = p./q;  % calculate late the EIR or 1/COP for each steady state conditions

% create the A matrix for the regressrion
A = [ones(size(z)) z x w (z.^2) (x.^2)  (w.^2) (z.*x) (z.*w) (x.*w) ...
     (z.^3) (x.^3) (w.^3) (z.^2).*x (z.^2).*w (x.^2).*z (x.^2).*w ...
     (w.^2).*z (w.^2).*x z.*x.*w f f.^2 f.*z f.*x f.*w];

cEIR = regress(eir,A);  % compute coefficients of the EIR curve
cQ = regress(q,A);      % computer coefficients of the Q curve
cP = regress(p,A);      % computer coefficients of the P curve

% save coefficients
save eircoefficients cEIR cQ cP
```

```
function IdentifyChillercurves()
%% function identifies the coefficients of the chiller's EIR model,
% cooling rate Q model, and power P model
% a 4-variable polynomial in compressor speed w, condenser fan speed f,
% outdoor air temperature x, and indoor zone air temperature z
format long
load CompMapData % load measured heat pump/chiller performanace data
```

```
% convert data structure objects to matlab matrices
for i=1:length(CompMapData)
   e(i) = CompMapData(i).averages(16); % evaporating temperature
   x(i) = CompMapData(i).averages(17); % outdoor air temperature
   w(i) = CompMapData(i).averages(56); % compressor speed
   f(i) = CompMapData(i).averages(57); % condenser fan speed
   p(i) = CompMapData(i).averages(33); % outdoor unit power consumption
   q(i) = CompMapData(i).averages(50); % cooling load on the evaporator
end
e = e'; x = x'; q = q'; w = w'; f = f'; p = p'; % create column vectors

eir = p./q;  % calculate late the EIR or 1/COP for each steady state conditions

% create the A matrix for the regressrion
A = [ones(size(e)) e x w (e.^2) (x.^2)  (w.^2) (e.*x) (e.*w) (x.*w) ...
     (e.^3) (x.^3) (w.^3) (e.^2).*x (e.^2).*w (x.^2).*e (x.^2).*w ...
     (w.^2).*e (w.^2).*x e.*x.*w f f.^2 f.*e f.*x f.*w];

cEIR = regress(eir,A);  % compute coefficients of the EIR curve
cQ = regress(q,A);      % computer coefficients of the Q curve
cP = regress(p,A);      % computer coefficients of the P curve

% save coefficients
save eircoefficients cEIR cQ cP
```

Appendix B. Thermal model identification testing

B.1 Thermal test chamber components

B.1.1 Radiant concrete floor

The layout of the Warmboard radiant subfloor, with grooves for pex pipe, is shown at right. The groove spacing is 12 inches. Six parallel water loops were installed, running down the length of the floor and back from the system manifold. The pressure drop per unit length of PEX is 0.016 psi/foot-pipe at 1 GPM for 1/2" PEX. The total pressure drop in the system is less than 1 foot of water column at the constant flow rate of 2.1 GPM, with roughly 0.35 GPM per loop.

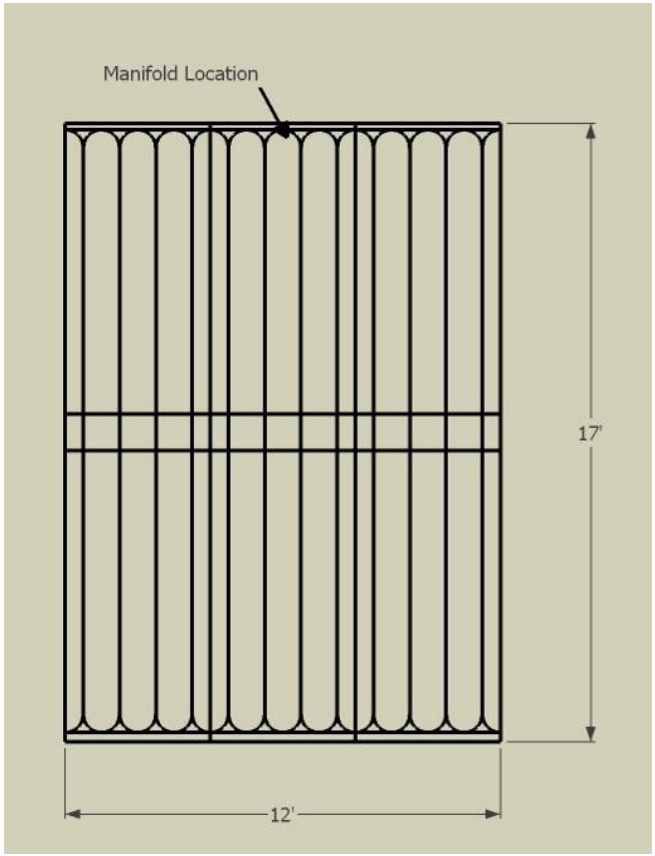

The PEX was installed in the Warmboard grooves and three layers of concrete pavers were installed over the top as shown in the picture below right. The concrete pavers have typical dimensions of eight inches by 16 inches by 1.5 inches, weighing 5.3 pounds. A picture of the radiant system manifold is shown below left.

The Matlab code below is an approximate physical model of the concrete floor in the LLCS test chamber. The greatest uncertainties in the model are the thermal conductivity of the concrete pavers, the contact resistance between the Warmboard aluminum surface and the bottom of the concrete pavers, and the contact resistance between the PEX pipe and the Warmboard aluminum surface. The contact resistances between the pipe and aluminum and aluminum and concrete pavers have been calibrated to match observations that show the typical temperature difference between the chilled water and the bottom of the concrete pavers is around eight to ten degrees Celsius. The thermal conductivity of the concrete pavers may vary anywhere between 0.3 W/mK for very lightweight concrete to 1.5 W/mK for concrete. Over this range, the percentage of the cooling delivered through the radiant floor lost to the outside of chamber, through the bottom of the floor, varies anywhere from 15 to 30 percent. The 25 percent cooling energy loss apparent for the low lift predictive control of the TABS system in Table 9 relative to the RCP system is within the range of possible losses from the floor.

```
function ModelConcreteFloor()

% Typical steady state temperature of the building slab and the chamber air
Tbuilding = 23+273;  % temperature of building floor K
Tchamber = 23+273; % temperature of the chamber in K
Tchw = 7+273; % Typical chilled water temperature K

% Properties of the plywood subfloor
kplywood = 0.13; % thermal conductivity of plywood W/mK
Lplywood = 1.5*0.0254; % thickness of plywood in m
Aplywood = 12*17*0.3048*0.3048; % area of plywood per loop in m^2
UAplywood = (kplywood/Lplywood)*Aplywood; % conductance of plywood in W/K
Rplywood = 1/UAplywood; % resistance of plywood in K/W

% Properties of the floor joists
kjoist = 0.15; % thermal conductivity of wood stud W/mK
Ljoist = 3.5*0.0254; % thickness of joist m
Ajoist = (1.5/12)*17*12*0.3048*0.3048; % area of joist m2
UAjoist = (kjoist/Ljoist)*Ajoist; % conductance of joists in W/K

% Properties of the floor insulation
kinsulation = 0.03; % thermal conductivity of insulation W/mK
Linsulation = (3*0.0254); % thickness of insulation m
Ainsulation = (10.5/12)*17*12*0.3048*0.3048; % area of insulation m2
Rinsulation = Linsulation/kinsulation; % resistance of insulaion in m^2-K/W
Uinsulation = 1/Rinsulation; % U value of insulation in W/m^2-K
UAinsulation = Uinsulation*Ainsulation; % conductance of insulation in W/K

% Properties of the composite subfloor construction
UAjoistcomposite = UAjoist+UAinsulation % Total conductance of joist/insulation W/K
Rjoistcomposite = 1/UAjoistcomposite; % Total resistance of joist/insulation K/W
Rsubfloor = Rplywood+Rjoistcomposite; % Total resistance of subfloor in K/W
Rsubfloorperloop = 6*Rsubfloor; % Resistance of subfloor per loop of pipe in K/W

% Properties of the concrete paver/slab
m = 0.4535*15;  % mass of one paver kg
```

```
volpaver = (1.75*8*16)*(0.0254^3) % volume of paver m3
rhopaver = m/volpaver; % concrete paver density kg/m^3
cp = 900;          % concrete slab specific heat(J/kg-K)
Aconcrete =12*17*(0.3048^2);       % concrete slab area m^2
kconcrete = 0.33;          % lightweight concrete thermal conductivity W/m-K, ranging from 0.2-1.5 W/mK
Lconcrete = (1.75*3)*0.0254;     % thickness of concrete m
Rslab = (Lconcrete/(kconcrete*Aconcrete)); % thermal resistance of slab K/W
Rfilm = 1/(10*Aconcrete);  % radiative and convective resistance at slab surface K/W
Rslabfilmperloop = 6*(Rslab+Rfilm); % total resistance from bottom of slab to chamber in K/W

% properties of the chilled water
cp = 4200; % specific heat of water W/kg-K;
kwater = 0.6; % thermal conductivity of water in W/mK
rho = 1000; % density of water in kg/m3
mu = 0.0013; % dynamic viscosity of water in kg/m-s
nu = mu/rho; % kinematic viscosity of water in m2/s

% properties of the PEX chilled water pipe
GPM = 2.2 % Total chilled water flow rate in GPM
GPMperloop = GPM/6; % chilled water flow rate per loop
kPex = 0.45; % thermal conductivity of pex in W/mK
ID = 0.475 *0.0254; % inner diameter in m
OD = 0.625*0.0254; % outer diameter in m
Ac = pi*(ID/2)^2; % cross sectional area of pipes in m2
X = 12*0.0254/2; % half width of spacing between tubes in m
Um = GPMperloop*0.000063/Ac; % mean velocity of fluid in m/s
Pr = cp*mu/kwater; % Prandtl number of water
Re = Um*ID/nu; % Reynolds number of water
Lpipe = 17*2*0.3048; % length of pipe in m

% poperties of the aluminum subfloor surface
kAlum = 222; % thermal conducitivyt of aluminum in W/mK
tAlum = 0.03*0.0254/2; % half thickness of aluminum in m

% Calculate Nusselt number based on Reynolds number
if(Re>3000)
   f = (0.790*log(Re)-1.64)^-2; % Friction factor
   Nu = ((f/8)*(Re-1000)*Pr)/(1+(12.7*(f/8)^0.5*(Pr^(2/3)-1))); % Nusselt number for turbulent flow
   disp(['Flow is turbulent, Nusselt number = ' num2str(Nu)])
elseif(Re>2300)
   f = (0.790*log(Re)-1.64)^-2; % Friction factor
   Nu = ((f/8)*(Re-1000)*Pr)/(1+(12.7*(f/8)^0.5*(Pr^(2/3)-1))); % Nusselt number for turbulent flow
   Nu = mean([Nu 4]); % take mean of laminar and Gnielinski in transition region
   disp(['Flow is transitional, Nusselt number = ' num2str(Nu)])
else
   Nu = 4; % laminar region, not uniform temperature (3.66) or uniform heat flux (4.36)
   disp(['Flow is laminar, Nusselt number = ' num2str(Nu)])
end

% Calculate heat transfer coefficient in the pipe using Nusselt number
h = Nu*kwater/ID; % W/m2K

%%
```

```
Rhc = 1/(pi*ID*h*Lpipe); % convective resistance K/W per loop
Rpipe = log(OD/ID)/(2*pi*kPex*Lpipe); % pipe wall resistance K/W per loop
Rcontactpipe = 0.003/(pi*OD*Lpipe); % pipe contact resistance K/W  assume R = del-T/q/m2 = 0.3K/100 W/m2 =
0.003 m2-K/W

% aluminum to concrete contact resistance, calibrated to 10K difference
% between water and bottom of slab
Rcontactconcrete = (12*17*0.3048^2)*10/1200; % contact resistance m^2-K/W
Rcontactplywood = 0.05; % m2K/W  assume R = del-T/q/m2 = 0.5K/100 W/m2 = 0.005 m2-K/W

% fin parameter (Perimeter Lpipe, Area = tAlum*Lpipe, h = 1/R_contact) for
% aluminum to concrete
mconcrete = (Lpipe/(kAlum*tAlum*Lpipe*Rcontactconcrete))^0.5;
RfintoSlab = ((Rcontactconcrete/(kAlum*tAlum*Lpipe*Lpipe))^0.5)*tanh(mconcrete*X)/2; % 1/2 resistance due to
two sides of aluminum on pipe

% fin parameter (Perimeter Lpipe, Area = tAlum*Lpipe, h = 1/R_contact) for
% aluminum to plywood
mplywood = (Lpipe/(kAlum*tAlum*Lpipe*Rcontactplywood))^0.5;  % fin parameter (Perimeter L, Area = t*L, h =
1/R_contact)
RfintoPlywood = ((Rcontactplywood/(kAlum*tAlum*Lpipe*Lpipe))^0.5)*tanh(mplywood*X)/2; % 1/2 resistance
due to two sides of aluminum on pipe

Rwatertofinbase = (Rhc+Rpipe+Rcontactpipe); % resistance from water loop to base of fin K/W
Rchambertofinbase = RfintoSlab+Rslabfilmperloop; % resistance from chamber air to base of fin K/W
Rbuildingtofinbase = Rsubfloorperloop+RfintoPlywood; % resistance from building floor to base of fin K/W

% base of fin temperature, the aluminum temperature near the chilled water
% pipe
Tfinbase = (Tchw/Rwatertofinbase+Tchamber/(Rslab+Rfilm+RfintoSlab)+Tbuilding/(Rsubfloor+RfintoPlywood))/ ...
   (1/Rwatertofinbase+1/(Rslab+Rfilm+RfintoSlab)+1/(Rsubfloor+RfintoPlywood));

% heat rate between the chamber and the aluminum near the chilled water
% pipe per loop
q1 = (Tchamber-Tfinbase)/Rchambertofinbase;
% heat rate between the building slab and the aluminum near the chilled
% water pipe per loop
q2 = (Tbuilding-Tfinbase)/Rbuildingtofinbase;

Q = (Tfinbase-Tchw)/Rwatertofinbase;  % Total heat rate per loop
Qtot = Q*6  % Total heat rate from the floor

ChamberFraction = q1/(q1+q2)
BuildingFraction = q2/(q1+q2)

UST = Tfinbase+q1*RfintoSlab; % underslab temperature
PLT = Tfinbase+q2*RfintoPlywood; % plywood temperature
SST = Tchamber-q1*6*Rfilm; % Slab surface temperature
[Tchw-273 Tfinbase-273  PLT-273 UST-273 SST-273 Tbuilding-273 Tchamber-273]
```

An analysis of the diurnal heat capacity (DHC) of the concrete floor relative to its thickness, the thermal conductivity of the concrete, and the heat transfer coefficient between the concrete surface and the room air shows the relative importance of these different concrete slab and heat transfer properties. DHC is a measure of the thermal storage capacity of a material, measured by the total energy it can store and release in a diurnal cycle per degree of temperature swing per unit area. The DHC of the slab as defined by Balcomb [1983b] is shown in the graph below at left, for which the temperature swing of the concrete surface is used. In general, increasing the depth of the concrete layer increases the DHC, or thermal storage capacity, up to a certain depth after which storage capacity begins to decline. Depending on the conductivity of the concrete, which may be as low as 0.2 W/mK for lightweight concrete, the optimal concrete thicknes may range from five to fifteen centimeters. A concrete depth of 10 to 15 centimeters is optimal for typical values of concrete thermal conductivity.

The net heat transfer coefficient, in W/m^{2}K, between the concrete surface and the chamber air and other surfaces also affects the thermal storage capacity of the concrete slab. The graph below at right shows the DHC relative to the zone air temperature swing for different values of the net heat transfer coefficient between the concrete surface and the zone, including both radiative and convective heat transfer. The DHC relative to the zone air temperature swing is lower than the DHC defined by Balcomb [1983b] and is strongly affected by the value of the net heat transfer coefficient. Slab depths greater than eight to twelve centimeters, for a typical concrete thermconductivity, do not yield higher DHCs.

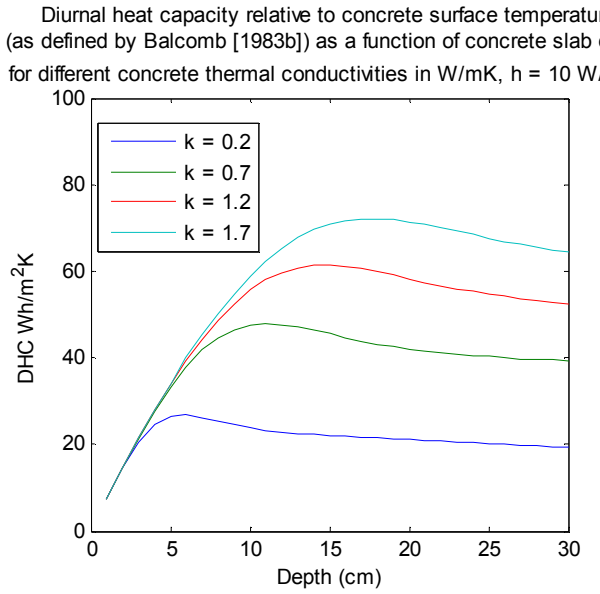

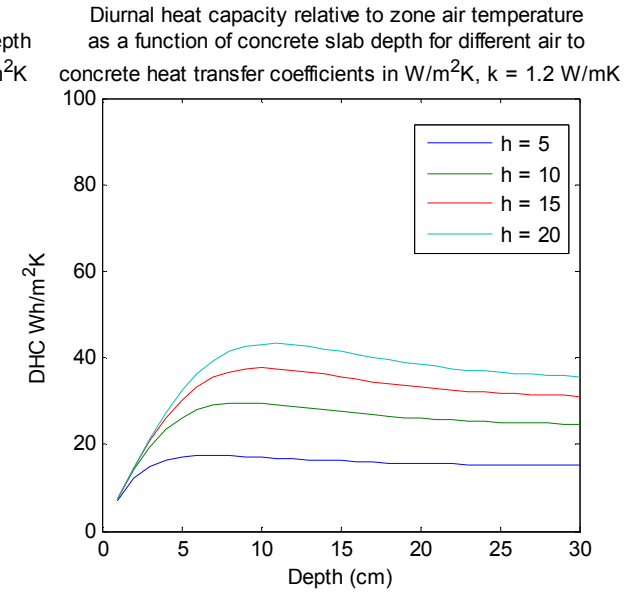

The Matlab code below calculates the DHC of a concrete slab as a function of depth, relative to the concrete surface and relative to the zone air.

```
function DHCslab(k,h)
% calculates the DHC of a concrete slab as a function of depth
% k is thermal conductivity in W/mK
% h is the net heat transfer coefficient between the slab surface and the
% zone in W/m^2 K
```

```
format long
depth = 0.01:0.01:0.3;   % trial concrete depths in meters
admittance = zeros(length(depth),length(h));
segments = 12; % segmented concrete slab
TempSwing = 5; % diurnal air temperature swing
for i=1:length(depth)
   rho = 2240;        % concrete slabdensity kg/m^3
   cp = 900;         % concrete slab specific heat(J/kg-K)
   area = 12*17*(0.3048^2);       % concrete slab area m^2
   Rfilm = 1/(h*area);  % radiative and convective resistance at slab surface K/W
   Cs = rho*cp*area*depth(i)/segments; % thermal capacity of slab J/K
   Rconc = (depth(i)/(k*area))/(segments+1); % resistance of concrete K/W
   inc = 60;    % 1 minute increments
   total = 60*60*24*4; % 4 days
   ts = 0:inc:total';  % timesteps
   u = 273+24+(TempSwing/2).*cos((2*pi/(24*60*60)).*ts); % room temperature driving function

   % create state space model of concrete response, 12 segments
   B = [1/((Rfilm+Rconc)*Cs) zeros(1,segments-1)]';
   A = diag([ones(segments-1,1)*(-2/(Rconc*Cs)); -1/(Rconc*Cs)],0)+diag(ones(segments-
1,1)*(1/(Rconc*Cs)),1)+diag(ones(segments-1,1)*(1/(Rconc*Cs)),-1);
   A(1,1) = -1/((Rfilm+Rconc)*Cs)-1/(Rconc*Cs);

   % output air temperature and heat rate and surface temperature
   C = [0  zeros(1,segments-1);...
      -1/(Rfilm+Rconc) zeros(1,segments-1);...
      Rfilm/(Rfilm+Rconc) zeros(1,segments-1)];
   D = [1; 1/(Rfilm+Rconc); 1-Rfilm/(Rfilm+Rconc)];
   x0 = (273+24).*ones(segments,1)';
   sys = ss(A,B,C,D);

   % simulate concrete floor state space model with sinusoidal room temperature driving function
   [Y T X] = lsim(sys,u,ts,x0);

   startindex = 60*24*2;  endindex = 60*24*3;
   delT = max(Y(startindex:endindex,1))-min(Y(startindex:endindex,1)); % air temperature swing
   delQ = max(Y(startindex:endindex,2))-min(Y(startindex:endindex,2)); % thermal load swing
   delST = max(Y(startindex:endindex,3))-min(Y(startindex:endindex,3)); % surface temperature swing
   Q = sum(Y(find(Y(startindex:endindex,2)>0),2)/60);  % total energy stored in a diurnal cycle
   DHC(i) = Q/delST/area;  % DHC per unit area
   DHCair(i) = Q/delT/area;  % DHC relative to air per unitarea
end
figure(1)
plot(depth*100,DHC)
hold all
plot(depth*100,DHCair)
xlabel('Depth (cm)')
ylabel('DHC Wh/m^2K')
title('Diurnal heat capacity as a function of concrete slab depth')
```

B.1.2 Internal Loads

The pictures on this page show the systems used to simulate internal loads from people, equipment and lights. Clockwise from the top right, the pictures show the simulated equipment loads, the simulated load from occupants, the view of the inside of a simulated internal load, and finally the lighting loads and the ceiling mixing fan.

Inside the simulated equipment and occupant loads are three light bulb sockets which can be used to change the amount of load to achieve the different load densities described in chapter 6.

The ceiling fan was used to create some air movement to make up for the concrete-core system cooling only from the floor, not from the floor and ceiling. Also, the companion DOAS would provide some air movement. The ceiling fan energy consumption was counted as part of the internal loads, but not as part of the system energy consumption. For an LLCS that required supplemental air movement, much higher efficiency fans could be used than that installed in the test chamber, which was intended only to simulate the effects of cooling from above and the DOAS.

During the temperature-CRTF model testing, the radiant heating panels shown in the picture at bottom left were used to apply internal radiant heating loads to the test chamber. A similar system was installed underneath the concrete floor to apply radiant thermal loads below the concrete floor prior to installation of the chilled water piping. Electrical convective heaters were used to simulate internal convective heating loads.

B.1.3 Climate chamber control

An image of the climate chamber HVAC control system is shown below. The system is a constant air volume system comprising a supply, a return fan, a chilled water coil, an electric pre-heat, an electric re-heat coil, and an economizer. The outdoor air supply and exhaust dampers were fixed shut, the pre-heat coil was disabled, and the mixed air damper was fixed open to force the system to only re-circulate indoor air. This was done to prevent humid outside air from entering the climate chamber, and ultimately the test chamber, resulting in latent loads. The system was programmed through time-of-day scheduling to follow the typical summer week in climates of choice, including Atlanta and Phoenix.

The system is controlled by a Landis & Gyr System Powers 600 control system, with Insight control software. This system is a predecessor to the Siemens Apogee control system.

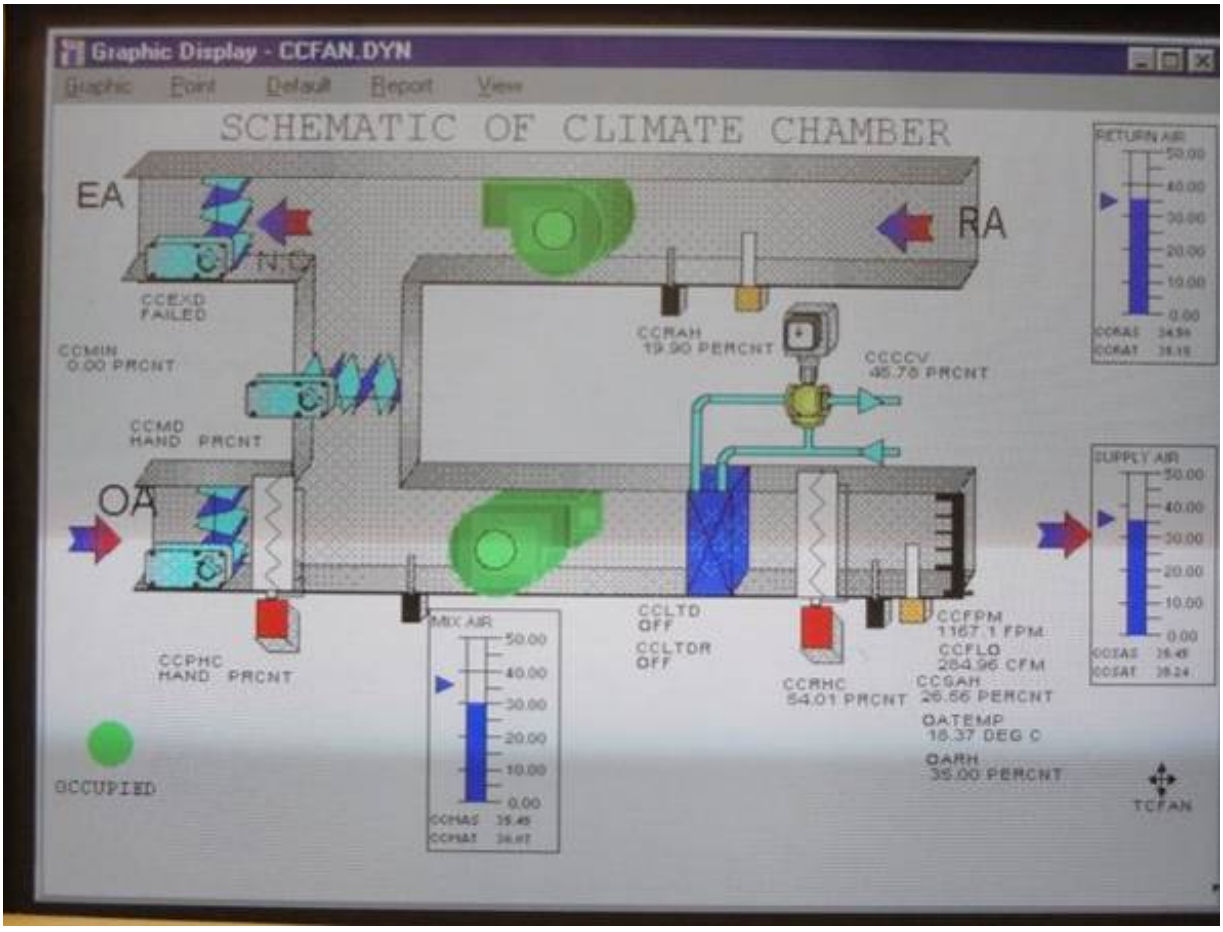

B.2 Thermal test chamber sensors and instrumentation

B.2.1 Table of sensors for thermal test chamber

Measurement description	Sensor Make/Model	Installation notes	Accuracy
Air temperature measurements	Omega/PR-T-24-SLE	Installed at locations described in sections B.2.2. Calibrated to measure within 0.01 K	0.5 C (rated)
Surface temperature measurements	Omega/PR-T-24-SLE	Installed at locations described in sections B.2.2. Calibrated to measure within 0.01 K	0.5 C (rated)
Concrete slab and under-slab temperature measurements	Omega/GG-T-28-SLE	Installed at locations described in sections B.2.2	0.5 C (rated)
Convective heater power, thermal model testing	F.W. Bell/PX-2221B1	Installed on the convective heat power supply	0.5 % (rated)
Radiant ceiling panel power, thermal model testing	F.W. Bell/PX-2221B1	Installed on the power supply to a variac, which supplied the radaint ceiling panels.	0.5 % (rated)
Radiant floor power, thermal model testing	Voltage divider DC current shunt		
Internal load power	Wattnode/ WNB-3Y-208P	Installed before a programmable switch relay.	0.5% of reading
Radiant concrete-core floor cooling rate	See Appendix C.2		

The data for the thermal test chamber was logged by a Campbell Scientific CR10X data logger. Three Campbell Scientific AM25T 25-channel multiplexers were used for logging thermocouple temperature measurements. The reference temperature sensors of the three loggers were calibrated relative to each other by enclosing the loggers in a well-insulated box and comparing the steady state temperature measured by each logger's reference temperature sensors. A 0.11 Kelvin offset for one of the loggers relative to the other two was identified and used to correct the data from that logger. Accounting for this offset, the relative accuracy of the three AM25T loggers is within 0.015 Kelvin. The internal loads were controlled using a Campbell Scientific SDM-CD16AC 16 channel AC/DC controller. The CR10X data logging code is shown below.

Thermal test chamber CR10X EdLog32 data-logging code (written primarily by P.R. Armstrong)

```
;{CR10X}
*Table 1 Program
  01: 60       Execution Interval (seconds)

; First AM25T, control port 1 and 2
1:  Do (P86)
  1: 42       Set Port 2 High
2:  Full Bridge (P6)
  1: 1        Reps
  2: 21       ñ 2.5 mV 60 Hz Rejection Range
  3: 1        DIFF Channel
  4: 1        Excite all reps w/Exchan 1
  5: 250      mV Excitation
  6: 1        Loc [ K_Vs_250  ]
  7: 1.0      Mult
  8: 0.0      Offset
3:  Do (P86)
  1: 41       Set Port 1 High
4:  Do (P86)
  1: 51       Set Port 1 Low
5:  Full Bridge (P6)
  1: 1        Reps
  2: 4        ñ 500 mV Slow Range
  3: 1        DIFF Channel
  4: 1        Excite all reps w/Exchan 1
  5: 250      mV Excitation
  6: 2        Loc [ Vx_250    ]
  7: .001     Mult
  8: 0.0      Offset
6:  Z=X/Y (P38)
  1: 1        X Loc [ K_Vs_250  ]
  2: 2        Y Loc [ Vx_250    ]
  3: 4        Z Loc [ RefTemp_C ]
7:  Z=X*F (P37)
```

```
 1: 4       X Loc [ RefTemp_C ]
 2: -.001   F
 3: 4       Z Loc [ RefTemp_C ]
8:  Z=X+F (P34)
 1: 4       X Loc [ RefTemp_C ]
 2: .09707  F
 3: 4       Z Loc [ RefTemp_C ]
9:  BR Transform Rf[X/(1-X)] (P59)
 1: 1       Reps
 2: 4       Loc [ RefTemp_C ]
 3: 10.025  Mult (Rf)
10:  Temperature RTD (P16)
 1: 1       Reps
 2: 4       R/R0 Loc [ RefTemp_C ]
 3: 80      Loc [ RefTemp1C ]
 4: 1.0     Mult
 5: 0.0     Offset
11:  Do (P86)
 1: 52      Set Port 2 Low
12:  Do (P86)
 1: 42      Set Port 2 High
13:  Beginning of Loop (P87)
 1: 0       Delay
 2: 25      Loop Count
14:  Do (P86)
 1: 41      Set Port 1 High
15:  Do (P86)
 1: 51      Set Port 1 Low
16:  Do (P86)
 1: 41      Set Port 1 High
17:  Do (P86)
 1: 51      Set Port 1 Low
18:  Thermocouple Temp (DIFF) (P14)
 1: 1       Reps
 2: 21      ñ 2.5 mV 60 Hz Rejection Range
 3: 1       DIFF Channel
 4: 1       Type T (Copper-Constantan)
 5: 80      Ref Temp Loc [ RefTemp1C ]
 6: 5    -- Loc [ TC_1_1   ]
 7: 1.0     Mult
 8: 0.0     Offset
19:  End (P95)
20:  Do (P86)
 1: 52      Set Port 2 Low

;Ssecond AM25T, control port 3 and 4
21:  Do (P86)
 1: 44      Set Port 4 High
22:  Full Bridge (P6)
 1: 1       Reps
 2: 1       ñ 5 mV Slow Range
 3: 1       DIFF Channel
 4: 1       Excite all reps w/Exchan 1
 5: 250     mV Excitation
 6: 1       Loc [ K_Vs_250  ]
 7: 1.0     Mult
 8: 0.0     Offset
23:  Do (P86)
 1: 43      Set Port 3 High
24:  Do (P86)
 1: 53      Set Port 3 Low
25:  Full Bridge (P6)
 1: 1       Reps
 2: 4       ñ 500 mV Slow Range
 3: 1       DIFF Channel
 4: 1       Excite all reps w/Exchan 1
 5: 250     mV Excitation
 6: 2       Loc [ Vx_250   ]
 7: .001    Mult
 8: 0.0     Offset
26:  Z=X/Y (P38)
 1: 1       X Loc [ K_Vs_250  ]
 2: 2       Y Loc [ Vx_250    ]
 3: 4       Z Loc [ RefTemp_C ]
27:  Z=X*F (P37)
 1: 4       X Loc [ RefTemp_C ]
 2: -.001   F
 3: 4       Z Loc [ RefTemp_C ]
28:  Z=X+F (P34)
 1: 4       X Loc [ RefTemp_C ]
 2: .09707  F
 3: 4       Z Loc [ RefTemp_C ]
29:  BR Transform Rf[X/(1-X)] (P59)
 1: 1       Reps
 2: 4       Loc [ RefTemp_C ]
 3: 10.025  Mult (Rf)
30:  Temperature RTD (P16)
 1: 1       Reps
 2: 4       R/R0 Loc [ RefTemp_C ]
 3: 81      Loc [ RefTemp2C ]
 4: 1.0     Mult
 5: 0.0     Offset
31:  Do (P86)
 1: 54      Set Port 4 Low
32:  Do (P86)
 1: 44      Set Port 4 High
33:  Beginning of Loop (P87)
 1: 0       Delay
 2: 25      Loop Count
34:  Do (P86)
 1: 43      Set Port 3 High
35:  Do (P86)
 1: 53      Set Port 3 Low
36:  Do (P86)
 1: 43      Set Port 3 High
37:  Do (P86)
 1: 53      Set Port 3 Low
38:  Thermocouple Temp (DIFF) (P14)
 1: 1       Reps
 2: 21      ñ 2.5 mV 60 Hz Rejection Range
 3: 1       DIFF Channel
 4: 1       Type T (Copper-Constantan)
 5: 81      Ref Temp Loc [ RefTemp2C ]
 6: 30   -- Loc [ TC_2_1   ]
 7: 1.0     Mult
 8: 0.0     Offset
39:  End (P95)
40:  Do (P86)
 1: 54      Set Port 4 Low ;

;Third AM25T, control port 5 and 6
41:  Do (P86)
 1: 46      Set Port 6 High
42:  Full Bridge (P6)
 1: 1       Reps
 2: 21      ñ 2.5 mV 60 Hz Rejection Range
 3: 1       DIFF Channel
 4: 1       Excite all reps w/Exchan 1
 5: 250     mV Excitation
 6: 1       Loc [ K_Vs_250  ]
 7: 1.0     Mult
 8: 0.0     Offset
```

```
43:  Do (P86)
 1: 45      Set Port 5 High
44:  Do (P86)
 1: 55      Set Port 5 Low
45:  Full Bridge (P6)
 1: 1       Reps
 2: 4       ñ 500 mV Slow Range
 3: 1       DIFF Channel
 4: 1       Excite all reps w/Exchan 1
 5: 250     mV Excitation
 6: 2       Loc [ Vx_250    ]
 7: .001    Mult
 8: 0.0     Offset
46:  Z=X/Y (P38)
 1: 1       X Loc [ K_Vs_250  ]
 2: 2       Y Loc [ Vx_250    ]
 3: 4       Z Loc [ RefTemp_C ]
47:  Z=X*F (P37)
 1: 4       X Loc [ RefTemp_C ]
 2: -.001   F
 3: 4       Z Loc [ RefTemp_C ]
48:  Z=X+F (P34)
 1: 4       X Loc [ RefTemp_C ]
 2: .09707  F
 3: 4       Z Loc [ RefTemp_C ]
49:  BR Transform Rf[X/(1-X)] (P59)
 1: 1       Reps
 2: 4       Loc [ RefTemp_C ]
 3: 10.025  Mult (Rf)
50:  Temperature RTD (P16)
 1: 1       Reps
 2: 4       R/R0 Loc [ RefTemp_C ]
 3: 82      Loc [ RefTemp3C ]
 4: 1.0     Mult
 5: 0.0     Offset
51:  Do (P86)
 1: 56      Set Port 6 Low
52:  Do (P86)
 1: 46      Set Port 6 High
53:  Beginning of Loop (P87)
 1: 0       Delay
 2: 25      Loop Count
54:  Do (P86)
 1: 45      Set Port 5 High
55:  Do (P86)
 1: 55      Set Port 5 Low
56:  Do (P86)
 1: 45      Set Port 5 High
57:  Do (P86)
 1: 55      Set Port 5 Low
58:  Thermocouple Temp (DIFF) (P14)
 1: 1       Reps
 2: 21      ñ 2.5 mV 60 Hz Rejection Range
 3: 1       DIFF Channel
 4: 1       Type T (Copper-Constantan)
 5: 82      Ref Temp Loc [ RefTemp3C ]
 6: 55    -- Loc [ TC_3_1    ]
 7: 1.0     Mult
 8: 0.0     Offset
59:  End (P95)
60:  Do (P86)
 1: 56      Set Port 6 Low ;

; CR10X measurements
;Chilled water pump power
61:  Pulse (P3)
 1: 1       Reps
 2: 1       Pulse Channel 1
 3: 20      High Frequency, Output Hz
 4: 112     Loc [ PumpPower ]
 5: 78.03   Multiplier
 6: 0.0     Offset
; 0.867 CT AMPs, 338.2 ohms.  0.025 Wh/pulse/AMP

;Internal load power
62:  Pulse (P3)
 1: 1       Reps
 2: 2       Pulse Channel 2
 3: 20      High Frequency, Output Hz
 4: 113     Loc [ LoadPower ]
 5: 6       Multiplier
 6: 0.0     Offset
; Load Watts, 0.6 W/Hz-CT-rated amps, 6 W/Hz, 0.0001667
Wh/pulse/Amp

;WRITE TO FINAL STORAGE
63:  If time is (P92)
 1: 0       Minutes into a
 2: 1       Minute Interval
 3: 10      Set Output Flag High
;assign array ID to final storage ID
64:  Set Active Storage Area (P80)^20345
 1: 1       Final Storage
 2: 105     Array ID
;time stamp
65:  Real Time (P77)^11008
 1: 1210    Year,Day,Hour/Minute (prev day at midnight)
;input locations written to final storage
66:  Resolution (P78)
 1: 01      High Resolution
67:  Sample (P70)^26349
 1: 3       Reps
 2: 80      Loc [ RefTemp1C ]
68:  Sample (P70)^24951
 1: 25      Reps
 2: 5       Loc [ TC_1_1    ]
69:  Sample (P70)^16309
 1: 25      Reps
 2: 30      Loc [ TC_2_1    ]
70:  Sample (P70)^8277
 1: 25      Reps
 2: 55      Loc [ TC_3_1    ]
71:  Average (P71)^15080
 1: 1       Reps
 2: 112     Loc [ PumpPower ]
72:  Average (P71)^24514
 1: 1       Reps
 2: 113     Loc [ LoadPower ]

*Table 2 Program
 02: 0.0       Execution Interval (seconds)
*Table 3 Subroutines
End Program
```

B.2.2 Thermocouple locations and dimensions

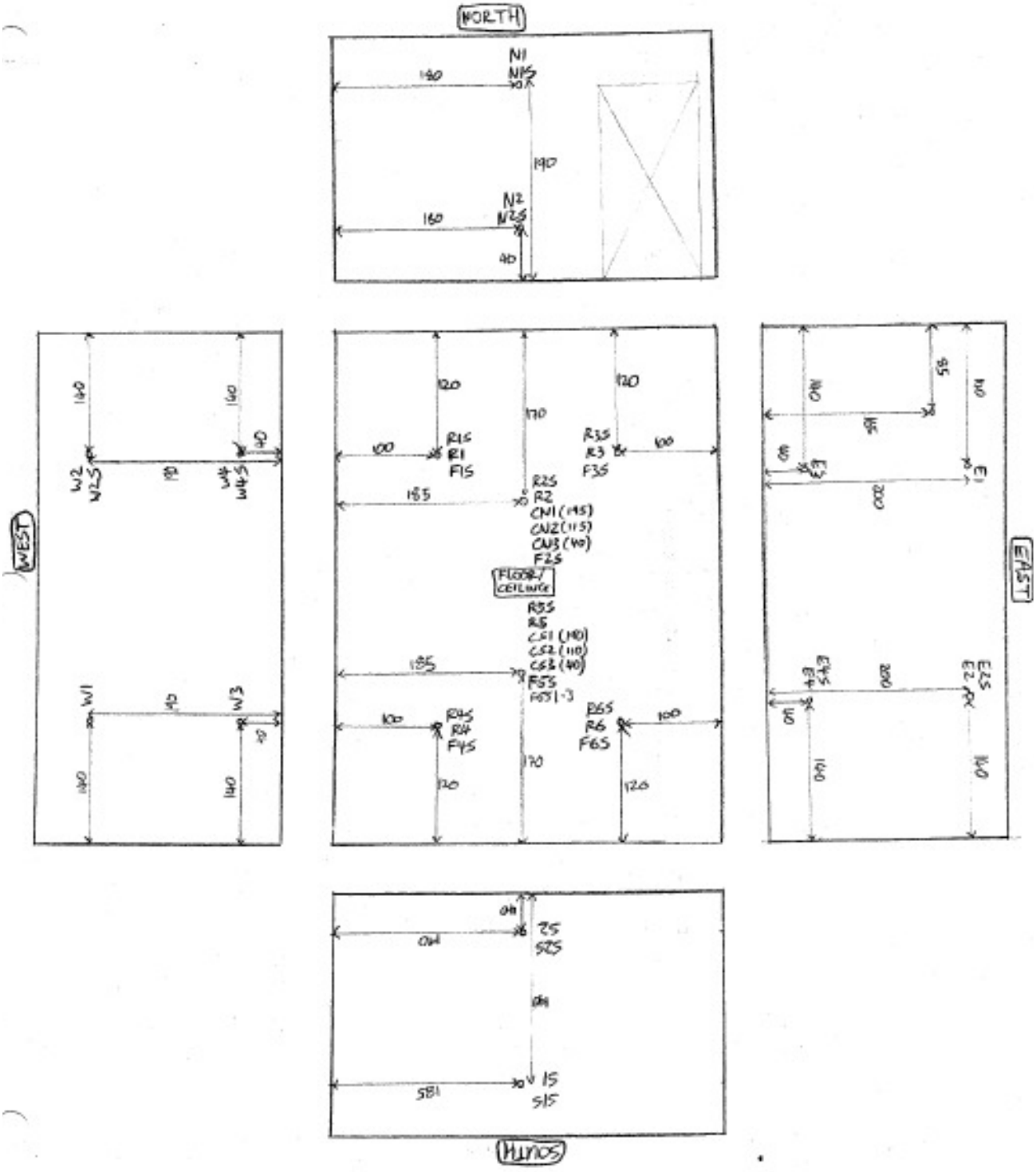

The diagram above shows the location and coordinates of each thermocouple installed in the test chamber. All dimensions are in centimeters. The South wall borders the climate chamber and has three large, double pane windows. The North wall has a doorway for access to the test chamber.

B.3 Temperature-CRTF model identification codes

The code below identifies temperature-CRTF model coefficients from data logged by the Test Chamber CR10X and the LLCS CR1000 data loggers. Thus, training data files come in pairs, one for the chamber and one for the LLCS system, described in Appendix C. An arbitrary number of training data sets can be added to the list of training data file names listed under the variables fnameschamber and fnameschiller, so long as they are in pairs and the data has been corrected to account for records skipped by each logger.

```
function [ZATrmse MRTrmse OPTrmse USTrmse RWTrmse] = IdentifyTCRTF(minutes,order)
% function Identify TCRTF uses a set of training data files to identify the
% coefficients of a temperature-CRTF model for the zone air temperature
% ZAT, the mean radiant temperature MRT, the operative temperature OPT, the
% under-slab temperature UST, and the return water temperature RWT.  The
% temperature CRTF applies a sampling interval of "minutes" and creates a
% model of order "order".  The function returns the RMSE for each
% temperature-CRTF and saves the model coefficients
format long

%% Column labels for the test chamber data files
srcHdr={'id','yyyy','jd','hhmm','Tref1','Tref2','Tref3','xE1','xE2','xE3','xE4','xS1','xS2','xW1','xW2','xW3','xW4',... % 17
   'xN1','xN2','xR1S','xR3S','xR1','xR3','xF1','xF2','xF3','xF4','xF5','x','x','x','x',... % 32
   'E1','E2','E3','E4','S1','S2','R4','R5','R6','F3','F5','F6','CS1','CS2','CS3','S1S','S2S',... % 49
   'E2S','E4S','R4S','R5S','R6S','F3S','F5S','F6S','W1','W2','W3','W4','N1','N2','R1','R2','R3',... % 66
   'F1','F2','F4','CN1','CN2','CN3','N1S','N2S','W2S','W4S','R1S','R2S','R3S','F1S','F2S','F4S',... % 82
   'PumpPower','LoadPower'}; % 86

%% Column labels for the chiller data files
chsrcHdr={'TIMESTAMP','RECORD','Tclimate_Avg','Tzone_Avg','Tcndair_Avg','dTcndair_Avg','Trhxliq_Avg', ...
   'Trhxsh_Avg','Tchwreturn_Avg','Tchwsupply_Avg','Trsuc2_Avg','Trdis2_Avg','Trexvin2_Avg','Trexvout2_Avg', ...
   'Wsystem_Avg','RunGPM_Avg','dutycycle_Avg','massflow_Avg'};

%% file names for all the training data sets.  Two files are required for
% each training data set, one for the data logged from the test chamber
% CR10X and one for the data logged from the LLCS chiller CR1000
 fnameschamber = {'FAN HI
OneMinuteChamberData.dat','AtlantaRadiantChamberData.dat','PhoenixRadiantChamberData.dat'};
 fnameschiller = {'FAN HI
OneMinuteChillerData.dat','AtlantaRadiantChillerData.dat','PhoenixRadiantChillerData.dat'};

%% Initialize regression data matrices
AZAT = [];
bZAT = [];
AMRT = [];
bMRT = [];
AUST = [];
bUST = [];
ARWT = [];
bRWT = [];
AOPT = [];
bOPT = [];
```

```
%% loop through all of the training data sets
for k=1:length(fnameschamber)
   fnamechamber = char(fnameschamber(k));
   fnamechiller = char(fnameschiller(k));
   % load the data-logger csv files
   [QC Psys RWT OAT2 ZAT2] = LoadOneMinuteChillerDataIM(fnamechiller);
   [QI AAT ZAT OAT OPT UST MRT Ppump chamtimes FLT] = LoadOneMinuteChamberDataIM(fnamechamber);

   % sampling the data at interval "minutes" with five-minute averaging
   nowmin = 1;
   index = 1;
   Ptot = Ppump+Psys;  % Sum the chiller power and the chilled water pump power
   while(nowmin+minutes<length(OPT))
           % Loads in Watts
           QC30(index) = mean(QC(nowmin:nowmin+minutes-1));
           QI30(index) = mean(QI(nowmin:nowmin+minutes-1));
           % Temperatures in Kelvins
           RWT30(index) = mean(RWT(nowmin:nowmin+minutes-1))+273;
           AAT30(index) = mean(AAT(nowmin:nowmin+4))+273;
           ZAT30(index) = mean(ZAT(nowmin:nowmin+4))+273;
           ZAT230(index) = mean(ZAT2(nowmin:nowmin+4))+273;
           OAT30(index) = mean(OAT(nowmin:nowmin+4))+273;
           OAT230(index) = mean(OAT2(nowmin:nowmin+4))+273;
           OPT30(index) = mean(OPT(nowmin:nowmin+4))+273;
           UST30(index) = mean(UST(nowmin:nowmin+4))+273;
           FLT30(index) = mean(FLT(nowmin:nowmin+4))+273;
           MRT30(index) = mean(MRT(nowmin:nowmin+4))+273;
           % Energy in Watt-hours
           Ptot30(index) = mean(Ptot(nowmin:nowmin+minutes-1))*(60/minutes);
           % Power in Watts
           Ppump30(index) = mean(Ppump(nowmin:nowmin+minutes-1));
           nowmin = nowmin+minutes;
           index = index+1;
   end

%% create regression data matrices from all of the training data sets
   startindex = 1;
   endindex = startindex+order;
   while(endindex<=length(ZAT30))
        AZAT = [AZAT; [ZAT30(startindex:endindex-1) AAT30(startindex:endindex) OAT30(startindex:endindex)
QC30(startindex:endindex) QI30(startindex:endindex)]];
        bZAT = [bZAT; ZAT30(endindex)];
        AMRT = [AMRT; [MRT30(startindex:endindex-1) AAT30(startindex:endindex) OAT30(startindex:endindex)
QC30(startindex:endindex) QI30(startindex:endindex)]];
        bMRT = [bMRT; MRT30(endindex)];
        AOPT = [AOPT; [OPT30(startindex:endindex-1) AAT30(startindex:endindex) OAT30(startindex:endindex)
QC30(startindex:endindex) QI30(startindex:endindex)]];
        bOPT = [bOPT; OPT30(endindex)];
        AUST = [AUST; [UST30(startindex:endindex-1) AAT30(startindex:endindex) OAT30(startindex:endindex)
QC30(startindex:endindex) QI30(startindex:endindex)]];
        bUST = [bUST; UST30(endindex)];
        if(Ppump30(endindex)>1)  % Identify a 2nd order model for RWT ONLY when the pump is on
          ARWT = [ARWT; [RWT30(endindex-2:endindex-1) UST30(endindex-2:endindex) QC30(endindex-
2:endindex)]];
```

```
            bRWT = [bRWT; RWT30(endindex)];
        end
        startindex = startindex+1; endindex = endindex+1;
    end
    % steady-state heat transfer constraints on temperature-CRTFs
    AeqOPT = [ones(1,order) ones(1,order+1) ones(1,order+1) zeros(1,order+1) zeros(1,order+1)];
    beqOPT = 1;
    AeqRWT = [ones(1,2) ones(1,3) zeros(1,3)];
    beqRWT = 1;

    % computer temperature-CRTF model coefficients
    cZAT = lsqlin(AZAT,bZAT,[],[],AeqOPT,beqOPT);
    cMRT = lsqlin(AMRT,bMRT,[],[],AeqOPT,beqOPT);
    cOPT = lsqlin(AOPT,bOPT,[],[],AeqOPT,beqOPT);
    cUST = lsqlin(AUST,bUST,[],[],AeqOPT,beqOPT);
    cRWT = lsqlin(ARWT,bRWT,[],[],AeqRWT,beqRWT);

    % computer temperature-CRTF RMSEs
    ZATrmse = mean((bZAT-AZAT*cZAT).^2).^0.5;
    MRTrmse = mean((bMRT-AMRT*cMRT).^2).^0.5;
    OPTrmse = mean((bOPT-AOPT*cOPT).^2).^0.5;
    USTrmse = mean((bUST-AUST*cUST).^2).^0.5;
    RWTrmse = mean((bRWT-ARWT*cRWT).^2).^0.5;
end

save thermalmodels cZAT cMRT cUST cRWT cOPT
```

The code below validates temperature-CRTF models from data logged by the Test Chamber CR10X and the LLCS CR1000 data loggers. Like the training data, validation data files come in pairs, one for the chamber and one for the LLCS system, described in Appendix C. An arbitrary number of validation data sets can be added to the list of validation data file names listed under the variables fnameschamber and fnameschiller, so long as they are in pairs and the data has been fixed to account for skipped records by each logger. The validate code will compute the root mean square error, in Kelvin, for predictions of zone air temperature (ZAT), mean radiant temperature (MRT), operative temperature (OPT), under-slab temperature (UST), and return water temperature (RWT) up to the number of look-ahead-hours selected by the input “lookaheadhours”.

```
function [ZATrmse MRTrmse OPTrmse USTrmse RWTonrmse] = ValidateTCRTF(minutes,order,lookaheadhours)
%% function ValidateTCRTF computes the RMSE of the temperature-CRTF models
% applied to one validation data set (not used in training) for
% temperature-CRTF models with sampling intervals of "minutes" minutes and
% of order "order".  The RMSE is computed for the a look-ahead predictive
% horizon that is "lookaheadhours" hours ahead.  The RMSE of the models
% relative to the validation data is computed and stored

format long
% load the temperature-CRTF model coefficients
load thermalmodels

%% Column labels for the test chamber data files
srcHdr={'id','yyyy','jd','hhmm','Tref1','Tref2','Tref3','xE1','xE2','xE3','xE4','xS1','xS2','xW1','xW2','xW3','xW4',... % 17
```

```
    'xN1','xN2','xR1S','xR3S','xR1','xR3','xF1','xF2','xF3','xF4','xF5','x','x','x','x',... % 32
    'E1','E2','E3','E4','S1','S2','R4','R5','R6','F3','F5','F6','CS1','CS2','CS3','S1S','S2S',... % 49
    'E2S','E4S','R4S','R5S','R6S','F3S','F5S','F6S','W1','W2','W3','W4','N1','N2','R1','R2','R3',... % 66
    'F1','F2','F4','CN1','CN2','CN3','N1S','N2S','W2S','W4S','R1S','R2S','R3S','F1S','F2S','F4S',... % 82
    'RCPwr','RFPrBad','RFamps','RFPwr'}; % 86

%% Column labels for the chiller data files
chsrcHdr={'TIMESTAMP','RECORD','Tclimate_Avg','Tzone_Avg','Tcndair_Avg','dTcndair_Avg','Trhxliq_Avg', ...
    'Trhxsh_Avg','Tchwreturn_Avg','Tchwsupply_Avg','Trsuc2_Avg','Trdis2_Avg','Trexvin2_Avg','Trexvout2_Avg', ...
    'Wsystem_Avg','RunGPM_Avg','dutycycle_Avg','massflow_Avg'};


%% file names for all the validation data sets.  Two files are required for
% each validation data set, one for the data logged from the test chamber
% CR10X (chamber) and one for the data logged from the LLCS (chiller) CR1000
fnames = {'VAL2 HI OneMinuteChamberData.dat'};
fnameschiller = {'VAL2 HI OneMinuteChillerData.dat'};

%% loop through chamberdata sets

fnamechamber = char(fnames(1));
fnamechiller = char(fnameschiller(1));
    % load the data-logger csv files
[QC Psys RWT OAT2 ZAT2 chilltimes] = LoadOneMinuteChillerDataIM(fnamechiller);
[QI AAT ZAT OAT OPT UST MRT Ppump chamtimes FLT] = LoadOneMinuteChamberDataIM(fnamechamber);

% sampling the data at interval "minutes" with five-minute averaging
nowmin = 1;
index = 1;
Ptot = Ppump+Psys;
while(nowmin+minutes<length(OPT))
    % Loads in Watts
    QC30(index) = mean(QC(nowmin:nowmin+minutes-1));
    QI30(index) = mean(QI(nowmin:nowmin+minutes-1));
    % Temperatures in Kelvin
    RWT30(index) = mean(RWT(nowmin:nowmin+minutes-1))+273;
    AAT30(index) = mean(AAT(nowmin:nowmin+4))+273;
    ZAT30(index) = mean(ZAT(nowmin:nowmin+4))+273;
    ZAT230(index) = mean(ZAT2(nowmin:nowmin+4))+273;
    OAT30(index) = mean(OAT(nowmin:nowmin+4))+273;
    OAT230(index) = mean(OAT2(nowmin:nowmin+4))+273;
    OPT30(index) = mean(OPT(nowmin:nowmin+4))+273;
    UST30(index) = mean(UST(nowmin:nowmin+4))+273;
    MRT30(index) = mean(MRT(nowmin:nowmin+4))+273;
    %Energy in Watt-hours
    Ptot30(index) = mean(Ptot(nowmin:nowmin+minutes-1))*(60/minutes);
    % Power in Watts
    Ppump30(index) = mean(Ppump(nowmin:nowmin+minutes-1));
    nowmin = nowmin+minutes;
    index = index+1;
end

% move through the entire validation data, for each data set, from the
```

```
% beginning of the data to the end, less the number of
% look-ahead-hours, to predict temperatures "lookaheadhours" hours ahead
% beginning with a segment of data order+1 samples long.  Starting with
% data samples 1 to order+1, predicting out to order+1+lookaheadsteps,
% then with samples 2 order+2, predicting out to
% order+1+lookaheadsteps, etc...
startpoint=1;
endpoint = startpoint+order;
% number of samples ahead to predict for a given sampling interval to
% predict "lookaheadhours" hours ahead
lookaheadsteps = lookaheadhours*(60/minutes);
while(endpoint+lookaheadsteps<length(ZAT30))
   endpoint = startpoint+order;

   % initialize matrices f
   AOPT = [];
   AZAT = [];
   AMRT = [];
   AUST = [];
   ARWT = [];
   RWTpredon=[];
   RWT30ton=[];

   % initialize the data from which the "lookaheadhour"-hour-ahead
   % prediction will be made
   RWTpred = RWT30(startpoint:endpoint-1);
   MRTpred = MRT30(startpoint:endpoint-1);
   OPTpred = OPT30(startpoint:endpoint-1);
   USTpred = UST30(startpoint:endpoint-1);
   ZATpred = ZAT30(startpoint:endpoint-1);
   QC30t = QC30(startpoint:startpoint+order+lookaheadsteps);
   QI30t = QI30(startpoint:startpoint+order+lookaheadsteps);
   RWT30t = RWT30(startpoint:startpoint+order+lookaheadsteps);
   AAT30t = AAT30(startpoint:startpoint+order+lookaheadsteps);
   ZAT30t = ZAT30(startpoint:startpoint+order+lookaheadsteps);
   OAT30t = OAT30(startpoint:startpoint+order+lookaheadsteps);
   OPT30t = OPT30(startpoint:startpoint+order+lookaheadsteps);
   UST30t = UST30(startpoint:startpoint+order+lookaheadsteps);
   MRT30t = MRT30(startpoint:startpoint+order+lookaheadsteps);

   % for the segment of data being used for prediction, predict the
   % temperatures ahead from step 1 to step lookaheadsteps (which is
   % sampling interval and model order dependent)
   startindex = 1;
   endindex = startindex+order;
   pumponindex=1;   % track the time the pump is on independently
   while(endindex<=1+order+lookaheadsteps)  % loop until all "lookaheadsteps" predictions have been made
      AZAT = [ZATpred(startindex:endindex-1) AAT30t(startindex:endindex) OAT30t(startindex:endindex)
QC30t(startindex:endindex) QI30t(startindex:endindex)];
      ZATpred(endindex) = AZAT*cZAT;
      AMRT = [MRTpred(startindex:endindex-1) AAT30t(startindex:endindex) OAT30t(startindex:endindex)
QC30t(startindex:endindex) QI30t(startindex:endindex)];
      MRTpred(endindex) = AMRT*cMRT;
```

```
    AOPT = [OPTpred(startindex:endindex-1) AAT30t(startindex:endindex) OAT30t(startindex:endindex)
QC30t(startindex:endindex) QI30t(startindex:endindex)];
    OPTpred(endindex) = AOPT*cOPT;
    AUST = [USTpred(startindex:endindex-1) AAT30t(startindex:endindex) OAT30t(startindex:endindex)
QC30t(startindex:endindex) QI30t(startindex:endindex)];
    USTpred(endindex) = AUST*cUST;
    if(Ppump30(endindex)>1)  % if the pump is on
      ARWT = [RWT30t(endindex-2:endindex-1) UST30t(endindex-2:endindex) QC30t(endindex-2:endindex)];
      RWTpred(endindex) = ARWT*cRWT;
      RWT30ton(pumponindex) = RWT30t(endindex);   % compile the actual RWT data while the pump is on
      RWTpredon(pumponindex) = RWTpred(endindex); % predict RWT from its transfer function model
      pumponindex = pumponindex+1;
    else
      RWTpred(endindex) = OAT30t(endindex);      % if the pump is off, assume RWT floats to ambient
temperature
    end
    startindex = startindex+1; endindex = endindex+1; % proceed to predict next time step
  end

  % compute the mean square error and relative mean square error for each
  % model for the current set of predictions
  ZATmse(startpoint) = mean((ZAT30t-ZATpred).^2);
  ZATrelmse(startpoint) = mean(((ZAT30t-ZATpred)./(max(ZAT30t)-min(ZAT30t))).^2);
  MRTmse(startpoint) = mean((MRT30t-MRTpred).^2);
  MRTrelmse(startpoint) = mean(((MRT30t-MRTpred)./(max(MRT30t)-min(MRT30t))).^2);
  OPTmse(startpoint) = mean((OPT30t-OPTpred).^2);
  OPTrelmse(startpoint) = mean(((OPT30t-OPTpred)./(max(OPT30t)-min(OPT30t))).^2);
  USTmse(startpoint) = mean((UST30t-USTpred).^2);
  USTrelmse(startpoint) = mean(((UST30t-USTpred)./(max(UST30t)-min(UST30t))).^2);
  if(~isempty(RWTpredon) && ~isempty(RWT30t) )
    RWTonmse(startpoint) = mean((RWT30ton-RWTpredon).^2);
    RWTonrelmse(startpoint) = mean(((RWT30ton-RWTpredon)./(max(RWT30ton)-min(RWT30ton))).^2);
  end
  startpoint= startpoint+1;
  endpoint=endpoint+1;
end
% compute the RMSE and relative RMSE for the entire validation data set,
% for all predictions based on all possible segments of data
ZATrmse = mean(ZATmse).^0.5
ZATrelrmse = mean(ZATrelmse).^0.5
MRTrmse = mean(MRTmse).^0.5
MRTrelrmse = mean(MRTrelmse).^0.5
OPTrmse = mean(OPTmse).^0.5
OPTrelrmse = mean(OPTrelmse).^0.5
USTrmse = mean(USTmse).^0.5
USTrelrmse = mean(USTrelmse).^0.5
RWTonrmse = mean(RWTonmse).^0.5
RWTonrelrmse = mean(RWTonrelmse).^0.5

save ALLRMSES ZATrmse ZATrelrmse MRTrmse MRTrelrmse OPTrmse OPTrelrmse USTrmse USTrelrmse
RWTonrmse RWTonrelrmse
```

B.4 Temperature-CRTF model coefficients

The temperature-CRTF model coefficients shown below are trained from data sampled at thirty minute intervals. An eighth order model in ZAT, MRT, OPT, and UST has been identified. The RWT model is a second order model.

Term	OPT	ZAT	MRT	UST
XXT(t-8)	-1.76E-02	-1.38E-02	-4.73E-02	-5.43E-02
XXT(t-7)	-2.81E-02	-3.96E-02	2.05E-03	1.03E-01
XXT(t-6)	-6.46E-03	-2.68E-02	4.12E-02	-1.17E-01
XXT(t-5)	-1.48E-02	-2.85E-02	-9.21E-02	-1.01E-01
XXT(t-4)	-5.17E-02	-9.04E-02	8.48E-02	2.31E-01
XXT(t-3)	-9.15E-02	3.82E-02	-3.63E-02	-1.23E-01
XXT(t-2)	2.76E-01	4.82E-01	-2.11E-01	1.33E-01
XXT(t-1)	9.26E-01	6.68E-01	1.25E+00	9.18E-01
AAT(t-8)	7.65E-04	8.05E-04	-7.29E-04	1.24E-03
AAT(t-7)	-4.46E-03	-4.03E-03	-3.74E-03	9.69E-03
AAT(t-6)	1.38E-04	3.55E-03	-2.89E-03	-6.16E-03
AAT(t-5)	-3.68E-03	-4.95E-03	-4.59E-03	-7.36E-03
AAT(t-4)	-5.36E-03	-7.84E-03	-5.47E-04	2.84E-03
AAT(t-3)	-1.02E-03	2.03E-03	-1.94E-03	3.88E-03
AAT(t-2)	2.65E-03	2.18E-03	-1.62E-03	2.95E-04
AAT(t-1)	1.18E-02	6.37E-03	1.95E-02	1.78E-03
AAT(t)	3.34E-03	7.02E-03	4.37E-04	-9.06E-04
OAT(t-8)	-1.71E-03	-1.99E-03	-1.15E-03	1.94E-03
OAT(t-7)	-1.93E-04	9.34E-04	-2.93E-03	-9.40E-04
OAT(t-6)	-7.45E-04	-2.93E-03	1.79E-03	5.08E-03
OAT(t-5)	1.45E-05	-3.12E-04	-1.10E-03	-1.20E-03
OAT(t-4)	-3.64E-03	-6.29E-03	-2.19E-03	-2.53E-03
OAT(t-3)	-8.15E-03	-1.14E-02	-2.44E-03	8.80E-03
OAT(t-2)	-2.39E-03	3.64E-03	-6.05E-03	-6.78E-03
OAT(t-1)	1.58E-03	4.18E-03	8.28E-04	-1.71E-02
OAT(t)	1.99E-02	1.99E-02	1.74E-02	1.78E-02
QC(t-8)	6.60E-07	-7.70E-07	2.77E-06	-5.47E-05
QC(t-7)	2.63E-06	5.63E-06	-5.19E-07	4.66E-05
QC(t-6)	2.85E-08	2.08E-06	1.10E-05	1.73E-05
QC(t-5)	2.14E-05	3.32E-05	3.13E-06	-2.19E-04
QC(t-4)	8.15E-06	1.80E-06	1.63E-05	1.16E-05
QC(t-3)	2.77E-05	3.24E-05	3.28E-05	-1.27E-04
QC(t-2)	-3.60E-05	-2.82E-05	-4.23E-05	-3.32E-04
QC(t-1)	1.14E-04	1.35E-04	9.67E-05	8.60E-04

Term	RWT
RWT(t-2)	-1.06E-01
RWT(t-1)	4.31E-01
UST(t-2)	2.14E+00
UST(t-1)	-6.24E+00
UST(t)	4.77E+00
QC(t-2)	1.83E-03
QC(t-1)	-2.39E-03
QC(t)	5.85E-03

OPT = Operative temperature (C)

ZAT = Zone air temperature (C)

MRT = Mean radiant temperature (C)

UST = Under-slab temperature (C)

RWT = Return water temperature (C)

t = current time t

t-k = time at previous time step t-k

XXT = OPT, ZAT, MRT or UST for each model

Term	OPT	ZAT	MRT	UST
QC(t)	-1.08E-06	1.03E-06	-2.66E-06	6.90E-05
QI(t-8)	7.90E-05	1.28E-04	1.05E-05	-1.62E-05
QI(t-7)	-2.46E-06	1.58E-05	-1.66E-05	-2.62E-05
QI(t-6)	-1.35E-04	-1.03E-04	-1.04E-04	-4.12E-05
QI(t-5)	7.77E-05	1.89E-04	-9.75E-06	1.41E-04
QI(t-4)	-8.99E-05	-2.50E-04	-1.71E-04	9.44E-05
QI(t-3)	-5.46E-04	-1.15E-03	-4.76E-05	-1.22E-04
QI(t-2)	-9.88E-04	-1.19E-03	-6.21E-04	1.44E-04
QI(t-1)	1.47E-03	2.03E-03	1.08E-03	3.97E-04
QI(t)	2.72E-04	5.34E-04	-1.11E-06	-4.04E-04

Appendix C. LLCS system testing

C.1 LLCS and SSAC components

Component	Description	Make/Model
Chiller/AC outdoor unit	This component contains the compressor, condenser fan, condenser heat exchanger, inverters and electronics supplying both the SSAC and the LLCS	Mitsubishi MUZ-A09NA-1
AC indoor unit	This is the air-heated evaporator used for the SSAC, containing the finned-tube evaporator heat exchanger and the evaporator fan	Mitsubishi MSZ-A09NA
Brazed plate heat exchanger	The BPHX is a counter-flow heat exchanger between R410A and the chilled water	Flatplate GB240-H10
Chilled water pump	The chilled water pump is installed on the supply side to the radiant floor	Laing D5 strong w/PWM P/N: P311
Radiant subfloor	The radiant subfloor, made by Warmboard, is a 5/8” plywood subfloor, topped by 0.03” aluminum, with 1/2" grooves at 12” spacing for PEX pipe installation	Warmboard
Chilled water pipe and fittings	The chilled water piping is constructed of PEX pipe embedded in the grooves of the Warmboard radiant subfloor.	Uponor 1/2” hePex with ProPex fittings
Radiant manifold	6-loop engineered plastic (EP) radiant manifold with flow meters.	Uponor PEXsupply SKU: A2670601

C.2 LLCS sensors and instrumentation

Table of sensors, make and model

Label	Sensor description	Sensor Make/Model	Installation notes	Accuracy
T_s	Suction refrigerant temperature	Omega/PR-T-24-SLE	Insulated pipe surface measurement	0.5 C (rated)
T_d	Discharge refrigerant temperature	Omega/PR-T-24-SLE	Insulated pipe surface measurement	0.5 C (rated)
T_{cnd}	Refrigerant condensing temperature	Omega/PR-T-24-SLE	Insulated pipe surface measurement	0.5 C (rated)
$T_{cnd,liq}$	Condenser outlet liquid refrigerant temperature	Omega/PR-T-24-SLE	Insulated pipe surface measurement	0.5 C (rated)
T_{xvi}	Expansion valve inlet refrigerant temperature	Omega/PR-T-24-SLE	Insulated pipe surface measurement	0.5 C (rated)
T_{xvo}	Expansion valve outlet refrigerant temperature	Omega/PR-T-24-SLE	Insulated pipe surface measurement	0.5 C (rated)
T_{hxi}	Brazed plate heat exchanger inlet refrigerant temperature	Omega/PR-T-24-SLE	Insulated pipe surface measurement	0.5 C (rated)
T_{hxo}	Brazed plate heat exchanger outlet refrigerant temperature	Omega/PR-T-24-SLE	Insulated pipe surface measurement	0.5 C (rated)
$T_{cnd,air,in}$	Condenser inlet air temperature	Omega/PR-T-24-SLE	Installed in condense rair inlet stream	0.5 C (rated)
T_{evp}	Refrigerant evaporating temperature	Omega/PR-T-24-SLE	Insulated pipe surface measurement	0.5 C (rated)
$\Delta T_{cnd,air}$	Condenser air temperature difference	Omega/PR-T-24-SLE 16 junction thermopile	A 16 junction thermopile	0.5 C (rated)
P_s	Suction refrigerant pressure	MEAS, INC MSP-300-500-P2-N1	Installed in the suction service port	1% of span
P_d	Discharge refrigerant pressure	MEAS, INC MSP-300-1000-P2-N1	Installed in the discharge service port	1% of span
P_{xvi}	Expansion valve inlet refrigerant pressure	MEAS, INC MSP-300-1000-P2-N1	Installed in the liquid line	1% of span

P_{xvo}	Expansion valve outlet refrigerant pressure	MEAS, INC MSP-300-500-P2-N1	Installed after the stop valve downstream of the expansion valve	1% of span
$\dot{m}_{ref}$	Refrigerant mass flowrate	Micromotion Meter: CMFS015M323N2BAEZZZ Transmitter: 2500D3ABBAEZZZ	A Micromotion Coriolis mass flow meter was installed in the liquid line, with roughly 5 feet of head.	0.05% of rate
W_{unit}	Total power to the outdoor unit, including inverters, condenser fan and compressor	Wattnode WNB-3D-240-P	Installed on the 208VAC power supply to the outdoor unit	0.5% of reading
$W_{3\varnothing,cmp}$	Three phase power from the inverter to the compressor	Yokogawa WT230	Installed between the compressor inverter and the compressor	0.1% of reading
RWT	Chilled water return temperature	Omega TMTSS-062G-6	Installed in the chilled water return pipe immediately exiting the chamber	0.5 C (rated)
SWT	Chilled water supply temperature	Omega TMTSS-062G-6	Installed in the chilled water supply pipe just before entering the chamber	0.5 C (rated)
$\forall$	Chilled water volumetric flowrate	Omega FTB8007B	Installed in the chilled water return line	1.5 % of reading
W_{QI}	Total power to the internal loads	Wattnode WNB-3Y-208-P	Installed on a power strip, to which all internal loads were connected	0.5% of reading
W_p	Total power to the chilled water pump	Wattnode WNB-3Y-208-P	Installed on the 120VAC power supplied to the chilled water pump power supply	0.5% of reading

The data measured from the LLCS test system was logged using a Campbell Scientific CR1000 data logger, with a slave Campbell Scientific AM25T 25-channel multiplexer for thermocouple measurements. The control code for the CR1000 data logger is shown below, and includes the control code for operating the internal loads and turning on the chilled water pump any time the chiller is in operation.

```
'CR1000 LLCS data logging, load control, and pump switching

'Declare Variables and Units
Public BattV
Public Pxvout, Pxvin, Pdis, Psuc 'Pressure measurements
''Trsuc-1, Trdis-2, Trxvin-3, Trxvout-4, Tcndliq-5, Tcnd-6, Tcndmix-7, Trevp-8, Trhxsh-9, Trhxliq-10
'Public Ref_Temps(10)
Public Trsuc, Trdis, Trxvin, Trxvout, Trcndliq, Trcnd, Trcndmix, Trevp, Trhxsh, Trhxliq, Trsuc2, Trdis2, Trexvin2, Trexvout2, Tsh
Public dTcndair 'channel 11
```

```
Public Tclimate, Tcndair, Tzone
Public Tchwreturn, Tchwsupply, Qcool
'Tclimate-12, Tcndair-13, Tzone-14
'Public Air_Temps(3)
Public RTemp_C
Public massflow, density
Public Wloads, Wsystem, Wpump, WsysAVG
Public FanSpd, CmpSpd
Public delta_mV, TdTref, dTresult, mV_TdT, i
Public Source(16)
Public DateArray(9)
Public dutycycle, Period, GPM, RunGPM, dutycycleprev
Public VaisT, RH, DT, a, b, gamma, DTplus2, ACYoko, BCYoko, Tot3ph

Units BattV=Volts

'Define Data Tables
DataTable(Table1,True,-1)
  DataInterval (0,0,Sec,10)
  Minimum (1,BattV,FP2,0,0)
  Sample(1,Tclimate,FP2)
  Sample(1,Tzone,FP2)
  Sample(1,Tcndair,FP2)
  Sample(1,dTcndair,FP2)
  Sample(1,Trsuc,FP2)
  Sample(1,Trdis,FP2)
  Sample(1,Trxvin,FP2)
  Sample(1,Trxvout,FP2)
  Sample(1,Trcnd,FP2)
  Sample(1,Trcndmix,FP2)
  Sample(1,Trcndliq,FP2)
  Sample(1,Trevp,FP2)
  Sample(1,Trhxliq,FP2)
  Sample(1,Trhxsh,FP2)
  Sample(1,Tchwreturn,FP2)
  Sample(1,Tchwsupply,FP2)
  Sample(1,Trsuc2,FP2)
  Sample(1,Trdis2,FP2)
  Sample(1,Trexvin2,FP2)
  Sample(1,Trexvout2,FP2)
  Sample(1,Psuc,FP2)
  Sample(1,Pdis,FP2)
  Sample(1,Pxvin,FP2)
  Sample(1,Pxvout,FP2)
  Sample(1,Wloads,FP2)
  Sample(1,Wsystem,FP2)
  Sample(1,FanSpd,FP2)
  Sample(1,CmpSpd,FP2)
  Sample(1,GPM,FP2)
  Sample(1,RunGPM,FP2)
  Sample(1,dutycycle,FP2)
  Sample(1,Tsh,FP2)
  Sample(1,massflow,FP2)
```

```
  Sample(1,density,FP2)
  Sample(1,VaisT,FP2)
  Sample(1,RH,FP2)
  Sample(1,Qcool,FP2)
EndTable

DataTable(Table2,True,-1)
  DataInterval (0,1,Min,10)
  Average(1,Tclimate,FP2,False)
  Average(1,Tzone,FP2,False)
  Average(1,Tcndair,FP2,False)
  Average(1,dTcndair,FP2,False)
  Average(1,Trhxliq,FP2,False)
  Average(1,Trhxsh,FP2,False)
  Average(1,Tchwreturn,FP2,False)
  Average(1,Tchwsupply,FP2,False)
  Average(1,Trsuc2,FP2,False)
  Average(1,Trdis2,FP2,False)
  Average(1,Trexvin2,FP2,False)
  Average(1,Trexvout2,FP2,False)
  Average(1,Wsystem,FP2,False)
  Average(1,RunGPM,FP2,False)
  Average(1,dutycycle,FP2,False)
  Average(1,massflow,FP2,False)
  Average(1,RH,FP2,False)
  Average(1,Qcool,FP2,False)
  Average(1,ACYoko,FP2,False)
  Average(1,BCYoko,FP2,False)
EndTable

'Main Program
BeginProg
  Scan(1,Sec,1,0)
    'Default Datalogger Battery Voltage measurement BattV
    Battery(BattV)
    'Reference Temperature measurement RTemp_C on the AM25T Multiplexer:
    AM25T(RTemp_C,0,mV2_5C,1,1,TypeT,RTemp_C,7,8,Vx2,True,0,250,1,0)

    'Temperature Measurements
    AM25T (Trsuc,1,mV2_5C,1,8,TypeT,RTemp_C,7,8,Vx2,True ,0,250,1.0,0)
    AM25T (Trdis,1,mV2_5C,2,8,TypeT,RTemp_C,7,8,Vx2,True ,0,250,1.0,0)
    AM25T (Trxvin,1,mV2_5C,3,8,TypeT,RTemp_C,7,8,Vx2,True ,0,250,1.0,0)
    AM25T (Trxvout,1,mV2_5C,4,8,TypeT,RTemp_C,7,8,Vx2,True ,0,250,1.0,0)
    AM25T (Trcndliq,1,mV2_5C,5,8,TypeT,RTemp_C,7,8,Vx2,True ,0,250,1.0,0)
    AM25T (Trcnd,1,mV2_5C,6,8,TypeT,RTemp_C,7,8,Vx2,True ,0,250,1.0,0)
    AM25T (Trcndmix,1,mV2_5C,7,8,TypeT,RTemp_C,7,8,Vx2,True ,0,250,1.0,0)
    AM25T (Trevp,1,mV2_5C,8,8,TypeT,RTemp_C,7,8,Vx2,True ,0,250,1.0,0)
    AM25T (Trhxsh,1,mV2_5C,9,8,TypeT,RTemp_C,7,8,Vx2,True ,0,250,1.0,0)
    AM25T (Trhxliq,1,mV2_5C,10,8,TypeT,RTemp_C,7,8,Vx2,True ,0,250,1.0,0)
    AM25T (Tclimate,1,mV2_5C,12,8,TypeT,RTemp_C,7,8,Vx2,True ,0,250,1.0,0)
    AM25T (Tcndair,1,mV2_5C,13,8,TypeT,RTemp_C,7,8,Vx2,True ,0,250,1.0,0)
    AM25T (Tzone,1,mV2_5C,14,8,TypeT,RTemp_C,7,8,Vx2,True ,0,250,1.0,0)
    AM25T (Tchwreturn,1,mV2_5C,15,8,TypeT,RTemp_C,7,8,Vx2,True ,0,250,1.0,0)
```

```
AM25T (Tchwsupply,1,mV2_5C,16,8,TypeT,RTemp_C,7,8,Vx2,True ,0,250,1.0,0)
AM25T (Trsuc2,1,mV2_5C,17,8,TypeT,RTemp_C,7,8,Vx2,True ,0,250,1.0,0)
AM25T (Trdis2,1,mV2_5C,18,8,TypeT,RTemp_C,7,8,Vx2,True ,0,250,1.0,0)
AM25T (Trexvin2,1,mV2_5C,19,8,TypeT,RTemp_C,7,8,Vx2,True ,0,250,1.0,0)
AM25T (Trexvout2,1,mV2_5C,20,8,TypeT,RTemp_C,7,8,Vx2,True ,0,250,1.0,0)
Tsh = Trhxsh-Trhxliq

'thermopile measurement
AM25T (delta_mV,1,mV25C,11,8,-1,RTemp_C,7,8,Vx2,True ,0,250,1.0,0)
delta_mV = delta_mV/16
TdTref = Tcndair
delta_mV = delta_mV*0.1
TdTref = TdTref*0.01
mV_TdT = delta_mV*TdTref*0.001
dTresult = 25.89-7.447*delta_mV+4.654*delta_mV^2-2.188*delta_mV^3
dTresult = dTresult-5.749*TdTref+1.635*TdTref-0.4475*TdTref
dTresult = dTresult+mV_TdT*5.557-2.107*mV_TdT*TdTref-3.793*mV_TdT*delta_mV
delta_mV = delta_mV*10
dTcndair = dTresult*delta_mV
TdTref = TdTref*100
' end of scaling for thermopile measurement

'Pressure measurements
VoltDiff (Psuc,1,mV250,1,True ,0,250,5,0)
VoltDiff (Pdis,1,mv5000,2,True ,0,250,0.25,-125)
VoltDiff (Pxvin,1,mv5000,3,True ,0,250,0.25,-125)
VoltDiff (Pxvout,1,mv5000,4,True ,0,250,0.125,-62.5)

' Mass flowrate measurement, R = 240.5, 4-20 mA, 0-100 kg/hr
VoltDiff (massflow,1,mV5000,6,True ,0,250,0.025987,-25)
' Density measurement, R = 240.4, 4-20 mA, 0-68 lbs/ft3
VoltDiff (density,1,mV5000,7,True ,0,250,0.0176788,-17)

'Pulse measurements, system power consumption and water flowrate
PulseCount (Wsystem,1,1,0,1,6,0) '0.6 W/Hz-CTamp = 6 W/Hz
PulseCount(GPM,1,2,0,0,6,0)
AvgRun (WsysAVG,1,Wsystem,4)

‘Vaisala sensor temperature and humidity measurements
AM25T (VaisT,1,mV2500,22,8,-1,RTemp_C,7 ,8 ,Vx2,True ,0,250,0.1,-40)
AM25T (RH,1,mV2500,21,8,-1,RTemp_C,7 ,8 ,Vx2,True ,0,250,0.1,0)

‘Dewpoint temperature calculation
a = 17.271
b = 237.7
gamma = ((a*VaisT)/(b+VaisT))+LN(RH/100)
DT = (b*gamma)/(a-gamma)

‘Yokogawa digital power meter measurements
AM25T (ACYoko,1,mV2500,23,8,-1,RTemp_C,7 ,8 ,Vx2,True ,0,250,0.6,0)
AM25T (BCYoko,1,mV2500,24,8,-1,RTemp_C,7 ,8 ,Vx2,True ,0,250,0.6,0)
Tot3ph = ACYoko+BCYoko
```

```
 dutycycleprev = dutycycle
 dutycycle = 0

‘initialize flow measurement when the system turns on
 If WsysAVG < 6 Then
   RunGPM = 0
 EndIf
 PWM (dutycycle,5,10000,uSec)
 AvgRun (RunGPM,1,GPM,60)

  ‘Calculate instantaneous cooling rate
 Qcool = RunGPM*((0.00378541/60)*1000)*4181.3*(Tchwsupply-Tchwreturn)

‘SDM-AC16 multiplexer control
 For i=1 To 16
   Source(i)=0
Next
 'Turn internal loads on and off at 8 am, 9 am, 5pm and 6pm
 RealTime(DateArray)
 If DateArray(8)>1 AND DateArray(8)<7 Then
   If DateArray(4) < 14 Then
     Source(1) = 0
     Source(3) = 0
     Source(5) = 0
     Source(9) = 0
     Source(11) = 0
   ElseIf DateArray(4) < 15 Then
     Source(1) = 1
     Source(3) = 0
     Source(5) = 1
     Source(9) = 1
     Source(11) = 1
   ElseIf DateArray(4) < 23 Then
     Source(1) = 1
     Source(3) = 1
     Source(5) = 1
     Source(9) = 1
     Source(11) = 1
   ElseIf DateArray(4) < 24 Then
     Source(1) = 1
     Source(3) = 0
     Source(5) = 1
     Source(9) = 1
     Source(11) = 1
   Else
     Source(1) = 0
     Source(3) = 0
     Source(5) = 0
     Source(9) = 0
     Source(11) = 0
   EndIf
 Else
   Source(1) = 0
```

```
    Source(3) = 0
    Source(5) = 0
    Source(9) = 0
    Source(11) = 0
   EndIf
    'Turn chilled water pump on any time the chiller is on
    If WsysAVG < 10 Then
      Source(7) = 0
    Else
      Source(7) = 1
    EndIf
   SDMCD16AC (Source,1,0)
   CallTable(Table1)
   CallTable(Table2)
  NextScan
EndProg
```

C.3 LLCS control codes

The Matlab codes listed below are the key control codes for implementing predictive control. This include supervisory control codes including the master control code, a code to process measured data, a pattern search optimization, and the optimization objective function. It also includes local control codes to automate chiller operation for one hour and implement PID control over the expansion valve based on evaporator superheat.

Master control code: LowLiftPredictiveControl()

```
function LowLiftPredictiveControl ()
nowtime = clock; lastchangehour = nowtime(4)-1; % initialize control hour
x0 = [15.*ones(1,24)]; % initialize compressor speeds, speeds < 19 = 0.

load speedhistory
if(~exist('speeds'))
      speeds = [];
      save speedhistory speeds
end

while(true) % run continously
   nowtime = clock;
   if(nowtime(4)~=lastchangehour) % execute new optimization if the hour has changed
      try
         StopCompressor;  pause(4); TurnOffFan; % stop the compressor and condenser fan
         PreparePredictionData (); % prepare data for prediction using temperature-CRTFs
         [X,FVAL,EXITFLAG,OUTPUT] =  PreCoolingOptimization(x0); % Perform pattern search optimization
         x0 = [X(2:end) 15]; % Use optimization outputs as the input at the next hour
         [f power] = PlotFutureTemperatures(X); % return the optimal fan speed and plot temperatures
         compstp = X(1);
         if(compstp<19) fanstp=0; compstp=0; else  fanstp = f; end  % compressor speeds<19 = 0
         load speedhistory
         speeds = [speeds; nowtime compstp fanstp]; % maintain record of speeds
         save speedhistory speeds
         AutomateHour(compstp,fanstp,[]); % operate compressor at compstp and fanstp for one hour
         lastchangehour = nowtime(4);
      catch  % stop the compressor if the controller fails
         cd('C:\Program Files\MATLAB\Precooling')
         StopCompressor; err = lasterror;
         SendNickEmail('System is off, failure in loop',err.message)
      end
   end
end
```

Data processing: PreparePredictionData()

```
function PreparePredictionData()
[chamhourmin QI30 AAT30 ZAT30 OAT30 OPT30 UST30 MRT30 Ppump30] = PrepareOneMinuteChamberData ();
[chillhourmin QC30 Psys30 RWT30] = PrepareOneMinuteChillerData ();
OATfuture = PredictOATTemperature();
QIfuture = PredictQI();
[OPTmin )_Tmax] = PredictOPTmaxmin();
QI30 = [QI30; QIfuture]; OAT30 = [OAT30; OATfuture]; OPTmax = [40.*ones(order,1); OPTmax];
OPTmin = [10.*ones(order,1); OPTmin]; AAT30 = [AAT30; AAT30(end).*ones(48,1)];
```

```
save predictiondata QI30 QC30 OAT30 OPTmax OPTmin OpT30 RWT30 AAT30 UST30 MRT30 ZAT30
```

Pattern Search: PreCoolingOptimization()

```
function [x,fval,exitflag,output] = PrecoolingOptimization(x0)

% Define lower and upper bounds, speeds <19 = 0, speeds above 50 cause freezing
lb = [  15 15 15 15 15 15 15 15 15 15 15 15 15 15 15 15 15 15 15 15 15 15 15 15 ];
ub = [  50 50 50 50 50 50 50 50 50 50 50 50 50 50 50 50 50 50 50 50 50 50 50 50 ];
 options = psoptimset;
% Modify options setting
options = psoptimset(options,'TolMesh', 0.5); % Stop when grid is less than 0.5
options = psoptimset(options,'TolX', 1);
options = psoptimset(options,'InitialMeshSize', 4); % Initial grid size = 4
options = psoptimset(options,'TimeLimit' ,300);
options = psoptimset(options,'ScaleMesh', 'off');
options = psoptimset(options,'MaxMeshSize', 4);
options = psoptimset(options,'CompletePoll', 'on');
options = psoptimset(options,'SearchMethod', @GPSPositiveBasis2N); % pattern search algorithm
options = psoptimset(options,'CompleteSearch', 'on');
options = psoptimset(options,'Display', 'off');
options = psoptimset(options,'OutputFcns', { [] });
[x,fval,exitflag,output] = patternsearch(@PredictFutureTemperatureAndPower,x0,[],[],[],[],lb,ub,[],options);
```

Objective Function: PredictFutureTemperatureAndPower(X)

```
function J = PredictFutureTemperatureAndPower(X)

% convert 24 compressor speed guesses to 48, one for each half hour, to sync with half hour sampling
factor = (48)/length(X(1,:));
for m=1:length(X) w(factor*(m-1)+1:factor*m) = X(m); end

%%  load pre-identified models for the chiller performance and room thermal response
load thermalmodels
load predictiondata
minutes = 30; order = 8; J=0; Jstage = zeros(size(w)); f = zeros(size(w));

for i=1:length(w)
   startindex = i;
   currentindex = startindex+order-1;
   currenthour = i/(60/minutes);
  % if the compressor is on, calculate the chiller power and cooling rate
   if(w(i)>=19 && w(i)<95)
      cd ChillerModel
     % initial EVT guess, EVT depends on QC and QC depends on EVT
      if(RWT30(currentindex)==OAT30(currentindex))  % if the compressor has been off, no info about RWT
         evaptempguess = max(-1,FUT30(currentindex)-10-(3.5+0.15*(w(i)-19))); % assume the
      else
         evaptempguess = max(-1,RWT30(currentindex)-(2+0.15*(w(i)-19)));
      end
     evaptempold=100;

    % iterate EVT and QC until EVT converges for a given QC
      while(abs(evaptempguess-evaptempold)>0.5)
```

```
            fguess(i) = FanMinEirFour(evaptempguess,OAT30(currentindex+1),w(i));
            QCguess = -0.77*CalculateQFour(evaptempguess,OAT30(currentindex+1),w(i),fguess(i));;
AZAT = [ZAT30(startindex:currentindex)'+273 AAT30(startindex:currentindex+1)'+273
…OAT30(startindex:currentindex+1)'+273 [QC30(startindex:currentindex); QCguess]'
…QI30(startindex:currentindex+1)'];
            ZAT30(currentindex+1) = AZAT*cZAT-273;
 AFUT = [FUT30(startindex:currentindex)'+273 AAT30(startindex:currentindex+1)'+273
…OAT30(startindex:currentindex+1)'+273 [QC30(startindex:currentindex); QCguess]'
…QI30(startindex:currentindex+1)'];
            FUT30(currentindex+1) = AFUT*cFUT-273;
ARWT = [RWT30(currentindex-1:currentindex)'+273 FUT30(currentindex-1:currentindex+1)'+273
[QC30(currentindex-1:currentindex); QCguess]'];
            RWT30(currentindex+1) = ARWT*cRWT-273;

            evaptemp = RWT30(currentindex+1)-(3.5+0.15*(w(i)-19));
            evaptempold = evaptempguess;
            evaptempguess = evaptemp;
        end
% if EVT is infeasible and has not converged, make it negative which will be heavily penalized
      evaptemp = max(evaptemp,-1);  if(isnan(evaptemp)) evaptemp = -1; end

% Compute optimal fan speed, chiller cooling rate and chiller power
      f(i) =FanMinEirFour(evaptemp,OAT30(currentindex+1),w(i));
      qchiller(i) = -0.77*CalculateQFour(evaptemp,OAT30(currentindex+1),w(i),f(i));
      pchiller(i) = (0.89*CalculatePFour(evaptemp,OAT30(currentindex+1),w(i),f(i))+19);
      cd ..
   else % if the compressor speed is out of range, chiller is off
      qchiller(i) = 0;
      pchiller(i) = 0;
   end

% Compute temperatures at next time step
QC30(currentindex+1) = qchiller(i);
AZAT = [ZAT30(startindex:currentindex)'+273 AAT30(startindex:currentindex+1)'+273
…OAT30(startindex:currentindex+1)'+273 QC30(startindex:currentindex+1)' QI30(startindex:currentindex+1)'];
ZAT30(currentindex+1) = AZAT*cZAT-273;
AMRT = [MRT30(startindex:currentindex)'+273 AAT30(startindex:currentindex+1)'+273
…OAT30(startindex:currentindex+1)'+273 QC30(startindex:currentindex+1)' QI30(startindex:currentindex+1)'];
 MRT30(currentindex+1) = AMRT*cMRT-273;
AOpT = [OpT30(startindex:currentindex)'+273 AAT30(startindex:currentindex+1)'+273
…OAT30(startindex:currentindex+1)'+273 QC30(startindex:currentindex+1)' QI30(startindex:currentindex+1)'];
OpT30(currentindex+1) = AOpT*cOpT-273;
AFUT = [FUT30(startindex:currentindex)'+273 AAT30(startindex:currentindex+1)'+273
….OAT30(startindex:currentindex+1)'+273 QC30(startindex:currentindex+1)' QI30(startindex:currentindex+1)'];
FUT30(currentindex+1) = AFUT*cFUT-273;
ARWT = [RWT30(currentindex-1:currentindex)'+273 FUT30(currentindex-1:currentindex+1)'+273
QC30(currentindex-1:currentindex+1)'];
   if(w(i)>=19 && w(i)<95)
      RWT30(currentindex+1) = ARWT*cRWT-273;
   else
      RWT30(currentindex+1) = OAT30(currentindex+1);
   end
```

```
   J=J+pchiller(i)*(minutes/60);  % penalize chiller energy consumption


   if(OpT30(currentindex+1)<(OPTmin(currentindex+1)+0.5)) % penalize for being too cold
      J = (((OPTmin(currentindex+1)+0.5)-OpT30(currentindex+1)).^2)*150+J;
   elseif(OpT30(currentindex+1)>OPTmax(currentindex+1)-0.5)  % penalize for being too hot
      J = ((OpT30(currentindex+1)-(OPTmax(currentindex+1)-0.5)).^2)*150+J;
   end

   if(w(i)>=19 && evaptemp<1.0) % penalize low refrigerant temperature
      J = (1.0-evaptemp)*10000+J;
   end
end
```

Compressor automation: AutomateHour()

```
function AutomateHour(compstp,fanstp,levstart)

timehourstarted = clock; nowtime = timehourstarted; % initialize hour clock
try
%% open com port to Mr Slim controller
delete(instrfind); s = serial('COM8'); s.Terminator = []; s.StopBits = 2; fopen(s)

%% initialize control variables
fan = 0;  % start with the fan off
compressor = 0; % start with the compressor off
safetorun = true; % assume it is safe to run when started
sloweddown = false; % the compressor has not been slowed down at start
pumpon = false; % assume pump is off
newcompressorspeed = true; % the program should change the compressor speed
timesloweddown = clock-400; % initialize time stamp for slow down control
timestopped = timesloweddown;
save chillercontrolpoints compressor fan safetorun sloweddown pumpon compstp newcompressorspeed
timesloweddown timestopped -append

%% loop continuosly for an hour
while(nowtime(4)==timehourstarted(4))
   tic  % match loop run time to sampling time of data loggers, 2 second intervals
   if(compstp==0 && fan~=0) % turn the fan on if the compressor is set to be on
      fan = 0;
      ChangeFanSpeed(fan,s);
   elseif(compstp~=0 && fan==0) % turn the fan off if the compressor is set to be off
      ChangeFanSpeed(fanstp,s);
      pause(16)
   end

   LoadShortIntervalChillerData();  %  load short-interval chiller data to perform superheat control and check safety

   CheckIfSafeToRunCompressor(s);  % determine if safe to run compressor, data is being logged, discharge
temperature is not high, evaporating temperature is above 1 Celsius
```

```
   CheckSlowDownCompressor(s); % Slow down the compressor, before shutting it down, to avoid freezing or
overheating

   load chillercontrolpoints
   if(safetorun && ~sloweddown)  % if safe to run and not slowed down, set the compressor to its optimal setpoint
      if(compressor~=compstp && isempty(levstart))
         ChangeCompressorSpeed(compstp,s);
         disp(['Compressor set to setpoint ' num2str(compstp)])
      elseif(compressor~=compstp)
         ChangeCompressorSpeed(compstp,s,levstart);
         levstart = [];
         disp(['Compressor set to setpoint ' num2str(compstp)])
      end
   end

   sh = SuperheatPID(s);   % run PID loop to control expansion valve position based on superheat across the BPHX

   load chillercontrolpoints
   pause(2-toc)  % synchronize superheat control to data logger sampling rate (2 seconds)

   load ShortChillerData
   if(chillerdata(1,20)<1)  %  additional emergency freeze protection
      safetorun=false; compressor = 0; timestopped = clock;
      ChangeCompressorSpeed(0,s);
      disp('Emergency compressor shut off')
      disp('Refrigerant temperature is too low')
   end
   nowtime = clock;

end
ChangeCompressorSpeed(0,s); %  shut down the compressor at the end of the hour to perform a new optimization
fclose(s)
delete(s)

catch  %  catch any errors, shut down the compressor if necessary
   try
      cd('C:\Program Files\MATLAB\Precooling')
      ChangeCompressorSpeed(0,s)
      fclose(s)
      delete(s)
      err = lasterror;
      SendNickEmail('System shut down',[err.message '  ' err.identifier])
      k = findstr(err.message,'dtstr2dtvecmx');
      if(~isempty(k))
         load chillercontrolpoints
         AutomateHour(compstp,fanstp,[])
      end
   catch
      err = lasterror;
      SendNickEmail('COM failure emergency',err.message)
   end
end
```

Expansion valve superheat control: SuperheatPID(s)

```
function sh = SuperheatPID(s)

shpidtime = clock;
load ShortChillerData
load chillercontrolpoints
shstp = 3.5+0.15*(compressor-19); % calculate superheat setpoint at given compressor speed
sh = chillerdata(1,21)-chillerdata(1,20); % calculate superheat
sherror = sh-shstp; % calculate superheat error

% wait for compressor speed to adjust before implementing superheat PID control
if(etime(shpidtime,timecompressorchanged)<15 || ~newpidchillerdata)
   return
end

% PID loop parameters
Ku = 0.9;  Tu = 100; Kp = 0.6*Ku; Ki = 2*Ku/Tu; Kd = Ku*Tu/8;

% calculate PID loop output (change in EXV position)
dtPID = etime(shpidtime,PIDtime);
integralerror = (sum(previouserrors)+sherror)*dtPID;  % finite sum integral term to avoid integral windup
derivative = (sherror-previouserrors(1))/dtPID;
previouserrors = [sherror; previouserrors(2:end)];
del_lev = Kp*sherror+Ki*integralerror+Kd*derivative;
% store time of PID change
PIDtime = shpidtime;
save chillercontrolpoints previouserrors PIDtime -append
levpos = lev+del_lev;
if(levpos~=lev)
   ChangeLEVposition(levpos,s)
end
```